REACTION OF MONOENERGETIC DEUTERIUM ATOMS WITH HYDROGEN AND MONOENERGETIC HYDROGEN ATOMS WITH PER-DEUTERO METHANE

Thesis by

Jeanette Asay Betts

In Partial Fulfillment of the Requirements

For the Degree of

Doctor of Philosophy

California Institute of Technology

Pasadena, California

1971

(Submitted September 24, 1970)

ACKNOWLEDGMENTS

I wish to express my appreciation to Dr. Aron Kuppermann for suggesting the projects described in this thesis and for discussion and advice given throughout the course of this work.

I wish to thank Dr. Donald R. Davis for the help and encouragement he gave me in starting this work and Dr. Avigdor Persky for helpful discussions during the course of this work.

Support in the form of a fellowship from the National Defense Foundation is appreciated.

Finally, I wish to thank my husband Tim for the encouragement and support he has given me in the preparation of this thesis.

ABSTRACT

Mixtures of $DBr-H_2$, $DI-H_2$ and $HBr-CD_4$ were photolyzed with monochromatic light. Thirteen different wavelengths were used in the $DBr-H_2$, $DI-H_2$ systems yielding deuterium atoms with initial laboratory energies ranging from 0.6 to 3.0 eV. We were able to obtain the integral reaction yield

$$A_{H + D_2} = \frac{k_1}{k_1 + k_2}$$

where k_1 and k_2 are effective bimolecular rate coefficients for the processes:

$$D^* + H_2 \rightarrow DH + H \qquad (1)$$

$$D^* + H_2 \rightarrow D + H_2 \qquad (2)$$

These processes describe rates of reaction and thermalization which accompany the injection of monoenergetic atoms into thermal H_2 gas. We were also able to obtain the integral reaction yield for the $H + CD_4$ system at five wavelengths with initial H atom laboratory energies ranging from 1.15 to 3.0 eV.

For both the $D + H_2$ and $H + CD_4$ systems we were able to show that the integral reaction yield is a monotonically increasing function of energy over the energy ranges scanned. For $D + H_2$ A ranged from 0 at about 0.6 eV to 0.66 at 2.86 eV initial laboratory energy while for $H + CD_4$ A ranged from 0.015 at 1.15 eV to 0.040 at 3.0 eV initial laboratory energy.

There is an order of magnitude difference between the integral reaction yields for H + CD_4 and either D + H_2 or H + D_2. These differences were attributed to the greater probability of inelastic collisions occuring in the H + CD_4 system than in the D + H_2 or H + D_2 systems. Finally, we were able to show how reaction cross sections can be extracted from the experimental integral reaction yield using a steady state Boltzmann equation.

We were also able to measure the abstraction fraction a for the reaction of H with DX (X = Br, I). The results were a(DBr) = 0.99 $\pm$ 0.03 and a(DI) = 0.97 $\pm$ 0.05.

Finally, using the integral reaction yield versus energy plot for D + H_2 plus additional DI-H_2, DI-He experiments we were able to determine the fraction f of iodine atoms produced in the excited $^2P_{1/2}$ state in the photolysis of DI at 4 wavelengths. The results are: f(2800Å) = -0.08 $\pm$ 0.27, f(2537Å) = 0.46 $\pm$ 0.05, f(2400Å) = 0.60 $\pm$ 0.07 and f(2138Å) = 0.33 $\pm$ 0.1.

TABLE OF CONTENTS

1. INTRODUCTION

The understanding of simple chemical reactions is a major area of interest in the field of chemical kinetics. It is profitable to study such systems experimentally since the results can be compared with detailed theoretical calculations leading to better understanding of detailed processes involved. One quantity in particular that is interesting to study is the reaction cross section. This quantity is important in that it enables chemists to gain greater insight into the molecular dynamics of chemical reactions. However, the amount of detailed information on this quantity, even on simple chemical systems, is small. The information available has been obtained by the elegant and complicated technique of molecular beams. However, this method has been used mainly in studies of reactions involving alkali atoms and/or halides, and even though it is now being extended to other systems, the energy dependence of total reaction cross sections for reactions with appreciable activation energy is not yet available. This study was undertaken to obtain cross section information on some elementary reactions by a relatively simple photochemical technique.

The two reactions reported here are the hydrogen isotope exchange reaction:

$$D + H_2 \rightarrow DH + H$$

and the reaction of hydrogen atoms with per-deutero methane:

$$H + CD_4 \rightarrow HD + CD_3.$$

The thesis is comprised of (in addition to this introduction)

4 papers, a section of conclusions and 6 appendices. It should be mentioned that the first 3 papers were written in conjunction with Drs. J. M. White, D. R. Davis and A. Kuppermann who contributed much to the work reported here. The first paper deals with the D + H_2 reaction, the second with the abstraction fraction for the reaction H + DX (X = I, Br), the third with the fraction of iodine atoms produced in the excited $^2P_{1/2}$ state in the photolysis of DI and the fourth with the H + CD_4 system. The appendices expand on details of experimental techniques and results not included in the papers.

PAPER 1

1. INTRODUCTION

The chemical reaction cross section is a very fundamental dynamical quantity which permits the formulation of bulk reaction properties in terms of the molecular level dynamics of reacting systems.[1] Furthermore, it contains information about the forces at play during reactive collisions of molecules.[2] Similar statements can be made about nuclear reaction cross sections, and indeed they have been extensively and profitably used by nuclear physicists in describing nuclear reactions and nuclear scattering processes and in developing a detailed understanding of these phenomena.[3] However, until ten or fifteen years ago, very little was known about chemical reaction cross sections. The main reasons were that experimentally no good methods were available for their determination and, theoretically, the calculations involved could not be carried out analytically and were far too elaborate to be done with the computational equipment then available.

The experimental difficulty was due to the fact that most measurements of reaction rates were made under thermal distribution conditions. For reasons described below, if the activation energy of the reaction is in excess of about 5 kcal/mole, such measurements do not contain information about the reaction cross section except relatively close to an effective threshold energy. Even with the use of the elegant and powerful crossed-molecular

beam technique,[4] it is still very difficult to determine the energy dependence of the cross section of such reactions over an extended energy range.

We will be concerned in this paper with the very important elementary process

$$D + H_2 \rightarrow DH + H$$

which, with its isotopic counterparts, has played a central role in the development of the foundations of chemical kinetics. In recent years, using a classical approximation to the motion of the nuclei during reaction,[2] it has been possible to calculate the energy dependence of the cross section of this reaction from first principles. In addition, theoretical formulations[5] and numerical techniques are presently being developed which should permit quantum mechanical calculations of good accuracy in the near future. For these reasons, it is highly desirable to obtain as much experimental information as possible about the cross section of this reaction and of its isotopic counterparts over a wide energy range. Information of this type is also desirable for systems too complex to perform a priori calculations, in order to test the validity of approximate models.

In this paper we describe a photochemical technique designed to measure the energy dependence of the integral reaction yield A [defined by Eq. (8)] of the $D + H_2$ exchange reaction, a quantity closely related to the reaction cross section. Preliminary results concerning the phenomenological energy threshold of this reaction have been previously described.[6]

In Section 2 we discuss the difficulties associated with obtaining reaction cross sections from thermal rate constants and crossed molecular beam measurements. In Section 3 we describe the basis of the present method, in Section 4 the experimental techniques, in Sections 5 and 6 the mode of analyzing the data and the results of the measurements of A for the relative energy range of 0.3 to 1.4 eV, and finally in Section 7 we discuss its relationship to reaction cross sections.

2. DIFFICULTIES IN OBTAINING TOTAL REACTION CROSS SECTIONS FROM THERMAL RATE CONSTANTS AND CROSSED MOLECULAR BEAM MEASUREMENTS

2.1. Thermal Rate Constants

Let us consider a homogeneous gas phase elementary bimolecular reaction between molecules A and B under conditions such that termolecular collisions are negligible. If all molecules A were in internal quantum state i and all B in state j and if collisions between A and B occurred at relative energy E, then the bimolecular rate coefficient for such a reaction would be

$$k_{ij}(E) = v(E)\,\sigma_{ij}(E) \qquad (1)$$

where $v(E)$ is the relative translational velocity of the reagents at energy E and $\sigma_{ij}(E)$ the total reaction cross section for such collisions. For more realistic conditions under which the reactants posses wider distributions of internal and relative translational energies, the bimolecular rate coefficient is given by[1]

$$k = \sum_{i,j} X_{A_i} X_{B_j} \int_0^\infty f_{ij}(E)\, \sigma_{ij}(E)\, dE \qquad (2)$$

where $f_{ij}(E)$ is the normalized distribution function of relative translational energies of A in state i and B in state j and X_{A_i} and X_{B_j} are respectively the fraction of A and B molecules in those states. The summation extends over all the states participating in the reaction. For the case in which f and the X are given by Boltzmann distributions at temperature T, k becomes the bimolecular reaction rate constant at that temperature and is expressable as

$$k(T) = \frac{1}{Z_A(T)\, Z_B(T)} \sum_{i,j} \exp\left[-(\epsilon_{A_i} + \epsilon_{B_j})/kT\right] (1/\pi\mu)^{1/2} (2/kT)^{3/2} \times \int \sigma_{ij}(E) E\, e^{-E/kT}\, dE \qquad (3)$$

Here Z_A and Z_B are the internal partition functions of A and B, ϵ_{A_i} and ϵ_{B_j} are the internal energies of A and B in states i and j respectively, μ is the reduced mass of the A + B system and k the Boltzmann constant. For convenience in the discussion which follows, it is helpful to consider the hypothetical case in which most of the contribution of k(T) comes from relatively few internal states i, j and $\sigma_{ij}(E)$ is almost independent of i, j for those states. This seems to be the case for the exchange reaction between hydrogen atoms and hydrogen molecules[2] and its isotopic counterparts (at temperatures below 1000°K), considered in this paper. Under these conditions, Eq. (3) reduces approximately to

$$k(T) = (1/\pi\mu)^{1/2} (2/kT)^{3/2} \int_0^\infty \sigma(E)\, E\, e^{-E/kT}\, dE \qquad (4)$$

It would seem at first glance that an experimental determination of k(T) followed by a numerical solution of the integral Eq. (4) should furnish $\sigma(E)$. For reactions whose activation energy E_a is large compared to kT, as is usually the case for $E_a > 5$ kcal/mole and $T < 1000^{\circ}K$, this method results in complete failure, and is responsible for the central difficulty in obtaining reaction cross sections from rate constants. The nature of this difficulty can be easily understood by considering a simple model for $\sigma(E)$ for reactions of the type being considered. Such a model is the hard-sphere line of center one given by

$$\sigma(E) = \begin{cases} \pi b^2 \left[1 - \frac{E_o}{E}\right] & \text{for } E \geq E_o \\ 0 & \text{for } E \leq E_o \end{cases} \qquad (5)$$

This cross section rises from zero at threshold energy E_o and approaches πb^2 at large energies. Its important feature is that its rate of rise with E is much slower than the rate of fall of $E \exp(-E/kT)$ for $E_o >> kT$. Since, to within a few kT, E_a is approximately equal to E_o (this result can be easily derived from Eqs. (4) and (5) and the usual definition of E_a as $-k\partial \ln k(T)/\partial(1/T)$) this last inequality is satisfied for reactions of the type being considered. If we consider a cross section with πb^2 of the order of $1A^2$ and E_o of the order of 7 kcal/mole (~0.3 eV) and a temperature below $1000^{\circ}K$, a major fraction of the contribution to the integral in Eq. (4) will come from the relatively narrow energy range of 7 to 9 kcal/mole (~0.3 to 0.4 eV).[7] In other words, the Boltzmann distribution of translational energies samples effectively

a relatively small energy range beyond the threshold energy, insofar as contributions to the rate constant are concerned. This conclusion is valid independently of the validity of Eq. (6), as long as $\sigma(E)$ can be characterized in terms of an effective threshold energy E_o such that for $E < E_o$ it is negligible [in terms of its contribution to k(T)] and for $E > E_o$ σE increases with energy much more slowly than exp (E/kT). Under these conditions, after a short range of rise, $\sigma E \exp(-E/kT)$ decays with E at a rate essentially characterized by the Boltzmann factor $\exp(-E/kT)$. This is likely to be the case for most reactions satisfying $E_a >> kT$. Therefore, for such reactions, even if Eq. (4) were accurate, i.e., if $\sigma_{ij}(E)$ were independent of i and j, it would be very difficult to obtain information about $\sigma(E)$ beyond a relatively narrow range (a few kT) of E around E_o. This point is further discussed elsewhere.[8] The actual dependence of $\sigma_{ij}(E)$ on i and j makes the situation worse, since several of these now contribute to k(T) in relative amounts which change with temperature. An attempt at increasing the energy range over which the reaction cross section is sampled by the Boltzmann distribution by substantially increasing the temperature and therefore shifting the tail of this distribution to higher energies brings with it an increase in the number of i, j states which may contribute significantly to k(T) and hence the number of significant and unknown $\sigma_{ij}(E)$. In many thermal experiments, in addition, as the temperature is substantially increased, processes of higher activation energy than the one of interest may start contributing

appreciably to the reaction mechanism, making it much more difficult to measure rate constants for the individual steps involved. Also, the rate of the reaction may increase by orders of magnitude which further increases the difficulties of accurate rate constant measurements. For all these reasons it has not been possible in the past to obtain much information from thermal experiments about the energy dependence of reaction cross sections with activation energy much greater than kT, and there is not much hope that such information can be gotten from such experiments in the future, except perhaps within a few kT of threshold for sufficiently low T. However, to understand the molecular dynamical properties of bimolecular chemical reactions and to test approximate theoretical calculations, reaction cross sections over a much wider energy range are highly desirable.

2.2. Crossed Molecular Beam Measurements

An alternative to thermal rate constant measurements for the determination of reaction cross sections is the elegant and powerful technique of crossed molecular beams.[4] In such experiments, the relative energy of the reactants can be maintained within a narrow distribution by keeping one of the beams at room temperature and velocity-selecting the other one. The information of greatest importance which has been derived from this technique up to the present has been the measurement of the angular and energy distribution of the products and its interpretation in terms of molecular dynamical models. For technical reasons, most

measurements to date have been limited to processes whose cross sections are greater than about 10Å^2 and/or which have essentially no activation energy (less than 2 kcal/mole). Even for such reactions the determination of the total cross sections has been made difficult and unreliable due to the necessity in many instances of including the contributions of large laboratory scattering angles, not always accessible to the detectors. In addition, if the beams are produced by thermal effusion ovens, the accessible relative energy range is relatively low. For beams of highly reactive free radicals, such as H or D atoms, it is not possible to produce acceleration by hypersonic expansion at high pressures[9] due to problems of radical recombination, and the lightness of such species precludes use of the seeding technique.[9] Finally, many elementary bimolecular reactions have activation energies of 5 kcal/mole or greater and reaction cross sections around threshold, as suggested by thermal rate constant measurements, of the order of 1Å^2. In addition, the reactants cannot in these cases usually be detected by surface ionization techniques. As a result of these circumstances, the crossed molecular beam technique has not been very successful in studying such processes, even at thermal energies. A particular example are the hydrogen atom-hydrogen molecule isotope exchange reactions

$$D + H_2 \rightarrow DH + H$$

$$H + D_2 \rightarrow HD + D$$

Early attempts[10,11] to study these reactions by crossed non-velocity-selected molecular beams were strongly limited by low signal

to noise ratios. However, a modulated-crossed beam experiment on the reaction of D with H_2 has been reported[12] recently in which the angular distributions of product HD were measured. However, no energy dependence measurements were made.

In summary, essentially no experimental information is available about the energy dependence of the hydrogen exchange reactions above from either thermal rate constant or crossed molecular beam studies, and furthermore there are no indications that such information, in the very important relative energy range from threshold to about 70 kcal/mole (~0.3 eV to ~3 eV), is forthcoming from these techniques. We now describe a method capable of furnishing such information.

3. FOUNDATIONS OF THE METHOD

3.1. The Integral Reaction Yield

It is well known[6,13-16] that translationally "hot" hydrogen atoms are formed in the photodissociation of HX (X = I,Br) and can be distinguished from thermal ones by their reaction properties (similar statements being also valid for the corresponding deuterium and tritium isotopes). Furthermore, if monochromatic radiation is used, these atoms are initially almost monoenergetic (there is a small spread associated to the thermal translation and rotation of the parent halide molecule), their average initial laboratory energy $E_1^{(0)}$ depending only on the wavelength λ of the photodissociating light. The method of studying the D + H_2

exchange reaction consists in photolyzing mixtures of DX (X = I,Br) and H_2 with monochromatic light, and in determining the integral reaction yield

$$A(E_1^{(0)}) = \frac{k_1(\lambda)}{k_1(\lambda) + k_2(\lambda)} \tag{8}$$

as a function of $E_1^{(0)}$. Here $k_1(\lambda)$ and $k_2(\lambda)$ are the effective bimolecular rate coefficients for the elementary processes

$$D^* + H_2 \rightarrow DH + H \qquad [1]$$

$$D^* + H_2 \rightarrow D + H_2 \qquad [2]$$

describing the rates of reaction and thermalization which accompany the injection of monochromatic deuterium atoms into a thermal H_2 gas. The asterisk is used to denote translationally "hot" deuterium atoms, as defined in Section 3.2. (A more rigorous definition of A, which does not invoke the concept of hot D, is given in Section 7.) These rate coefficients depend on the energy with which the D* are initially formed and therefore on λ. The integral reaction yield is a measure of the competition between reactive collisions and non-reactive ones, and its variation with λ is related to the energy dependencies of the corresponding cross sections. If information is available about the differential non-reactive cross sections, from either theoretical calculations or independent experiments, the exchange reaction cross section $\sigma(E)$, averaged over the distribution of rotational states of H_2 at the temperature of the experiment, can be obtained from the experimental $A(E_1^{(0)})$ according to methods to be described in a succeeding paper. The present one is limited to the experimental determination

of $A(E_1^{(0)})$ and to giving the formal relations between it and the cross sections just mentioned.

3.2. Hot and Cold Deuterium Atoms

During photolysis of the DX plus H_2 mixtures, a steady state is expected to prevail. Therefore, the deuterium atoms will be characterized by a distribution function $F_{E_1^{(0)}}(E_1)$ of laboratory energies E_1. This steady state $F_{E_1^{(0)}}(E_1)$ is considerably broadened towards lower energies compared to the one at formation, due to the non-reactive collisions the D atoms undergo with the H_2 molecules. These collisions are predominantly deactivating because in all our experiments $E_1^{(0)} >> kT$, where T is the temperature of the H_2 gas. There is strong reason to believe that $F_{E_1^{(0)}}(E_1)$ will be bimodal, with one peak at the initial energy $E_1^{(0)}$ and the other at an energy of the order of kT, because of the thermalization process. We may then conceptually consider $F_{E_1^{(0)}}(E_1)$ as the superposition of two distribution functions, one thermal at temperature T and the other having a peak at the initial energy $E_1^{(0)}$. The deuterium atoms described by these two distributions will be called respectively "cold" (or "thermal") and "hot", and in the mechanism below designated by D and D*.

This conceptual classification is not essential for a quantitative analysis of the experiments. In Section 7, for instance, we use a Boltzmann equation formalism which does not invoke it. Nevertheless, it is a very useful classification for a physical

understanding of what is happening in the system. The steady state distribution function $f_E(0)(E)$ of relative energies E of D with respect to H_2 will have a hot component peaked approximately at $E^{(0)} = (1/2)E^{(0)}$ (the factor 1/2 being the ratio of the reduced mass of the D + H_2 system to that of the D atom), in addition to the thermal one, as indicated schematically in Fig. 1. The cross section $\sigma(E)$ of reaction [1], for one internal quantum state of H_2, is also depicted. We can make this hot peak "scan" $\sigma(E)$ by varying the photolysis wavelength. This is the essential characteristic of these experiments, which distinguishes them from thermal ones in which the hot peak is absent. Fundamentally, it is this peak which permits the determination of reaction cross sections from these experiments.

3.3. Kinetic Analysis

The concept of hot and cold deuterium atoms as introduced above suggests a kinetic method of analyzing the experimental data. The validation of this method of analysis from a Boltzmann equation formalism will be given in Section 7.

Let us consider the cold D and hot D* as two chemically distinct species in that their reactive properties differ due to different energy distributions. To indicate how the integral reaction yield A can be obtained, let us assume that the following mechanism is a correct description of the processes occurring in the DX + H_2 system

Figure 1. Schematic representation of steady state distribution function $f_E(0)(E)$ of D atom energies E relative to H_2 and of cross section $\sigma(E)$ of reaction $D + H_2 \rightarrow DH + H$.

(a) "thermal" peak.

(b) "hot" peak.

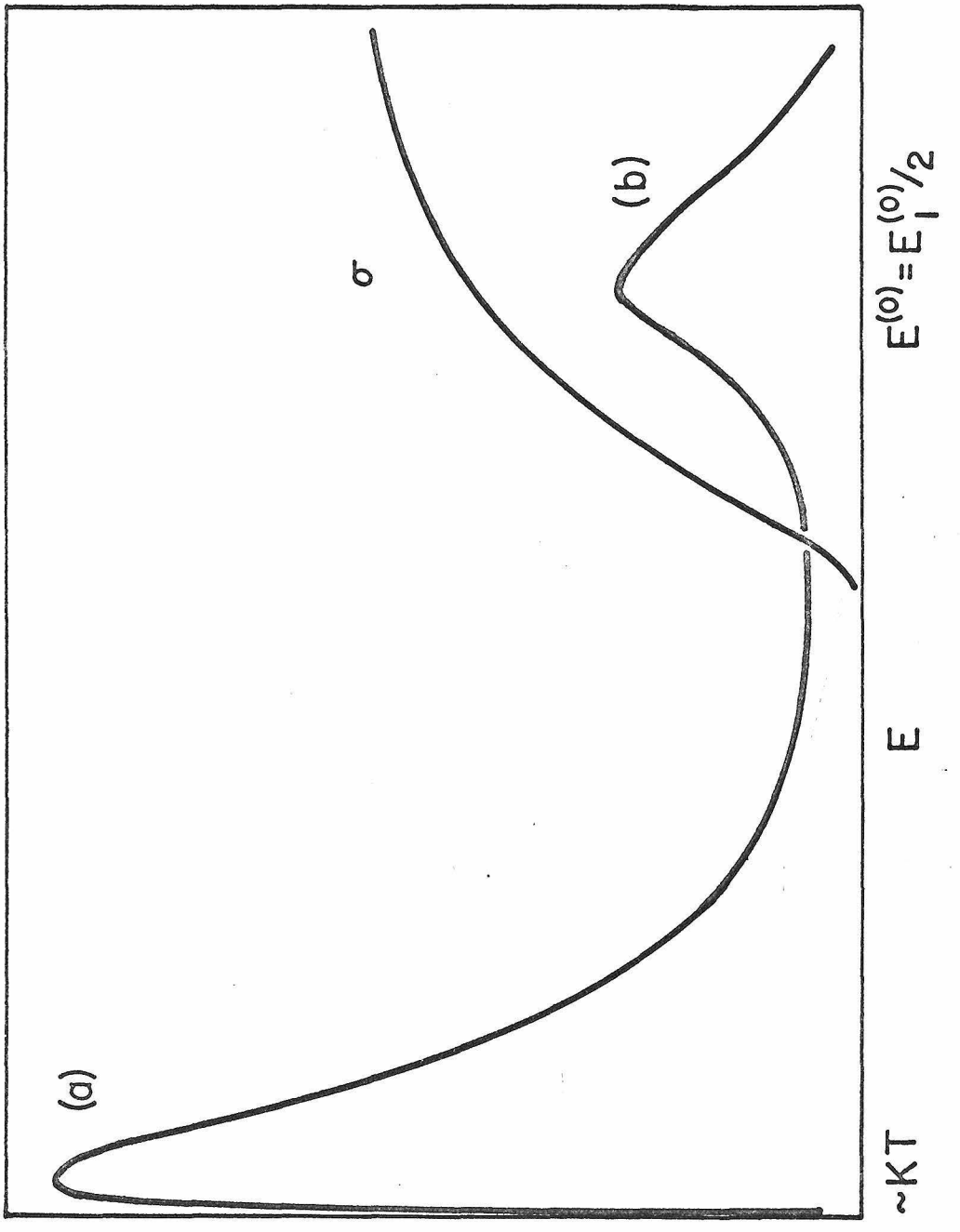
(a)
(b)
σ
~KT
E
$E^{(0)}=E_1^{(0)}/2$

$$DX + h\nu \rightarrow D^* + X \qquad [0]$$

$$D^* + H_2 \rightarrow DH + H \qquad [1]$$

$$D^* + H_2 \rightarrow D + H_2 \qquad [2]$$

$$D^* + DX \rightarrow D_2 + X \qquad [3]$$

$$D^* + DX \rightarrow D + DX \qquad [4]$$

$$D + DX \rightarrow D_2 + X \qquad [5]$$

$$H + DX \rightarrow HD + X \qquad [6]$$

$$H + DX \rightarrow HX + D \qquad [7]$$

$$X + X + M \rightarrow X_2 + M \qquad [8]$$

where the third body M is either a species in the gas phase or a surface. Neglect of other possible steps is justified in detail in Section 6.2.1. As shown in that section, there is strong reason to believe that the atomic product of [1] is translationally hot and should be denoted by H*, requiring that we consider its reactions in the mechanism. This complicates somewhat the resulting kinetic expressions but leaves the method of determination of the integral reaction yield A unchanged. For this reason we postpone inclusion of the H* reactions to that section.

Assuming steady state concentrations of [D*], [D] and [H], a kinetic analysis of the mechanism above furnishes

$$\frac{[D_2]}{[HD]} = \left(\frac{[D_2]}{[HD]}\right)_0 + \frac{(k_3 + k_4)}{(1 + a)k_1}\frac{[DX]}{[H_2]} \qquad (9)$$

where

$$\left(\frac{[D_2]}{[HD]}\right)_0 = \frac{(1 - a) + (k_2/k_1)}{(1 + a)} \qquad (10)$$

and

$$a = \frac{k_6}{k_6 + k_7} \tag{11}$$

Therefore, we should expect $[D_2]/[HD]$ to be a linear function of $[DX]/[H_2]$ with positive intercept and slope, as found previously by Carter, Hamill and Williams[14] and by Martin and Willard[15]. This turns out indeed to be the case also in our experiments (see Section 5) and can be justified theoretically from a more rigorous Boltzmann equation formalism as will be seen in Section 7. From Eqs. (8) and (11) we obtain

$$A = \frac{([HD]/[D_2])_0}{1 + a + a([HD]/[D_2])_0} \tag{12}$$

Under the simplifying conditions above, a determination of A requires the measurement of the quantity $([HD]/[D_2])_0$, which is the reciprocal of the intercept of Eq. (9), and of a. This latter quantity is the exchange fraction defined as the ratio of abstraction to abstraction plus exchange yields in H + DX collisions under the conditions of our experiments. These H atoms, formed by reaction [1], undergo many collisions with H_2 before reacting with DI, especially in the limit $[DI]/[H_2] \to 0$ used in determining $([D_2]/[HD])_0$. Therefore, they should have a thermal energy distribution, and k_6 and k_7 should be thermal rate constants. Consequently, the exchange fraction can be determined from independent thermal experiments.

Eq. (9) contains a paradox. We know that if DX is made sufficiently small, the rate of the thermal reaction [5] will

become negligible compared with the rate of the thermal reaction

$$D + H_2 \rightarrow DH + D \qquad [9]$$

this latter occurring due to the high-energy tail of the distribution of thermal D energies. This means that as $[DX]/[H_2] \rightarrow 0$ we should have $[D_2]/[HD] \rightarrow 0$, in disagreement with Eqns. (9) and (10). The reason for this paradox is that Eq. (9) is not supposed to be valid for $[D_2]/[HD]$ too close to zero, exactly because of the exclusion of reaction [9] from the mechanism. If that reaction is included, we get a generalization of Eq. (9) valid down to vanishingly small $[DX]/[H_2]$:

$$\frac{[D_2]}{[HD]} = \frac{1}{1+a} \frac{1 - a + \frac{k_2}{k_1} + a\frac{k_3}{k_1}\frac{k_9}{k_5} + \left(\frac{k_3}{k_1} + \frac{k_4}{k_1}\right)\frac{[DX]}{[H_2]}}{1 + \frac{k_9}{k_5}\left[\left(1 + \frac{k_2}{k_1}\right)\frac{[H_2]}{[DX]}\frac{k_4}{k_1}\right]} \qquad (13)$$

The curve represented by Eq. (13) goes through the origin as expected. Under conditions such that

$$\frac{k_9}{k_5}\left[\left(1 + \frac{k_2}{k_1}\right)\frac{[H_2]}{[DX]} + \frac{k_4}{k_1}\right] \ll 1 \qquad (14)$$

Eq. (13) represents a straight line which <u>does not</u> go through the origin; it has a slope equal to that of Eq. (9) and a positive intercept $([D_2]/[HD])_0$ which exceeds that of Eq. (9) by the amount $a(k_3/k_1)(k_9/k_5)$. In terms of the receprocal of this corrected intercept, the integral reaction yield is given by

$$A = \frac{([HD]/[D_2])_0}{1 + a + a([HD]/[D_2])_0\left(1 - \frac{k_3}{k_1}\frac{k_9}{k_5}\right)} \qquad (15)$$

which differs from Eq. (12) by the $(k_3/k_1)(k_9/k_5)$ term in the denominator of the right hand side. We show in Section 6.2 that

$$k_5/k_9 \sim 10^5 \tag{16}$$

and that, as soon as the laboratory D atom energy $E_1^{(0)}$ rises slightly above twice the relative threshold energy for reaction [1],

$$k_3/k_1 < 10^2 \tag{17}$$

The meaning of Eqs. (16) and (17) is that DX is five orders of magnitude more efficient in scavenging thermal D atoms than H_2 (because of the much smaller activation and threshold energies of reaction [5] compared to that of reaction [9], whereas for relative D + H_2 energies in excess of the threshold for reaction [1], the energy advantage of [3] over reaction [1] disappears and DX and H_2 become about equally efficient scavengers of D except perhaps very close to that threshold.)

Physically, the non-vanishing intercept $([D_2]/[HD])_0$ is due to the smallness of k_9/k_5, so that even a relatively small amount of DX suffices to scavenge the D atoms which were thermalized before reacting while hot with H_2. The positive slope of Eq. (9) is due to the competition between DX and H_2 for hot deuterium atoms; the intercept excludes this competition and is therefore a measure of the contribution of the D* with H_2 only.

We show in Section 6.2 that Eq. (14) is equivalent to

$$\frac{[DX]}{[H_2]} \gg \frac{1}{A}\frac{k_9}{k_5} \tag{18}$$

The smallest A in our experiments (see Table I) is about 0.02. In view of Eq. (16), a sufficient condition for the validity of the last inequality is that

$$\frac{[DX]}{[H_2]} \gg 5 \times 10^{-4} \qquad (19)$$

Since the lowest $[DX]/[H_2]$ value used in our experiments was 0.1, this condition is amply satisfied. As a result of this and the validity of Eqs. (16) and (17), Eqs. (13) and (15) can be replaced by Eqs. (9) and (12) respectively, justifying the elimination of reaction [9] from the mechanism. From the straight line corresponding to Eq. (9) we therefore get $([D_2]/[HD])_0$ quite independently of what the actual behavior of $[D_2]/[HD]$ is at values of $[DX]/[H_2]$ very close to zero.

It is interesting to note that for sufficiently small $[DX]/[H_2]$ [much smaller than $(1/A)(k_9/k_5)$] Eq. (13) represents a straight line going through the origin with slope

$$\frac{[(1 - a)k_1 + k_2]\,(k_5/k_9)\quad ak_3}{(1 + a)(k_1 + k_2)} \simeq \left[\frac{1 - a + \dfrac{k_2}{k_1}}{1 + a}\right] A(k_5/k_9) \qquad (20)$$

The term in square brackets on the right hand side of Eq. (20) is equal to the slope of Eq. (9). Therefore, the slope of Eq. (13) at the origin is more that 2000 times greater than that of Eq. (9). This means that for conditions under which the mechanism being considered is valid, as $[DX]/[H_2]$ increases from zero there is a sharp rise in the $[D_2]/[HD]$ ratio followed by a sharp bending over at $[DX]/[H_2] \sim (1/A)(k_9/k_5)$. Schematically, the full behaviour

of Eq. (13) is represented in Figure 2.

One important detail was left out in the mechanism considered. A certain amount of HX impurity (about 3% for the iodide and 1% for the bromide) was always present. In order to correct for this, we performed experiments of DX plus He or Ne (plus the unavoidable HX impurity) similar to the DX plus H_2 ones. The corresponding more general mechanisms and kinetic analysis are described in Section 6.2.

In summary, the method for determining the integral reaction yield A defined by Eq. (8) consists in photolyzing mixtures of DX plus H_2 with monochromatic light and measuring the resulting $[D_2]/[HD]$ ratio as a function of the $[DX]/[H_2]$ one. From this, the intercept $([D_2]/[HD])_0$ is determined and used to obtain A from a modified version of Eq. (12) which corrects for the effects of the HX impurity, as determined from similar DX plus rare gas experiments. Scanning of the photolysis wavelength furnishes the energy dependence of A.

4. EXPERIMENTAL

4.1 Apparatus

The equipment used in these experiments consisted of four parts: (1) a high vacuum line for preparing the reactant mixtures, (2) a photolysis system, (3) a high vacuum line for the removal of the products, and (4) an analysis system.

Figure 2. Schematic representation of Eq. (13). For clarity, the slope of the line for $[DI]/[H_2] = (1/A)(k_9/k_5)$ has been greatly exagerated compared to the slope of line passing through origin.

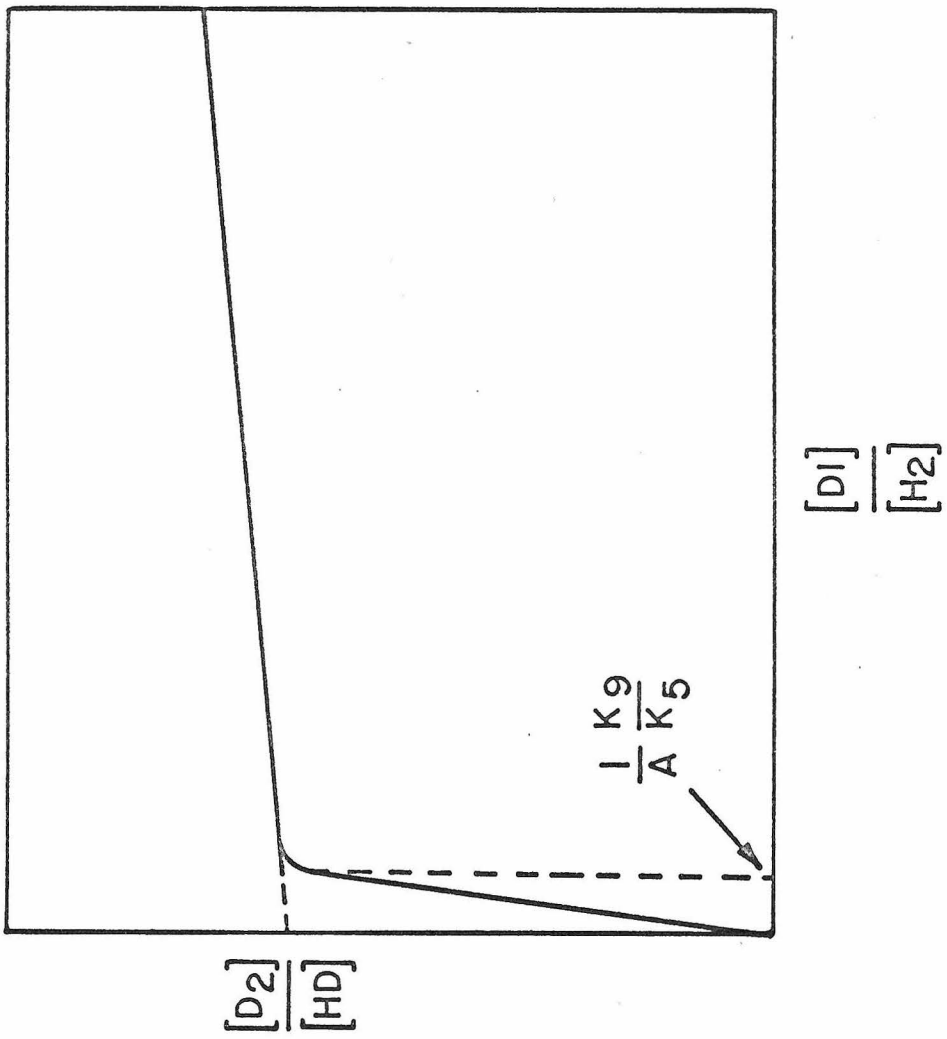
[D2]/[HD]
1 + K9/A K5
[D1]/[H2]

The high-vacuum line used to prepare the reactant mixture was entirely mercury free, because DX reacts rapidly with mercury and also to avoid mercury-photosensitized reactions in the photolysis system. Gas pressures were measured with the help of a Pace Electronics Co. (North Hollywood, California) model P7D-0.1 differential pressure transducer as a null detector balanced against a mercury manometer.

The photolysis system, as depicted schematically in Fig. 3, consisted of a light source system (A), a reaction vessel (B), and a light detection system (C). Different light source systems were used for different wavelengths, as follows[17]:

(a) For experiments at wavelengths of 3340Å, 3130Å, 2891Å, 2483Å and 2400Å a 2500 watt Hanovia medium pressure mercury-xenon lamp was used. The output was passed through a 2:1 nickel sulfate-cobalt sulfate filter solution (20g $NiSO_4 \cdot 7H_2O$, 10g $CoSO_4 \cdot 6H_2O$ and 1 ml 16M sulfuric acid per liter of water in a 5 cm pathlength cell) to remove energy in the visible and infrared, and then through the entrance slit of a Bausch and Lomb model 33-86-01 monochromator. The bandpasses used varied depending on the wavelength and are listed in Table I. At 3340Å a 5 mm thick Corning 0160 glass filter and at wavelengths 2481Å, 2400Å and 2891Å a 2 mm thick Corning 7910 glass filter were placed at the exit of the monochromator to remove shorter wavelength radiation.

(b) For experiments at 3261Å a cadmium Phillips spectral lamp was used in conjunction with the 5 mm Corning 0160 glass filter.

Figure 3. Schematic drawing of the photolysis system. A - light source system; A_1 - lamp; A_2 - filter A_3 - monochromator; A_4 - filter; B - reaction vessel; C - light detection system.

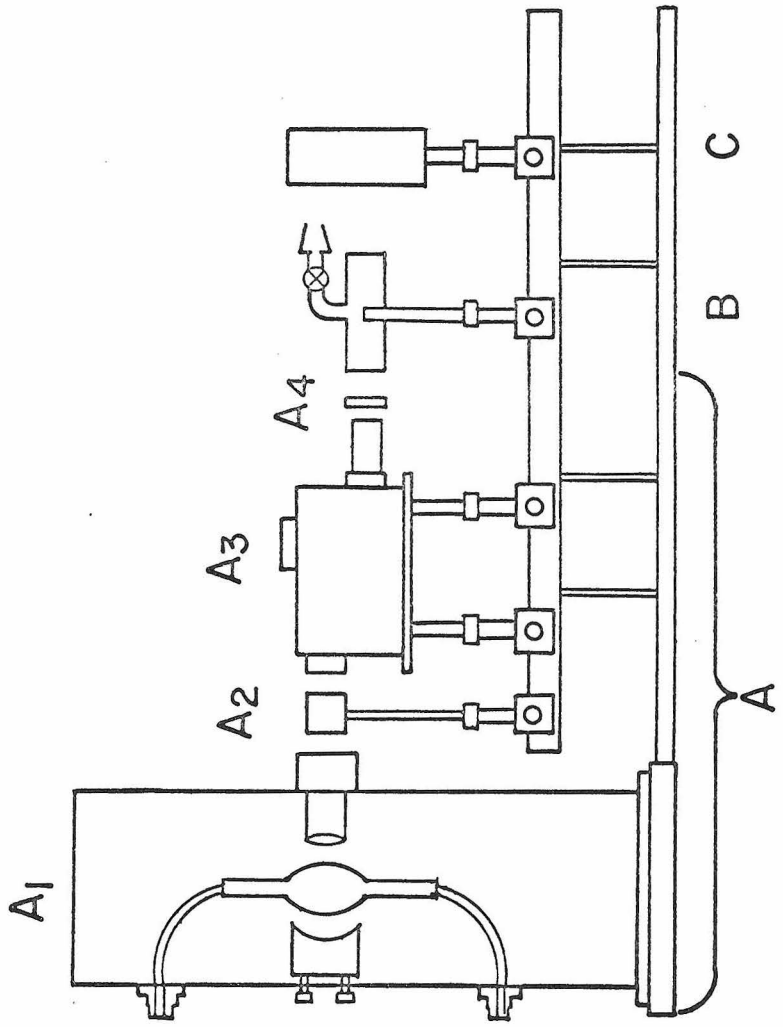
A1
A2
A3
A4
A
B
C

(c) For experiments at 2537Å and 1849Å a Hanovia SC 2537 low pressure mercury lamp was used. To isolate the 2537Å line a 2 mm thick lithium fluoride window irradiated with a dose of one million rad of Co^{60} gamma rays was used to remove the 2537Å radiation. The absorbance of the filter was always 2.5 or greater at 2537A and 0.45 at 1849Å. The lamp emitted 10% 1849Å radiation, so approximately 10% of all light passing through the filter was 2537Å. Since the extinction coefficient of DBr at 1849Å is over 100 times greater than at 2537A the correction for the 2537Å light passing through the filter is less than 0.1%. The window tended to fade during irradiation with 2537Å light and was reirradiated with Co^{60} gamma rays if the absorbance at 2537Å fell below 2.0.

(d) For photolyses at 2300Å and 3250Å a 6000 watt Hanovia high pressure xenon lamp was used in conjunction with the nickel sulfate-cobalt sulfate filter described previously. A 2 mm thick Corning 0160 glass filter was placed at the exit of the monochromator in the 3250A experiment.

(e) At 2138Å a zinc Phillips spectral lamp was used with a cis-2-butene gas filter (100 torr pressure, 5 cm pathlength) to remove shorter wavelength radiation. The spectrum of the filter taken using the Cary spectrophotometer showed that its transmission was 60% at 2138Å and less than 0.02% at 2050Å.

Several different reaction vessels were used in these experiments. They were all cylindrical in shape and made out of pyrex or fused silica. The windows at each end were of optical quality

pyrex or quartz. The length of the vessels was about 20 cm and the internal diameter 25mm. In some experiments a teflon tube of 22 mm internal diameter was inserted in a specially constructed vessel of larger internal diameter, in order to check for surface reactions. In all vessels, a high vacuum pyrex stopcock was attached to its side to permit the addition or removal of reactants and products. The light beam during most photolyses was not allowed to irradiate the inner cylindrical surfaces of the vessel. Light beams coming from the Bausch and Lomb monochromator had a rectangular cross section of approximate dimensions of 19 mm by 2 mm. However, in the experiments at 2537Å and 1849Å the light beam did irradiate the inner cylindrical surfaces of the vessel. Experiments described in Section 4 show that this introduced no error.

The light intensity was measured by either an Eppley thermopile or a photocell calibrated by the thermopile. A Jarrell-Ash scanning monochromator with photomultiplier detector was used to measure the wavelength distribution of the light source system output and to carefully check for light of shorter wavelength than the one desired. The bandpasses ($\Delta\lambda$) listed in Table I were determined from the full width at half-height of the photomultiplier output. The shape of this output peak was approximately gaussian.

The high vacuum line for removal of products included a mercury diffusion pump, a mercury toepler pump and a cell for thermally equilibrating mixtures of H_2, HD, and D_2. This cell

included a platinum or chromel-A filament which could be heated by passage of an electric current.

The analysis system was either an isotope ratio mass spectrometer[18,19] which accurately measured the ratio of the intensities of the peaks at m/e 3 and 2, or a Consolidated Electrodynamics Corporation Model 21-103C mass spectrometer.

A more detailed description of the apparatus can be found elsewhere.[20]

4.2 Reagents

The deuterium iodide and bromide were supplied by Merck, Sharp and Dohme of Canada, Ltd. The stated isotopic purity was 98% for DI and 99% for DBr. The actual isotopic purity, as measured in these experiments, was 97% for the DI and 98.7% for the DBr. Attempts to improve this purity for the iodide, by exchange with purer D_2 over platinized asbestos at 550°K in a carefully predeuterated line were unsuccessful.[20] The DI and DBr were stored in black bulbs and purified prior to use as described below.

Two kinds of hydrogen were used. One was Matheson Co. prepurified grade with a reported minimum chemical purity of 99.9%. The other was deuterium-depleted hydrogen, with a deuterium abundance about 100 times less than natural abundance.[21] Because of the lower HD background resulting from this H_2, more accurate measurements of the experimental $[D_2]/[HD]$ ratios could be obtained. The Matheson hydrogen was further purified by passage through a

deoxocatalytic unit (Engelhardt Industries Inc., Gas Equipment Division, East Newark, N. J.) and the deuterium depleted hydrogen by passage through a liquid nitrogen trap.

The helium and neon used were research grade obtained from the Linde Co., with a minimum purity of 99.99%. Mass spectrometric analysis on the CEC-103C showed no detectable impurities in the m/e range 12 through 60.

4.3 Experimental Procedure

4.3.1 Preparation of Reaction Mixture

Using the mercury-free line, the DX is transferred from a storage bulb to a cold finger dipped in liquid nitrogen. It is then pumped to remove any residual D_2 which could have been formed from some prior decomposition of the DX, and distilled from a dry ice-acetone bath (-78° C) into the reaction vessel. This step is to remove any X_2 which may have been formed in that same decompsition. The DX pressure is measured with the help of the differential pressure transducer plus mercury manometer and cathetometer. Pressures of DX ranged from 25 to 60 torr. Hydrogen or rare gas is then added, and the pressure of the mixture measured. From the two pressure measurements, the $[DX]/[H_2]$ or [DX]/[rare gas] ratios are determined. They range from about 0.2 to about 1.5. Blank experiments without photolysis showed no detectable D_2 and no HD above that introduced by the H_2.

The vacuum line and reaction vessel were deuterated prior to use by exposure to DX for approximately 24 hours. They were then

flushed several times with clean DX and were not further exposed to air to keep them in the same condition throughout a series of experiments for which the [HX]/[DX] was determined. Separate vacuum lines were used for the DI and DBr experiments since a small amount of DI in the DBr could drastically alter the results for the latter, because the DI has a much higher extinction coefficient than the DBr in the wavelength region used and produces D atoms of higher energy by photodissociation.

4.3.2 Photolyses

The intensity of the photolysis light, as determined by the calibrated photocell, varied from about 2×10^{14} photons/sec to about 10^{16} photons/sec, depending on the light source used. During a given photolysis it stayed constant to within about 10%, which is sufficient for our purposes since the results were shown to be independent of light intensity over a much wider intensity range.

The photolysis times ranged from 15 minutes to 12 hours depending on the wavelength used and the extent of conversion of the DX desired. The latter varied from 0.01% to 2.1%.

4.3.3 Analysis of Products

After photolysis, one end of the reaction vessel is placed in liquid nitrogen for 15 minutes or more to freeze out the DX and HX. The noncondensible gases are then transferred on a vacuum line into a glass sample bulb with the help of a mercury toepler

pump.

When the isotope ratio mass spectrometer was used, part of this sample was transferred to the equilibration cell mentioned in Section 4.1, to convert all of the D_2 into HD. The ratio of intensities of the mass spectral peaks at m/e 3 and 2 was then determined for the equilibrated and nonequilibrated samples, as well as for a sample of H_2 used in the experiment, and from these measurements, corrections for H_3 contributions to m/e 3 and calibration curves the $[D_2]/[HD]$ in the photolysis product was determined. After these experiments were completed, it was noticed that in the analysis of the products of the DX + He photolyses there was an unsuspected contribution from the He to the peak at m/e 3. Due to this, and to the availability of the deuterium-depleted hydrogen, use of the isotope ratio mass spectrometer was discontinued in favor of the CEC-103C one. The results with asterisks in Table I were obtained by this method and the helium interference was approximately corrected for a posteriori.

When the CEC-103C mass spectrometer was used, the entire product sample in the glass bulb was analyzed. As previously, corrections for the H_3 contribution to m/e 3 were made, as well as for the HD contribution from the H_2 gas. Also, the instrument was calibrated with mixtures of known $[D_2]/[HD]$ ratios whose composition was analogous to that of the photolysis samples. The resolution of this instrument of about 1/500 permitted adequate separation of the m/e peaks for He and D_2. Reproducibility of repeated analysis of the same sample was within 2%.

5. RESULTS OF $([D_2]/[HD])_0$ MEASUREMENTS

Photolyses were done at thirteen different wavelengths. At each wavelength a series of DX plus H_2 and DX plus rare gas experiments were performed at [DX]/[G] ratios (G = H_2, rare gas) varying in general between 0.3 and 1.5. In some instances this ratio was as low as 0.2 and as high as 2.0. In each series of experiments the reaction vessel and vacuum line were soaked in DX between runs, without being exposed to air, to keep the deuterated condition of the internal surfaces unchanged. They were then evacuated to 10^{-6} torr for 1 hour prior to filling. At some wavelengths as many as four different series of experiments were done over the course of several years. For each series of experiments the plot of the $[D_2]/[HD]$ ratio in the products against the [DX]/[G] ratio in the reactants was always a straight line of positive slope and intercept. These two quantities and their standard deviations were determined by a least mean square fit to the experimental points. The intercepts are labelled $([D_2]/[HD])_0^{H_2}$ and $([D_2]/[HD])_0^{M}$ for the DX plus H_2 and DX plus rare gas experiments respectively, M standing for helium or neon.

An important quantity to correct for the effect of HX impurity in the DX in the determination of the integral reaction yield A is

$$\Delta = ([HD]/[D_2])_0^{H_2} - ([HD]/[D_2])_0^{M} \qquad (24)$$

where the quantities in the right hand side are the reciprocals of the corresponding intercepts defined above. If there were no

HX impurity present, $([HD]/[D_2])_0^M$ would vanish and Δ would be equal to $([HD]/[D_2])_0^{H_2}$. In particular, at the phenomenological reaction threshold both A and Δ should vanish.

The effects of dark reactions, total pressure, light intensity, oxygen impurity, extent of DX conversion, temperature and nature of internal reaction vessel surfaces close to the photolysis volume were investigated, with the following results.

(a) Effects of dark reactions. In blank experiments, for which the same experimental procedure of actual experiments was followed, except that the photolysis light was not turned on, no formation of D_2 or HD was ever detected. This excludes the presence of nonphotochemically initiated (i.e., "dark") thermal reactions.

(b) Effect of total pressure. Two reaction vessels were filled at the same time with the same DI plus H_2 mixture, but the pressure in one of them was decreased by expansion into an evacuated volume. With total pressures of 64.9 and 36.0 torr, photolysis at 3030Å furnished the same $[D_2]/[HD]$ product ratio to within 1%, indicating no total pressure effects over an approximate two-fold variation in pressure.

(c) Effect of light intensity. Two reaction vessels were filled at the same time with the same DI plus H_2 mixture and photolyzed for the same length of time at 3030Å with light intensities of about 2.5×10^{14} and 1.2×10^{15} photons/sec respectively. The resulting $[D_2]/[HD]$ ratios agreed to within 2%, indicating the absence of significant light intensity effects over

a five-fold range.

(d) Effect of oxygen impurity. Two reaction vessels were filled as follows. One of them, in clean condition, was filled with a certain DI plus H_2 mixture. The other was filled with 20 torr of oxygen for 6 hours and evacuated to approximately 10^{-4} torr. The stopcock of the first vessel was then opened for about 2 seconds allowing expansion into the second vessel. Both cells were then photolyzed under the same conditions at 3030Å and the resulting $[D_2]/[HD]$ ratios agreed to within 3%, indicating a small oxygen effect. Since in our experiments no such exposure to oxygen or air was allowed, this shows that no oxygen effects were present in them.

(e) Effect of extent of DX conversion. Several DI plus H_2 mixtures were photolyzed at 3030Å. For eight of them the extent of DI conversion was allowed to reach 0.55%, for another six 1.2% and a final set of six 2.1%. The corresponding $([D_2]/[HD])_0^{H_2}$ values were 3.00 ± 0.18, 3.20 ± 0.15 and 2.87 ± 0.18 respectively. A similar study was performed with 3340Å light at 0.45% and 0.9% conversions furnishing intercepts equal to 2.78 ± 0.19 and 2.62 ± 0.15 respectively. Finally photolyses of DBr at 2537Å at 0.5% and 1% conversion furnished intercepts equal to 2.70 ± 0.07 and 2.70 ± 0.03 respectively. The differences within each set of intercepts are within experimental error and show no systematic trend with extent of conversion. All our experiments were performed at extents of DX conversion ranging from 0.15 to 2.1%, with most of them between 0.2 and 0.7%, as shown in Table I.

Under these conditions the results are not significantly dependent on the extent of conversion.

(f) Effect of temperature. Temperature dependence studies were performed for DI plus H_2 mixutres at 3030Å and 2537Å as follows. Two identical vessels were filled with DI plus H_2 mixtures having the same $[DI]/[H_2]$ ratio of 0.50 and photolyzed with 3030Å light at room (20°C) and at dry ice (-78°C) temperatures respectively. The corresponding $[D_2]/[HD]$ ratios were 2.78 and 2.69. The difference between these results is within experimental accuracy. At 2537Å a series of experiments with varying $[DI]/[H_2]$ ratios were performed at dry ice and at room temperature. The corresponding straight lines of $[D_2]/[HD]$ versus $[DI]/[H_2]$ had intercepts of 1.38 ± 0.15 and 1.45 ± 0.07 and slopes of 1.76 ± 0.09 and 1.57 ± 0.06 respectively. The intercepts are equal within experimental error. We conclude that no temperature effects on $([D_2]/[HD])_0^{H_2}$ are detectable in the -78°C to 20°C range. We also conclude that it is unnecessary to keep the reaction vessel thermostated at room temperature, since small temperature variations from day to day or during an experiment should not, within our experimental accuracy, alter the results.

(g) Effect of teflon lining and nature of the reaction vessel.

It is conceivable that some of the species generated in the light beam region could diffuse to nearby walls and undergo heterogeneous reactions. To test for such effects, we compared the results obtained for reaction vessels lined with a teflon tube insert with those for unlined vessels and also the results obtained

with both quartz and silica reaction vessels. Since using different reaction vessels may affect the amount of HX impurity formed as a result of exchange of the DX with the surfaces to which it was exposed, the quantity Δ, defined by Eq. (18) above, is the important one to consider. The values of $([HD]/[D_2])_0^{H_2}$ and $([HD]/[D_2])_0^{He}$ for photolysis of DI and H_2 mixtures at 3030Å were 0.364 ± 0.013 and 0.100 ± 0.003 for a lined pyrex vessel and 0.420 ± 0.032 and 0.150 ± 0.006 for an unlined one leading to Δ values of 0.26 ± 0.01 and 0.27 ± 0.03 respectively. Experiments were done a year earlier comparing lined pyrex and silica vessels. The Δ values were 0.22 ± 0.02 for the pyrex vessel and 0.20 ± 0.01 for the silica one. At 3340Å, which is close to the phenomenological threshold for Δ and A, the Δ values were 0.053 ± 0.014 for a lined pyrex vessel and 0.10 ± 0.03 for an unlined one. At 2537Å DI-H_2 photolyses were done comparing lined and unlined silica vessels. The Δ values were 0.64 ± 0.02 for the lined silica vessel and 0.67 ± 0.02 for the unlined one. The results for DBr-H_2 photolyses show less scatter than those for DI-H_2 indicating that the nature of surface is less important for DBr. Hence we conclude that a small surface effect may exist near threshold, but that at higher energies it should not significantly alter the value of Δ.

(h) Effect of irradiating the sides of the reaction vessel. Photolyses of DBr-H_2 mixtures with $[DBr]/[H_2]$ = 1.46 were done using 3 low pressure mercury lamps with different geometries. The first lamp was the Hanivia SC 2537 lamp which sent out a

divergent beam of light initially 1 inch in diameter which irradiated the windows and also some of the inner cylindrical surface of the reaction vessel. The second lamp was a General Electric germicidal lamp which was placed so it irradiated the sides of the vessel. The third lamp was a low pressure mercury Phillips spectral lamp with a light area approximately 1 inch high and 1/2 inch across which irradiated only the windows of the vessel. The $[HD]/[D_2]$ ratios obtained were 0.240, 0.245 and 0.250 respectively. This is within the experimental error of the experiments indicating that light hitting the inner cylindrical surfaces of the reaction does not alter the results.

Illustrative examples of lines of $[D_2]/[HD]$ versus $[DX]/[G]$ are given in Figs. 4 and 5. The ones in Fig. 4 correspond to photolysis of DI mixtures at 3340Å and furnish $\Delta = 0.053 \pm 0.015$. The ones in Fig. 5 correspond to photolysis of DBr mixtures at 2138Å and furnish $\Delta = 1.32 \pm 0.05$. The results of all experiments together with the experimental conditions are summarized in Table I. Column 1 gives the central photolysis wavelength, column 2 the wavelength range (full width at half maximum), column 3 the substance photolyzed, columns 4, 5 and 6 the initial laboratory velocity, initial laboratory energy with associated spread and initial energy relative to stationary H_2 of the D atoms produced in the photodissociation (calculated as described in Section 6.1), column 7 the extent of the DX conversion, column 8 the ratio of molar extenction coefficients of HX and DX as described in Section 6.3 and column 9 specifies the nature of the reaction vessel.

Figure 4. Plot of $[D_2]/[HD]$ versus $[DI]/[G]$ at $\lambda = 3340\text{Å}$.

He line: intercept = 3.34 ± 0.12; slope = 0.90 ± 0.20

H_2 line: intercept = 2.83 ± 0.06; slope = 0.69 ± 0.07.

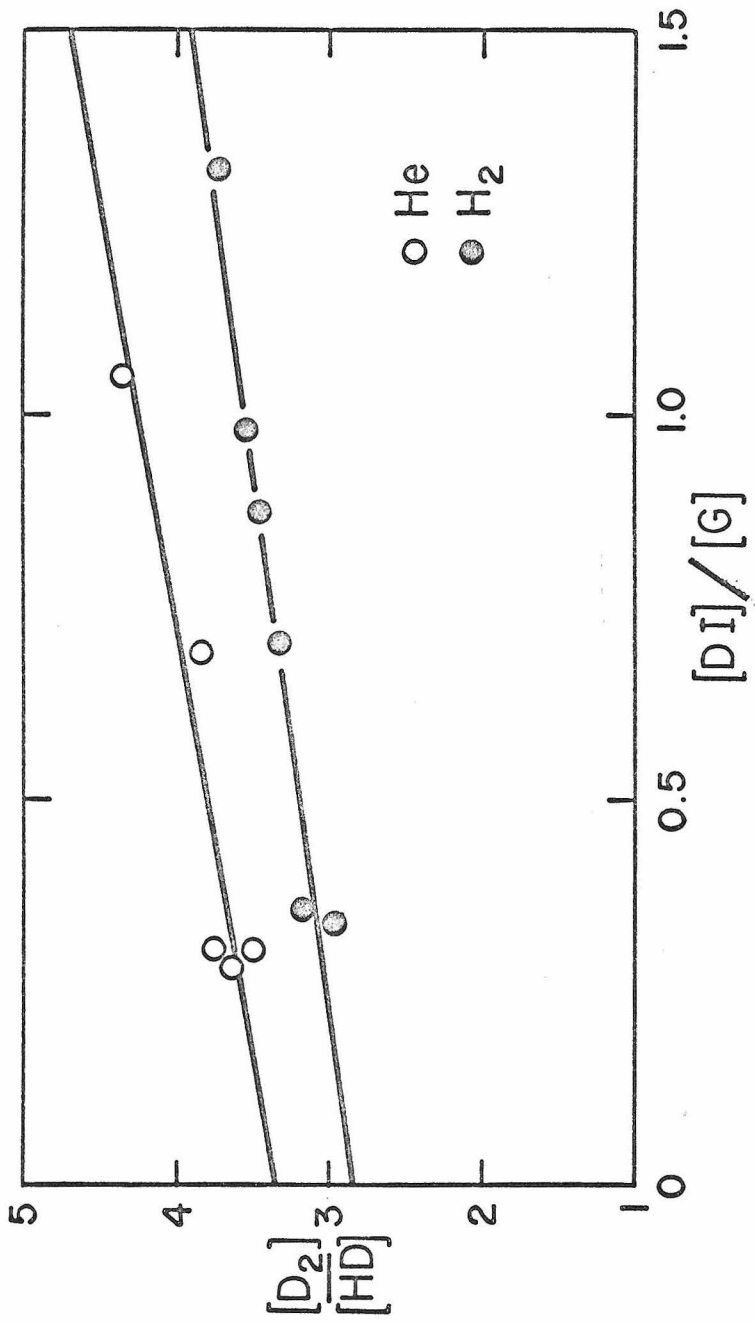
5
4
3
2
1
0
0.5
1.0
1.5
[D2]/[HD]
[DI]/[G]
He
H2

Figure 5. Plot of $[D_2]/[HD]$ versus $[DBr]/[G]$ at $\lambda = 2138$Å.

He line: intercept = 29.1 ± 0.2; slope = 2.8 ± 0.2

H_2 line: intercept = 0.74 ± 0.03; slope = 0.91 ± 0.03

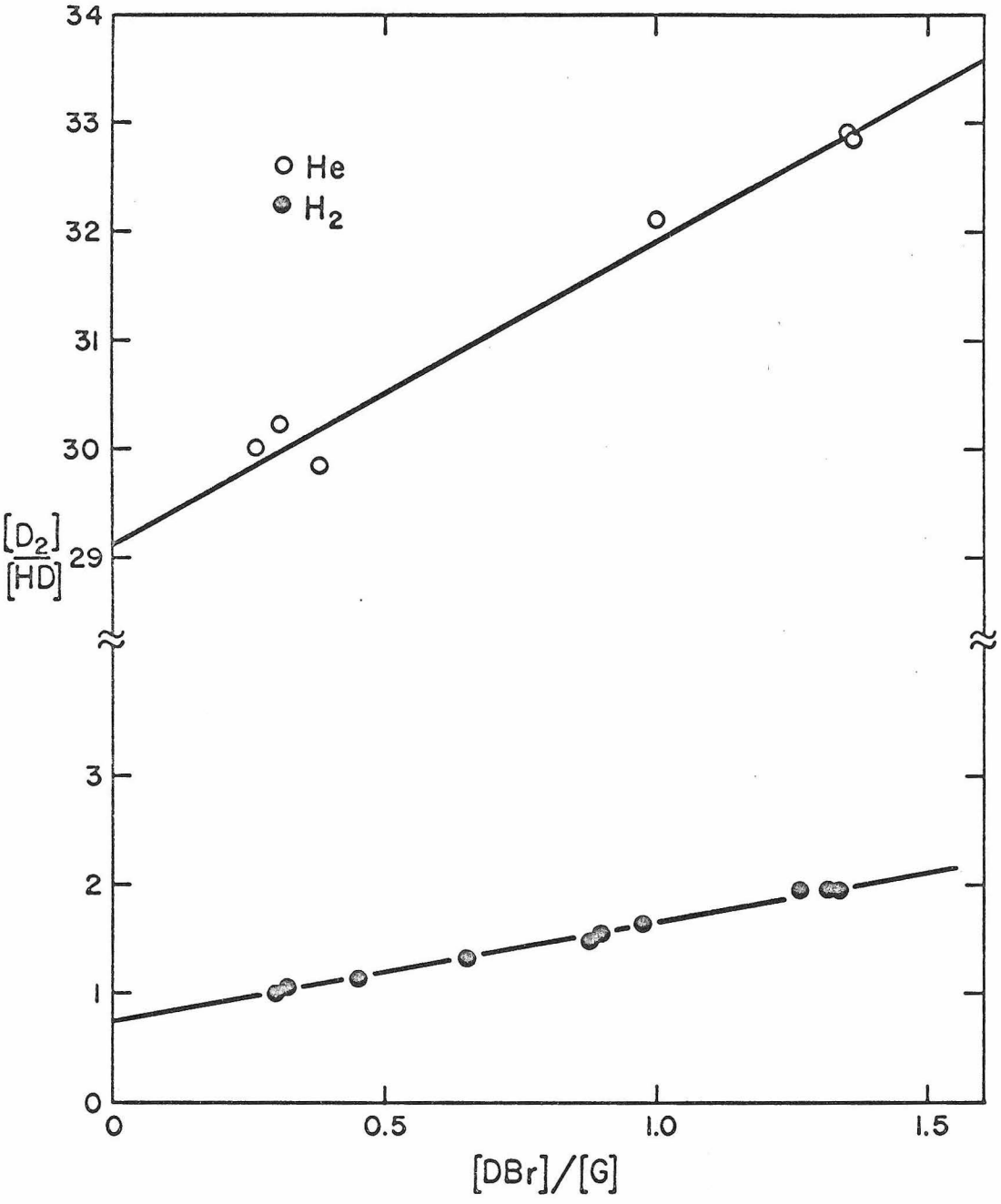
34
33
32
31
30
29
3
2
1
0
0
0.5
1.0
1.5
He
H_2
$\frac{[D_2]}{[HD]}$
[DBr]/[G]

TABLE I. Summary of Results for D + H_2

λ(Å)	Δλ (Å)	Substance Photolyzed	Initial Laboratory Velocity (10^5cm/sec)	Initial Laboratory Energy (eV)	Initial Relative Energy (eV)
3340	4.5[a] 4.5[a] 64[b]	DI	7.72	0.622 ± 0.023	0.311
3261	1[c] 1[c]	DI	8.27	0.714 ± 0.018	0.357
3251	30[a]	DI	8.33	0.724 ± 0.053	0.362
3130	16[a] 16[a] 32[b]	DI	9.11	0.866 ± 0.038 0.866 ± 0.038 0.866 ± 0.058	0.433
3030	10.3[a] 10.3[a] 32[b] 10.3[a]	DI	9.79	1.000 ± 0.031 1.000 ± 0.031 1.000 ± 0.058 1.000 ± 0.031	0.500
2891	11[a]	DI	10.66	1.182 ± 0.038	0.591
2537	1[c] 1[c]	DBr	10.19	1.084 ± 0.024	0.542
2500	33[a]	DBr	10.52	1.154 ± 0.087	0.577
2483	24[a]	DBr	10.66	1.186 ± 0.072	0.593
2446	34[a]	DBr	10.99	1.260 ± 0.090	0.630
2300	22[a]	DBr	12.36	1.594 ± 0.081	0.897
2138	1[c]	DBr	13.75	1.973 ± 0.024	0.986
1849	1[c]	DBr	16.54	2.856 ± 0.024	1.428

a. width at half height of peak
b. bandpass of monochromator
c. line source - no monochromator

TABLE I (continued)

λ(Å)	Extent DX Conversion[d] (%)	$x = \frac{HX}{DX}$	Nature of Reaction Vessel	Reciprocal Intercept $([HD]/[H_2])_0^{H_2}$
3340	0.15 - 0.56 0.45 + 0.9 0.02	12 ± 1	lined pyrex	0.353 ± 0.008 0.355 ± 0.014 0.362 ± 0.011
3261	0.18 + 0.36 0.27 - 0.49	7.4 ± 0.3	lined pyrex	0.353 ± 0.019 0.292 ± 0.026
3251	0.46	7.0 ± 0.08	lined pyrex	0.326 ± 0.021
3130	0.39 - 1.9 0.38 0.10	3.85 ± 0.07	lined pyrex	0.279 ± 0.012 0.270 ± 0.008 0.280 ± 0.004
3030	1.0 - 3.0 0.61 0.2 0.55 + 1.2	2.54 ± 0.07	lined pyrex	0.303 ± 0.012 0.364 ± 0.012 0.325 ± 0.012 0.326 ± 0.012
2891	0.5	1.72 ± 0.03	unlined silica	0.420 ± 0.006
2537	0.7 0.50 + 1.0	6.7 ± 0.3	unlined silica	0.423 ± 0.007 0.370 ± 0.005
2500	0.25	5.4 ± 0.1	unlined silica	0.399 ± 0.009
2483	0.35	4.9 ± 0.1	unlined silica	0.476 ± 0.014
2446	0.40	4.19 ± 0.08	unlined silica	0.485 ± 0.066
2300	0.20	2.39 ± 0.04	unlined silica	0.896 ± 0.064
2138	0.50	1.47 ± 0.02	unlined silica	1.36 ± 0.13
1849	0.40	0.78 ± 0.01	unlined silica	3.22 ± 0.13

d. If A - B means variable conversion between limits
If A + B means conversion study at conversions listed.

TABLE I (continued)

λ(Å)	Slope of DX-H_2 Experiments	Reciprocal Intercept $([HD]/[H_2])_0^{He}$	Slope of DX-He Experiments	$\alpha = \frac{[HX]}{[DX]}$
	0.74 ± 0.06	0.300 ± 0.011	1.1 ± 0.2	0.020
3340	0.69 ± 0.074	0.308 ± 0.011	0.9 ± 0.2	0.018
	1.03 ± 0.05	0.296[e]	1.8 ± 0.2	0.023
3261	1.4 ± 0.3	0.299 ± 0.012	0.8 ± 0.3	0.023
	1.5 ± 0.3	0.187 ± 0.013	0.6 ± 0.3	0.021
3251	1.0 ± 0.2	0.197 ± 0.006[f]	1.0 ± 0.2	0.021
	1.3 ± 0.2	0.135 ± 0.008	1.0 ± 0.7	0.020
3130	1.5 ± 0.2	0.130 ± 0.006	1.3 ± 0.5	0.023
	1.5 ± 0.1	0.150[e]	4.1 ± 0.2	0.021
	1.30 ± 0.10	0.092 ± 0.003	2.4 ± 0.5	0.021
	2.00 ± 0.07	0.100 ± 0.003	3.0 ± 0.5	0.019
3030	1.56 ± 0.05	0.151[e]	3.4 ± 0.5	0.023
	1.44 ± 0.11	0.107 ± 0.003	0.4 ± 0.5	0.023
2891	1.87 ± 0.03	0.072 ± 0.004	2.0 ± 0.8	0.019
2537	1.32 ± 0.05	0.098 ± 0.001	2.0 ± 0.1	0.012
	1.25 ± 0.05	0.074 ± 0.002	1.1 ± 0.5	0.012
2500	0.88 ± 0.08	0.062 ± 0.001	1.5 ± 0.5	0.012
2483	1.45 ± 0.07	0.075 ± 0.0003	2.2 ± 0.6	0.013
2446	1.18 ± 0.04	0.061 ± 0.001	2.9 ± 0.6	0.013
2300	1.09 ± 0.08	0.0402 ± 0.0004	2.1 ± 0.4	0.012
2138	0.91 ± 0.03	0.034 ± 0.0006	2.8 ± 0.2	0.013
1849	0.73 ± 0.02	0.025 ± 0.0004	0.1 ± 1.0	0.013

e. Isotope ratio mass spectrometer measurements approximately corrected for He interference (see text).

f. Ne used as rare gas.

TABLE I (continued)

λ(Å)	Δ	A	A (a = 0.96 ± 0.04)	A (a = 0.93 ± 0.03)
3340	0.053 ± 0.015 0.042 ± 0.015 0.066 ± 0.015	0.025 ± 0.007 0.020 ± 0.007		
3261	0.054 ± 0.022 0.105 ± 0.028	0.025 ± 0.010 0.050 ± 0.013		
3251	0.129 ± 0.025	0.060 ± 0.011		
3130	0.149 ± 0.013 0.135 ± 0.011 0.130 ± 0.010	0.070 ± 0.006 0.064 ± 0.005 0.062 ± 0.005		
3030	0.210 ± 0.01 0.264 ± 0.01 0.174 ± 0.01 0.219 ± 0.01	0.098 ± 0.005 0.120 ± 0.005 0.080 ± 0.005 0.101 ± 0.006		
2891	0.345 ± 0.007	0.154 ± 0.006		
2537	0.325 ± 0.007 0.295 ± 0.006	0.133 ± 0.004[g] 0.123 ± 0.005[g]	0.135 ± 0.004 0.125 ± 0.005	0.137 ± 0.004 0.127 ± 0.005
2500	0.337 ± 0.010	0.140 ± 0.005[g]	0.143 ± 0.005	0.145 ± 0.005
2483	0.401 ± 0.015	0.161 ± 0.006[g]	0.164 ± 0.006	0.167 ± 0.007
2446	0.425 ± 0.006	0.170 ± 0.004[g]	0.173 ± 0.005	0.177 ± 0.005
2300	0.85 ± 0.04	0.29 ± 0.01[g]	0.30 ± 0.01	0.31 ± 0.01
2138	1.32 ± 0.05	0.39 ± 0.01[g]	0.40 ± 0.01	0.41 ± 0.01
1849	3.2 ± 0.1	0.61 ± 0.02[g]	0.63 ± 0.02	0.65 ± 0.02

g. A(a = 0.99 ± 0.03)

Columns 10 through 13 give the reciprocal of the intercepts and the slopes of the $[D_2]/[HD]$ versus $[DX]/[G]$ lines, column 14 the impurity ratio $[HX]/[DX]$ determined as described in Section 6.3, column 15 the Δ value defined by Eq. (8) and finally columns 16 through 18 the values of A calculated as described in Section 6.3.

The results of the DBr plus H_2 experiments at 1849A can be compared with those of Martin and Willard.[15] They correct for the HBr impurity by a slightly different technique than ours (i.e., by subtracting $[HD]/[D_2]$ determined from "pure" DBr photolysis as compared to our DBr plus rare gas mixtures), but this correction is of the order of a few percent only both in their and in our experiments, and therefore a comparison is meaningful. Their corrected $([HD]/[D_2])_0$ is 3.2 ± 0.1 whereas our (i.e., Δ) is $3.2_0 \pm 0.1_3$. This excellent agreement is very gratifying.

Inspection of the columns of Table I giving $([HD]/[D_2])_0^{H_2}$, $([HD]/[D_2])_0^{M}$ and Δ shows that the effect of the HX, even though this impurity amounts to only a few percent of the DX, is a major one in the case of DI. The reason is that in the wavelength region used, the ratio of molar extinction coefficients $\epsilon_{HI}/\epsilon_{DI}$ is greater than unity, tending to favor the absorption of light by the HI. The reason for this is discussed in Section 6.1. If we take 3340Å as an extreme example, even though the [HI]/[DI] ratio may be only 0.03, its product by $\epsilon_{HI}/\epsilon_{DI}$ is 0.36, i.e., about 26.5% of the light absorbed is absorbed by the 3% HI impurity. A second magnifying factor is that at such a long wavelength (i.e., low

initial D atom energy) a relatively small fraction of the D* atoms is expected to react with H_2 to form HD, whereas a large fraction (of the order of unity) of the H* atom formed by the photodissociation of the HI is expected to react with DI after thermalization giving HD. A combination of these two effects is responsible for the relatively large $([HD]/[D_2])_0^M$ values in spite of the relatively small [HX]/[DX] ones, indicating that care must be taken to correct for this effect appropriately. How this is done is described in Section 6.2.

The errors in some of the slopes of the plots of $[D_2]/[HD]$ versus [DX]/[G] are large, as indicated in columns 12 and 14 of Table I. This is particularly true in the DX-He experiments. However, the scatter which leads to the large error in these slopes does not lead to a corresponding large error in the intercepts in which we are interested. For instance, in the case of DBr-He at 1849Å which is the worst case the $[D_2]/[HD]$ ratios were of the order of 40. Hence a large error (~1000%) in the slope led to only a 2.5% error in the intercept. Also as the wavelength decreases, the intercept of the helium experiments contributes less to Δ. Hence a large error in the intercept of the helium experiments can occur without leading to large errors in Δ.

6. DETERMINATION OF INTEGRAL REACTION YIELDS

6.1 Initial Energy of Photochemically Produced Deuterium Atoms

Because of its central role in these experiments, we will discuss the basis for knowledge of the initial laboratory translational energy of the D atoms in some detail. The absorption spectra of the hydrogen halides have been measured by several workers.[22] Measurements of HBr, DBr, HI and DI were repeated in this laboratory[23] and used to obtain the ratios of molar extinction coefficients

$$x = [HX]/[DX] \qquad (21)$$

listed in Table I.

Mulliken[24] has made a theoretical analysis of the lower lying electronic states in the hydrogen halides. He concludes that the only three important transitions from the $^1\Sigma^+$ ground state are to the $^3\Pi_1$, $^1\Pi$, and $^3\Pi_0$ states. He designates these states as N, $^3Q_1$, ^1Q and Q_0, respectively. The potential energy curves that he deduced for DI (or HI) are shown in Figure 6. The curves for DBr should be analogous. The Q_0 state dissociates to give ground state D and excited $^2P_{1/2}$ iodine atoms. At wavelengths longer than 3070Å in DI and 2710Å in DBr, it is energetically possible to form only ground state $^2P_{3/2}$ halogen atoms. At shorter wavelengths both ground state and excited halogen atoms can be formed. The first excited state of the deuterium atom is at 10.2 eV. and cannot be produced with the wavelengths used in these experiments.

Figure 6. Potential energy curves for HI.

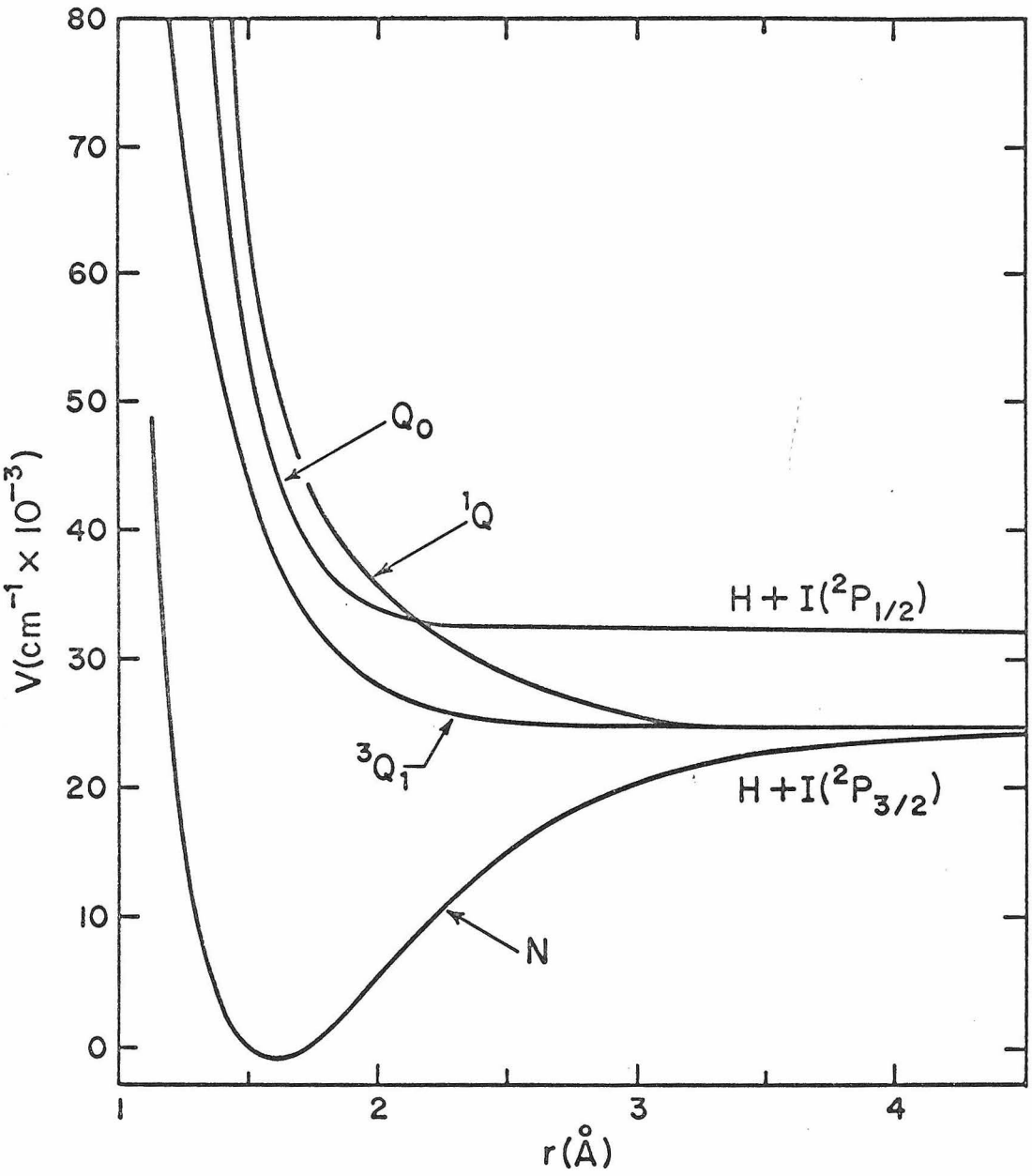
80
70
60
50
40
30
20
10
0
V(cm⁻¹ × 10⁻³)
1
2
3
4
r(Å)
Q0
1Q
3Q1
H + I(2P1/2)
H + I(2P3/2)
N

The initial kinetic energy of the deuterium atom can be calculated if the final electronic states of the atoms formed by the dissociation of DX are known. If only ground state atoms are formed, the energy available for products is

$$E_t = E_\nu - D_0^0 \tag{22}$$

where E_ν is the energy of a photon of frequency ν and D_0^0 is the dissociation energy of the ground vibrational state of DX. The fraction of this energy which goes to the deuterium in the center of mass system of DX is m_X/m_{DX}. When we add the small contributions due to rotation and translation of the DX, the following expression for the average initial laboratory energy $E_1^{(0)}$ of the D atoms is obtained:

$$E_1^{(0)} = \frac{m_X}{m_{DX}}\left(\frac{hc}{\lambda} - D_0^0\right) + \frac{m_X}{m_{DX}}\langle E_{rot}\rangle + \frac{m_D}{m_{DX}}\langle E_{DX}^L\rangle \tag{23}$$

where $\langle E_{DX}^L\rangle$ and $\langle E_{rot}\rangle$ are the average room temperature laboratory translational and rotational energy of the DX molecules. Over the wavelength range of these experiments, the first term in the right hand side of Eq. (23) varies from 0.60 eV to 1.16 eV for DI and 1.06 eV to 2.84 eV for DBr. The second term is 0.020 eV for DI and 0.025 eV for DBr and third one is correspondingly 0.0006 eV and 0.0010 eV.

Since the photolysis light used is not completely monochromatic, and since the translational and rotational energies of the DX have thermal spreads, the D atoms formed with average energy $E_1^{(0)}$ are characterized by a distribution function which can be calculated from the wavelength distribution in the photolysis

light, the wavelength dependence of the DX absorption coefficient and the Boltzmann distribution of its translational and rotational energies. However, a qualitative description of this distribution is contained in the spread $\Delta E_1^{(0)}$ defined as the root mean square of the spreads of the three terms in the right hand side of Eq. (23), each one of these being associated to an interval containing 70% of the corresponding molecules. For DI, the spreads in the second and third terms in the right hand side of Eq. (23) are 0.018 eV and 0.00045 eV, respectively, whereas for DBr they are 0.025 and 0.0007 eV. In column 5 of Table I are given the values of $E_1^{(0)} + \Delta E_1^{(0)}$, these intervals including approximately 70% of the initial D atoms.

At wavelengths shorter than 3070Å in DI and 2710Å in DBr photolyses the formation of electronically excited $^2P_{1/2}$ halogen atoms is allowed energetically and we may expect D atoms of two different initial energies to be formed; one given by Eq. (23) and the second by a similar equation obtained by replacing D_0^0 by $(D_0^0 + E(^2P_{1/2}))$. $E(^2P_{1/2})$ is the electronic excitation energy of the $^2P_{1/2}$ state. For all but two wavelengths used to dissociate DI the $^2P_{1/2}$ state of I is not accessible. However, in the case of DBr it is energetically possible to form $Br(^2P_{1/2})$ at every wavelength used.

Satisfying the energy criterion is a necessary but not sufficient condition for the formation of excited halogen atoms. In principle the oscillator strengths of the various transitions and the details of the dissociation process (for example, the influence

of curve crossing) must be known in order to properly evaluate the extent of the excited halogen atom formation. We summarize here what is known about the oscillator strengths. Little is known about the influence of the curve crossings shown in Fig. 6.

Figure 7 shows plots of the molar extinction coefficient ratios $\epsilon_{DI}/\epsilon_{HI}$ and $\epsilon_{DBr}/\epsilon_{HBr}$ versus wavenumber. There is some structure in the plot of $\epsilon_{DI}/\epsilon_{HI}$ while there is none in the case of the bromides. The structure is attributed to the presence of the $Q_0 \leftarrow N$ transition, in addition to the $^3Q_1 \leftarrow N$ one. The absence of structure for the bromides suggests that a second transition is at most very weak. Mullikan[24] predicts theoretically that the $Q_0 \leftarrow N$ transition will be 15 to 20 times less intense in HBr than in HI, and that consequently the number of excited bromine atoms formed will be small. Donovan and Husain[25] have used flash photolysis of HI and HBr in the ultraviolet and vacuum ultraviolet to determine the fraction of iodine or bromine atoms formed in the excited state. Using a continuous source they observed approximately 20% excited iodine atoms in the flash photolysis of HI at wavelengths longer than 2000Å. They observed no excited bromine atoms in the flash photolysis of HBr when wavelengths greater than 2000Å were used but saw a weak spectrum of excited bromine atoms when the wavelengths extended down to 1850Å. From the above observations and arguments we conclude that only ground state deuterium and bromine atoms are important dissociation products of DBr except at wavelengths shorter than 2000Å where small amounts of excited Br atoms may be formed. In addition,

Figure 7. Molar extinction coefficient ratio as a function of wavenumber.

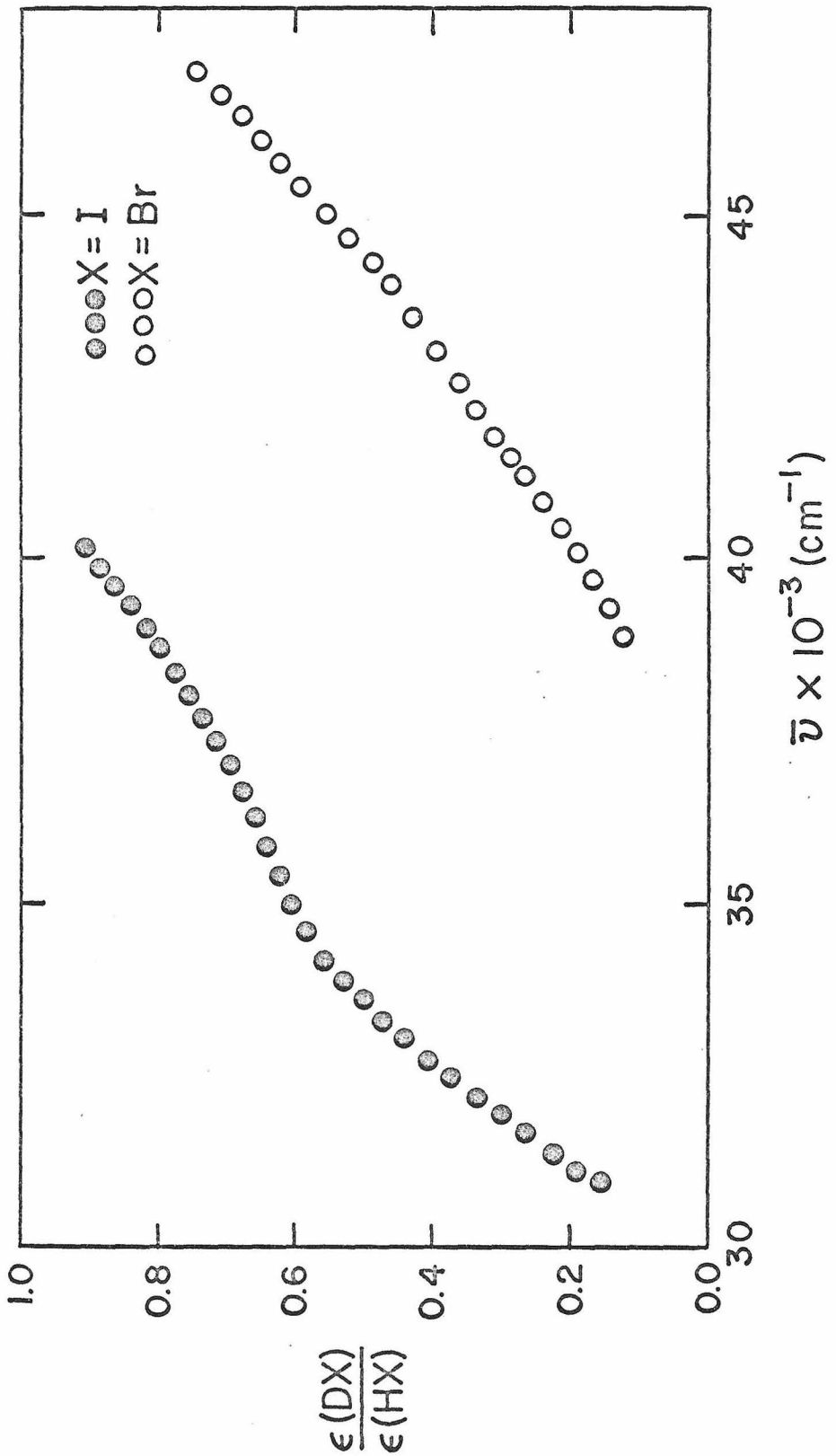
●●●X = I
○○○X = Br
1.0
0.8
0.6
0.4
0.2
0.0
30
35
40
45
$\frac{\epsilon(DX)}{\epsilon(HX)}$
$\bar{\upsilon} \times 10^{-3}$ (cm^{-1})

since for the iodides the structure in Fig. 7 is very small for less than 34600 cm^{-1}, we conclude that between 3070Å and 2890Å the amount of excited iodine atoms from the photodissociation of DI is unimportant.

The $\nu = 0$ state of DX has been assumed as the absorbing state in the E_{lab} calculations. Absorption by the $\nu = 1$ state of DI would furnish D atoms with 0.20 eV more energy than given in Table I. The $\nu = 1$ state will be most significant at long wavelengths (3340A) where it makes the largest relative contribution to the total absorption and to the initial laboratory energy of the resulting D atom. We show below that under all our experimental conditions absorption by this state can be neglected.

The population ratio $N_{\nu=1}/N_{\nu=0}$ is 4×10^{-4} at 20° C for the vibrational energy level spacing of 1630 cm^{-1}. Simple theoretical calculations described below indicate that the ratio of extinction coefficients for these two states at 3340Å is about 12. Hence the ratio of absorption by molecules in the first excited state and in the ground state is approximately 5×10^{-3}. Therefore, at this most unfavorable wavelength, about 99.5% of the D atoms are formed with a lab energy around 0.62 eV and about 0.5% with a lab energy around 0.82 eV. The effect of the latter may be ignored in view of the results of Fig. 8, to be described and discussed in Section 6.5. The calculated extinction coefficient ratio $\epsilon_1/\epsilon_0 = 12$ for the two vibrational states is approximately equal to the ratio of $|\psi|_1^2/|\psi|_0^2$ of the square of the absolute values of the harmonic oscillator wavefunctions evaluated at the

internuclear distances which result in absorption of 3340A light. This ratio is an approximation to a more exact expression which includes also the wavefunctions of the photo-produced repulsive upper state. The approximation is discussed by Coolidge, James and Present[26] and by Herzberg[27] and has been used by Goodeve and Taylor[22a] to analyze the spectra of HI and HBr. Using harmonic oscillator wave functions it leads to

$$\epsilon_1/\epsilon_0 = 2ay_1^2 \exp[a(y_0^2 - y_1^2)] \qquad (24)$$

where $a = \mu\omega_0/\hbar = 96.5\text{Å}^{-2}$ and $y_i = r_i - r_0$ is the displacement of the internuclear distance r_i for state i (i = 0,1) from the equilibrium value, corresponding to absorption of photons of the frequency ν for which ϵ_1/ϵ_0 is being obtained. To calculate $y_i(\nu)$ it is necessary to have expressions for the lower and upper electronic state potential energy functions. For the former we took a quadratic potential corresponding to the observed vibrational spectrum of HI and for the later an exponential function of the form $\nu = D_0^0 + Ee^{-GX}$. The parameters E and G were determined by fitting the calculated DI absorption spectrum to the observed one we observed, yielding 13,400 cm^{-1} and 3.1 Å^{-1}, respectively. For 3340Å this resulted in $y_0 = 0.321\text{Å}$, $y_1 = 0.126\text{Å}$ and $\epsilon_1/\epsilon_0 = 11.7$. A similar calculation using a linear function for the upper state potential gives $\epsilon_1/\epsilon_0 = 17$.[28]

In summary, in the totality of experiments here reported, electronically excited I or Br atoms are either completely absent or present in negligible amounts, and the effect of light absorption

by vibrationally excited DX molecules is also negligible. Equation (23) furnishes the average laboratory energy of the D atoms at formation, given in Table I, column 5 together with its spread.

6.2 Mechanisms and Kinetic Analysis

In Section 3.3 we have already considered a simplified mechanism for the photolysis of DX + H_2 mixtures. In this section we justify the neglect of certain other conceivable elementary steps and extend the kinetic analysis to the DX + HX + H_2 and DX + HX + rare gas systems made necessary by the unavoidable presence of small amounts of HX impurity.

6.2.1 The DX + H_2 System

The kinetic analysis given in Section 3.3 has shown that in the mechanism given by reactions [1] through [9], the thermal reaction [9] can be neglected as long as relations (16) and (17) can be justified and (18) shown to be a sufficient condition for the validity of (14). Let us now show that this is indeed the case.

(a) Validity of Eq. (16). From studies of the thermal decomposition of DI + I_2 mixtures, Sullivan[29] determined the rate constant of the reaction

$$I + D_2 \rightarrow DI + D \qquad [10]$$

to be 1.9×10^3 $cm^3.mole^{-1}.sec^{-1}$. From this value and a simple statistical thermodynamic calculation of the equilibrium constant

between the two sides of this equation, we determine the value of the rate constant of the reverse reaction

$$D + DI \rightarrow D_2 + I \qquad [11]$$

to be 1.4×10^{13} $cm^3.mole^{-1}.sec^{-1}$. Sullivan[30] has also shown that the activation energy for the reaction

$$H + HI \rightarrow H_2 + I \qquad [12]$$

is zero and inferred that the activation energy for reaction [11] should also be zero or very close to zero. Therefore, we conclude that $297^{\circ}K$ k_{11} (which is the same as k_5 for X = I) should be 1.4×10^{13} $cm^3.mole^{-1}.sec^{-1}$ also.

From the data of Ridley, Schulz and LeRoy,[31] the value of k_9 at $297^{\circ}K$ is 2.08×10^8 $cm^3.mole^{-1}.sec^{-1}$, whereas from that of Westenberg and de Haas[32] it is 1.61×10^8 $cm^3.mole^{-1}.sec^{-1}$. The value of the k_5/k_9 ratio at $297^{\circ}K$, for X = I, is therefore of the order of 10^5, as given by Eq. (16).

(b) Validity of Eq. (13). Previous information about the hot atom reaction

$$D^* + DI \rightarrow D_2 + I \qquad [13]$$

is not available. However, we may infer something about its cross section from the lack of temperature dependence of the rate constant of its thermal counterpart, reaction [11]. This implies that the cross section for this reaction has a threshold energy smaller than kT (which at $700^{\circ}K$ is 0.06 eV), and it may even be zero. It also implies that over the energy range sampled by a thermal Boltzmann distribution, it does not depend strongly on energy. If, for example, it were inversely proportional to

relative energy and independent of the internal DI states participating in the reaction, i.e., if

$$v(E) = \sigma_{ij}(E) = C \tag{25}$$

with C a constant independent of E, i and j, Eqs. (1) and (2) would furnish

$$k = C \tag{26}$$

for any distribution functions f including thermal ones. This means that Eq. (26) predicts a thermal rate constant rigorously independent of temperature. If, on the other hand, σ_{ij} were equal to a constant $\sigma^{(11)}$ independent of energy and of the internal states of the participating DI, Eq. (3) would furnish

$$k_{11}(T) = \sigma^{(11)} \left(\frac{8kT}{\pi\mu}\right)^{1/2} \tag{27}$$

which has a $T^{1/2}$ temperature dependence, but which in an Arrhenius plot over a temperature range of a few hundred degrees absolute would furnish an activation energy indistinguisable from zero within experimental accuracy. Since assuming $\sigma^{(13)}$ (E) to be constant will furnish a larger k_{13} than assuming $\sigma^{(13)}(E)v(E)$ to be constant, and since according to Eq. (17) we are interested in establishing an upper limit for k_{13}/k_1, we will use the former assumption and Eq. (27) to estimate k_{13}. Replacement of $\sigma_{ij}(E)$ by the constant $\sigma^{(13)}$ into Eqs. (1) and (2) furnishes

$$k_{13} = \sigma^{(13)} \langle v \rangle \tag{28}$$

where $\langle v \rangle$ is the relative velocity averaged over the distribution function of relative hot atom energies. Since, as discussed in Section 3.2, the distribution function of laboratory D energies should peak at the initial laboratory energy $E_1^{(0)}$, and since

$(m_D/m_{DI}) \ll 1$, we have

$$k_{13} \sim \sigma^{(11)} \left(\frac{2E_1^{(0)}}{m_D} \right)^{1/2} \tag{29}$$

In order to estimate k_1, we may use the $\sigma(E)$ values obtained from the trajectory calculations of the type reported by Karplus, Porter and Sharma.[2] The cross section $\sigma^{(1)}$ for reaction [1], averaged over the distribution of H_2 rotational states at 300°K, shows[33] a threshold relative energy of about 2.29 eV, and values of about 0.1, 1.0 and 1.7 Å^2 at energies of 0.31, 0.6 and 1.2 eV, respectively. From Eqs. (1) and (2) we may write

$$k_1 \sim \sigma^{(1)} \langle v^{(1)} \rangle \tag{30}$$

where $\sigma^{(1)}$ is the rotationally averaged cross section just described and $\langle v^{(1)} \rangle$ is the relative velocity of D with respect to H_2 averaged over the hot atom distribution function of relative energies. As for the D + DI case we write

$$\langle v^{(1)} \rangle \sim \left[\frac{2E_1^{(0)}}{(1/2)m_D} \right]^{1/2} \tag{31}$$

From Eqs. (29) through (31) we get

$$\frac{k_1}{k_{13}} \sim \sqrt{2} \frac{\sigma^{(1)}}{\sigma^{(13)}} \tag{32}$$

Because of the assumed energy independence of $\sigma^{(13)}$ it is equal to $\sigma^{(11)}$. From Eq. (27) and the value of k_{11} (700°K) given above we get $\sigma^{(13)} = 0.5$ Å^2. However, if the cross section of reaction [13] increased from 0.5Å^2 at thermal energies (~0.05 eV) to a few times that value at energies of the order of 1 eV, this would

probably not change the values of the experimental $k_{11}(T)$. The important point, however, is that in view of the absence of long range forces between D and DI, there is no reason why $\sigma^{(13)}$ should ever exceed a few Å^2. On the other hand, as mentioned above, $\sigma^{(1)}$ varies from 0.1 to 1.7 Å^2 as the D atom energy relative to H_2 varies from 0.02 eV above threshold to 1.2 eV, corresponding to laboratory energies of 0.62 to 2.4 eV approximately. Therefore, in this energy range k_1/k_{13} exceeds 0.28 if we use the 0.5 Å^2 for $\sigma^{(13)}$; if we use instead a very conservative upper limit of 5 Å^2, k_1/k_{13} is larger than 0.028 which justifies Eq. (17) for X = I. The important point is that in the energy range of interest the cross section for reactions [1] and [13] should not differ by more than about one or (closer to the threshold of [1]) two orders of magnitude, and therefore k_1 and k_3 can also not differ by more than that. A similar arguments holds for X = Br.

(c) Validity of Eq. (18). The condition (14) of Eq. (13) to represent a straight line with a positive intercept can be written as

$$\frac{[DX]}{[H_2]} >> \frac{1}{A}\frac{k_9}{k_5}\,\frac{1}{1-(k_4/k_1)(k_9/k_5)} \tag{33}$$

This is equivalent to Eq. (18) if

$$\frac{k_4}{k_2}\cdot\frac{k_2}{k_1}\cdot\frac{k_9}{k_5} << 1 \tag{34}$$

That this inequality is indeed satisfied results from the following facts: 1) k_4/k_2 is smaller than unity since D* atoms are thermalized much more efficiently by H_2 molecules than DI ones because

of the better matching of collision partner masses; 2) throughout our experiments A exceeds 0.02 (see Table I) and therefore, as a result of Eq. (8), k_2/k_1 is smaller than 50; 3) from Eq. (16) $k_9/k_5 \sim 10^{-5}$. As a result, the left hand side of Eq. (34) is smaller than 5×10^{-4} and this inequality is satisfied, making (18) valid for X = I. Similar arguments hold for X = Br.

We have now completed the justification of the neglect of reaction [9]. Since halogen atoms are formed in the initial photodissociation of the halides as well as in reactions [3], [5] and [6], consideration must be given to steps involving these atoms:

$$X + H_2 \rightarrow HX + H \qquad [14]$$

$$X + DX \rightarrow X_2 + D \qquad [15]$$

$$X^* + H_2 \rightarrow HX + H \qquad [16]$$

$$X^* + DX \rightarrow X_2 + D \qquad [17]$$

Reaction [14] has an activation energy of 33 Kcal/mole[34] and 19 Kcal/mole[35] for I and Br, respectively. The X + HX counterpart of reaction [15] has an activation energy of 36.5 Kcal/mole[36] and 41.7 Kcal/mole[35] for I and Br, respectively. The fastest of these reactions is therefore [14] for X = Br. We must compare its rate with that of reaction [8]. The lifetime of Br atoms with respect to reaction [14] is $(k_{14}[H_2])^{-1}$, which is about 25 hours for 100 torr of H_2 and $k_{14} = 2 \times 10^{-3}$ liter.mole^{-1}sec^{-1}. This is several orders of magnitude in excess of the lifetime with respect to reaction [8] under our experimental conditions. Indeed, the ratio of the rates of reactions [8] and [14] is about

$(k_8^{1/2}/k_{14})(I_o\epsilon_{DX}/AN)^{1/2}([DX]/[H_2])^{1/2}$ as can be seen by estimating the steady state concentration of X atoms from reactions [0], [5] and [8] and taking M to be $[H_2]$. In the preceding expression, I_o is the intensity of the photolysis light beam, A its cross-sectional area, ϵ_{DX} the molar extinction coefficient of DX and N Avogadro's number. Assuming k_8 to be of the order of 10^{10} liter.mole^{-2}.sec^{-1},[32] that ratio exceeds 10^4 under all of our experimental conditions. Therefore, we are justified in neglecting reactions [14] and [15] in our mechanism. We also calculate that reaction [8] itself occurs partly in the gas phase and partly on wall surfaces. This is in agreement with the experimental finding that in the DI experiments with teflon-lined vessels, if after a few tens of hours of photolysis a cross-sectional cut is made through the cylindrical teflon sleeve, a purple ring, attributed to iodine, appears near the inner surface.

In reactions [16] and [17] the asterisk denoted translational excitation, since as pointed out in Section 6.1 electronically excited X atoms from reaction [0] are unimportant under our experimental conditions. The fraction of the excess of the photon energy E_ν over the DX bond dissociation energy D_0^0 which is given to the X atom (in the DX center of mass system) is m_D/m_{DX}. For a stationary DX and H_2 this leads to a X + H_2 relative energy of $(m_D/m_{DX})^2(E_\nu - D_0^0)$, which ranges from about 1.4×10^{-4} eV to about 1.6×10^{-3} eV in our experiments. These values are small compared with average room temperature thermal energies of 3.9×10^{-2} eV, and we can therefore neglect reaction [16]. For X + DX collisions

the corresponding energies range from 0.46×10^{-2} eV to 3.3×10^{-2} eV, which are not negligible compared to average thermal energies. For the highest energy, the total average relative energy due to the thermal motion of the DX and the translational hotness of the X is then about 7.2×10^{-2} eV. A thermal distribution of relative energies having this average value would correspond to a temperature of about 550°K. The rate coefficient for reaction [17] will therefore not exceed that of reaction [15] taken at 550°K, since it is the high energy tail of the distribution function of relative energies that contributes to the rate coefficients, and the one for reaction [15] at 550°K should be much more important than that for [17] with hot X of equal total average relative energy. Since the activation energy of [15] exceeds 33 Kcal/mole, we conclude that k_{17} is less than 7×10^{10} times k_{15} (300°K). The activation energy of reaction [14] for X = Br is less than that of reaction [15] by at least 14 Kcal/mole and therefore k_{14}^{Br} (300°K) > 1.6×10^{10} k_{15} (300°K). As a result, $k_{17} < k_{14}^{Br}$ (300°K) and since, as shown in the previous paragraph, k_{14}/k_8 is less than 10^{-4} under all our experimental conditions, k_{17} is negligible compared to k_8, and we may therefore also eliminate reaction [17] from our mechanism.

We next consider reactions

$$D + X_2 \rightarrow DX + X \qquad [18]$$

$$H + X_2 \rightarrow HX + X \qquad [19]$$

The ratios of their rates to those of reactions [5] and [6] are respectively

$$\frac{r_{18}}{r_5} = \frac{k_{18}}{k_5}\frac{[X_2]}{[DX]} \tag{35}$$

$$\frac{r_{19}}{r_6} = \frac{k_{19}}{k_6}\frac{[X_2]}{[DX]} \tag{36}$$

The halogen molecules are in general much better scavengers for hydrogen atoms than the corresponding halides. The k_{18}/k_5 and k_9/k_6 are approximately equal to each other and independent of temperature and have values of 22.7[37] for X = Br and 12 to 17[38] for X = I. In order to minimuze the scavenging of H and D atoms by halogen molecules, we kept the fractional conversion c of the DX into products as low as possible. The $[X_2]/[DX]$ ratio at the end of an experiment is c/2 if adsorption of X_2 on walls is ignored, and its average value throughout an experiment is c/4. The r_{18}/r_5 and r_{19}/r_6 ratios for small conversions are then approximately 5.5 c for X = Br and 3.5 c for X = I. As seen from Table I, c had values ranging from 0.2% to 1% for X = Br, and from 0.15% to 2.1% for X = I. Therefore, these ratios ranged from 0.01 to 0.05 for X = Br and from 0.005 to 0.07 for X = I but were about 0.02 for most of the iodide experiments. As seen in Section 5, the values of $([D_2]/[HD])_0^{H2}$ were independent of c within the experimental accuracy, even at the higher values of 2.1%. The reason seems to be that the small amount of X_2 scavenges both H and D atoms, showing therefore a demagnified effect of the $[D_2]/[HD]$ ratio. Therefore, under our experimental conditions, we can neglect reactions [18] and [19] with respect to [5] and [6], respectively, although at somewhat higher conversions than those

we used this might not have been the case.

Finally, as mentioned in Section 3.3, we must consider the effect of translationally hot H atoms. The source of such atoms is reaction [1]. As translationally hot D atoms with a relative translational energy in excess of the potential barrier height of the D + H_2 system react with H_2, the excess energy must appear in internal or translational degrees of freedom of the DH H products. Let us consider, for simplicity, the case in which the H_2 reagent is stationary in the laboratory system of reference. In this case, conservation of linear momentum guarantees than even if the relative energy of the products is zero, the laboratory energy E_H of the H atom produced in the reaction must be equal to one quarter of the relative energy E_{rel} of the reactants. If the relative energy of the products is not zero, E_H depends in addition on the scattering angle and on the difference E between the internal energies of the reagent H_2 and product HD. For the H + H_2 system and the relative energies typical of our experiments, there are theoretical indications[39] that the diatomic reaction product is predominantly back-scattered in the center of mass system. Assuming the same to hold true in the D + H_2 system, a simple kinematic analysis shows that for $E \sim 0$ E_H would be about twice E_{rel} whereas for $E \sim 0.5$ eV (corresponding to HD being formed vibrationally excited), E_H would again be about one quarter of E_{rel}. The final conclusion is that we expect the H atoms produced by reaction [1] to have laboratory energies considerable in excess of thermal.

In addition accurate quantum mechanical calculations for an electronically adiabatic, collinear model of the H H_2 system, using a parameterized energy surface[40] yield the following results. For relative energies of 0.2 to 0.6 eV reaction occurs with no vibrational excitation with probability of about 1.0. For relative energies in the range 0.6 to 0.85 eV reaction still proceeds with no vibrational excitation with a probability of about 0.55, while reaction with vibrational excitation occurs with a probability of about 0.45. Threshold for vibrational excitation occurs at a relative energy of approximately 0.52 eV. However, the probability of excitation does not become significant until a relative energy of approximately 0.6 eV is reached. The 0.1 eV difference is much greater than the energy of thermal H and thus, the contribution of thermal H from the H + H_2 reaction is insignificant in comparison with the non-thermal H from the same reaction. Therefore, if we extrapolate these results to the D + H_2 system, we would expect that the majority of the H product of this reaction would come off with energies in excess of thermal as was indicated by the arguments above.

The H* atom reactions which must be added to the mechanism are:

$$H^* + H_2 \rightarrow H + H_2 \qquad [20]$$

$$H^* + DX \rightarrow HD + X \qquad [21]$$

$$H^* + DX \rightarrow HX + D^* \qquad [22]$$

$$H^* + DX \rightarrow H + DX \qquad [23]$$

Process [20] includes both non-reactive and reactive collisions.

In reaction [22] the atomic product should come out translationally hot for reasons similar to those invoked for reaction [1].

Consideration of reactions [0] - [8] and [20] - [23] yields the following steady state expression for the ratio of rates of production of D_2 to HD:

$$\frac{d[D_2]/dt}{d[HD]/dt} = \frac{[D_2]}{[HD]} = \frac{g}{f}\left(\frac{[DX]}{[H_2]}\right) + \frac{b - \frac{ge}{f}}{f} + \frac{c - \frac{e}{f}\left(b - \frac{ge}{f}\right)}{f\left(\frac{[DX]}{[H_2]}\right) + e} \tag{37}$$

where:

$$c = (1 - a) + k_2/k_1 \tag{38}$$

$$b = \frac{k_2}{k_1}\left(\frac{k_{21} + k_{22} + k_{23}}{k_{20}}\right) + \frac{k_3 + k_4}{k_1} + (1-a)\frac{k_{23}}{k_{20}} \tag{39}$$

$$g = \left(\frac{k_{21} + k_{22} + k_{23}}{k_{20}}\right)\left(\frac{k_3 + k_4}{k_1}\right) \tag{40}$$

$$e = 1 + a \tag{41}$$

$$f = \frac{2k_{21} + k_{22} + k_{23}(1 + a)}{k_{20}} \tag{42}$$

This equation is linear in $[DX]/[H_2]$ if

$$\frac{[DX]}{[H_2]} \ll \frac{e}{f} \tag{43}$$

i.e.

$$\frac{[DX]}{[H_2]} \ll \frac{(1 + a)\,k_{20}}{2k_{21} + k_{22} + k_{23}(1 + a)} \tag{44}$$

In order to show that the above inequality is satisfied under the conditions of our experiments we first note that a has been shown elsewhere[41] to between 0.90 and 1.0. For the purposes of this discussion we will assume that a = 1. Using a = 0.9 makes the

right hand side of Eq. (44) less than when a = 1. With a = 1 the right hand side of Eq. (44) becomes:

$$\frac{(1 + a)k_{20}}{2k_{21} + k_{22} + k_{23}(1 + a)} \simeq \frac{2k_{20}}{2k_{21} + k_{22} + 2k_{23}}$$

$$\equiv \frac{k_{20}}{k_{21} + 1/2\, k_{22} + k_{23}} > \frac{k_{20}}{k_{21} + k_{22} + k_{23}} \qquad (45)$$

We now note that k_{20} is the total rate coefficient (reactive plus nonreactive) of $H^* + H_2$ whereas $(k_{21} + k_{22} + k_{23})$ is the equivalent rate coefficient for $H^* + DX$. It is reasonable to assume that

$$k_{20} >> (k_{21} + k_{22} + k_{23}) \qquad (46)$$

because k_{20} is dominated by its elastic part which is large whereas the elastic part of $(k_{21} + k_{22} + k_{23})$ is small, and although the reactive one is large it should not be as large as the elastic one of k_{20}. Therefore, Eq. (46) coupled with Eq. (45) yields

$$\frac{(1 + a)k_{20}}{2k_{21} + k_{22} + k_{23}(1 + a)} >> 1 \geq \frac{[DX]}{[H_2]} \qquad (47)$$

since $[DX]/[H_2]$ is always less than or equal to 1 in our experiments. Therefore Eq. (44) is satisfied and Eqn. (37) becomes:

$$\frac{[D_2]}{[HD]} = \left(\frac{[D_2]}{[HD]}\right)_0 + \left(\frac{k_3 + k_4}{k_1}\right)\left(\frac{k_{21} + k_{22} + k_{23}}{2k_{21} + k_{22} + (1 + a)k_{23}}\right)\frac{[DX]}{[H_2]} \qquad (48)$$

where

$$\left(\frac{[D_2]}{[HD]}\right)_0 = \frac{(1 - a) + (k_2/k_1)}{(1 + a)} \qquad (49)$$

The intercept of this equation $([D_2]/[HD])_0$ is the same as arrived at in Section 3.3, Eq. (10). However, the slope differs from the one derived in that section by an amount

$$\delta = \left(\frac{k_3 + k_4}{k_1}\right)\left[\frac{k_{21} + k_{22} + k_{23}}{2k_{21} + k_{22} + (1 + a)k_{23}} - \frac{1}{1 + a}\right] \qquad (50)$$

The quantity $(k_{21} + k_{22} + k_{23})/[2k_{21} + k_{22} + (1 + a)k_{23}]$ varies from 1/2 to a maximum of 1 as the fraction $k_{21}/(k_{21} + k_{22} + k_{23})$ varies from 1 to 0. In order to maximize the difference we will use a = 1.0. Therefore, δ ranges from 0 to $0.5[(k_3 + k_4)/k_1]$. We can obtain a crude estimate of $(k_3 + k_4)/k_1$ from the slopes of the $[D_2]/[HD]$ versus $[DX]/[H_2]$ lines by neglecting HX impurity and assuming that Eqs. (9) and (48) are valid descriptions of the slopes. Since the experimental slopes vary from 0.7 to 1.5 (see Table I), we find that $(k_3 + k_4)/k_1$ can be anywhere between 0.7 and 3.0. Hence the change in the slope δ could be as much as 1.5 which is not negligible. This indicates that the H* reactions [20] - [23] should be included in the overall mechanism, even though they don't contribute to the intercept. This inclusion is required if information is to be obtained from the slopes of these lines.

The reactions

$$D^* + X_2 \rightarrow DX + X \qquad [24]$$

$$H^* + X_2 \rightarrow HX + X \qquad [25]$$

must also be considered since they can compete effectively with reactions [3] and [21] for hot deuterium or hydrogen atoms. The ratios of the rates of these reactions to those of [3] and [21] are respectively:

$$\frac{r_{24}}{r_3} = \frac{k_{24}}{k_3}\frac{[X_2]}{[DX]} \qquad (51)$$

$$\frac{r_{25}}{r_{21}} = \frac{k_{25}}{k_{21}} \frac{[X_2]}{[DX]} \qquad (52)$$

The k_{24}/k_3 and k_{25}/k_{21} are approximately equal to each other and independent of temperature and wavelength. They have values of 3.5 for X = Br[42] and 3.8 to 4.4 for X = I.[43] The $[X_2]/[DX]$ ratio at the end of an experiment is c/2 (where c is the fractional conversion) if absorption of X_2 on the walls is ignored, and its average value throughout an experiment is about c/4. The r_{24}/r_3 and r_{25}/r_{21} ratios are then approximately 0.9 c for X = Br and 1.1 c for X = I. As seen from Table I, c had values ranging from 0.2% to 1% for X = Br and from 0.15% to 2.1% for X = I. Therefore, these ratios ranged from 0.0018 to 0.009 for X = Br and from 0.0016 to 0.02 for X = I. Consequently, at the $[X_2]/[DX]$ ratios attained in our experiments reactions [24] and [25] are not expected to contribute significantly to the mechanism. This is verified experimentally as seen in Section 5 since no conversion effect was observed.

6.2.2. The DX + HX + H_2 System

In the presence of HX impurity, the following reactions must be added to the mechanism:

$$HX + h\nu \rightarrow H^* + X \qquad [26]$$

$$D^* + HX \rightarrow DX + H^* \qquad [27]$$

$$D^* + HX \rightarrow HD + X \qquad [28]$$

$$D + HX \rightarrow DX + H \qquad [29]$$

$$D + HX \rightarrow HD + X \qquad [30]$$

These reactions, along with reactions [0] - [8] and [20] - [23] give rise to the following steady state expression for the rate of formation of D_2 divided by the rate of formation of HD:

$$\frac{[D_2]}{[HD]} = \frac{\frac{k_3}{k_2}u + E + E(1-a)\,H(u)}{h + \alpha\frac{k_{27}}{k_2}u + G + \left[\frac{k_{21}}{k_{20}}u + a + G(1-a)\right]H(u)} \tag{53}$$

where

$$H(u) = \frac{\alpha x\left(\frac{k_3 + \alpha k_{27} + \alpha k_{28}}{k_2}\right)u + \alpha\frac{k_{28}}{k_2}u + \alpha x(1 + h) + h}{1 + \left(\frac{k_{21} + k_{22}(1 + \alpha x)}{k_{20}}\right)u} \tag{54}$$

and

$$u = [DX]/[H_2] \tag{55}$$

$$a = \frac{k_6}{k_6 + k_7} \tag{56}$$

$$\alpha = [HX]/[DX] \tag{57}$$

$$E = \frac{1}{1 + \alpha(C + aD)} \tag{58}$$

$$G = \frac{\alpha(C + aD)}{1 + \alpha(C + aD)} \tag{59}$$

$$C = k_{30}/k_5 \tag{60}$$

$$D = k_{29}/k_5 \tag{61}$$

$$x = \epsilon_{HX}/\epsilon_{DX} \tag{62}$$

$$h = k_1/k_2 \tag{63}$$

As discussed further in Section 6.3.2, the quantity a has been determined experimentally and the quantities C and D have been estimated, so that E and G can be evaluated if α is known. If we take an α of 0.020 as observed for the DI-He experiments (see Section 6.3.1 for a discussion of how this is obtained), E and G can be evaluated for DI to be 0.97 ± 0.04 and 0.05 ± 0.01 respectively. The ratios k_{22}/k_{21}, k_{27}/k_{28} and k_{27}/k_3 are estimated in the appendix to be $k_{22}/k_{21} = k_{27}/k_{28} = 1.9 \pm 0.3$ and $k_{28}/k_3 = 0.8 \pm 0.2$. Using these values Eq. (53) can be reduced to an equation containing only k_1/k_2, k_3/k_2 and k_{21}/k_{20}. The ratio k_1/k_2 can be calculated from the values of A listed in Table I. If we further make the assumption that $k_3/k_2 = k_{21}/k_{20}$, the values of $[D_2]/[HD]$ as calculated from Eq. (53) as a function of $[DX]/[H_2]$ and k_3/k_2 can be compared with experimental data. At 3030Å experiments were done with $[DI]/[H_2]$ ratios ranging from 0.3 to 3.2. Hence there is a wide range over which to compare theory and experiment. The best fit to the experimental data occurs for $k_3/k_2 = 0.25$. A plot of the experimental and theoretical values is shown in Fig. 8. This gives a straight line for $[DX]/[H_2]$ values from 0.3 to 1.5 which then curves over at higher $[DX]/[H_2]$ ratios. Hence the above mechanism can explain the experimentally observed straight line behavior of a plot of $[D_2]/[HD]$ versus $[DX]/[H_2]$. A similar fit was performed for DI-H_2 photolyses at 2537Å yielding the best fit for values of k_3/k_2 between 1.1 and 1.4. Hence, some approximate information about the hot atom rate constant ratio k_3/k_2 can be extracted from the plot of

Figure 8. Effect of varying k_3/k_2 on the $[D_2]/[HD]$ ratio.

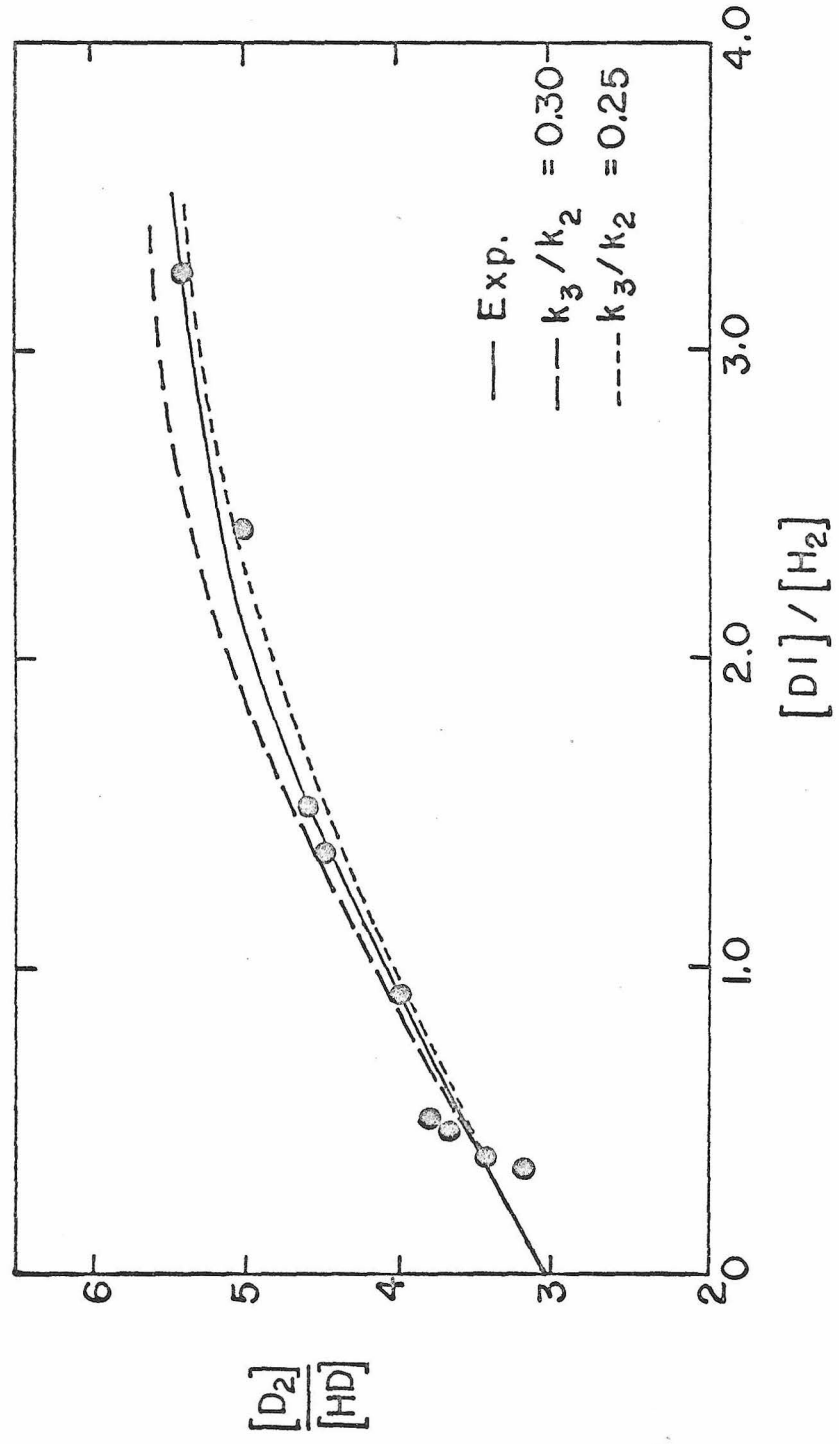
Exp.
k_3/k_2 = 0.30
k_3/k_2 = 0.25
$\frac{[D_2]}{[HD]}$
$[DI]/[H_2]$
2
3
4
5
6
1.0
2.0
3.0
4.0

$[D_2]/[HD]$ versus $[DX]/[H_2]$.

In the limit of zero $[DX]/[H_2]$ the reciprocal of Eq. (53) reduces to:

$$\left(\frac{[HD]}{[D_2]}\right)_0^{H_2} = \alpha(C + aD) + [1 + \alpha(C + aD)]\left[\frac{h + a[\alpha x(h + 1) + h]}{1 + (1-a)[\alpha x(h + 1) + h]}\right] \quad (64)$$

where a, C, D, α, x and h are defined by Eqns. (56) and (60) - (63) respectively. Eq. (64) will be used in Section 6.2.4 to derive an expression for the integral reaction yield A in terms of the above quantities.

6.2.3. The DX + HX + He System

For photolysis of DX with a small amount of HX impurity, the mechanism to be considered includes reactions [0], [3] - [8] and [21] - [28]. In addition, the reactions:

$$D^* + M \rightarrow D + M \qquad [31]$$

$$H^* + M \rightarrow H + M \qquad [32]$$

where M is rare gas must be included. Using this mechanism, the following steady state expression for the rate of formation of D_2 divided by the rate of formation of HD is obtained:

$$\frac{[D_2]}{[HD]} = \frac{\left(\frac{k_4}{k_{29}} + 1\right)E + \frac{k_3}{k_{31}}y + (1-a)E\left(\frac{k_{28}}{k_{32}}y + 1\right)Z(y)}{\alpha\frac{k_{28}}{k_{31}}y + \left(\frac{k_4}{k_{31}} + 1\right)G + \left\{\frac{k_{21}}{k_{32}}y + \left[\frac{k_{23}}{k_{32}}y + 1\right][a + (1-a)G]\right\}Z(y)} \quad (65)$$

where a, E, G and α have been defined by Eqs. (56), (58), (59) and (57), $y = [DX]/[He]$ and

$$Z(y) = \frac{\alpha xy\left(\frac{k_3}{k_{31}} + \alpha\frac{k_{27}}{k_{31}} + \alpha\frac{k_{28}}{k_{31}}\right) + \alpha x + \alpha y\,\frac{k_{27}}{k_{31}}}{\left(\frac{k_{21} + k_{22}}{k_{32}}\right) y + 1 + \alpha x\,\frac{k_{22}}{k_{32}}\,y} \qquad (66)$$

As mentioned in Section 6.2.2, good estimates of a, E, G and α are available. If we again assume that $k_{22}/k_{21} = 1.9$ $k_{26}/k_3 = 0.8$ and likewise that $k_3/k_{31} = k_{21}/k_{32}$, Eq. (65) can be reduced to an equation containing only k_3/k_{31}. This equation can be fit to the experimental slopes. A plot of $[D_2]/[HD]$ versus $[DX]/[He]$ from Eq. (65) shows this plot is approximately linear over the range $0 \leq [DX]/[He] \leq 1.5$ but shows decreasing slope as $[DX]/[He]$ increases. The best fit to the experimental at 3030Å comes for $k_3/k_{29} = 0.4 \pm 0.1$. The large experimental error in the slope (due to fluctuations in α during a series of experiments) precludes more accurate fitting of theory to experiment. If the $[D_2]/[HD]$ ratios were known very accurately (to 6 or 8 significant figures) more information could be extracted from Eq. (65) with the help of computers.

In the limit as $y \to 0$, the reciprocal of Eq. (65) becomes:

$$\left(\frac{[HD]}{[D_2]}\right)_0^{He} = \alpha\left[C + aD + ax\left(\frac{1 + \alpha(C + aD)}{1 + \alpha Bx}\right)\right] \qquad (67)$$

Note that since the mechanism for the helium experiments is the same as for the hydrogen experiments with the exception of reactions [1] and [2], it would seem intuitive that replacing $([HD]/[D_2])_0$ by the difference between the reciprocal of the intercepts of plots of $[D_2]/[HD]$ versus $[DX]/[G]$ for $G = H_2$ and He respectively, should give a good value for the integral

reaction yield corrected for HX impurity. In the next section we give the exact formula for the integral reaction yield and show its dependence on

$$\Delta = \left(\frac{[HD]}{[D_2]}\right)^{H_2} - \left(\frac{[HD]}{[D_2]}\right)^{He} \tag{68}$$

6.2.4. Exact expression for the integral reaction yield

An exact expression for the integral reaction yield can be arrived at by subtracting Eq. (67) from Eq. (64) to obtain an expression for Δ and then solving this expression for A. When this is done the following equation is obtained for the integral reaction yield:

$$A = \frac{\Delta(1 + \alpha Bx)}{1 + a(1+\Delta) + \alpha(1 + \alpha Bx)^{-1}[xa^2 + (C + aD)(a + 1 + \alpha x)]} \tag{69}$$

If we perform an expansion in a power series in α and drop the terms of order α^2 and higher (this is justified since the maximum value of α is 0.03, the coefficient in α is less than 3 and the coefficient in α^2 ranges from 0.07 to 1. At most only a 1% error results from dropping the terms of order α^2 and higher.) the following expression for A is obtained:

$$A = \frac{\Delta}{1 + a(1+\Delta)}\left\{1 + \alpha \frac{[1 + a(1+\Delta)]Bx - [xa^2 - (C + aD)(a + 1)]}{[1 + a(1+\Delta)]}\right\} \tag{70}$$

Note that the quantity preceding the parenthesis is the result obtained in Eq. (12) when pure DX was considered with Δ replacing $([HD]/[D_2])_0^{H_2}$. The quantity in parenthesis varies from 0.92 to 0.99 depending on wavelength which shows the utility of Δ in determining the integral reaction yield.

6.3. Determination of the integral reaction yield

In order to use Eq. (69) to obtain the integral reaction yield, values of α and a must be known. In the following subsection we will describe how these values were determined and will show how the errors in these and other factors affect the calculated value of A.

6.3.1. Determination of HX impurity in DX

We obtained the quantity $\alpha = [HX]/[DX]$, which is a measure of the amount of HX impurity present in the DX, from the reciprocal of the intercepts of the appropriate plots of the helium runs. Eq. (67) gives the explicit steady state solution for $([HD]/[D_2])_0^{He}$. This equation is a quadratic equation in α and can be solved to obtain:

$$\alpha = \frac{-p \pm \sqrt{p^2 + 4aI(C + aD)}}{2a(C + aD)} \tag{71}$$

where

$$p = C + aD - ax - xI(1 - a) \tag{72}$$

and

$$I = \left(\frac{[HD]}{[D_2]}\right)_0^{He} \tag{73}$$

For the DI experiments the resulting α was 0.03 ± 0.004 while for DBr it was 0.013 ± 0.001.

The estimation of the ratios $C = k_9/k_4$ and $D = k_8/k_4$ which are needed to determine both α and A is discussed in another paper.[41] These ratios were estimated from experimental data of Timmons and

Weston[44] and Sullivan[29] using transition state theory. Independent experiments in these laboratories[45] were also used to confirm these estimates. The results of these estimates are, for DI, $C = 1.45 \pm 0.15$ and $D = 1.2 \pm 0.1$ and for DBr, $C = 2.0 \pm 0.2$ and $D = 1.35 \pm 0.14$. It will be shown in Section 6.3.2 that these ratios are not needed with a high degree of accuracy for the final determination of the integral reaction yield.

6.3.2. Determination of the abstraction fraction of H + DX

The abstraction fraction $a = k_6/(k_6 + k_7)$ was determined by additional helium experiments. The basis of the method is variable wavelength photolysis of 3-6% HX in DX mixtures in helium. The extinction coefficient ratio $\epsilon_{HX}/\epsilon_{DX}$ is strongly wavelength dependent,[23] and a plot of the $([HD]/[D_2])_0^{He}$ values versus $\epsilon_{HX}/\epsilon_{DX}$ is linear and allows calculation of a. Further details are contained in a separate paper.[41] The resulting values are $a(DI) = 0.97 \pm 0.05$ and $a(DBr) = 0.99 \pm 0.03$. However, other experiments[45] based on the photolysis of mixtures of DX and HX in the concentration ratio of about 1 to 4 give $a(DI) = 0.95 \pm 0.03$ and $a(DBr) = 0.93 \pm 0.03$. The agreement is well within experimental error in the case of the iodides and barely so in the case of the bromides. Since there is no basis for concluding which measurement is most accurate, we list values of the integral reaction yield for the bromide experiments based on each of the values of a(DBr) and also on their average, i.e., 0.93 ± 0.03, 0.99 ± 0.03 and 0.96 ± 0.04, respectively.

6.3.3. Results for the integral reaction yield.

The integral reaction yield $A(\lambda)$ was calculated from the experimental Δ's listed in Table I using Eq. (69) and values of a and α calculated as described above. The results for $A(\lambda)$ at each wavelength are listed in Table I. A plot of A versus $E_1^{(0)}$ is shown in Fig. 9.

The contributing errors in A were determined by taking its derivatives with respect to the five independent variables Δ, a, α, C and D and multiplying each derivative by the absolute standard error of the variable considered. The total error was taken as the square root of the sum of the squares of these errors. The associated confidence is 70%.

The uncertainty in A is usually dominated by the uncertainty in a single one of the variables on which it depends. For small A, the error in Δ dominates. At about A = 0.1 the errors in Δ and in a contribute equally. For larger A, the error in a(DBr) dominates. Therefore, a more accurate value for a(DBr) would permit us to reduce the uncertainties in $A > 0.1$. In no case is the uncertainty in α, C or D important. At worst an error of 10% in one of them causes an error of 0.04% in A.

In order to check the self-consistency of the values of $A(E_1^{(0)})$ it is important to have the initial energy range spanned by the D atoms from DI overlap the range of initial energies spanned by the D from DBr. The experiment at 2891Å with DI is important in this connection. This was the shortest wavelength used with DI to avoid the formation of electronically excited iodine atoms. The

Figure 9. Plot of $A = k_1/(k_1 + k_2)$ versus laboratory energy. Values of a(DBr) = 0.96 and a(DI) = 0.97 were used in computing A.

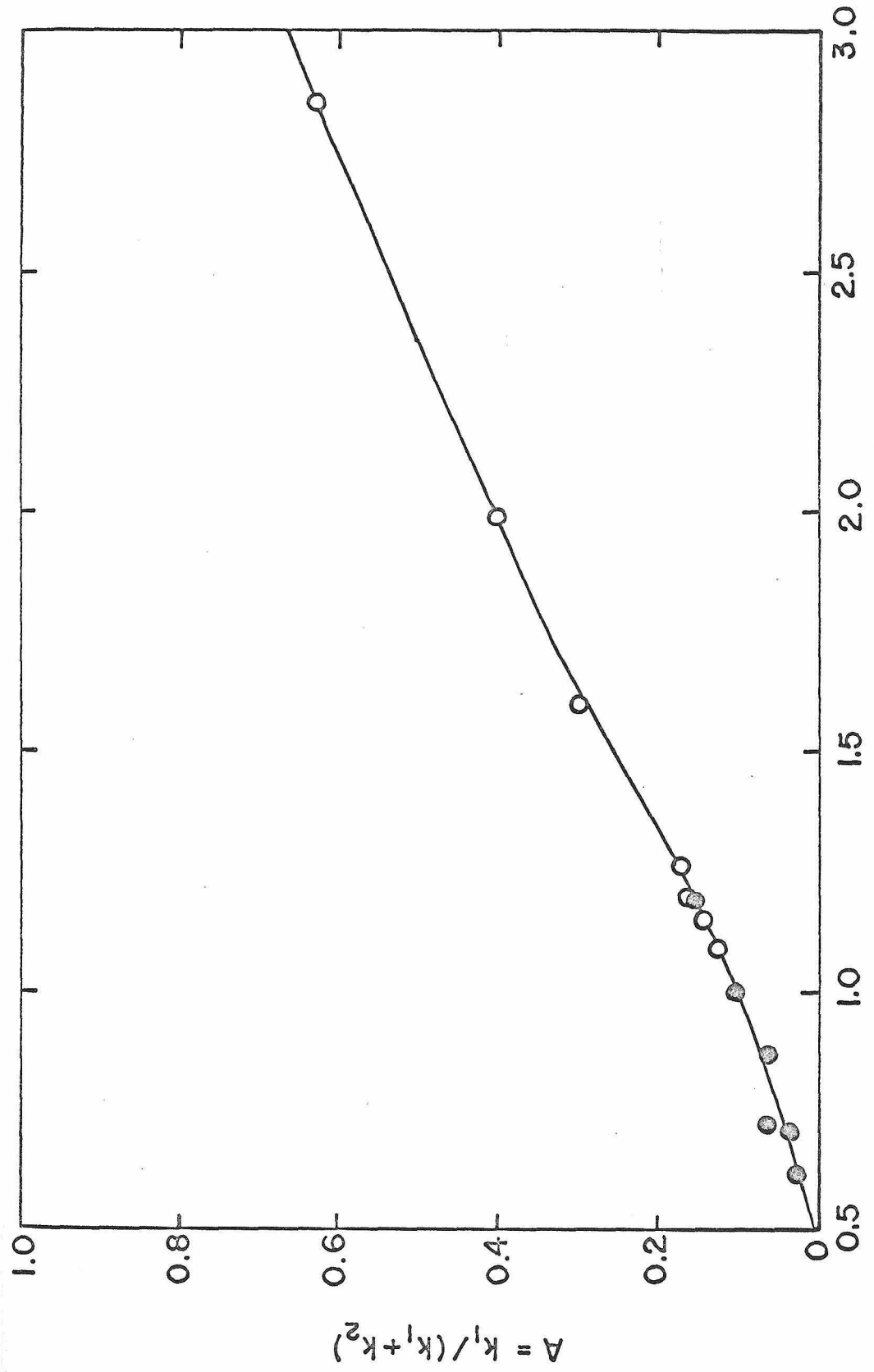
A = k1/(k1+k2)
1.0
0.8
0.6
0.4
0.2
0
0.5
1.0
1.5
2.0
2.5
3.0
E1(0) (eV)

fact that this point lies on a smooth curve going through the DBr points is a manifestation of the consistency of the interpretation.

As stated in Section 6.1, it is energetically possible to form excited bromine atoms in the DBr photolysis, but the best theoretical and experimental evidence available indicates that the fraction of the Br atoms which are excited is negligible. Nevertheless, if such excited Br atoms were present in significant amounts, the experimental A values would correspond to lower energies than those used for Fig. 9. Therefore, the A's reported in this paper for DBr photolyses are lower limits and are correct only if the assumption of no excited bromine atoms is correct. Further experimental evidence is needed to confirm this assumption. Any direct measurements of the fraction of bromine atoms produced in DBr photolysis as a function of wavelength could be used to correct our values of A.

For example, if it were found that at 2138Å 10% of the Br atoms were excited, but that at 2460Å none were, the corrected A value corresponding to no excited Br at 2138Å ($E_1^{(0)}$ = 1.973eV) would be 0.44 compared to the present value of 0.41, indicating that we would have made an error of 7%.

An additional complication which could result as a result of formation of the $^2P_{1/2}$ excited Br atoms is that these atoms could react with either H_2 or DBr, thus complicating the mechanism. However, Donovan and Husain[46] observed no excited bromine atom reactions except quenching and 3-body recombination in their study

of excited bromine atoms. Therefore, excited bromine atoms would not be expected to cause further complications.

7. DISCUSSION

7.1. Shape of $A(E_1^{(0)})$

Our experiments show that the integral reaction yield is a monotonically increasing function of the laboratory energy over the range 0.48 eV to 3.0 eV. It has a value of 0.66 at 2.86 eV dropping to near zero at 0.48 eV.

A region of interest in the A versus $E_1^{(0)}$ plot is near A = 0. The experimental value where A first equals zero occurs approximately at a laboratory energy of 0.48 eV corresponding to a relative $D + H_2$ energy of 0.24 eV for stationary H_2. This is however not the energy at which the reaction cross section goes to zero. The reason for this can be seen by considering the behavior of k_1 near threshold. This behavior is a good approximation to the behavior of the integral reaction yield $A = k_1/(k_1 + k_2)$ since k_1 is changing rapidly near the threshold whereas k_2 (which depends on the non-reactive cross section) is a slowly increasing function of $E_1^{(0)}$ in this region and hence can be considered a constant with respect to k_1.

The rate constant $k_1(E_1^{(0)})$ is related to the reaction cross section by the expression:

$$k_1(E_1^{(0)}) = \int_0^\infty S_R(E)\, v(E)\, f_{E_1^{(0)}}(E)\, dE \qquad (74)$$

where $S_R(E)$ is the reactive cross section, $v(E)$ is the relative velocity of D and H_2 and $f_{E_1^{(0)}}(E)$ is the steady state distribution function of relative energies E for D atoms with an initial laboratory energy $E_1^{(0)}$. In the following, approximations will be made to $S_R(E)$ and $f_{E_1^{(0)}}$ in order to obtain a qualitative description of the behavior of k_1. For this purpose $S_R(E)$ will be assumed to be the simple line of centers hard sphere cross section[1]:

$$S_R(E) = \begin{cases} 0 & \text{for } E \leq E_0 \\ \pi b^2[1 - E_0/E] & \text{for } E > E_0 \end{cases} \tag{75}$$

where b is the distance between the centers of the hard spheres at contact, i.e., the sum of their radii, and E_0 is the minimum energy along the line of centers for reaction to occur and is therefore the threshold energy E_{thrs} for this cross section. As an approximation to $f_{E_1^{(0)}}(E)$ we will consider the relative energy distribution of D with respect to H_2 before any collision takes place for D atoms with a sharply defined laboratory velocity v_D^*. The distribution function $\phi(v_{H_2})$ of the laboratory velocity v_{H_2} of the H_2 molecules will be assumed to be a Boltzmann distribution at temperature T:

$$\phi(v_{H_2})\, d_{v_{H_2}} = \left(\frac{m_2}{2\pi kT}\right)^{3/2} \exp -\left(\frac{m_2 v_{H_2}^2}{2kT}\right) dv_{H_2} \tag{76}$$

where m_2 is the mass of H_2 and k is the Boltzmann factor. The resulting distribution function of relative energies described above is:

$$f_{E_1^{(0)}}(E)\,dE = \frac{1}{\mu v_D^*}\left(\frac{m_2}{2\pi kT}\right)^{1/2}\left\{\exp -\left[\frac{m_2}{2kT}(v_D^* - v)^2\right] - \exp -\left[\frac{m_2}{2kT}(v_D^* + v)^2\right]\right\} dE \qquad (77)$$

where v is the relative velocity, μ is the reduced mass and v_D^* and v are considered to be functions of $E_1^{(0)}$ and E_{rel} according to:

$$E_1^{(0)} = 1/2\; m_D v_D^{*2} \qquad (78)$$

$$E_{rel} = 1/2\; \mu\, v^2 \qquad (79)$$

This distribution function has been shown to have a width of[47]

$$\Delta E = 2\mu(6kT\, E_D/m_D m_2)^{1/2} \qquad (80)$$

Hence its energy spread is 0.22 eV at a relative energy of 0.3 eV which is close to the threshold energy. The above expression for $f_{E_1^{(0)}}(E)$ should be a good approximation for calculations in the region near threshold since it should differ from the real distribution involving multiple collisions mainly in the low energy side, (i.e., for $E < (\mu/m_D)\, E_1^{(0)} = 1/2\, E_1^{(0)}$) leaving the high energy tail, which contributes most to the integral in Eq. (74) for $E_1^{(0)} < 2E_{thr}$ basically unchanged. $k_1(E_1^{(0)})$ was evaluated from Eq. (74) using Eqs. (75) and (77). The integrals involving $\exp[-(m_2/2kT)\cdot(v_D^* + v)^2]$ contribute negligibly to Eq. (74) and may be dropped (Their contribution is less than 10^{-15} of the one resulting from the $\exp[-(m_2/2kT)\cdot(v_D^* - v)^2]$ term). The resulting expression is:

$$k_1(E_1^{(0)}) = \frac{b^2}{v_D^*}\left\{\frac{1}{2\sqrt{\pi}s^{1/2}}(v_D^* + v_0)\exp[-s(v_0 - v_D^*)^2]\right.$$

$$\left.\frac{1}{2}\left(\frac{1}{2s} + v_D^{*2} - v_0^2\right)\operatorname{erfc}[s^{1/2}(v_0 - v_D^*)]\right\} \qquad (81)$$

where $s = m_2/2kT$ and $v_0^2 = 2E_0/\mu$. Erfc is the complementary error function.[48] Since the above equation increases linearly with v_D^* at large v_D^*, a more suitable function is k_1/v_D^* which approaches asymptotically to the maximum value πb^2. The expression for $k_1(E_1^{(0)})$ was evaluated at 300°K and $E_0 = 0.3$ eV. The results of this calculation are shown in Fig. 10 as well as a plot of the line of centers cross section used in the calculation. Note that the two curves nearly coincide except at low energies where k_1/v_D^* goes asymptotically to zero and $S_R(E)$ has a sharp cutoff. This low velocity tail in k_1/v_D^* comes from the Boltzmann spread of the velocities of the H_2 target; and makes it difficult to estimate the threshold velocity v_0 and corresponding threshold energy E_0 of $S_R(E)$. If we define a phenomenological threshold as the energy at which (k_1/v_D^*) becomes a certain fraction ζ of its maximum value, then for ζ respectively equal to 0.01, 0.03 and 0.10 the corresponding phenomenological threshold energies are equal to 0.17 eV, 0.21 eV and 0.294 eV respectively compared to the correct assumed value of 0.30 eV. Therefore, we may expect significant errors to occur if we try to estimate the reaction cross section threshold energy from the energy at which A vanishes.

This calculation points out the need for a more rigorous analysis than the one carried out above in order to obtain the

Figure 10. Plot of calculated k_1/v_D^* and the line of centers cross section used in its calculation versus relative energy.

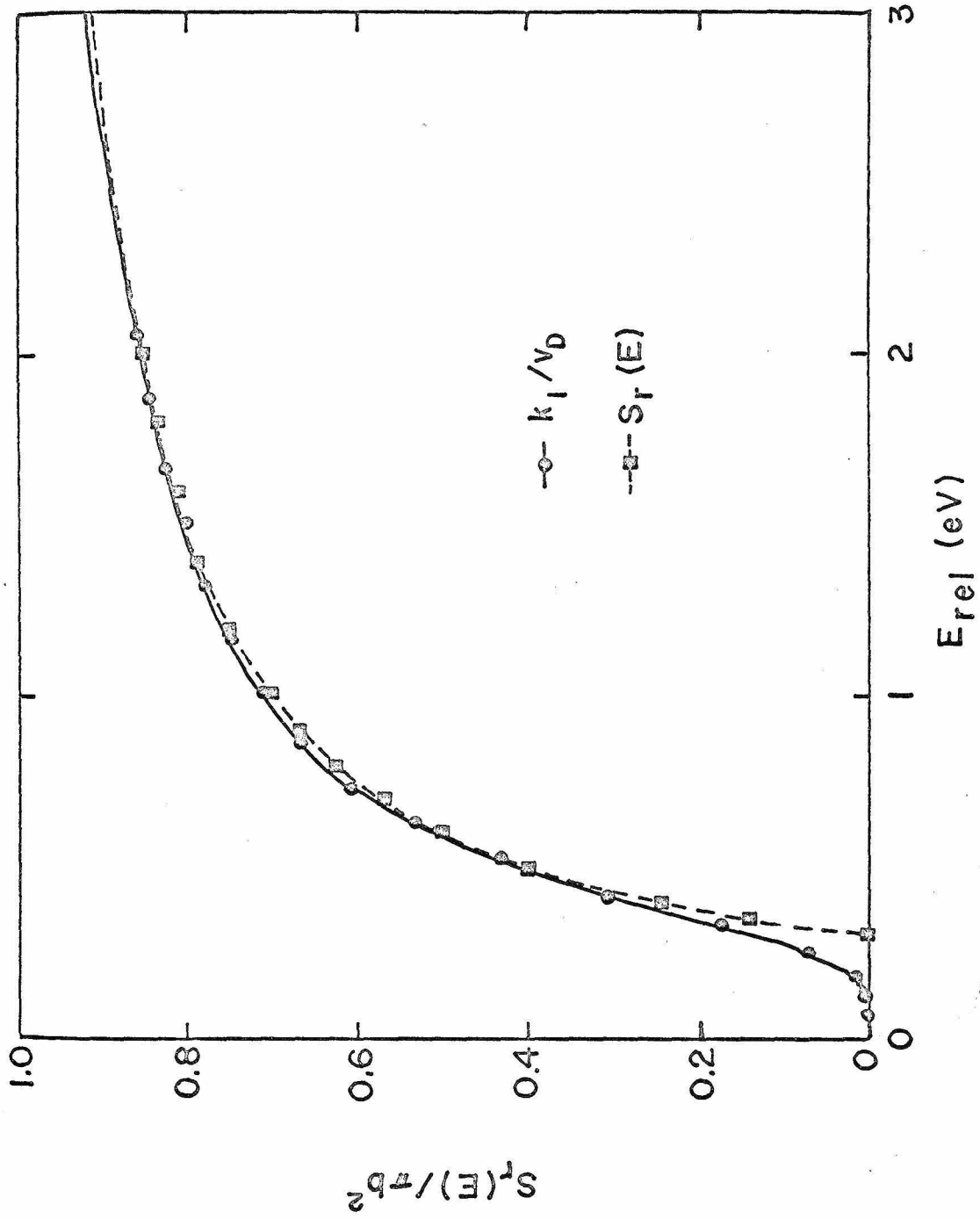
$S_r(E)/\pi b^2$
1.0
0.8
0.6
0.4
0.2
0
0
1
2
3
E_{rel} (eV)
k_1/v_D
$S_r(E)$

threshold energy of the cross section for the reaction of D with H_2. Calculations are also required to extract the reaction cross section from the experimental data. An outline of the method used to obtain cross sections and threshold energies from experimental data is given in the next section. A more detailed description and the associated results will be given in a forthcoming paper.

7.2. Determination of reaction cross sections from integral reaction yields

7.2.1. Boltzmann Equation

The behavior of the DX-H_2 photolysis system can be described by a steady-state Boltzmann equation. The details of this derivation are given elsewhere[47] and the results will be summarized here. Let R_0 be the rate of initial D atom production due to photolysis and $\phi_{v_D^*}(v_D)$, the normalized initial distribution function of D atom laboratory velocities. This is a narrow function centered at v_D^*. Let $G_{v_D^*}(v_D)\, dv_D$ be the concentration of D atoms under steady state photolysis conditions in the laboratory velocity range v_D to $v_D + dv_D$. It satisfies the following steady-state Boltzmann equation:

$$R_0 \phi_{v_D^*}(v_D) - K_t(v_D) G_{v_D^*}(v_D) + \int_{v_D'} H(v_D^*, v_D)\, G_{v_D^*}(v_D')\, dv_D' = 0 \quad (82)$$

In the above $K_t(v_D)$ is defined as:

$$K_t = K^{H_2} + K^{DX} \quad (83)$$

$$K^{H_2} = K_R^{H_2} + K_{NR}^{H_2} \tag{84}$$

$$K^{DX} = K_R^{DX} + K_{NR}^{DX} \tag{85}$$

$$K_R^{H_2} = [H_2] \int \phi_T^{H_2}(v_D, v)\, v\, S_R^{H_2}(v)\, dv \tag{86}$$

$$S_R^{H_2} = \sum_i g_i^{H_2} S_R^{H_2,i} \tag{87}$$

$$K_{NR}^{H_2} = [H_2] \int \phi_T^{H_2}(v_D, v)\, v\, S_{NR}^{H_2}(v)\, dv \tag{88}$$

$$S_{NR}^{H_2} = \sum_i g_i^{H_2} S_{NR}^{H_2,i} \tag{89}$$

$$K_R^{DX} = [DX] \int \phi_T^{DX}(v_D, v')\, v'\, S_R^{DX}(v')\, dv' \tag{90}$$

$$S_R^{DX} = \sum_i g_i^{DX} S_R^{DX,i} \tag{91}$$

$$K_{NR}^{DX} = [DX] \int \phi_T^{DX}(v_D, v')\, v'\, S_{NR}^{DX}(v')\, dv' \tag{92}$$

$$S_{NR}^{DX} = \sum_i g_i^{DX} S_{NR}^{DX,i} \tag{93}$$

where v is the relative velocity of D with respect to H_2 and v' is the relative velocity of D with respect to DX. $\phi_T^{H_2}(v_D, v)$ is the distribution function of D + H_2 relative velocities for D atoms with a laboratory velocity v_D and H_2 molecules with a Boltzmann distribution of laboratory velocities and $\phi_T^{DX}(v_D, v')$ is a similar distribution for D + DX. $S_R^{H_2}(v)$ is the reactive cross section for D + H_2 averaged over the internal states of H_2 at temperature T and $S_{NR}^{H_2}(v)$ is the corresponding total non-reactive cross section averaged over these internal states. S_R^{DX} and S_{NR}^{DX} are similarly the reactive and non-reactive cross sections for D + DX and $g_i^{H_2}$ and g_i^{DX} are mole fractions of an initial internal state i of

either H_2 or DX. It is assumed that thermalization of D by DX is negligible compared to thermalization by H_2 and hence K_{NR}^{DX} is set equal to zero when applying Eq. (82). This is valid since the masses of D and H_2 are equal and hence exchange energy very efficiently compared to D and DX where the difference in mass is greater. The quantity $H(v_D', v_D)$ is defined as follows:

$$H(v_D', v_D) = H^{H_2}(v_D', v_D) + H^{DX}(v_D', v_D) = \frac{[H_2]}{2} \int_{v_{H_2}', \chi, \eta} \phi_T^{H_2}(v_{H_2}') \sum_i g_i$$

$$\cdot \sum_j v_{if}' \sigma_{i \to f}^{H_2}(v_{if}', \chi, \eta) \left| \frac{\partial \cos \gamma_{if}}{\partial v_D} \right| \sin\chi \, dv_{H_2}' \, d\chi \, d\eta$$

$$+ \frac{[DX]}{2} \int_{v_{DX}', \chi, \eta} \phi_T^{DX}(v_{DX}') \sum_i g_i \sum_j v_{if}' \sigma_{i \to f}^{DX}(v_{if}', \chi, \eta)$$

$$\cdot \left| \frac{\partial \cos \gamma_{if}}{\partial v_D} \right| \sin\chi \, dv_{DX}' \, d\chi \, d\eta \qquad (94)$$

In the above v_{H_2}' and v_{DX}' are the laboratory velocities of H_2 and DX respectively before collision, v_{if}' is the magnitude of the relative velocity vector of D with respect to either H_2 or DX, χ and η are scattering angles which define the directions of these vectors after collision and γ_{if} is the angle between between v_D' and v_{H_2}' or v_{DX}' before collision. The quantity $\sigma_{i \to f}^{H_2}(v_{if}', \chi, \eta)$ is the differential non-reactive cross section for the collision of a D atom with a H_2 molecule in internal state i to give a D atom and a H_2 molecule in internal state f. $\sigma_{i \to f}^{DX}$ is a similarly defined quantity defined for D + DX. $\phi_T^{H_2}(v_{H_2}')$ is the Maxwell Boltzmann distribution function of H_2 velocities in laboratory coordinates while $\phi_T^{DX}(v_{DX}')$ is a similar distribution for DX velocities. g_i

is the distribution function for initial internal states of H_2 or DX. If inelastic collsions are unimportant, the summation over f in Eq. (94) may be dropped. Again, since thermalization of D by DX is negligible compared to thermalization by H_2, $H^{DX}(v_D', v_D)$ is set equal to zero.

The physical interpretation of Eq. (82) is very simple despite the complexities of some of its terms. The first term represents the rate of formation of D atoms in the velocity range $v_D + dv_D$ directly from the photolysis source. The second represents their rate of removal from the same velocity range by all collisions with H_2 and reactive collisions with DX. Finally, the third term represents the rate of production of D atoms in the velocity range $v_D + dv_D$ due to all non-reactive collisions of D atoms at all other velocities with H_2 and DX. The net rate of production of D atoms in any given velocity range must vanish under steady state conditions and hence the sum of terms in Eq. (82) is set equal to zero.

7.2.2. Relation between $A(v_D^*)$ and the reaction cross section

The integral reaction yield $A(v_D^*)$ is related to the above quantities by the expression:

$$A(v_D^*) = \frac{1}{R_0} \int K_R^{H_2}(v_D)\, G_{v_D^*}(v_D)\, dv_D \qquad (95)$$

where $K_R^{H_2}(v_D)$ is defined by Eq. (86). The Boltzmann equation given by Eq. (82) can be reexpressed in terms of $A(v_D^*)$ as[49]

$$K_R^{H_2}(v_D) - K_t(v_D)\, A(v_D) + \int H(v_D, v_D')\, A(v_D')\, dv_D' \qquad (96)$$

In the limit of dilute [DX] which corresponds to the intercept of a plot of $[D_2]/[HD]$ versus $[DX]/[H_2]$ we have

$$K_t(v_D) = K_R^{H_2} + K_{NR}^{H_2} \qquad (97)$$

Using this relation in Eq. (96) and rearranging, the following expression is obtained for $K_R^{H_2}$:

$$K_R^{H_2}(v_D) = \frac{1}{1 - A(v_D)} \left[K_{NR}^{H_2} A(v_D) - \int H^{H_2}(v_D, v_D')\, A(v_D')\, dv_D' \right] \qquad (98)$$

Therefore, if the differential non-reactive scattering cross sections $\sigma_{i\,f}^{H_2}(v_{if}', \chi, \eta)$ are known, they can be used to determine $K_{NR}^{H_2}(v_D)$. To a first approximation we may in H^{H_2} use the term coming from the elastic process only, since it usually predominates over the inelastic ones. In this case only $\sigma_{el}(v', \chi, \eta)$ is needed to calculate $H^{H_2}(v_D, v_D')$.

Once $K_R^{H_2}(v_D)$ is known, Eq. (86) is an integral equation in which the total internal-state-averaged reaction cross section $S_R^{H_2}(v)$ is the only unknown. One way to solve it is to transform it into an equivalent partial differential equation with the help of Fourier transforms. The result[49] is that if $u(v,v')$ is the solution of the differential equation

$$\frac{\partial u}{\partial T'} = - \frac{k}{2m_{H_2}} \frac{\partial^2 u}{\partial v^2} \qquad (99)$$

subject to the initial condition

$$u(v,0) = \frac{v}{[H_2]} K_R^{H_2}(v) \qquad (100)$$

then $S_R^{H_2}(v)$ is given by

$$S_R^{H_2}(v) = \frac{u(v,T)}{v^2} \qquad (101)$$

where T is the H_2 temperature at which the experiment was conducted and u(v,T) is obtained by solving Eq. (99) numerically subject to Eq. (100).

Therefore, a knowledge of $\sigma_{el}^{H_2}(v',\chi,\eta)$ and the experimentally known $A(v_D)$ furnishes the $S_R^{H_2}(v)$. $\sigma_{el}^{H_2}(v',\chi,\eta)$ has been calculated by Karplus and Tang[50] in a central field approximation. Hence all pertinent information is available to calculate $S_R^{H_2}(v)$ from the present experiments. The results of this calculation will appear in the near future.

7.2.3. Consequences of the simplified Boltzmann equation.

In sections 3.2 and 3.3 it was stated that the Boltzmann equation leads to a steady-state distribution function of D atom energies which is bi-modal, having a "hot" atom peak, as indicated in Fig. 1, and that the variation of $[D_2]/[HD]$ with $[DX]/[H_2]$ was as depicted in Fig. 2. In order to validate these statements let us consider a simplified model. Assume that the H_2 and DX are stationary (i.e., that the experiment is conducted at $T = 0^oK$ but that the system is still gaseous), that the energy dependence of the cross sections of reactions [1] and [3] are independent of the molecular reagents and that the contribution of non-reactive collisions of D* with DI to thermalization of the D* is negligible compared to the contribution of the D* + H_2 collisions and that

the latter are dominated by elastic collisions having a differential cross section $\sigma_{el}^{H_2}$ independent of internal state and orientation of the H_2. Under these conditions, Eq. (82) becomes, using the laboratory energy E_1 of the D atoms instead of their velocities as the independent variable:

$$R_0\phi_{E_1}^{(0)}(E_1) - K_t(E_1)G_{E_1}^{(0)}(E_1) + \int_{E_1}^{\infty} H(E_1',E_1)\, G_{E_1}^{(0)}(E_1')\, dE_1' = 0 \quad (102)$$

where the K's and H aquire the simplified forms

$$K_t(E_1) = K_{NR}^{H_2}(E_1) + K_R^{H_2}(E_1) + K_R^{DX}(E_1) \quad (103)$$

$$K_{NR}^{H_2}(E_1) = [H_2]\, v_D\, S_{NR}^{H_2}(v_D) \quad (104)$$

$$K_R^{H_2}(E_1) = [H_2]\, v_D\, S_R^{H_2}(v_D) \quad (105)$$

$$K_R^{DX}(E_1) = [DX]\, v_D\, S_R^{DX}(v_D) \quad (106)$$

$$H(E_1',E_1) = [H_2]\, 2\, v_D'\, \sigma_{NR}^{H_2}(E_1',E_1) \quad (107)$$

In these expressions, the laboratory velocity v_D becomes equal to the velocity v relative to either H_2 or DX and is related to the laboratory energy E_1 by

$$v_D = [2E_1/m_D]^{1/2} \quad (108)$$

In addition, the S are the internal-state-independent total cross sections, and $\sigma_{NR}^{H_2}(E_1',E_1)$ (where E_1 is the D laboratory energy before collision and E_1' is that after collision) is related to the differential elastic cross section $\sigma_{el}^{H_2}(v',\chi)$ by

$$\sigma_{NR}^{H_2}(E_1', E_1) = \frac{2}{E_1'}\sigma_{el}^{H_2}(v', \chi) \tag{109}$$

where v' is the relative velocity before collision and χ is the scattering angle. The total non-reactive cross section is related to the differential one by

$$S_{NR}^{H_2}(v_D) = 2\pi\int_0^{E_1} \sigma_{NR}^{H_2}(E_1, E_1')\, dE_1' \tag{110}$$

Model calculations with particular but reasonably realistic choices of the cross sections $S_R^{H_2}(v)$, $S_R^{DX}(v)$ and $\sigma_{NR}^{H_2}(v', \chi)$ have been performed and are described elsewhere.[49] The results are indeed that $G_{E_1}(0)(E_1)$ and therefore the distribution function $f_{E_1}(0)(E)$ are bimodal and that the behavior of $[D_2]/[HD]$ versus $[DI]/[H_2]$ is the one depicted in Fig. 2.

APPENDIX

Photolysis of DI Containing a Small Amount of HI Impurity

In sections 6.2.2 and 6.2.3 we needed crude estimates of k_{22}/k_{21}, k_{27}/k_{28} and k_{28}/k_3 in order to evaluate the slopes of plots of $[D_2]/[HD]$ versus $[DX]/[H_2]$ and $[D_2]/[HD]$ versus $[DX]/[He]$ to test whether the mechanism given in that section could be fit to the experimental data.

To obtain such estimates, we performed a series of experiments in which "pure" DI (except for the small amount of HI impurity) was photolyzed. The resulting $[D_2]/[HD]$ ratio depended on the previous history of the reaction vessel, presumably due to various states of deuteration of its surface and the consequent variation of HI impurity. However, the ratio of $[HD]/[D_2]$ at two wavelengths obtained in consecutive experiments was reproducible.

In a series of pairs of consecutive experiments at 3030Å and 2537Å, in the same reaction vessel, the lowest $[HD]/[D_2]$ obtained were 0.0397 and 0.0337 respectively and correspond therefore to the smallest α. In view of the results in Table I we will assume this α to be 0.020. From these results, we may estimate the rate constant ratios mentioned above as follows.

The mechanism characterizing these experiments is the same as for the DX-HX-He system excluding reactions [31] and [32]. The corresponding steady state expression for the ratio of the rate of formation of [HD] to that of $[D_2]$ is

$$\frac{[HD]}{[D_2]} = \alpha\left\{\frac{k_{28}}{k_{23}} + \frac{x\left[1 + \alpha\frac{k_{28}}{k_3}\left(1+\frac{k_{27}}{k_{28}}\right)\right] + \frac{k_{27}}{k_3}}{1 + \frac{k_{22}}{k_{21}}(1 + \alpha x)}\right\} \qquad (111)$$

In this expression, not only x but also the ratios of rate coefficients should be functions of wavelength, the latter via the initial energy of the D and H atoms. However, since k_{28}/k_3 represents the isotope effect of the abstraction reaction, it is reasonable to assume that it is approximatly energy independent. The k_{22}/k_{21} ratio represents the ratio of exchange to abstraction and we should allow it to be energy dependent. However, it is reasonable to make it equal to k_{27}/k_{28} at the energies used, since this represents an isotope effect on the exchange to abstraction ratio.

Calculations of the energy dependence of the ratio of the probabilities of exchange to abstraction in single H + DI collisions were performed using the statistical theory.[51] They show that this ratio increases by 24% as the relative collision energy increases from 0.570 eV to 1.00 eV. In our experiments, the initial energy of H with respect to DX is 0.500 eV at 3030Å and 0.89 eV. at 2537Å (for DI dissociating into ground state iodine atoms). The k_{22}/k_{21} ratio is not equal to the monoenergetic probability ratio since they involve averages over the distribution functions characteristic of our experiments. Therefore, on the basis of these statistical theory results, we would expect this rate constant ratio to change by less than 20%. Let θ be

the fractional increase just mentioned in k_{22}/k_{21} in going from 3030Å to 2537Å:

$$\theta = \frac{(k_{22}/k_{21})_{2537Å} - (k_{22}/k_{21})_{3030Å}}{(k_{22}/k_{21})_{3030Å}} \qquad (112)$$

If we apply Eq. (111) at these 2 wavelengths, use the assumptions above and consider θ to be known, we get a system of 2 equations in the two unknowns k_{28}/k_3 and $(k_{22}/k_{21})_{3030Å}$, since the extinction coefficient ratio x is known from independent experiments described elsewhere.[23] Solving them furnishes the results given in Table II.

The reproducibility of the quantities $([HD]/[D_2])_{\lambda_1}/([HD]/[D_2])_{\lambda_2}$ for pairs of consecutive experiments mentioned in the beginning of this appendix can be understood by assuming α to be unchanged in these experiments. Using (111) at wavelengths λ_1 and λ_2 and dividing the resulting expressions eliminates the main dependence on α. The remaining dependence is negligible as can be verified by direct substitution into this expression of the value of α and of the rate coefficients of Table II.

Table II shows also that the effect of θ on the rate coefficient ratios over the energy range of interest is not excessively pronounced. Although they represent crude estimates, these ratios should be adequate for the purposes for which they were used in Sections 6.2.2 and 6.2.3.

TABLE II

Estimates of k_{28}/k_3, k_{22}/k_{21} and k_{27}/k_{28}

	$\theta = 0.0$		$\theta = 0.24$	
λ(Å)	3030	2537	3030	2537
k_{28}/k_3	0.82	0.82	0.80	0.80
k_{22}/k_{21}	1.9	2.3	2.3	2.8
k_{28}/k_{27}	1.9	2.3	2.3	2.8

REFERENCES

1. M. A. Eliason and J. O. Hirschfelder, J. Chem. Phys., 30, 1426 (1959).
2. M. Karplus, R. N. Porter and R. D. Sharma, J. Chem. Phys., 43, 3259 (1965).
3. J. M. Blatt and V. F. Weisskopf, Phil. Mag., 44, 356 (1953).
4. For reviews see: (a) D. Herschbach, Adv. Chem. Phys., 10, 319, (1966); (b) H. Pauly and J. P. Toennies, Methods of Experimental Physics, 7, 227 (1968).
5. M. Karplus, personal communication to A. Kuppermann.
6. J. M. White and A. Kuppermann, J. Chem. Phys., 44, 4352 (1966).
7. A. Kuppermann, Nobel Symposium 5, Stig Claesson, ed. (Interscience Publishers, New York, 1967) pp. 131-140.
8. L. Melton and A. Kuppermann, to be published.
9. J. B. Anderson, R. P. Andres and J. B. Fenn, Adv. Chem. Phys., 10, 275 (1966).
10. S. Datz and E. H. Taylor, J. Chem. Phys., 39, 1896 (1963).
11. W. L. Fite and R. T. Brackmann, (a) Atomic Collision Processes, M. R. C. McDowell, ed. (North-Holland Publishing Company, Amsterdam, 1964) pp. 955-963; (b) J. Chem. Phys., 42, 4057 (1965).
12. J. Geddes, H. F. Krause and W. L. Fite, J. Chem. Phys., 52, 3296 (1970).
13. (a) R. A. Ogg, Jr. and R. R. Williams, Jr., J. Chem. Phys., 13, 586 (1945); (b) R. R. Williams, Jr. and R. A. Ogg, Jr., J. Chem. Phys., 15, 691 (1947).

14. (a) H. H. Schwarz, R. R. Williams, Jr. and W. H. Hamill, J. Am. Chem. Soc., 74, 6007 (1952); (b) R. J. Carter, W. H. Hamill and R. R. Williams, Jr., J. Am. Chem. Soc., 77, 6457 (1955).

15. R. M. Martin and J. E. Willard, J. Chem. Phys., 40, 3007 (1964).

16. (a) C. C. Chou and F. S. Rowland, J. Am. Chem. Soc., 88, 1612 (1966); (b) C. C. Chou and F. S. Rowland, J. Chem. Phys., 46, 812 (1967); (c) C. C. Chou and F. S. Rowland, J. Chem. Phys. 50, 2763 (1969).

17. D. R. Davis and J. A. Betts, forthcoming. (The main details that will appear are in Appendix A of this thesis).

18. Instrument in geochemistry department of California Institue of Technology and made available by Professor Samuel Epstein of that department.

19. A. O. Nier, Rev. Sci. Instr., 18, 398 (1947).

20. J. M. White, Ph.D. Thesis, University of Illinois, Urbana, Illinois (1966), p. 80.

21. natural abundance HD supplied by Dan Quinn, High Energy Physics Laboratory, Stanford University.

22. (a) C. F. Goodeve and A. W. C. Taylor, Proc. Roy. Soc. (London) 154A, 181 (1936); (b) B. J. Huebert and R. M. Martin, J. Phys. Chem., 72, 3046 (1968); (c) J. P. Bates, J. O. Halford and L. C. Anderson, J. Chem. Phys., 3, 415 (1935); (d) J. Romand, Ann. de Phys., 4, 527 (1948); (e) A. A. Gordus, D. A. Caughey, and T. R. Wilcox, personal communication to J. M. White and A. Kuppermann.

23. J. A. Betts, D. R. Davis, J. M. White and A. Kuppermann, to be published.

24. (a) R. S. Mulliken, J. Chem. Phys., 8, 382 (1940); (b) R. S. Mulliken, Phys. Rev., 51, 310 (1937).

25. (a) R. J. Donovan and D. Husain, Trans. Faraday Soc., 62, 1050 (1966); (b) R. J. Donovan and D. Husain, Ibid., 62, 2643, 2987 (1966).

26. A. S. Coolidge, H. M. James and R. D. Present, J. Chem. Phys., 4, 193 (1936).

27. G. Herzberg, Spectra of Diatomic Molecules, (D. van Nostrand Co., Inc., Princeton, New Jersey, 1950) pp. 199-201, 392-3.

28. J. M. White, Ph.D. Thesis, University of Illinois, Urbana, Illinois (1966).

29. J. H. Sullivan, J. Chem. Phys., 39, 3001 (1963).

30. J. H. Sullivan, J. Chem. Phys., 36, 1925 (1962).

31. B. A. Ridley, W. R. Schulz and D. J. Le Roy, J. Chem. Phys., 44, 3344 (1966).

32. A. A. Westenberg and N. de Haas, J. Chem. Phys., 47, 1393 (1967).

33. M. Karplus, private communication to A. K.

34. J. A. Sullivan, J. Chem. Phys., 30, 1292 (1959).

35. A. F. Trotman-Dickenson and G. S. Milne, National Standard Reference Data Series - National Bureau of Standards 9, p. 22 (1967).

36. J. A. Sullivan, J. Chem. Phys., 36, 1925 (1962).

37. R. A. Fass, J. Phys. Chem., 74, 984 (1970).

38. A. F. Trotman-Dickenson and G. S. Milne, National Standard Reference Data Series - National Bureau of Standards 9, p. 12 (1967).

39. (a) M. Karplus, R. N. Porter and R. D. Sharma, J. Chem. Phys., 43, 3254 (1965); (b) N. C. Blais and D. L. Bunker, J. Chem. Phys., 41, 2377 (1964).

40. D. G. Truhlar and A. Kuppermann, J. Chem. Phys., 52, 3841 (1970).

41. D. R. Davis, J. A. Betts, J. M. White and A. Kuppermann, forthcoming (this is Paper 2 in this thesis).

42. R. A. Fass, J. Phys. Chem., 74, 984 (1970).

43. R. D. Penzhorn and B. deB. Darwent, J. Phys. Chem., 72, 1639, (1968).

44. R. B. Timmons and R. E. Weston, J. Chem. Phys., 41, 1654 (1964).

45. A. Persky and A. Kuppermann, forthcoming.

46. R. J. Donovan and D. Husain, Trans. Faraday Soc., 62, 2987 (1966).

47. A. Kuppermann, J. Stevensen and P. O Keefe, Disc. Faraday Soc., 44, 46 (1967).

48. M. Abramowitz and L. A. Stegun, National Bureau of Standards Applied Mathematics Series 55, 1964, p. 295.

49. A. Kuppermann and R. N. Porter, forthcoming.

50. M. Karplus and K. T. Tang, Disc. Faraday Soc., 44, 56 (1967). Also, M. Karplus, personal communication to A. Kuppermann.

51. D. G. Truhlar and A. Kuppermann, J. Phys. Chem., 73, 1722 (1969).

PAPER 2

REACTIONS OF H ATOMS WITH DBr AND DI

INTRODUCTION

The reaction of thermal hydrogen atoms with deuterium iodide or bromide may result in either of the two processes,

$$H + DX \rightarrow HD + X \qquad [1]$$

$$H + DX \rightarrow HX + D \qquad [2]$$

We have measured the ratio $k_1/(k_1 + k_2)$ for the iodide and bromide reactions at 300°K. These results are needed for the interpretation of hot atom experiments[1-3] in which DX serves as an H-atom scavenger and for adjusting parameters in theoretical treatments of these reactions.[4-5]

The method is an indirect one based on photodissociation of HX-DX mixtures with essentially monochromatic light. Over the range of wavelengths utilized, the extinction coefficient ratio $\epsilon_{HX}/\epsilon_{DX}$ varies by about a factor of 10. This ratio must be known as well as certain other rate constant ratios in order to evaluate $k_1/(k_1 + k_2)$. The photoproduced atoms are born with 0.6 to 3 eV kinetic energy depending on the photolysis wavelength, but in the presence of increasing amounts of added helium, the average energy of the atoms at the time of reaction is shifted toward thermal energies. Our results are extrapolated to infinite dilution in He, which gives ordinary thermal rate constants characteristic of the temperature of the helium.

MECHANISM

The following mechanism is used to interpret the extrapolated results.

$$HX + h\nu \rightarrow H^* + X \qquad [3]$$

$$DX + h\nu \rightarrow D^* + X \qquad [4]$$

$$H + DX \rightarrow HD + X \qquad [1]$$

$$H + DX \rightarrow HX + D \qquad [2]$$

$$D + HX \rightarrow HD + X \qquad [5]$$

$$D + HX \rightarrow DX + H \qquad [6]$$

$$D + DX \rightarrow D_2 + X \qquad [7]$$

$$H + HX \rightarrow H_2 + X \qquad [8]$$

$$X + X + M \rightarrow X_2 + M$$

The last reaction occurs both on the walls and by a termolecular mechanism in the gas. The ratio $\alpha = [HX]/[DX]$ is kept small (0.02-0.06) to minimize the importance of reactions [5] and [6] and to permit neglect of reaction [8] in the mechanism. The effect of including reaction [8] is discussed in a later section. Neglect of several other reactions is justified elsewhere.[2]

The quantum yields of [3] and [4] are one,[6-8] so the ratio of photoproduced H and D is simply $\epsilon_{HX}/\epsilon_{DX}$. If one knows this ratio and the auxilliary rate constant ratios involving reactions [5], [6] and [7], then a single measurement of the extrapolated product ratio $[HD]/[D_2]$ suffices to determine $k_1/(k_1 + k_2)$. But accurate direct knowledge of α is difficult to obtain, and one can instead vary the wavelength (and hence $\epsilon_{HX}/\epsilon_{DX}$) with α constant. Then

$k_1/(k_1 + k_2)$ and α can be calculated from measurements of the product ratio, the auxilliary ratios and the wavelength dependence of $\epsilon_{HX}/\epsilon_{DX}$.

The mechanism neglecting reaction [8] with a steady state assumption for the H and D concentrations yields for the extrapolated product ratio,

$$\left(\frac{[HD]}{[D_2]}\right)_o^{He} = \alpha\left[C + aD + \frac{ax[1 + \alpha(C + aD)]}{1 + \alpha(1 - a)x}\right] \qquad (1)$$

where

$$a = k_1/(k_1 + k_2) \qquad k_1/k_2 = a/(1 - a)$$

$$C = k_5/k_7 \qquad \alpha = [HX]/[DX]$$

$$D = k_6/k_7 \qquad x = \epsilon_{HX}/\epsilon_{DX}$$

The complete mechanism which accounts for the positive slope of a plot of $[D_2]/[HD]$ versus $[DX]/[He]$ has been discussed elsewhere.[2] There it was shown that very little information content could be extracted from the slope unless it was known to within 6 to 8 significant figures. However, the intercept value given by Eq. (1) is sufficient to give the needed information on a and α. On the basis of Eq. (1) it is expected that a plot of the extrapolated product ratio versus $x/[1 + \alpha(1-a)x]$ will be linear with

$$\text{slope } s = \alpha a[1 + \alpha(C + aD)] \qquad (2)$$

$$\text{intercept } i = \alpha(C + aD) \qquad (3)$$

From this it follows that

$$a = s\left[\frac{C + K}{i(i + 1) + sK}\right] \qquad (4)$$

$$\alpha = \frac{i(i + 1) + sK}{(1 + i)(C + K)} \tag{5}$$

where $K = (k_6/k_2).(k_1/k_7)$ has been introduced because it is more readily estimated by theory than the related $D = k_6/k_7$. The term $(1 - a)$ occurring in the expression for $([HD]/[D_2])_0^{He}$ is obtained by first assuming $a = 1$ and calculating a and α from a plot of $([HD]/[D_2])_0^{He}$ versus x. These calculated values of a and α are then used to make a new plot of $([HD]/[D_2])_0^{He}$ versus $x/[1 + \alpha(1-a)x]$, the slope and intercept of which are used to calculate new values of a and α. This process is repeated until the results converge, which usually takes 3 or 4 iterations. Calculation of the ratios C and K will be discussed later.

If reaction [8] is added to the mechanism, the expression for the extrapolated product ratio becomes

$$\frac{[HD]}{[D_2]}_0^{He} = \alpha\left[C + \frac{aD}{1 + \alpha G} + \frac{aX\left[1 + \alpha\left(C + aD\left[\frac{\alpha G + 1}{\alpha aG + 1}\right]\right)\right]}{\alpha aG + 1 + \alpha x(1 - a)}\right] \tag{6}$$

where $G = k_8/k_1$. Then a plot of $([HD]/[D_2])_0^{He}$ versus $x/[\alpha aG + 1 + \alpha x(1 - a)]$ is expected to be linear with

$$\text{slope } s = \alpha a\left\{1 + \alpha\left[C + aD\left(\frac{\alpha G + 1}{\alpha aG + 1}\right)\right]\right\} \tag{7}$$

$$\text{intercept } i = \alpha\left(C + \frac{aD}{1 + \alpha G}\right)$$

Solving for a in Eq. (8) and using this in Eq. (7) one obtains a 5th order equation in α which can be solved using Newton's root method.[9] In the worst case in our experiments corresponding to the largest value of α of 0.06 in DBr, we find

that a = 0.99 when reaction [8] is neglected and a = 1.00 when reaction [8] is included in the mechanism. This is within experimental error and justifies neglecting reaction [8].

EXPERIMENTAL

Preparation, photolysis and analysis of the mixtures was carried out by techniques described elsewhere.[2,10] DBr and DI were obtained from Merck, Sharp and Dohme of Canada Ltd. The DI, after transfer to the photolysis vessel, contained 3% of HI and was used in that form. Under similar conditions the DBr contained less HBr impurity and we added HBr to it. Ultra high purity helium was obtained from Matheson. Separate vacuum lines and photolysis cells were used for DI and DBr. The wavelengths used are given in Table I. Great care was taken[10] to insure that the light was sufficiently monochromatic to avoid significant error. Conversion of halide ranged from 0.2 to 2% in about 1 hour for most experiments. At each wavelength the product ratio $[D_2]/[HD]$ was plotted versus [DX]/[He] for about 5 to 15 photolysis mixtures with [DX]/[He] ranging from about 0.1 to 2. Such plots are linear[2,3] and a linear least squares fit gave the desired extrapolated intercept and a measure of its uncertainty due to random errors (mostly caused by lack of constancy of α). The plots are shown in Figs. 1 and 2.

Figure 1. Plots of photolysis results for DBr-He mixtures

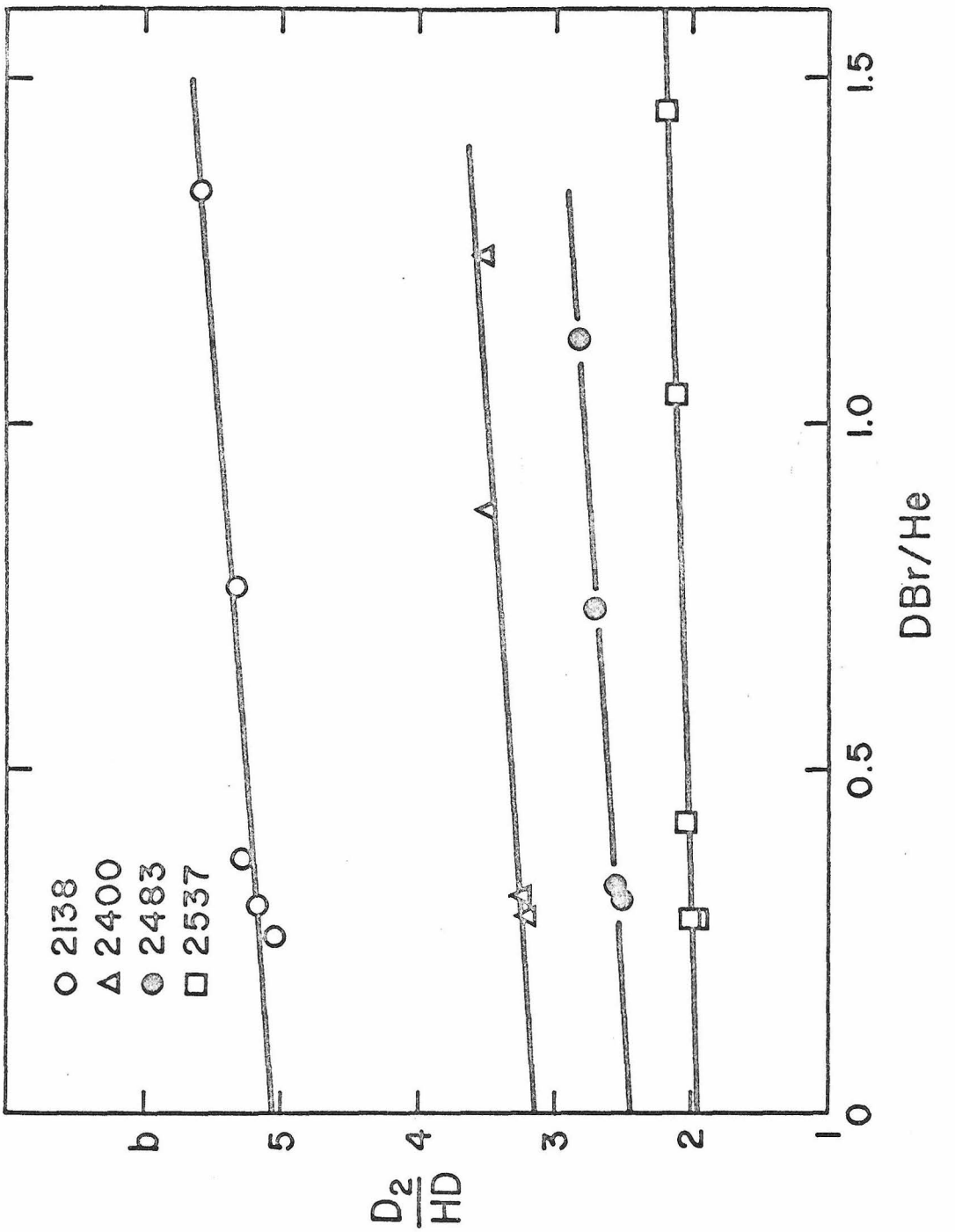
○ 2138
△ 2400
● 2483
□ 2537
b
5
4
3
2
1
0
0.5
1.0
1.5
$\frac{D_2}{HD}$
DBr/He

Figure 2. Plots of photolysis results for DI-He mixtures.

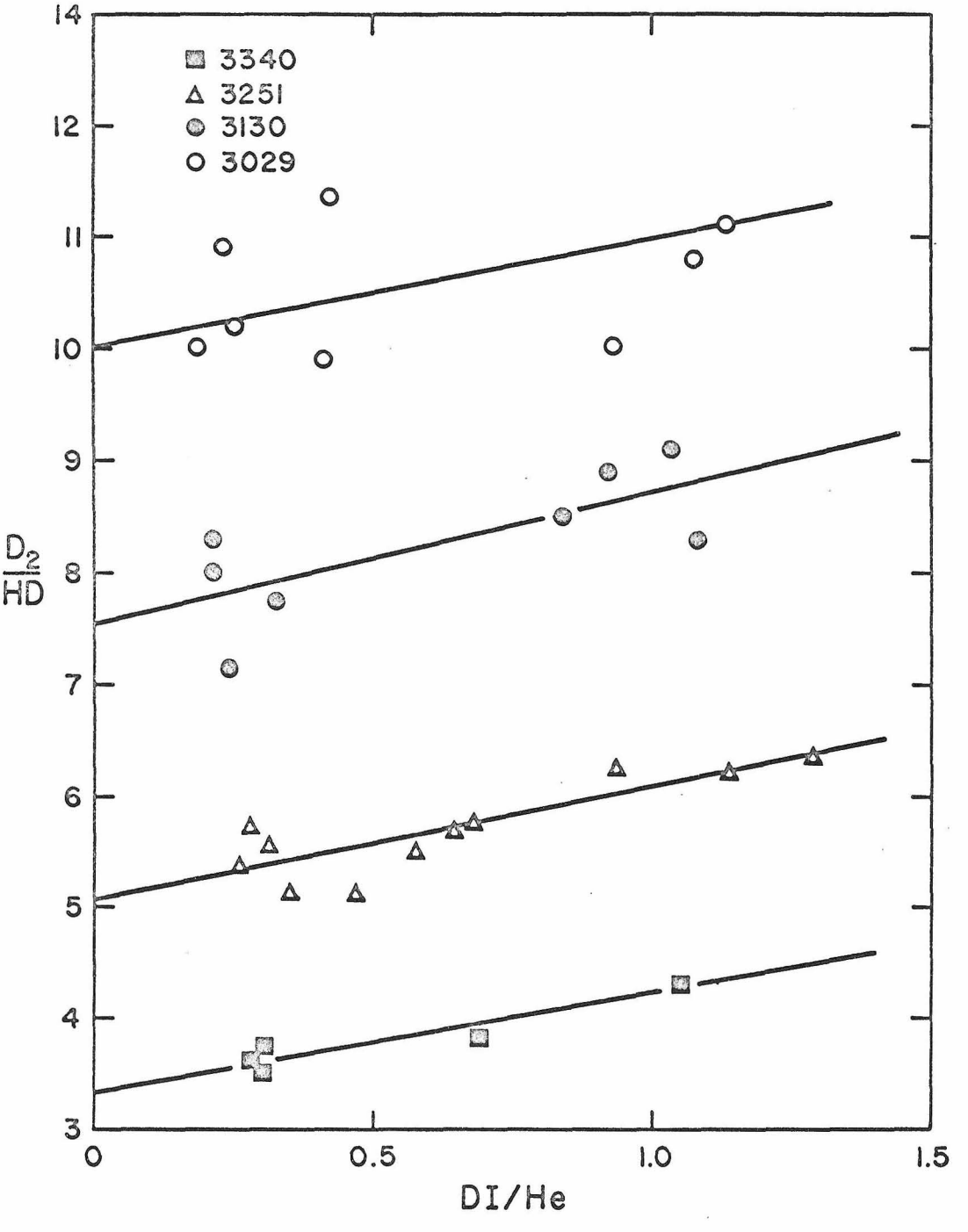
14
12
11
10
9
8
7
6
5
4
3
0
0.5
1.0
1.5
$\frac{D_2}{HD}$
DI/He
3340
3251
3130
3029

RESULTS AND DISCUSSION

Results of the variable wavelength photolyses of HX-DX mixtures in helium are presented in Table I. Plots of extrapolated $[HD]/[D_2]$ ratios versus $x/[1 + \alpha(1-a)x + \alpha aG]$ are shown in Fig. 3. The values and standard errors of the resulting slopes (s) and intercepts (i) were obtained from a least squares fit which took into account errors in both the ordinate and abcissa[11] of each point. Finally, values of a and α are shown for each series. The standard error shown is the square root of the sum of squares of individual errors. The later were obtained from products of derivatives of Eqs. (1) and (4) with the appropriate estimated standard errors for each variable.

In order to evaluate the expressions for a(DX) and α from Eqs. (4) and (5), one must have the rate constant ratios $C = k_5/k_7$ and $K = (k_6/k_2)(k_1/k_7)$ or, if the effect of reaction [8] is to be included and Eqs. (7) and (8) used, we need $G = k_8/k_1$ in addition. The ratio k_6/k_2 is estimated by equilibrium statistical mechanics to be 4.2 for the bromides and 3.5 for the iodides. We can estimate k_5/k_7 and k_8/k_1 from transition state theory or make an independent measurement of these quantities.

Timmons and Weston[12] give force constants and internuclear distances for the H-H-Br activated complex. These parameters are assumed to be isotope independent. Thus, the following formulas can be used to calculate the needed frequencies:

Table I. Summary of results of photolysis of DX in He. The indicated uncertainties are the least squares standard errors. Standard errors are calculated as described in the text.

Halide	λ	$x = \frac{HX}{DX}$	No. of Photolyses	$\left(\frac{[HD]}{[D_2]}\right)_0^{He}$	s	i	α	a
I	3029	2.50 ± 0.07	8	0.094 ± 0.005	0.024 ± 0.001	0.038 ± 0.006	0.023 ± 0.002	0.97 ± 0.05
	3130	3.68 ± 0.08	8	0.133 ± 0.006				
	3252	6.8 ± 0.3	11	0.197 ± 0.01				
	3340	11.0 ± 1.0	5	0.300 ± 0.01				
Br	2138	1.42 ± 0.02	5	0.198 ± 0.002	0.065 ± 0.002	0.120 ± 0.008	0.059 ± 0.005	0.99 ± 0.03
	2400	3.25 ± 0.09	5	0.317 ± 0.006				
	2483	4.99 ± 0.14	5	0.410 ± 0.004				
	2537	6.78 ± 0.29	5	0.512 ± 0.003				

Fig. 3. Plots of $([HD]/[D_2])_0^{He}$ ratios measured at different wavelengths.

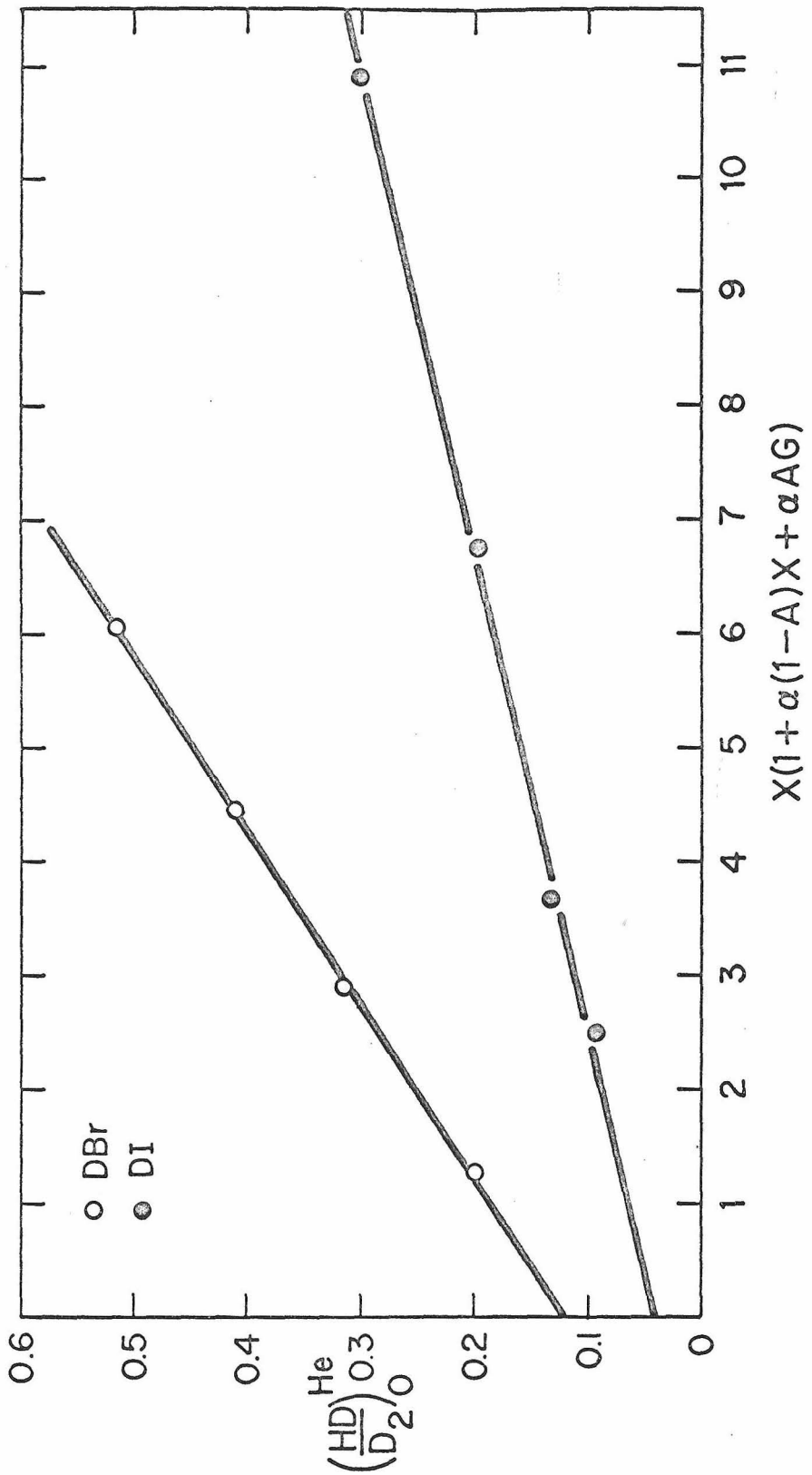
0.6
0.5
0.4
0.3
0.2
0.1
0
$\left(\frac{HD}{D_2O}\right)^{He}$
o DBr
• DI
1
2
3
4
5
6
7
8
9
10
11
$X(1+\alpha(1-A)X+\alpha AG)$

$$\lambda_1^{\neq} + \lambda_3^{\neq} = (\mu_X + \mu_Y)f_{XY} + (\mu_Y + \mu_Z)f_{YZ} - 2\mu_Y f_{int} \tag{9}$$

$$\lambda_1^{\neq}\lambda_3^{\neq} = (f_{XY}f_{YZ} - f_{int}^2)(\mu_X\mu_Y + \mu_X\mu_Z + \mu_Y\mu_Z) \tag{10}$$

$$\lambda_2^{\neq} = \frac{f_\alpha}{R_{XY}R_{YZ}}\left[\frac{R_{XY}\mu_Z}{R_{YZ}} + \frac{R_{YZ}\mu_X}{R_{XY}} + \frac{(R_{XY} + R_{YZ})^2\mu_Y}{R_{XY}R_{YZ}}\right] \tag{11}$$

where $\lambda_i^{\neq} = 4\pi^2\nu_i^{\neq 2}$ and $\nu_i^{\neq}$ is the vibrational frequency of the activated complex, $\nu_2^{\neq}$ is the bending frequency of the activated complex and $\nu_3^{\neq}$ is the imaginary frequency corresponding to motion along the reaction coordinate at the saddle point of the potential energy surface. The f_{ij}'s are force constants corresponding to a linear XYZ type molecule, the R_{ij}'s are the internuclear distances and $\mu_i = 1/m_i$ where the m_i's are the masses of the atoms. The ratio k_5/k_7 can be expressed in terms of the above calculated frequencies as

$$k_5/k_7 = \frac{\nu_{DX}}{\nu_{HX}}\exp\left[\frac{E_{HX} - E_{DX}}{RT}\right]\frac{(\nu_1^{\neq}\nu_2^{\neq 2}\nu_3^{\neq})_{DHX}}{(\nu_1^{\neq}\nu_2^{\neq 2}\nu_3^{\neq})_{DDX}}\cdot\frac{\sinh(1/2\ u_{1DDX})}{\sinh(1/2\ u_{1DHX})}\cdot$$

$$\left(\frac{\sinh(1/2\ u_{2DDX})}{\sinh(1/2\ u_{2DHX})}\right)^2 \tag{12}$$

where ν_{DX} and ν_{HX} are the vibrational frequencies of DX and HX, $(E_{HX} - E_{DX})$ is the difference in zero point energy and $u = hc\nu/kT$. The vibrational frequencies of HBr and DBr are 1650 cm^{-1} and 1898 cm^{-1} respectively.[13] The zero point energy difference is 376 cm^{-1}. The ratio k_8/k_1 is calculated by the same expression with DHX replaced by HHX and DDX replaced by HDX. Likewise

$$k_1/k_7 = \frac{(\nu_1^{\neq}\nu_2^{\neq 2}\nu_3^{\neq})_{HDX}}{(\nu_1^{\neq}\nu_2^{\neq 2}\nu_3^{\neq})_{DDX}} \cdot \frac{\sinh(1/2\ u_{1DDX})}{\sinh(1/2\ u_{1HDX})} \quad \frac{\sinh(1/2\ u_{2DDX})}{\sinh(1/2\ u_{2HDX})}^2 \quad (13)$$

Using sets A and C of force constants and internuclear distances given by Timmons and Weston, we obtain $k_5/k_7 = 2.2$, $k_1/k_7 = 1.2$ and $k_8/k_1 = 2.2$. Experiments done in this laboratory[14] indicate that $k_5/k_7 = 2.0 \pm 0.2$, $k_1/k_7 = 1.35 \pm 0.14$, and $k_8/k_1 = 2.0 \pm 0.2$. These latter experimental values were used in interpreting the data.

For the iodides the only work on isotope effects is by Sullivan. We calculate $k_8/k_7 = 1.75 \pm 0.15$ from his frequencies. Then, experiments done in this laboratory[14] used this number to obtain $k_5/k_7 = 1.45 \pm 0.15$, $k_1/k_7 = 1.21 \pm 0.12$ and $k_8/k_1 = 1.45 \pm 0.15$.

The extinction coefficients for HBr, DBr, HI and DI have been measured in this laboratory.[15] These values were used to obtain the x's listed in Table I. With the above values for k_5/k_7, k_1/k_7 and k_8/k_1 the abstraction fraction a is 0.97 ± 0.05 for DI and 0.99 ± 0.03 for DBr as shown in Table I.

Our major sources of error are due to uncertainty in k_5/k_7, the slope and the intercept. The ratio k_5/k_7 contributes 2.6% error to a(DBr) and 2.5% error to a(DI). The slope contributes errors of 1.0% to a(DBr) and 2.1% to a(DI) while the intercept error is 1.7% in DBr and 4.5% in DI. There error due to K is negligible. The errors reported in this paper are standard errors.

A systematic error in the extinction coefficients could alter the results. For example for the iodides a decrease of x(3340A) to 9.6 from 11.0 and of x(3250A) to 6.25 from 6.77 would increase a(DI) to 1.00. A flow system such as that used by LeRoy et al.[16] in the study of hydrogen isotope reactions is being set up by one of us (D. R. Davis) to achieve a more direct measurement of a.

The abstraction fraction has been studied theoretically[4] using a statistical phase space theory of chemical kinetics. This theory contains no adjustable parameters and gives values of a(DI) = 0.98 and a(DBr) = 0.97 at 300°K. As can be seen from Table I, these values are in good agreement with the experimental values of a(DI) = 0.97 ± 0.05 and a(DBr) = 0.98 ± 0.03. The reason the theory predicts abstraction fractions near 1 is that the exchange reaction leading to HX and D is endothermic and hence is statistically less likely to occur. The theory also predicts that the abstraction fraction will decrease with increasing temperatures as the endothermicity of reaction [2] is overcome. However, the temperature dependence of the abstraction fraction was not measured.

REFERENCES

1. A. Kuppermann and J. M. White, J. Chem. Phys., 44, 4352 (1966).
2. J. M. White, D. R. Davis, J. A. Betts and A. Kuppermann, forthcoming (this is Paper I in this thesis).
3. R. M. Martin and J. E. Willard, J. Chem. Phys., 40, 3007 (1964).
4. D. G. Truhlar and A. Kuppermann, J. Phys. Chem., 73, 1722 (1969).
5. C. A. Parr, Ph.D. Thesis, California Institute of Technology, 1968.
6. E. Warburg, Sitzb. Preuss. Akad., 300 (1918).
7. A. Bodenstein and C. Lieneweg, Zeit. Phys. Chem., 119, 123 (1926).
8. B. Lewis, Proc. Natl. Acad. Sci., 13, 720 (1927).
9. M. Abramowitz and L. A. Stegun, National Bureau of Standards Applied Mathematics Series 55, 1964, p. 18.
10. D. R. Davis and J. A. Betts, forthcoming (this is Appendix A of this thesis).
11. W. E. Deming, Statistical Adjustment of Data (John Wiley and Sons, Inc., New York, 1943).
12. R. B. Timmons and R. E. Weston, Jr., J. Chem. Phys., 41, 1654 (1964).
13. G. Herzberg, Molecular Spectra and Molecular Structure, II, Spectra of Diatomic Molecules (D. Van Nostrand Co., Inc., New York, 1950). pp. 534-540.
14. A. Persky and A. Kuppermann, forthcoming.

15. J. A. Betts, D. R. Davis, J. M. White and A. Kuppermann, forthcoming.

16. B. A. Ridley, W. R. Schulz and D. J. LeRoy, J. Chem. Phys., 44, 3344 (1966).

PAPER 3

EXCITED IODINE ATOMS BY PHOTOLYSIS OF DI

INTRODUCTION

Deuterium iodide has a broad, continuous absorption which extends from the near ultraviolet to the vacuum ultraviolet, reaching a maximum around 2225Å. Only three excited states ($^3\pi_0^+$, $^1\pi$, $^3\pi$) can contribute to this absorption.[1,2] All three are repulsive and lead to dissociation of the iodide. The dissociation of the $^3\pi_0$ and $^1\pi$ states leads to ground state iodine atoms, $^2P_{3/2}$, while that of the $^3\pi_0^+$ states leads to an excited iodine atom, $^2P_{1/2}$, which is 0.942 eV above the ground state. This is depicted in Fig. 1. Therefore, at a given wavelength photodissociation of DI can occur into two channels:

$$DI + h\nu \rightarrow D + I\,(^2P_{3/2}) \qquad [1]$$

$$DI + h\nu \rightarrow D + I^*(^2P_{1/2}) \qquad [2]$$

We have measured the fraction

$$f(\lambda) = k_2/(k_1 + k_2) \qquad (1)$$

of iodine atoms produced in excited states by photolysis of DI as a function of wavelength. This fraction f is zero unless the photon absorbed has sufficient energy both to break the D-I bond and to excite the iodine. The critical wavelength corresponding to this energy in DI is 3070Å.

Cadman, Polanyi and Smith[3] measured the sum of f in HI at

Figure 1. Potential Energy Curves for HI.

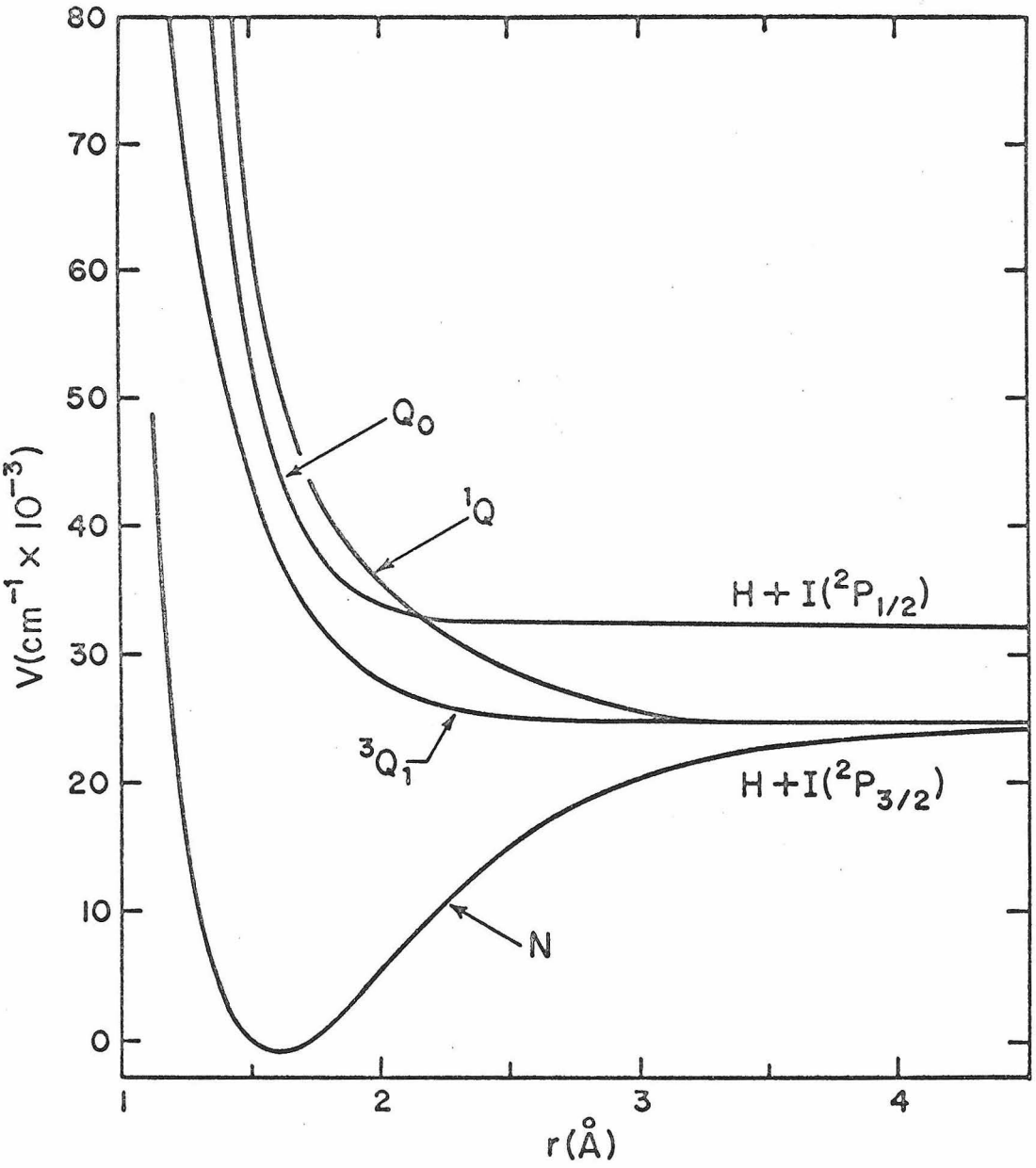
80
70
60
50
40
30
20
10
0
1
2
3
4
V(cm^{-1} × 10^{-3})
r(Å)
Q_0
^1Q
$^3Q_1$
N
H + I($^2P_{1/2}$)
H + I($^2P_{3/2}$)

2537Å and the fraction of iodine atoms which are produced excited in the reactions:

$$H + HI \rightarrow H_2 + I\,(^2P_{3/2}) \qquad [3]$$

$$H + HI \rightarrow H_2 + I^*(^2P_{1/2}) \qquad [4]$$

They reported $C = k_2/(k_2 + k_1) + k_4/(k_4 + k_3)$ to be 1.5 ± 0.4. In a later paper Cadman and Polanyi[4] used a new experimental measurement of the Einstein transition probability to reinterpret their data to give $C = 0.55 \pm 0.25$. They also estimated $k_4/(k_4 + k_3)$ to be 0.02 ± 0.015 indicating that $f = 0.53 \pm 0.25$. Donovan and Husain[5] used flash photolysis of HI in the ultraviolet to determine the fraction of iodine atoms formed in the excited state. Using a continuous source, theyobserved an average f of approximately 0.2 for wavelengths longer than 2000Å. Compton and Martin[6] used a method similar to ours to obtain f's in HI of 0.93 ± 0.15, 0.81 ± 0.15 and 1.00 ± 0.15 at wavelengths of 2537Å, 2288Å and 1849Å, respectively.

METHODS

Our measurement of $f(\lambda)$ follows from the fact that the deuterium atom produced in process [1] has nearly 1 eV more kinetic energy (in the laboratory system) than that produced in [2]. In other work from this laboratory[7] we have shown the yield of HD from the reaction

$$D^* + H_2 \rightarrow HD + H \qquad [5]$$

is a sensitive function of the initial kinetic energy (denoted by the asterisk) of the deuterium atom.

Figure 2 presents the fraction A of D* atoms which undergo reaction [5] in H_2 as a function of the initial laboratory energy at 300°K. A is called the integral reaction yield of D* with H_2. The quantity (1 - A) is the fraction of those atoms which are thermalized by elastic collisions with H_2 and are removed by thermal reaction with a scavenger, in our case DI or DBr. The function $A(E_{lab})$ can be used as a calibrated "energy measuring device" for deuterium atoms in the photolysis of DI in the presence of H_2. This calibration is based on measurements of A for D* produced by photolysis of DI and DBr with monochromatic radiation for which E_{lab} is known (i.e., for which f is zero or very small).

Photolysis of DI at wavelength λ greater than 3070Å yields D* having an average laboratory energy of

$$E_{lab} = \frac{m_I}{m_{DI}}\left(\frac{hc}{\lambda} - D_0^0\right) + \frac{m_I}{m_{DI}}\langle E_{rot}\rangle + \frac{m_D}{m_{DI}}\langle E_{DI}^L\rangle \qquad (2)$$

If the DI is at 300°K, this gives

$$E_{lab} = \frac{m_I}{m_{DI}}\left(\frac{hc}{\lambda} - D_0^0\right) + 0.026\text{eV} + 0.001\text{eV} \qquad (3)$$

In the above D_0^0 is the bond dissociation energy of DI, $\langle E_{rot}\rangle$ is the average rotational energy of DI and $\langle E_{DI}^L\rangle$ is the average laboratory translational energy of DI molecules. If at a given wavelength iodine is produced in both the $^2P_{3/2}$ and $^2P_{1/2}$ states, D atoms of two different energies are formed; one is given by Eq. (2) when D_0^0 is replaced by $[D_0^0 + E(^2P_{1/2})]$. $E(^2P_{1/2})$ is the electronic excitation energy of the $^2P_{1/2}$ state and is 0.9426 eV

Figure 2. The fraction of D atoms having laboratory energy E_{lab} which react with pure H_2 to form HD ($T = 300^{\circ}K$).

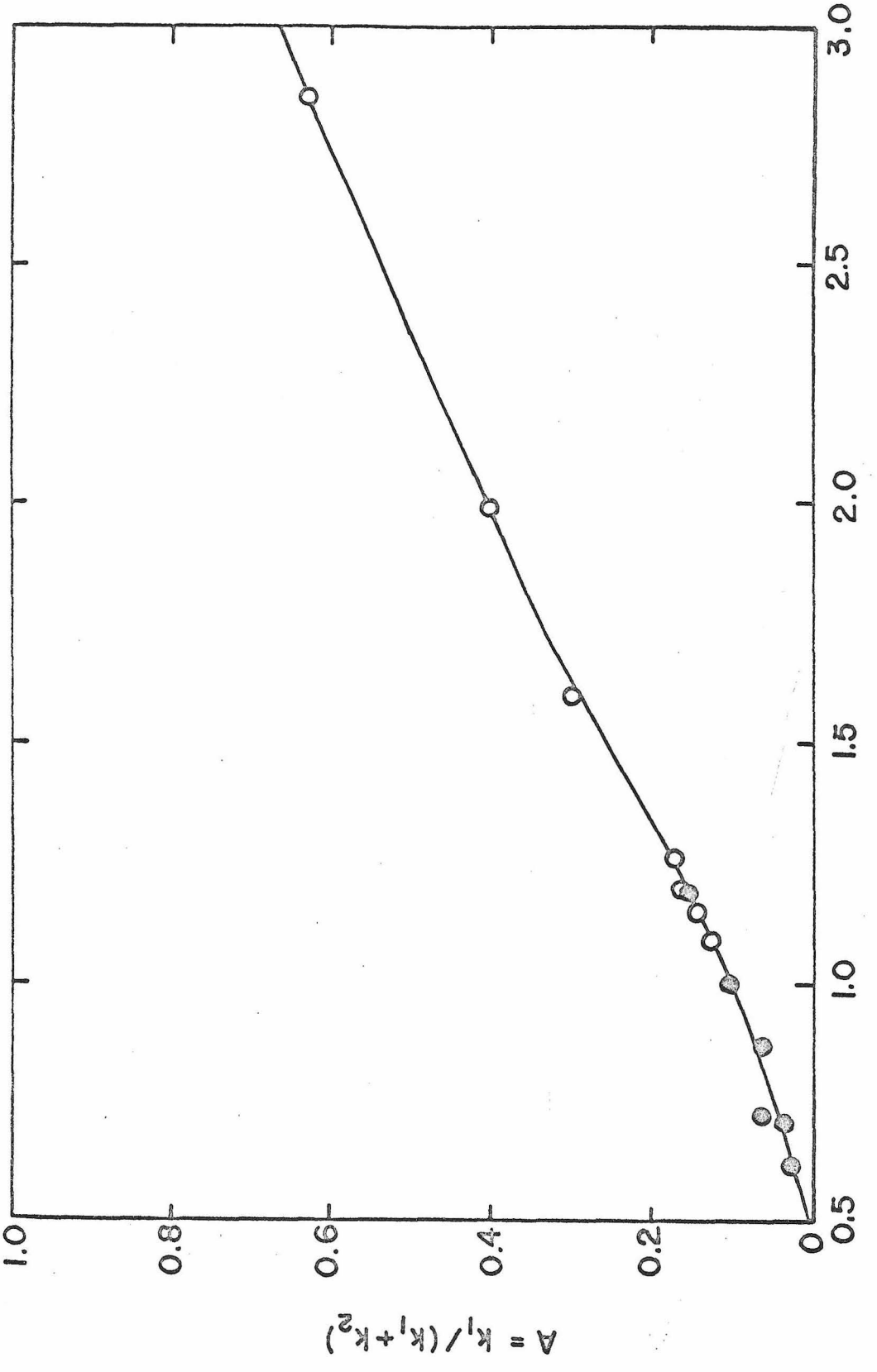
A = k1/(k1+k2)
1.0
0.8
0.6
0.4
0.2
0
0.5
1.0
1.5
2.0
2.5
3.0
E1(0) (eV)

for iodine atoms. $\langle E_{rot} \rangle$, $\langle E_{DI}^{L} \rangle$ and E_{lab} have distribution functions associated with them due to thermal spreads and the fact that the photolysis light is not completely monochromatic. The spreads in the second and third terms have been shown to be 0.018 eV and 0.00045 eV respectively.[7] The spreads due to the photolysis light are less than 0.02eV in these experiments so the D* atoms are produced in a nearly monoenergetic distribution.

The quantity f can be determined from a measurement of the average A for D atoms produced in H_2 by photolysis of DI at the desired wavelength, and from interpolated values of $A(E_1)$ and $A(E_2)$ from Fig. 2. Of the D* atoms produced, a fraction f have $E_{lab} = E_1$ and a fraction (1 - f) have $E_{lab} = E_2 + E_1 - E(^2P_{1/2})$. Thus the fraction of all D* atoms which yield HD is

$$A(\lambda) = f \cdot A(E_1) + (1 - f) \cdot A(E_2) \qquad (4)$$

where $A(\lambda)$ is the observed average. Solving, we get

$$f = \frac{A(E_2) - A(\lambda)}{A(E_2) - A(E_1)} \qquad (5)$$

EXPERIMENTAL

DI-H_2 and DI-He mixtures were prepared using a mercury-free vacuum line. The cylindrical reaction vessel was 50 mm in diameter and 75 mm long and was made of fused silica with high optical quality windows.

A Hanovia SC 2537 low pressure mercury lamp with a 2 mm Corning 7910 filter to remove the 1849Å line was used for photolysis

at 2537Å. A Hanovia 2500 watt medium pressure mercury lamp was used for photolysis at 2800Å and 2400Å. The light was passed through a Bausch and Lomb model 33-86-01 monochromator with a 2 mm thick Corning 7910 filter at the exit to remove short wavelength radiation (transmission 10% at 2240Å, 1% at 2175Å). A zinc Phillips spectral lamp with a cis-2-butene gas filter (100 torr pressure, 5 cm pathlength) was used for photolysis at 2138Å (transmission 60% at 2138Å, less than 0.01% at 2050Å). The light intensities were of the order 5×10^{15} photons/sec at all wavelengths.

At all wavelengths about 1% of the DI was decomposed. After photolysis, the DI was frozen in liquid nitrogen and the volatile gases transferred to an analysis bulb via a toepler pump. The products were analyzed for HD and D_2 on a calibrated CEC-21-103C mass spectrometer. Unirradiated blanks showed no products. The hydrogen used was depleted in deuterium atoms with respect to their natural abundance and contained only 5 ppm HD and corrections for this HD amounted to less than 1%. Further details are given elsewhere.[7]

RESULTS AND DISCUSSION

At each wavelength a series of DI-H_2 and DI-He experiments were performed at [DI]/[G] (G stands for H_2 or He) ratios varying from 0.3 to 1.5. The product ratio $[D_2]/[HD]$ was then plotted against the reactant ratio [DI]/[G]. These plots were linear for

both hydrogen and rare gas runs. A typical plot is shown in Fig. 3. A linear least squares analysis gave the intercepts $([D_2]/[HD])_0^{H_2}$ and $([D_2]/[HD])_0^{He}$ and their standard deviations. The intercepts $([D_2]/[HD])_0^{He}$ are needed to correct the results for HI impurity in the DI; they would be infinite if there were no impurity. The quantity $A(DI,\lambda)$ is derived elsewhere[7] and is

$$A(\lambda) = \frac{\Delta(1 + \alpha Bx)}{1 + a(1+\Delta) + \alpha(1 + \alpha Bx)^{-1}[xa^2 + (C + aD)(a + 1 + \alpha x)]} \quad (6)$$

where $\alpha = \frac{[HI]}{[DI]}$, $x = \frac{\epsilon_{HI}}{\epsilon_{DI}}$

and $a = \frac{k_6}{k_6 + k_7}$, $C = \frac{k_9}{k_5}$, $D = \frac{k_8}{k_4}$, $B = 1 - a$,

$$\Delta = ([HD]/[D_2])_0^{H_2} - ([HD]/[D_2])_0^{He},$$

where the rate constants above correspond to the thermal reactions:

$$D + DI \rightarrow D_2 + I \quad [5]$$

$$H + DI \rightarrow HD + I \quad [6]$$

$$H + DI \rightarrow HI + D \quad [7]$$

$$D + HI \rightarrow DI + H \quad [8]$$

$$D + HI \rightarrow HD + I \quad [9]$$

We used $a(DI) = 0.97 \pm 0.04$, $C = 1.45 \pm 0.15$ and $D = 0.14 \pm 0.02$; the determination of these rate constant ratios is discussed elsewhere,[8] as is the determination of α and the measurement of x. We used $a(DBr) = 0.96 \pm 0.04$ to calculate the upper portion of the curve in Fig. 2. This value could be either 0.93 or 0.99 as discussed in reference 7. The effect of changing this

Fig. 3 Plots of product ratio $[D_2]/[HD]$ versus reactant ratios $[DI]/[H_2]$ or $[DI]/[He]$ for photolysis of DI-H_2 and DI-He mixtures at 2537Å. Linear least-squares intercepts are 1.48 ± 0.06 and 11.1 ± 0.6.

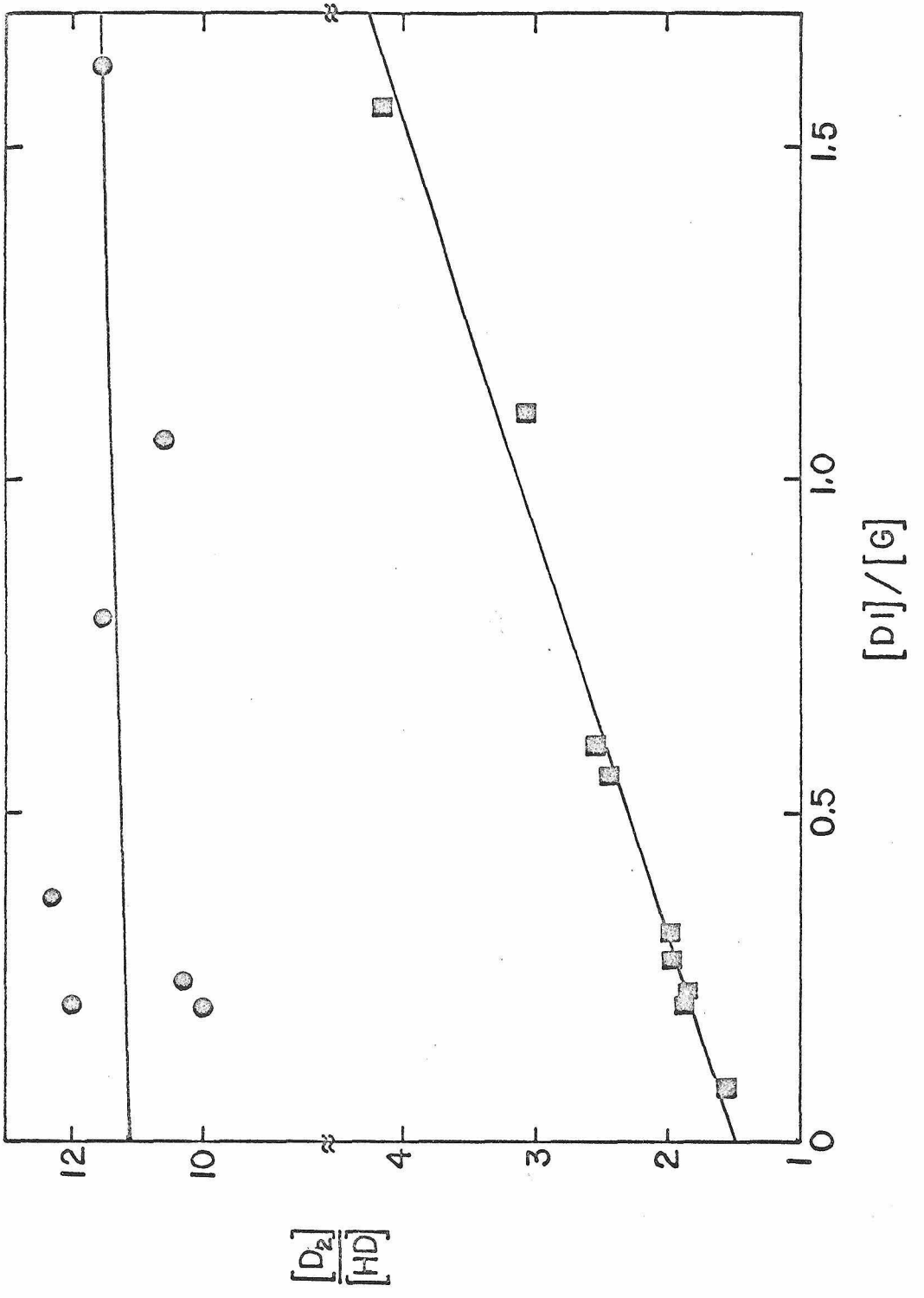
[D2]/[HD]
12
10
≈
4
3
2
1
0
0.5
1.0
1.5
[D1]/[G]

value will be shown later. The results of all the experiments are shown in Table I.

The main sources of error are the random error in the experiments, errors in the values of a(DI) used to calculate A(obs) and a(DBr) used to obtain the upper portion of the curve in Fig. 1, and errors in interpolating the values of $A(E_i)$. For the latter we have used errors the size of the error bars in Fig. 2. The standard errors listed for the A(obs) take into account errors in all the quantities that go into determining A. This is discussed in detail elsewhere.[7]

The errors in $A(\lambda)$ are important in all experiments. The experiments at 2800Å include only 4 points so the random error contributes almost the entire total error listed. At 2537Å and 2400Å $A(\lambda)$ and $A(E_2)$ contribute almost equally to the error while at 2138Å the major source of error comes from $A(E_2)$. Since $A(E_2)$ is dependent mainly on a(DBr), changes in this quantity greatly affect the reported f. For example, if a (DBr) = 0.91, f(2138Å) = 0.41, while if a(DBr) = 0.99, f(2138Å) = 0.24, a change of almost 50%. The results at other wavelengths are not as dependent on a(DBr).

We have used the interpolated values of $A(E_2)$ with the assumption that the observed A values are not strongly biased by production of excited bromine atoms in DBr photolysis. Although there is no reason to believe that a significant fraction of these bromine atoms are excited,[1,2,7] our values of $f(DI,\lambda)$ would have to be revised if $f(DBr,\lambda)$ were found non-zero. For example, if

TABLE I. Summary of Results

	λ(Å)	2800	2537	2400	2138
H_2	slope	2.0 ± 0.4	1.64 ± 0.08	1.65 ± 0.07	1.36 ± 0.02
	intercept	1.4 ± 0.4	1.48 ± 0.06	1.25 ± 0.07	0.45 ± 0.02
He	slope	0.4 ± 0.1	0.66 ± 0.11	3.4 ± 0.2	0.9 ± 0.1
	intercept	11.1 ± 0.9	10.8 ± 0.8	12.1 ± 0.2	9.4 ± 0.8
	Δ	0.62 ± 0.2	0.58 ± 0.02	0.72 ± 0.05	2.10 ± 0.09
	A(λ)	0.229 ± 0.05	0.218 ± 0.008	0.257 ± 0.014	0.505 ± 0.02
	E_1(eV)	0.402	0.854	1.128	1.736
	E_2(eV)	1.326	1.780	2.056	2.682
	A(E_1)	0.0 ± 0.001	0.065 ± 0.005	0.143 ± 0.03	0.336 ± 0.03
	A(E_2)	0.212 ± 0.02	0.35 ± 0.02	0.427 ± 0.03	0.590 ± 0.03
	f	-0.08 ± 0.27	0.46 ± 0.05	0.60 ± 0.07	0.33 ± 0.1

f(DBr, 2250Å) = 0.05 then f(DI, 2537Å) would increase by 0.019.

We can compare our DI results with the HI results of Cadman and Polanyi and Compton and Martin. Cadman and Polanyi obtain f(HI, 2537Å) = 0.53 ± 0.25, while we obtain f(DI, 2537Å) = 0.46 ± 0.05. Compton and Martin obtain f(HI, 2537Å) = 0.07 ± 0.15. Further experiments are needed to establish f(HI) and to show whether there is a measurable real difference between f(HI) and f(DI). It is difficult to compare our results with those of Donovan and Husain since they measured an average f over a continuum of wavelengths. Our results agree qualitatively with theirs.

The isotope effect to be expected in going from DI to HI can be estimated using the following approximate theory. First, we assume that the extinction coefficient to the i th electronic state is:

$$\epsilon(\nu,i) = \nu K(i)\,\psi_o^{\,2} \tag{7}$$

In the above $\psi_o^{\,2}$ is the square of the normalized ground state vibrational wavefunction, ν is the wavenumber and K(i) is related to the integral over the electronic wavefunctions and is assumed to be constant. This approximation is further discussed by Coolidge, James and Present[9] and by Herzberg[10] and has been used by Goodeve and Taylor[11] in analyzing their HI and HBr spectra. The total extinction coefficient at each wavelength is just

$$\epsilon = \sum_i \epsilon(\nu,i) \tag{8}$$

Secondly we assume that the upper electronic state potential curves are given by the expression:

$$\nu_i(\rho) = D_0(i) + E(i)\, e^{-F(i)\rho} \tag{9}$$

where $\rho = r - r_e$ and r_e is the equilibrium distance of the oscillator, the $D_0(i)$'s are dissociation energies for each excited state and the E(i)'s and F(i)'s are isotope independent parameters to be fitted to the experimental data. The isotope dependency is included in ψ_o and the $D_0(i)$'s. For DI, D(1) = D(3) = 24,660 cm^{-1} and D(2) = 32,263 cm^{-1}.[10]

In the following discussion we have assumed the ground state vibrational wavefunction to be a Morse wavefunction[12] of the form:

$$\psi_o^2 = \frac{a(2b - 1)(2b)^{2b - 1}}{(2b)} \exp[2b(-a\rho - e^{-a\rho}) + a\rho] \qquad (10)$$

In the above, $a = 0.12177\, \omega_e \sqrt{\mu/D_e}$ where ω_e is the vibrational frequency equal to 2309.5 cm^{-1} for HI and 1640 cm^{-1} for DI,[10] D_e is the dissociation energy from the bottom of the potential and equals 25,804.7 cm^{-1} for both HI and DI and μ is the reduced mass and $b = 2D_e/\omega_e$.

An attempt was made to fit the parameters K(i), E(i) and F(i) to the experimental data illustrated in Fig. 4. These attempts were largely unsuccessful in providing precise agreement with our data although qualitative agreement could be obtained. This analysis is sufficient to determine the magnitude of the isotope effect to be expected in going from DI to HI. For example for our best fit with K(1) = 1.2 x 10^{-4} l. $mole^{-1}$, E(1) = 13370 cm^{-1}, F(1) = 3.1 cm^{-1}, K(2) = 7.0 x 10^{-4} l. $mole^{-1}$, E(2) = 11772 cm^{-1}, F(2) = 6.0 cm^{-1}, K(3) = 6.0 x 10^{-4} l. $mole^{-1}$, E(3) = 29370 cm^{-1} and F(3) = 1.5 cm^{-1}, we obtain f(DI, 2550Å) = 0.76 and f(HI, 2550Å) = 0.82. Changing the above parameters changes the predicted

percent isotope effect only slightly. This predicted isotope effect is consistant with that observed by comparing our results for DI and Cadman and Polanyi's results for HI. However, it is not consistent if we compare our results with those of Compton and Martin for HI. In the above analysis we did not take into account the possibility than an absorption to the $^3\pi$ state could cross to the $^3\pi_0^+$ state producing an excited iodine atom. Such intersystem crossing has been observed in other systems (see for instance Herzberg[13]). If this intersystem crossing were much more efficient in DI than in HI it could explain the differences in our results and those of Compton and Martin.

One value of the experiments is to determine to what extent each of the three possible transitions to excited states contribute to the total extinction coefficient of DI. According to Mullikan[1,2] at low energies the extinction coefficient would be due to transitions to the $^3\pi_0$ state. At energies above about 0.6 eV transition to the $^3\pi_0^+$ state contributes. At even greater energies come contributions from transitions to the $^1\pi$ state. Since only the $^3\pi_0^+$ state leads to an excited iodine atom, we have assumed that the quantity f which we measured is equal to the fractional contribution of this state to the total extinction coefficient. In this analysis we will neglect intersystem crossing as there is no criterion for deciding how much it would contribute. If we assume that all excited iodine atoms produced come from a transition to the $^3\pi_0^+$ state, the fraction f multiplied by the

total extinction coefficient gives the contribution of this state to the extinction coefficient at each wavelength measured. Fig. 4 shows the resulting breakdown of the extinction coefficient of DI versus wavelength into component parts. The extinction coefficients used were measured in this laboratory. Our analysis indicates that there is a maximum in the curve showing absorption to the $^3\pi_0^+$ state at approximately 2300Å. No attempt was made to determine the contribution from transitions to the $^1\pi$ state.

Figure 4. Contribution of the DI excited states to the total extinction coefficient as a function of wavelength. The upper line is the measured extinction coefficient from reference 8 while the lower slashed lines are the contributions of each state.

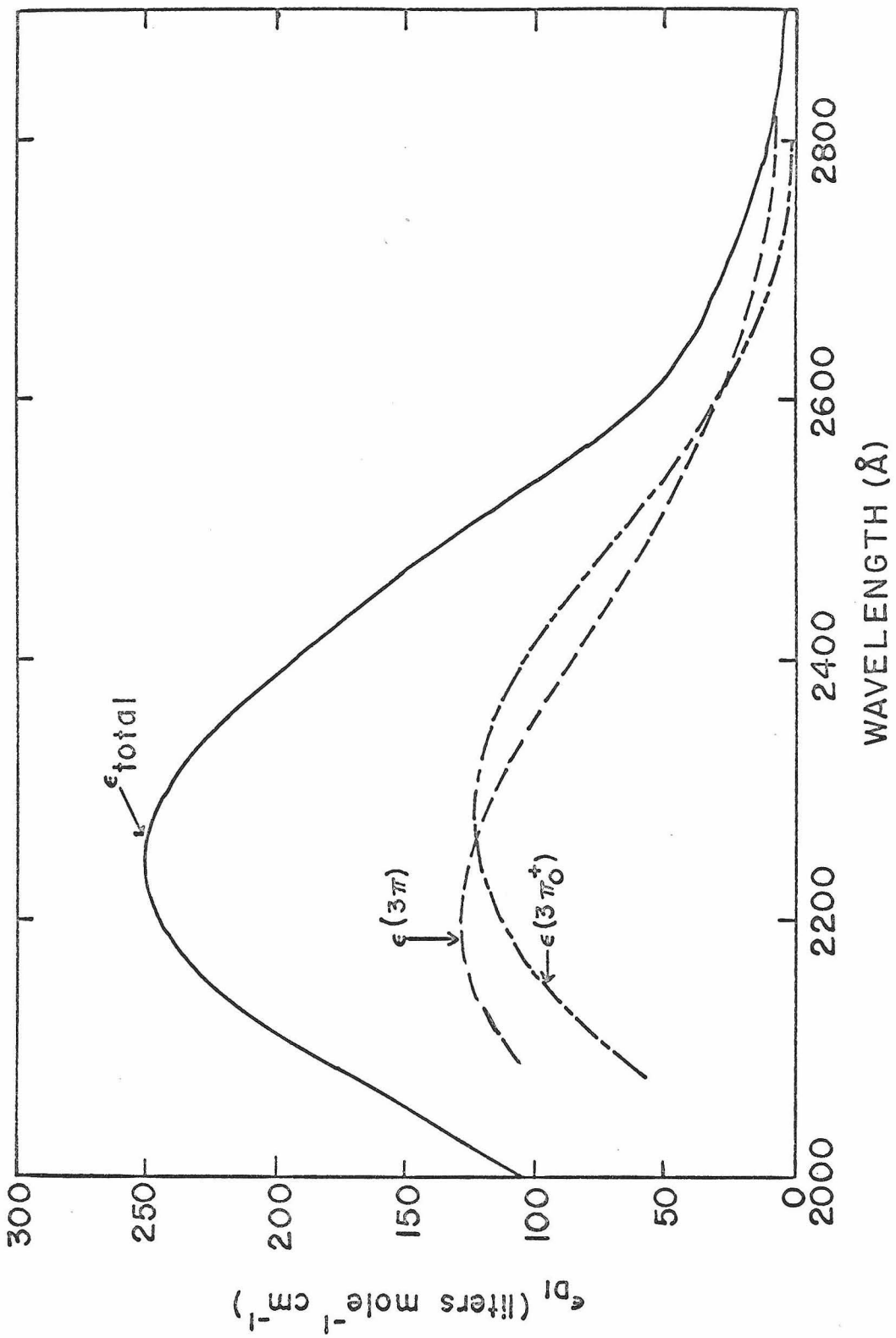
300
250
200
150
100
50
0
2000
2200
2400
2600
2800
WAVELENGTH (Å)
ϵ_{bl} (liters mole^{-1} cm^{-1})
ϵ_{total}
$\epsilon(3\pi)$
$\epsilon(3\pi_0^+)$

REFERENCES

1. R. S. Mulliken, J. Chem. Phys., 8, 382 (1940).
2. R. S. Mulliken, Phys. Rev., 51, 310 (1937).
3. P. Cadman, J. C. Polanyi and I. W. M. Smith, J. Chim. Phys., 64, 111 (1967).
4. P. Cadman and J. C. Polanyi, J. Phys. Chem., 72, 3715 (1968).
5. R. J. Donovan and D. Husain, Trans. Faraday Soc., 62, 1050 (1966).
6. L. E. Compton and R. M. Martin, J. Phys. Chem., 73, 3474 (1969).
7. J. M. White, D. R. Davis, J. A. Betts, and A. Kupperman, forthcoming (this is Paper I in this thesis).
8. D. R. Davis, J. A. Betts, J. M. White and A. Kuppermann, forthcoming (this is Paper II in this thesis).
9. A. S. Coolidge, H. M. James and R. D. Present, J. Chem. Phys., 4, 193 (1936).
10. G. Herzberg, Spectra of Diatomic Molecules, (D. Van Nostrand Co., Inc., Princeton, New Jersey, 1950) pp. 199-201, 392-3.
11. C. F. Goodeve and A. W. C. Taylor, Proc. Roy. Soc., A152, 221 (1935).
12. P. H. Morse, Phys. Rev., 34, 57 (1929).
13. G. Herzberg, Spectra of Diatomic Molecules, (D. Van Nostrand Co., Inc., Princeton, New Jersey, 1967) pp. 359, 368.

PAPER 4

1. INTRODUCTION

The chemical reaction cross section is a very fundamental dynamical quantity which permits the formulation of bulk reaction properties in terms of the molecular level dynamics of reacting systems.[1] In a previous paper[2] (designated here as I) the importance of chemical reaction cross sections and the experimental difficulties in obtaining them were discussed. A photochemical technique was presented which gives the energy dependence of the integral reaction yield A for the reaction:

$$D^* + H_2 \rightarrow HD + H \qquad [1']$$

where A is defined as the fraction of the hot D* atoms (produced monoenergetically) which react according to [1'] rather than with a dilute scavenger of thermalized D atoms. It describes the competition between reaction [1'] and the thermalization process:

$$D^* + H_2 \rightarrow D + H_2 \qquad [2']$$

and was shown to be closely related to the cross sections for these collision processes.

In this paper we extend the technique to obtain the integral reaction yield of the reaction:

$$H^* + CD_4 \rightarrow HD + CD_3 \qquad [1]$$

as a function of energy.

In (I) we discussed the many experimental difficulties associated with obtaining the cross sections of reaction [1'] and its isotopic counterparts. Neither thermal rate constant

measurements nor molecular beam experiments are able at present to furnish the cross sections for these reactions in the energy range from 0 to 3 eV. As explained in (I), such information would be extremely useful for comparison with either a priori or more approximate model calculations. This information can be obtained using our technique.

In this paper we discuss the details pertinent to the H + CD_4 system. In section 2 we outline the basis of the present method and in section 3 the experimental techniques employed. In sections 4 and 5 we discuss the results of the experiments and the manner of analyzing these results to obtain the integral reaction yield. In section 6 we discuss the relation of the integral reaction yield to the reaction cross section.

2. METHOD

2.1 Integral reaction yield

The method consists of photolyzing mixtures of HBr and CD_4 with monochromatic radiation to produce translationally "hot" monoenergetic hydrogen atoms. These either react "hot" or are thermalized in the system. The integral reaction yield:

$$A(E_1^{(0)}) = \frac{k_1(\lambda)}{k_1(\lambda) + k_2(\lambda)} \qquad (1)$$

is measured as a function of the initial laboratory energy $E_1^{(0)}$ of the hydrogen atoms produced when the HBr is photolyzed with light of wavelength λ. In the above, $k_1(\lambda)$ and $k_2(\lambda)$ are the

effective bimolecular rate coefficients for the elementary processes:

$$H^* + CD_4 \rightarrow HD + CD_3 \qquad [1]$$

$$H^* + CD_4 \rightarrow H + CD_4 \qquad [2]$$

describing the rates of reaction and thermalization which accompany the injection of monochromatic hydrogen atoms into thermal CD_4 gas. The asterisk denotes translationally hot hydrogen atoms which are defined in section 2.2.

The rate coefficients k_1 and k_2 depend on the energy with which the hydrogen atoms are initially formed. The integral reaction yield is a measure of the competition between reactive collisions and non-reactive ones, and its variation with wavelength is related to the energy dependencies of the corresponding cross sections. If information is available about the differential non-reactive cross sections from either theoretical calculations or independent experiments, the exchange reaction cross section, averaged over the appropriate internal states of the CD_4, can be obtained from the experimental $A(E_1^{(0)})$ by methods which will be described later.

2.2 Hot and thermal hydrogen atoms

As in (I), the steady state distribution function of laboratory energies of hydrogen atoms is expected to be bimodal with one peak at the initial energy $E_1^{(0)}$ and the other at an energy of the order of kT where T is the temperature of the reaction mixture. This distribution may, for descriptive purposes, be considered as

the superposition of two distribution functions, the hydrogen atoms described by the one peaked at $E_1^{(0)}$ being called "hot" and denoted as H*, and the hydrogen atoms described by the one peaked at kT being called "thermal" and denoted as H.

2.3 Kinetic analysis

In the following kinetic analysis we consider the thermal H and hot H* as two chemically distinct species since their reactive properties differ due to their different energy distributions. If the CD_3H impurity in the CD_4 is neglected, the following mechanism is expected for the HBr-CD_4 system:

$$HBr + h\nu \rightarrow H^* + Br \qquad [0]$$

$$H^* + CD_4 \rightarrow CD_3 + HD \qquad [1]$$

$$H^* + CD_4 \rightarrow H + CD_4 \qquad [2]$$

$$H^* + HBr \rightarrow H_2 + Br \qquad [3]$$

$$H^* + HBr \rightarrow H + HBr \qquad [4]$$

$$H + HBr \rightarrow H_2 + Br \qquad [5]$$

$$CD_3 + HBr \rightarrow CD_3H + Br \qquad [6]$$

$$Br + Br + M \rightarrow Br_2 + M \qquad [7]$$

where the third body M is either a species in the gas phase or a surface. Neglect of other possible steps is justified in section 5.

Assuming steady state concentrations of [H*], [H] and [CD_3], a kinetic analysis of the above mechanism gives:

$$\frac{[H_2]}{[HD]} = \frac{k_2}{k_1} + \frac{[HBr]}{[CD_4]}\left(\frac{k_3}{k_1} + \frac{k_4}{k_1}\right) \qquad (2)$$

Therefore we should expect a plot of $[H_2]/[HD]$ versus $[HBr]/[CD_4]$ to be linear with positive slope and intercept as found previously by Carter, Hamill and Williams[3] and by Martin and Willard.[4] This turns out to be the case in our experiments.

From equation (1) we can see that:

$$A = \frac{\left(\frac{[HD]}{[H_2]}\right)_0}{1 + \left(\frac{[HD]}{[H_2]}\right)_0} = \frac{1}{1 + \left(\frac{[H_2]}{[HD]}\right)_0} \qquad (3)$$

where $([HD]/[H_2])_0$ is the reciprocal of the intercept of the above straight line. A determination of A requires therefore only the measurement of $([HD]/[H_2])_0$. Small corrections are made for competing reactions as discussed in section 5.

In summary, the method for determining the integral reaction yield A consists in photolyzing mixtures of HBr and CD_4 with monochromatic light and measuring the resulting $[H_2]/[HD]$ product ratios as a function of the reactant ratios $[HBr]/[CD_4]$. This provides a linear plot, the intercept $([H_2]/[HD])_0$ of which is used to determine A.

3. EXPERIMENTAL

3.1 Apparatus

A mercury free vacuum line with an oil diffusion pump was used in preparing reactant mixtures. Pressures were measured with a mercury manometer and cathetometer using a Pace differential transducer as a null device. The reaction vessel was made

of fused silica with optical quality quartz windows. It was cylindrical in shape being 6 inches long and 1 1/2 inches in diameter and had a stopcock attached for addition and removal of gases. The windows were fused onto its ends.

The photolysis apparatus consisted of an optical bench on which the light sources, filters and reaction vessel were mounted. The light sources used were as follows:

1849Å - An Hanovia low pressure mercury lamp which draws 110 ma current at 280 volts was used for photolysis at this wavelength. A 2 mm thick ^{60}Co gamma-irradiated lithium flouride window was placed in front of the lamp to remove the 2537Å radiation. The absorbance of the filter was always 2.5 or greater at 2537Å and approximately 0.5 at 1849Å. The lamp emitted 10% 1849Å radiation, so approximately 10% of all light passing through the filter was 2537Å. Since the absorption coefficient of HBr at 1849Å is over 100 times greater than that at 2537Å, the correction for the 2537Å light passing through the filter is less than 0.1%. The intensity of the lamp with the lithium flouride filter was approximately 9×10^{13} photons/sec.

2061Å - An iodine lamp[5] powered by a microwave source was used for photolysis at this wavelength. There were impurity lines at approximately 1820Å, 1830Å and 1860Å which were less than 0.5% of the peak at 2061Å. These lines were removed by the quartz window of the reaction vessel and by an additional thickness of quartz placed in front of the window. The intensity of the lamp was approximately 1.8×10^{16} photons/sec.

2138Å - A zinc Phillips spectral lamp with a cis-2-butene filter (100 torr pressure, 5 cm pathlength) was used for photolysis at this wavelength. The transmission of the filter was 60% at 2138Å and less than 0.02% at 2050Å. The lamp had impurity lines at 2025Å and 2062Å, each of which was 14% of the peak at 2138Å. Less than 0.06% of all light passing through the filter was 2025Å or 2062Å radiation. The intensity of the lamp was approximately 6.7×10^{15} photons/sec.

2288Å - A cadmium Phillips spectral lamp was used for photolysis at this wavelength. A small peak at 2145Å was removed with a cis-2-butene filter (650 torr pressure, 5 cm pathlength). The transmission of the filter was 35% at 2288Å and 0.1% at 2145Å. There was also a peak at 2266Å which was 10% of the peak at 2288Å. The resulting data were corrected for the presence of this peak as described in section 6. The intensity of the lamp was approximately 8×10^{15} photons/sec.

2537Å - A General Electric germicidal lamp was used for photolysis at this wavelength. A Corning 7910 glass filter was placed in front of the lamp to remove any 1849Å radiation.

A McPherson Model 235 fifty centimeter vacuum ultraviolet scanning monochromator with a grating blazed for 3000Å was used to scan the output of the light sources to check for unwanted lines. A RCA 935 phototube was used to measure light intensities during a photolysis.

Products were handled on a mercury vacuum line. This line contained a dewar cooled by pumped liquid nitrogen (to produce

temperatures of about -212° C), a 1 1/2 liter toepler pump and analysis bulbs.

A CEC-103C mass spectrometer was used to analyze the reaction products.

3.2 Reagents

The HBr was obtained in lecture bottles from the Matheson Company. It was frozen in liquid nitrogen and pumped to remove any hydrogen impurity and then distilled from a dry ice-acetone bath at -78°C to remove any bromine. It was stored in black 1-liter bulbs after purification and was repurified prior to a photolysis. The CD_4 was from Merck, Sharp and Dohme of Canada Ltd. It had a minimum stated isotopic purity of 99% D atoms. Our mass spectrometric analysis showed 0.9 atom percent H atoms. There was also 0.43% nitrogen and 0.16% oxygen impurity present.

3.3 Procedure

Prior to use the HBr was again frozen in liquid nitrogen in a cold finger and pumped and then distilled into the reaction vessel from a dry ice-acetone bath. The pressure of the HBr was measured and found to range from 30 to 45 torr. The CD_4 was then added to the reaction vessel and the pressure of the mixture measured. From the two pressure measurements, the pressure of the CD_4 was determined. Pressures of CD_4 ranged from 30 to 150 torr and $[HBr]/[CD_4]$ ratios ranged from 0.25 to 1.3.

The reaction vessel was then moved to an optical bench

where the contents were photolyzed by one of the light sources described above. Blank experiments were also performed as described in section 4.

After photolysis one end of the reaction vessel was placed in liquid nitrogen for 15 minutes or longer to remove the HBr and some of the CD_4. The contents were then passed with the help of a toepler pump through a trap cooled to -212°C or less (as measured by a copper-constantan thermocouple inserted in the dewar) by pumped liquid nitrogen and were then transferred to a glass bulb for analysis. With one such pass we were able to increase the ratio of $([HD] + [H_2])/[CD_4]$ from a value of the order of a few times 10^{-3} to at least 0.098.

The HD and H_2 were measured on the CEC mass spectrometer. Corrections were made for the contributions of the remaining CD_4 to the m/e 2 peak and the CD_3H to the m/e 3 peak. In no case did the correction to the m/e 2 peak exceed 50% and it was usually of the order of 20-30% of this peak's height. The correction to the m/e 3 peak was always less than 10% of its measured height. Calibration mixtures with composition analogous to photolysis mixtures were prepared. These were then passed through the trap cooled to -212°C and analyzed. This served to calibrate the mass spectrometer and also to check the efficiency of the trap. Reproducibility for a given sample was 2% or better.

4. RESULTS OF $[H_2]/[HD]$ MEASUREMENTS

A series of photolyses was carried out at each of five different wavelengths. For each series the $[HBr]/[CD_4]$ ratios varied from 0.25 to 1.3. The product ratio $[H_2]/[HD]$ was then plotted against the reactant ratio $[HBr]/[CD_4]$. The plots were linear with positive slopes and intercepts. These slopes and intercepts and their standard deviations were determined by a linear least squares analysis. The plots of $[H_2]/[HD]$ versus $[HBr]/[CD_4]$ at all 5 wavelengths are shown in Figure 1, together with the root mean square fitted straight lines.

The effects of dark reactions, light intensity and extent of conversion were investigated. The extent of each of these effects is as follows:

(a) Dark reactions - Blank experiments were run at intervals in which the same experimental procedure as other experiments was followed except for the actual photolysis. No products were observed in these experiments indicating that dark reactions do not contribute to the mechanism.

(b) Light intensity - Two experiments with the same $[HBr]/[CD_4]$ ratio were photolyzed for the same length of time at 2288Å with light intensities of about 1.2×10^{16} and 6.0×10^{15} photons/sec respectively. The results agreed to within the 2% experimental reproducibility indicating there was no detectable effect of intensity over this range of intensities.

(c) Conversion - Two series of experiments with $[HBr]/[CD_4]$

Figure 1. Variation of $[H_2]/[HD]$ with $[HBr]/[CD_4]$ at several photolysis wavelengths.

◇ 1849Å

● 2061Å

□ 2138Å

△ 2288Å

○ 2537Å

The straight lines are root mean square fits to the points at each wavelength.

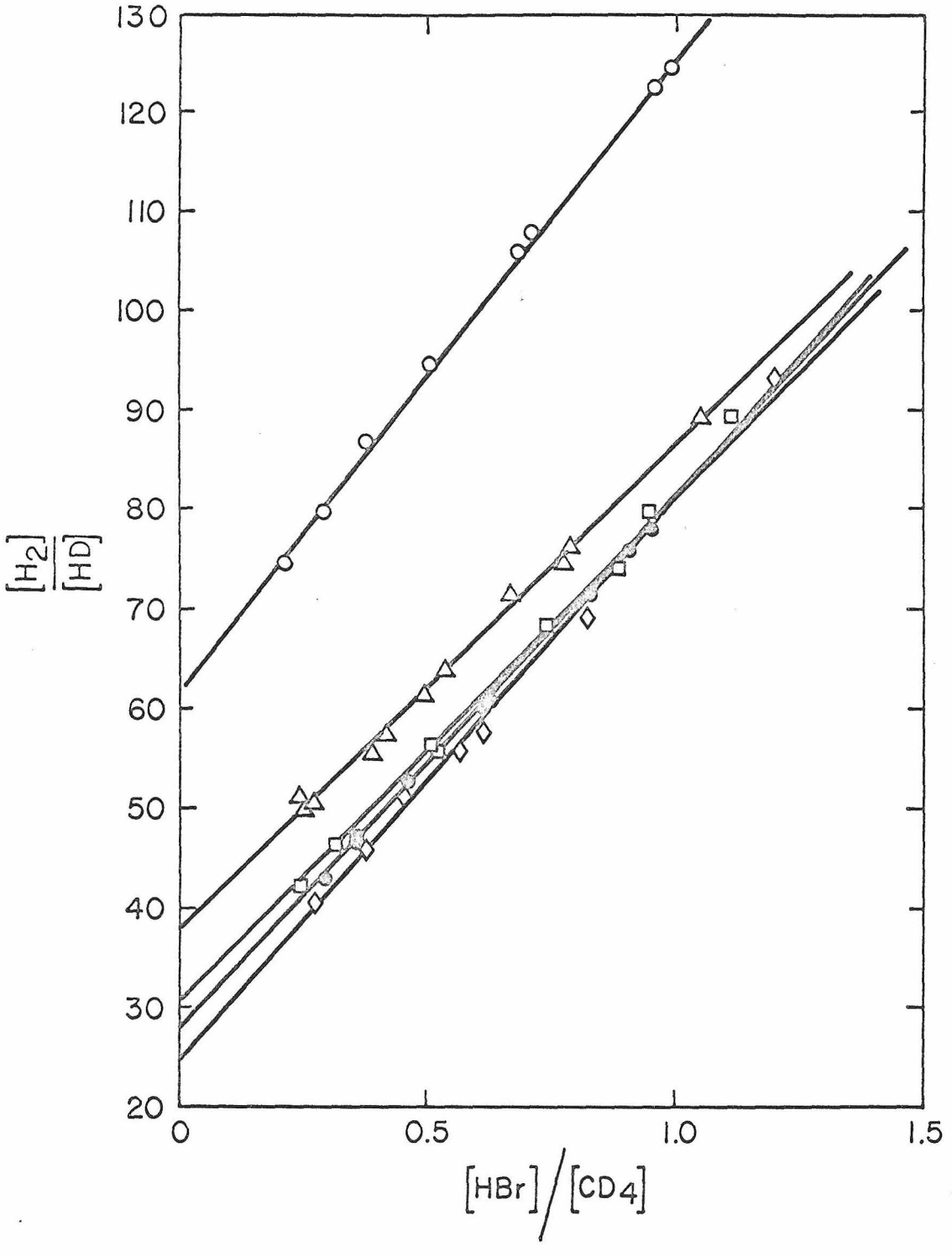
130
120
110
100
90
80
70
60
50
40
30
20
0
0.5
1.0
1.5
[H2]/[HD]
[HBr]/[CD4]

ratios ranging from 0.25 to 1.0 were done at 2288Å at different HBr conversions. Since the conversion is approximately equal to:

$$\frac{([HD] + 2[H_2])}{[HBr]} = \frac{\frac{[HD]}{[He]}\left(1 + 2\frac{[H_2]}{[HD]}\right)}{[HBr]/[He]} \qquad (4)$$

the conversion could be measured by adding a known amount of helium to the reaction vessel after a photolysis and analyzing for helium as well as H_2 and HD. Only one experiment of this kind was performed at each wavelength and the intensity of the lamp and the photolysis time were kept constant for the remaining experiments. One series was done at 0.45% conversion and the other at 0.90% conversion. The intercepts were 37.7 ± 0.9 and 37.1 ± 0.8 and the slopes were 49.1 ± 1.8 and 49.3 ± 1.2 respectively. These agree within experimental error. However, experiments with $[HBr]/[CD_4]$ ratios ranging from 0.03 to 0.12 showed a marked conversion effect. The reason for this will be discussed in section 5.

The results of all experiments along with experimental conditions are given in Table I. Column 1 gives the photolysis wavelength and columns 2, 3 and 4 the initial laboratory velocity, initial laboratory energy and initial energy relative to stationary CD_4 of the hydrogen atoms produced in the photodissociation. Column 5 gives the extent of HBr conversion and columns 6 and 7 give the reciprocal of the intercepts and the slopes of the $[H_2]/[HD]$ versus $[HBr]/[CD_4]$ least mean square straight line plots. Finally column 8 gives the values of the reaction fraction

TABLE I. Summary of Experiments

λ(Å)	$v_1^{(0)}$(10^6 cm/sec)	$E_1^{(0)}$(eV)	E_{rel}(eV)	conversion	$([H_2]/[HD])_0$	slope	A
2537	1.481	1.143	1.098	1.0%	61.8 ± 0.7	63.8 ± 1.0	0.0155 ± 0.0002
2288	1.797	1.684	1.609	0.52-1.04%	37.8 ± 0.5	48.7 ± 0.9	0.0251 ± 0.0003
2138	1.980	2.043	1.941	0.8%	30.3 ± 0.8	50.5 ± 1.1	0.0311 ± 0.0008
2061	2.081	2.257	2.154	0.56%	27.8 ± 0.4	53.0 ± 0.6	0.0338 ± 0.0005
1849	2.374	2.938	2.850	0.60%	24.6 ± 1.0	56.5 ± 1.5	0.0381 ± 0.0015

A calculated as described in section 5.

The results of the HBr plus CD_4 experiments at 1849Å can be compared with those of Martin and Willard.[4] We obtained a value of 24.6 ± 1.0 for the intercept while they obtained a value of 15. This large discrepancy can be explained by the fact that Martin and Willard did experiments at $[HBr]/[CD_4]$ ratios ranging from 0.02 to 0.1 at high conversions (~10%). The discussion in section 5 shows that this discrepancy is to be expected due to the different experimental conditions and that our procedure and values are the correct ones to use to obtain information about processes [1] and [2].

5. DETERMINATION OF INTEGRAL REACTION YIELDS

5.1 Initial Energy of Photochemically Produced Hydrogen Atoms

A detailed discussion of the factors involved in determining the initial laboratory translational energy in the photolysis of DBr is included in (I). Since the same discussion applies for HBr, only a summary of the conclusions will be given here.

Mullikan[6] has concluded that the only important transitions from the $^1\Sigma^+$ ground state of HBr to excited states are to the $^3\Pi_1$, $^1\Pi$ and $^3\Pi_0$ states. He designates the ground state and excited states as N, $^3Q_1$, ^1Q and Q_0 respectively. The $^3Q_1$ and ^1Q states dissociate to give hydrogen and bromine atoms in their ground states, ^1S and $^2P_{3/2}$ respectively. The Q_0 state dissociates to give ground state hydrogen and excited $^2P_{1/2}$ bromine atoms. At

the wavelengths used in these experiments it is energetically possible to form bromine atoms in both these states. However, theoretical arguments and experimental evidence as presented in (I) indicate that only ground state $^3P_{3/2}$ bromine atoms are formed in the photolysis of HBr at these wavelengths. The first excited state of the hydrogen atoms is at 10.2 eV and cannot be produced with the wavelengths used in these experiments.

The initial kinetic energy of the hydrogen atoms is calculated assuming a knowledge of the final electronic states in the dissociation of HBr. For only ground state atoms the photon energy available to products is

$$E_t = E_\nu - D_0^0 \tag{5}$$

where E_ν is the energy of a photon of frequency ν and D_0^0 is the dissociation energy of the ground vibrational state of HBr. The fraction of this energy which goes to the hydrogen in the center of mass system of HBr is m_{Br}/m_{HBr}. When we add the small contributions due to rotation and translation of the HBr, the following expression for the average initial laboratory energy $E_1^{(0)}$ of the D atoms is obtained:

$$E_1^{(0)} = \frac{m_{Br}}{m_{HBr}}\left(\frac{hc}{\lambda} - D_0^0\right) + \frac{m_{Br}}{m_{HBr}}\langle E_{rot}\rangle + \frac{m_H}{m_{HBr}}\langle E_{HBr}^L\rangle \tag{6}$$

Here $\langle E_{HBr}^L\rangle$ and $\langle E_{rot}\rangle$ are the average room temperature laboratory translational and rotational energies of the HBr molecules. Over the wavelength range of these experiments the first term in the right hand side of Eq. (6) varies from 1.12 to 2.91 eV, the second term is 0.024 eV and the third term is 0.0005 eV.

In (I) we showed that the contribution of excited vibrational states of DBr to the light absorption is negligible. The same arguments hold in the case of HBr.

In summary, we conclude that electronically excited bromine atoms are present in negligible amounts and that the absorption by vibrationally excited HBr molecules is also negligible. Eq. (6) gives the laboratory energy of hydrogen atoms at formation.

5.2 Mechanisms and Kinetic Analysis

A mechanism for the photolysis of HBr-CD_4 mixtures has already been considered in section 2.3. In this section we will justify the neglect of other reactions and include reactions involving the CD_3H impurity in the CD_4.

5.2.1 List of reactions in the HBr-CD_4 system (in the absence of CD_3H impurity)

Contributions of the following processes should be considered:

$HBr + h\nu$	→	$H^* + Br$	[0]
$H^* + CD_4$	→	$CD_3 + HD$	[1]
$H^* + CD_4$	→	$CD_4 + H$	[2]
$H^* + HBr$	→	$H_2 + Br$	[3]
$H^* + HBr$	→	$H + HBr$	[4]
$H + HBr$	→	$H_2 + Br$	[5]
$CD_3 + HBr$	→	$CD_3H + Br$	[6]
$Br + Br + M$	→	$Br_2 + M$	[7]
$H + Br_2$	→	$HBr + Br$	[8]

$$H + CD_4 \rightarrow HD + CD_3 \quad [9]$$

$$Br + CD_4 \rightarrow DBr + CD_3 \quad [10]$$

$$Br + HBr \rightarrow Br_2 + H \quad [11]$$

$$H^* + Br_2 \rightarrow HBr + Br \quad [12]$$

$$H^* + CD_4 \rightarrow CD_3H + D \quad [13]$$

$$D + HBr \rightarrow HD + Br \quad [14]$$

$$D + HBr \rightarrow H + DBr \quad [15]$$

$$Br^* + CD_4 \rightarrow DBr + CD_3 \quad [16]$$

$$Br^* + HBr \rightarrow Br_2 + H \quad [17]$$

In the following we will show that reactions [8] through [17] may be neglected in the kinetic analysis of this system.

(a) Reaction [9]

If reaction [9] is included in the mechanism together with reactions [1] through [7], the following expression for $[H_2]/[HD]$ results:

$$\frac{[H_2]}{[HD]} = \frac{\frac{k_2}{k_1} + \frac{k_3}{k_1}\frac{k_9}{k_5} + \left(\frac{k_3}{k_1} + \frac{k_4}{k_1}\right)\frac{[HBr]}{[CD_4]}}{1 + \frac{k_9}{k_5}\left[\left(1 + \frac{k_2}{k_1}\right)\frac{[CD_4]}{[HBr]} + \frac{k_4}{k_1}\right]} \quad (7)$$

The above expression goes through the origin as one would expect if experiments were done in the limit of zero $[HBr]/[CD_4]$. However, if the lowest $[HBr]/[CD_4]$ ratio considered satisfies the relation:

$$\frac{k_9}{k_5}\left[\left(1 + \frac{k_2}{k_1}\right)\frac{[CD_4]}{[HBr]} + \frac{k_4}{k_1}\right] << 1 \quad (8)$$

the plot from this $[HBr]/[CD_4]$ ratio upwards is a straight line

plot with a non-zero intercept. This intercept is greater than the one given by Eq. (2) by $(k_3/k_1).(k_9/k_5)$. As shown in (I) for the DBr-H_2 system, condition (8) is equivalent to:

$$\frac{[HBr]}{[CD_4]} >> \frac{1}{A}\ \frac{k_9}{k_5} \tag{9}$$

provided that:

$$\frac{k_4}{k_2}\frac{k_2}{k_1}\frac{k_9}{k_5} << 1 \tag{10}$$

One can show that the above approximations are correct by the following arguments.

First, the measurements of LeRoy et.al.[7] extrapolated to 25°C yield $k_9 = 5 \times 10^3\ M^{-1}sec^{-1}$. Similar extrapolations to 25°C from the measurements of Skinner and Ringrose[8] and Steiner[9] yield $k_5 = 5 \times 10^8\ M^{-1}sec^{-1}$. Hence:

$$k_9/k_5 \cong 10^{-5} \tag{11}$$

Secondly, $k_4/k_2 < 1$ since H* atoms are thermalized more efficiently by CD_4 than by HBr. This is true because the masses of H and CD_4 are more similar than those of H and HBr.

Finally, $k_2/k_1 < 65$ since in our experiments A always exceeds 0.015.

Thus we can conclude that:

$$\frac{k_4}{k_2}\frac{k_2}{k_1}\frac{k_9}{k_5} = 6 \times 10^{-4} << 1 \tag{12}$$

and therefore that Eq. (10) is satisfied.

In view of the above arguments, a sufficient condition for the validity of Eq. (9) is that:

$$\frac{[HBr]}{[CD_4]} >> 7 \times 10^{-4} \tag{13}$$

Since the lowest $[HBr]/[CD_4]$ ratio used in our experiments was 0.25, this condition is satisfied.

We must also show that

$$\frac{k_3}{k_1}\frac{k_9}{k_5} << \frac{k_2}{k_1} \tag{14}$$

in order that Eq. (7) reduce to Eq. (2). For the $DBr-H_2$ system (I) we were able to show that k_3 and k_1 should not differ by more than two orders of magnitude. A similar argument holds for the $HBr-CD_4$ system. Further confirmation comes from the fact that the slope of a plot of $[H_2]/[HD]$ versus $[HBr]/[CD_4]$ (see table I) is never greater than 65. Noting from Eq. (7) that this slope is equal to $(k_3/k_1 + k_4/k_1)$ we necessarily conclude that:

$$k_3/k_1 < 65 \tag{15}$$

On the other hand, from Eq. (12)

$$\frac{k_2}{k_1} = \frac{1 - A}{A} \tag{16}$$

and therefore k_2/k_1 is a decreasing function of A. Since the largest value of A is, from Table I, 0.038, k_2/k_1 always exceeds 25 in the energy range of these experiments. Collecting the above estimates together we can write:

$$\frac{k_3}{k_1}\frac{k_9}{k_5} = 6 \times 10^{-4} << 25 < \frac{k_2}{k_1} \tag{17}$$

which again validates Eq. (12). This reasoning is apparently circular since the experimental determination of A already assumes

that relation (14) is valid, and we then use the resulting A to prove the validity of (13). The process is however self-consistent and valid and is essentially an iterative approach in which the value of A determined assuming the validity of (14) corresponds to a first iteration and the second iteration is shown to agree with the first one. A further discussion of the effects of reaction [9] near the intercept is given in (I).

(b) Reaction [8]

Since bromine is a much better scavenger of hydrogen atoms than HBr (k_8/k_5 = 22.7 at 27°C[10]), the small amount of bromine formed during a photolysis could appreciably reduce the $[H_2]/[HD]$ ratio by effectively competing with HBr for hydrogen atoms. The amount of Br_2 formed should increase with the extent of conversion of HBr, and therefore, the $[H_2]/[HD]$ ratio should decrease concomitantly. As discussed in section 4, experiments with $[HBr]/[CD_4]$ ratios ranging from 0.25 to 1.0 were done at two different conversions. The slopes and intercepts of the straight line plots for these experiments agreed within experimental error indicating that effects due to bromine molecule reactions are negligible at these conversions. However, experiments with $[HBr]/[CD_4]$ ratios ranging from 0.03 to 0.1 showed a marked conversion effect. To illustrate this, the photolysis time, experimental conversion and experimental $[H_2]/[HD]$ are tabulated in Table II for a fixed $[HBr]/[CD_4]$ ratio of 0.075 for 2288A radiation. The above $[H_2]/[HD]$ is plotted versus photolysis time and % conversion in Fig. 2. The value of $[H_2]/[HD]$ extrapolated to zero

Figure 2. Variation of $[H_2]/[HD]$ with time for $[HBr]/[CD_4]$ 0.075.

--- $k_3/k_1 = 47.8$, $k_4/k_1 = 1.0$

—— $k_3/k_1 = 1.0$, $k_4/k_1 = 47.8$

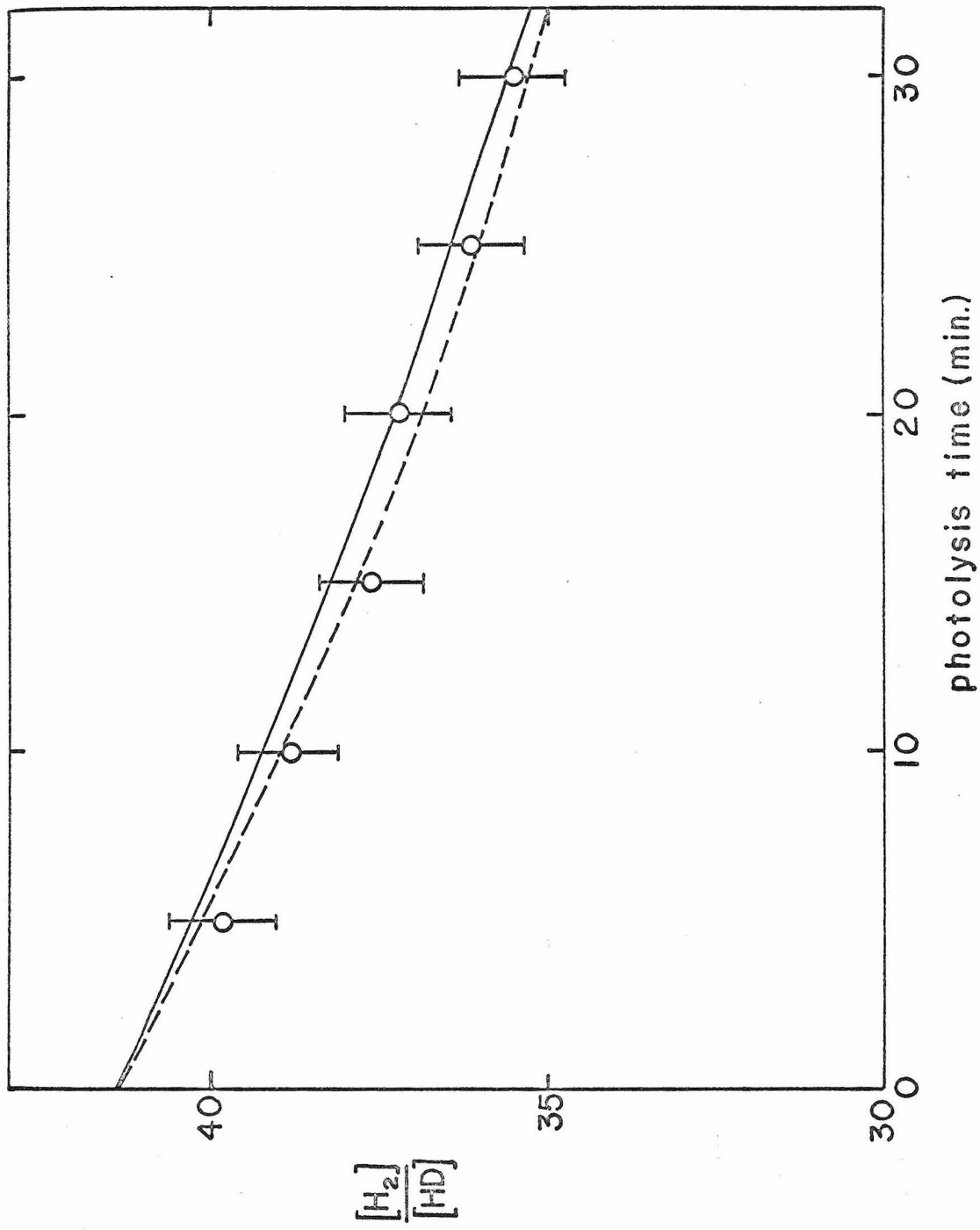
40
35
30
0
10
20
30
photolysis time (min.)
[H2]/[HD]

conversion fits nicely on the plot of $[H_2]/[HD]$ versus $[HBr]/[CD_4]$ for $[HBr]/[CD_4]$ ratios ranging from 0.3 to 1.0 (zero conversion value is 41.5, value from least squares fit of straight line of Fig. 1 is 41.4). Likewise, two series of experiments with $[HBr]/[CD_4]$ ratios ranging from 0.03 to 0.1 were done at the two conversions 0.6% and 1.2%. Plots of $[H_2]/[HD]$ versus $[HBr]/[CD_4]$ were linear with intercepts of 34.7 and 31.9 respectively. These intercepts were then linearly extrapolated to zero conversion. The extrapolated intercept of 37.5 is within experimental error equal to the intercept of 37.8 ± 0.8 of Fig. 1 obtained at 2288A in the experiments with $[HBr]/[CD_4]$ ratios ranging from 0.3 to 1.0. Hence it appears that the extent of reaction of H atoms with bromine must depend on the $[HBr]/[CD_4]$ ratio.

A theoretical justification of the above behavior is obtained by calculating the bromine concentration as a function of conversion and CD_4 concentration from the assumed mechanism. If reactions [1] through [7] are included we find:

$$[Br_2] = \frac{[HBr]_{t=0}}{2} \left[1 - \exp(-2 \epsilon_{HBr} I_o t/NA) \right] \qquad [18]$$

where $[HBr]_{t=0}$ is the initial concentration of HBr, ϵ_{HBr} is the HBr molar extinction coefficient, I_o is the incident photon intensity in photons/sec, N is Avogadro's number and A is the light beam cross sectional area. In terms of $[Br_2]/[HBr]$ this is:

$$\frac{[Br_2]}{[HBr]} = \frac{1}{2} \left[\exp(2 \epsilon_{HBr} I_o t/NA) - 1 \right] \cong \frac{\epsilon_{HBr} I_o t}{NA} \qquad [19]$$

for $I_o \epsilon_{HBr} t/NA \ll 1$. Note that there is no dependence on CD_4

concentration. If reaction [8] is included the following two simultaneous first order differential equations are obtained:

$$\frac{d[HBr]}{dt} = -\frac{\epsilon_{HBr} I_o}{NA}[HBr]\left\{1 + \frac{[CD_4] + \frac{k_3}{k_1}[HBr] + \left(\frac{k_2}{k_1}[CD_4] + \frac{k_4}{k_1}[HBr]\right)}{\left(\frac{k_1 + k_2}{k_1}\right)[CD_4] + \left(\frac{k_3 + k_4}{k_1}\right)[HBr]} x \left(\frac{[HBr] - \frac{k_8}{k_5}[Br_2]}{[HBr] + \frac{k_8}{k_5}[Br_2]}\right)\right\} \quad (20)$$

and

$$\frac{d[Br_2]}{dt} = -\frac{1}{2}\frac{d[HBr]}{dt} \quad (21)$$

These equations were solved numerically to obtain the concentrations of Br_2 and HBr as a function of photolysis time (conversion) and CD_4 concentration. The value of $q = \epsilon_{HBr} I_o/NA$ was chosen so the theoretical conversion matched the experimental one. At 2288A ϵ_{HBr} is 30 $M^{-1}cm^{-1}$, A is 8 cm^2 and I_o ranged from 1.7 x 10^{15} photons/sec to 1.9 x 10^{15} photons/sec. This gives a q ranging from 0.00065 to 0.00070. The initial concentration of HBr was taken as 1.626 x 10^{-3} M (30 torr pressure at 23°C) and the initial concentration of CD_4 ranged from 1.626 x 10^{-3} M to 5.42 x 10^{-2} M depending on the $[HBr]/[CD_4]$ ratio desired. Values of k_2/k_1, k_3/k_1 and k_4/k_1 are also needed for the above calculations. These values were obtained as follows. From Eq. (2) and the plot of $[H_2]/[HD]$ versus $[HBr]/[CD_4]$ at 2288A shown in Fig. 1, we obtain $k_2/k_1 = 39.0$ and

$$(k_3/k_1 + k_4/k_1) = 48.7 \qquad (22)$$

The values of k_3/k_1 and k_4/k_1 were then adjusted within the limits of the restraint given by Eq. (22). The effect of varying these ratios will be shown below.

Differential equations for $[H_2]$ and [HD] were also solved numerically (these are given in the appendix) so the theory could be compared with experimental values of $[H_2]/[HD]$. Results of the calculation at 2288A for $[H_2]/[HD]$ versus time for a fixed $[HBr]/[CD_4]$ ratio of 0.075 are shown in Table II and in Fig. 2 where they are compared with experiment. The top line in Fig. 2 corresponds to $k_3/k_1 = 47.8$ and $k_4/k_1 = 1.0$ while the lower line corresponds to $k_3/k_1 = 1.0$ and $k_4/k_1 = 47.8$. Hence the values chosen for k_3/k_1 and k_4/k_1 cannot be determined by fitting the theory to the experimental data. However, the excellent fit to the experimental data indicates that the proposed mechanism is correct.

The independence of the conversion to the ratio

$$u = \frac{k_4/k_1}{k_4/k_1 + k_3/k_1} \qquad (23)$$

can be further illustrated as follows. Eqn. (20) can be written in terms of the extent conversion x by making the substitutions:

$$[HBr] = [HBr]_0 (1 - x) \qquad (24)$$

and

$$[Br_2] = \frac{1}{2} x [HBr]_0 \qquad (25)$$

The following differential equation in x then results:

$$\frac{dx}{dt} = q(1-x)\ 1 + \frac{[1+(1-u)aw(1-x)][\ 1-x+\frac{c}{2}x] + [\ b+uaw(1-x)][\ 1-x-\frac{c}{2}x]}{[1+b+aw(1-x)][1-x+\frac{c}{2}x\ ]}$$

$$= q(1-x)\left(1 + \frac{A'}{D'}\right) \qquad (26)$$

where $q = \epsilon_{HBr}I_o/NA$, $a = k_3/k_1 + k_4/k_1$, $b = k_2/k_1$, $c = k_8/k_5$ and $w = [HBr]_0/[CD_4]$. By substituting the known values of a, b, c and w in the above equation, assuming a conversion of 1% we find that A' can be written as

$$A' = 39.8 - 0.83u \qquad (27)$$

Note that in A' is the only place where u appears in the above equation. Hence varying u within its limits of from 0 to 1 produces at most only a 2% change in A'. D' can be evaluated to be 48.5 indicating that A'/D' is approximately equal to 0.82. Hence varying u within its limits only produces a 2% change in dx/dt.

The calculated $[Br_2]$, $[Br_2]/[HBr]$ and $[H_2]/[HD]$ (using equations (20) and (21)) for various $[HBr]/[CD_4]$ ratios are given in Table III and compared with those calculated using Eqns. (18) and (19). Note that at the end of a 10 minute experiment there is 7.2% less bromine in experiments with an $[HBr]/[CD_4]$ ratio of 0.03 than would be the case if reaction [8] did not contribute and 3.4% less bromine in experiments with an $[HBr]/[CD_4]$ ratio of 1.0. This corresponds in changes in $[H_2]/[HD]$ from time 0 of 6.6% and 3.5% respectively. This indicates that the effect of reaction [8] is greatest at low $[HBr]/[CD_4]$ ratios. We also note that for an $[HBr]/[CD_4]$ ratio of 1.0, the $[H_2]/[HD]$ ratio would decrease from its value for zero HBr conversion at t = 0 by 1.7% after 5 minutes and by 3.5% after 10 minutes. This predicted

1.7% change in the $[H_2]/[HD]$ due to conversion is of the order of our experimental error and hence was not observed experimentally. However, our experiments do show the predicted decrease of $[H_2]/[HD]$ with decreasing $[HBr]/[CD_4]$ at low $[HBr]/[CD_4]$ ratios. Since our experimental results where the $[HBr]/[CD_4]$ ratios vary from 0.3 to 1.0 agree so well with those at lower $[HBr]/[CD_4]$ ratios extrapolated to zero conversion, we conclude that the above corrections due to bromine molecule reactions are not important for $[HBr]/[CD_4]$ ratios from 0.3 to 1.0.

The difference between our results and those of Martin and Willard[4] can be explained by a similar calculation. Their net decomposition of HBr was approximately 10%.[4,11] We find that with this conversion the theory predicts that their $[H_2]/[HD]$ ratio would be 17.0 at an $[HBr]/[CD_4]$ ratio of 0.03 compared to their experimental value of 17.2 (determined from their least squares fit to their plot of $[H_2]/[HD]$ versus $[HBr]/[CD_4]$. The value of $[H_2]/[HD]$ extrapolated to zero conversion would be 26.3 compared to our experimental value of 26.4 (determined from our least squares fit to our data). Thus we conclude that the discrepancies between our results and those of Martin and Willard is due to their not having taken into account the HBr conversion effect at low $[HBr]/[CD_4]$ ratios.

c) Reaction [13]

If reaction [13] is included in the mechanism the following steady state expression for $[H_2]/[HD]$ is obtained:

$$\frac{[H_2]}{[HD]} = \left(\frac{[H_2]}{[HD]}\right)_0 + \frac{[HBr]}{[CD_4]}\left(\frac{k_4}{k_1} + \frac{k_3}{k_1}\right)\Bigg/\left(1 + \frac{k_{13}}{k_1}\frac{k_{14}}{k_{14} + k_{15}}\right) \quad (28)$$

where

$$\left(\frac{[H_2]}{[HD]}\right)_0 = \left(\frac{k_2}{k_1} + \frac{k_{13}}{k_1}\frac{k_{15}}{k_{14} + k_{15}}\right)\Bigg/\left(1 + \frac{k_{13}}{k_1}\frac{k_{14}}{k_{14} + k_{15}}\right) \quad (29)$$

In order to justify neglect of this reaction we must show that:

$$\frac{k_{13}}{k_1}\frac{k_{14}}{k_{14} + k_{15}} \ll 1 \quad (30)$$

For the reaction of T* with CD_4, Chou and Rowland[12] found that k_{13}/k_1 is a monotonically increasing function of energy with a value of less than 0.01 at 2288A increasing to 0.065 at 1849A. We will use the largest of these values for our analysis.

On the basis of transition state theory we expect k_{13}/k_1 to be similar for both the T* + CD_4 and H* + CD_4 systems. This is because the transition states leading to abstraction and exchange are the same and hence ratios between T* + CD_4 and H* + CD_4 would be the same for both abstraction and exchange. Also, recent theoretical calculations[13] indicate that k_{13}/k_1 should decrease as the mass of the attacking atom decreases.

The fraction

$$k_{14}/(k_{14} + k_{15}) \quad (31)$$

has been determined in our laboratories by independent experiments[14] and is 0.80 ± 0.05.

From Eq. (29) and these considerations we obtain, at 1849A:

$$\left(\frac{[H_2]}{[HD]}\right)_0 = \frac{k_2/k_1 + 0.012}{1.05} \quad (32)$$

Using this expression and Eq. (1) to determine A produces a value that differs by 5% from the one obtained from Eq. (3). This correction becomes less than 1% at 2288A. Since as mentioned above k_{13}/k_1 is expected to be smaller for the H* + CD_4 system than for the T* + CD_4 system, no correction has been applied for the contribution of reaction [13].

d) Reactions [10], [11], [16] and [17]

The above reactions were considered in (I) where CD_4 is replaced by H_2. For both H_2 and CD_4 consideration of activation energies indicates that [10] is faster than [11]. For the case of Br + H_2 k_{10} equals 2×10^{-3} $M^{-1}sec^{-1}$ whereas for Br + CD_4 it equals 3.8×10^{-3} $M^{-1}sec^{-1}$.[15] By similar agruments to those used in (I) we can show that $k_7/k_{10} > 10^4$ under all experimental conditions. Thus reactions [10] and [11] can be neglected

In reactions [16] and [17] the asterisk denotes translational excitation. As shown in (I) the Br + CD_4 relative energy is $(m_H/m_{HBr})^2(E - D_0^0)$ which ranges from 2.02×10^{-4} to 4.2×10^{-4} eV in our experiments. These values are small compared with average room temperature thermal energies of 3.9×10^{-2} eV and hence reaction [16] can be neglected with respect to [10].

Reaction [17] for DBr was considered in (I). There it was shown that reaction [17] is negligible compared to reaction [8]. The same arguments hold for HBr. Hence all bromine atom reactions except 3-body recombination can be neglected.

e) Reaction [12]

Fass[10] found k_{12}/k_3 to be 5.3 ± 0.04 independent of temperature and wavelength for temperatures from 300°K to 523°K and wavelengths from 1849A to 2480A. The $[Br_2]/[HBr]$ ratio at the end of an experiment with conversion c is approximately c/2 for small c; the average $[Br_2]/[HBr]$ ratio during the experiment is therefore approximately c/4. Taking into account the above rate constant ratio, the average ratio of H* reacting with Br_2 compared to H* reacting with HBr is 1.4c. Since c ranges from 0.005 to 0.01, reaction of H* with Br_2 amounts to only 0.6% to 1.4%. This effect is negligible within the accuracy of our experiments since varying c produced no significant change in the $[H_2]/[HD]$ ratio.

5.2.2 Consideration of CD_3H impurity

Since the CD_4 used in these experiments contained about 3.8% CD_3H impurity, reactions involving CD_3H must be considered in interpreting the experiments. The additional processes to be considered are as follows:

$$H^* + CD_3H \rightarrow HD + CD_2H \qquad [18]$$

$$H^* + CD_3H \rightarrow H_2 + CD_3 \qquad [19]$$

$$H^* + CD_3H \rightarrow H + CD_3H \qquad [20]$$

$$CD_2H + HBr \rightarrow CD_2H_2 + Br \qquad [21]$$

We have shown in the last section that reactions [8] through [17] can be neglected. Similar arguments hold for reactions similar to [9], [10], [13] and [16] where CD_4 is replaced by CD_3H. Consideration of reactions [0] - [7] and [18] - [21] gives rise

to the following steady state expression:

$$\frac{[H_2]}{[HD]} = \frac{1}{\left(1 + \frac{[CD_3H]k_{18}}{[CD_4]\,k_1}\right)}\left[\frac{k_2}{k_1} + \frac{[CD_3H]}{[CD_4]}\left(\frac{k_{19} + k_{20}}{k_1}\right) + \frac{[HBr]}{[CD_4]}\left(\frac{k_3}{k_1} + \frac{k_4}{k_1}\right)\right] \quad (33)$$

Again we expect a linear plot of $[H_2]/[HD]$ versus $[HBr]/[CD_4]$ with positive slope and intercept.

From the intercept of this plot we can see that the integral reaction yield A is:

$$A = \frac{\left(\frac{[HD]}{[H_2]}\right)_0}{\left(\frac{[HD]}{[H_2]}\right)_0\left[-\frac{[CD_3H]}{[CD_4]}\left(\frac{k_{19} + k_{20}}{k_1}\right)\right] + 1 + \frac{k_{18}}{k_1}\frac{[CD_3H]}{[CD_4]}} \quad (34)$$

To evaluate this expression we need values for k_{18}/k_1, k_{19}/k_1, k_{20}/k_1 and $[CD_3H]/[CD_4]$. Arguments based on probability considerations and neglect of isotope effects would lead one to expect $k_{18}/k_1 = 0.75$ and $k_{19}/k_1 = 0.25$. These are at least upper limits to the true values since statistical mechanical calculations for thermal reactions predicts k_{19}/k_1 to be even smaller than the above. Likewise we expect k_{20}/k_1 to be close to k_2/k_1 since k_{20}/k_2 should be close to unity and $k_{20}/k_1 = (k_{20}/k_2).(k_2/k_1)$. The impurity ratio $[CD_3H]/[CD_4]$ measured on the mass spectrometer was 0.038.

Using values of the rate constants listed above and Eq. (34) we find that neglect of the CD_3H impurity contributes less than 1% error at all wavelengths.

5.2.3 Determination of the Integral Reaction Yield

The integral reaction yield A was calculated from the experimental $([HD]/[H_2])_0$ using equation (3). The results for A are listed in Table I. A plot of A versus $E_1^{(0)}$ is shown in Fig. 3.

The error in A due to $([HD]/[H_2])_0$ was determined by taking the derivative of A with respect to $([HD]/[H_2])_0$ and multiplying it by the standard experimental error of $([HD]/[H_2])_0$. Other corrections were neglected.

As mentioned in section 5.1 it is energetically possible to form excited bromine atoms in the HBr photolysis. If excited bromine atoms are important, the measured A values would correspond at each wavelength, to contributions of two different initial laboratory energies, one being the value assumed in this paper and the other a value smaller than it by 0.45 eV due to the 0.457 eV spacing between the $^2P_{3/2}$ and $^2P_{1/2}$ levels. Due to the monotonically increasing nature of A versus initial laboratory energy, the A's reported in this paper for HBr photolysis are at the very least lower limits to the idealized values. Further experiments could either confirm or indicate the slight corrections due to the neglect of excited Br atoms. More extensive measurements on the fraction of such atoms as a function of wavelength could be used to refine our values of A.

Figure 3. Plot of $A = k_1/(k_1 + k_2)$ versus initial laboratory energy.

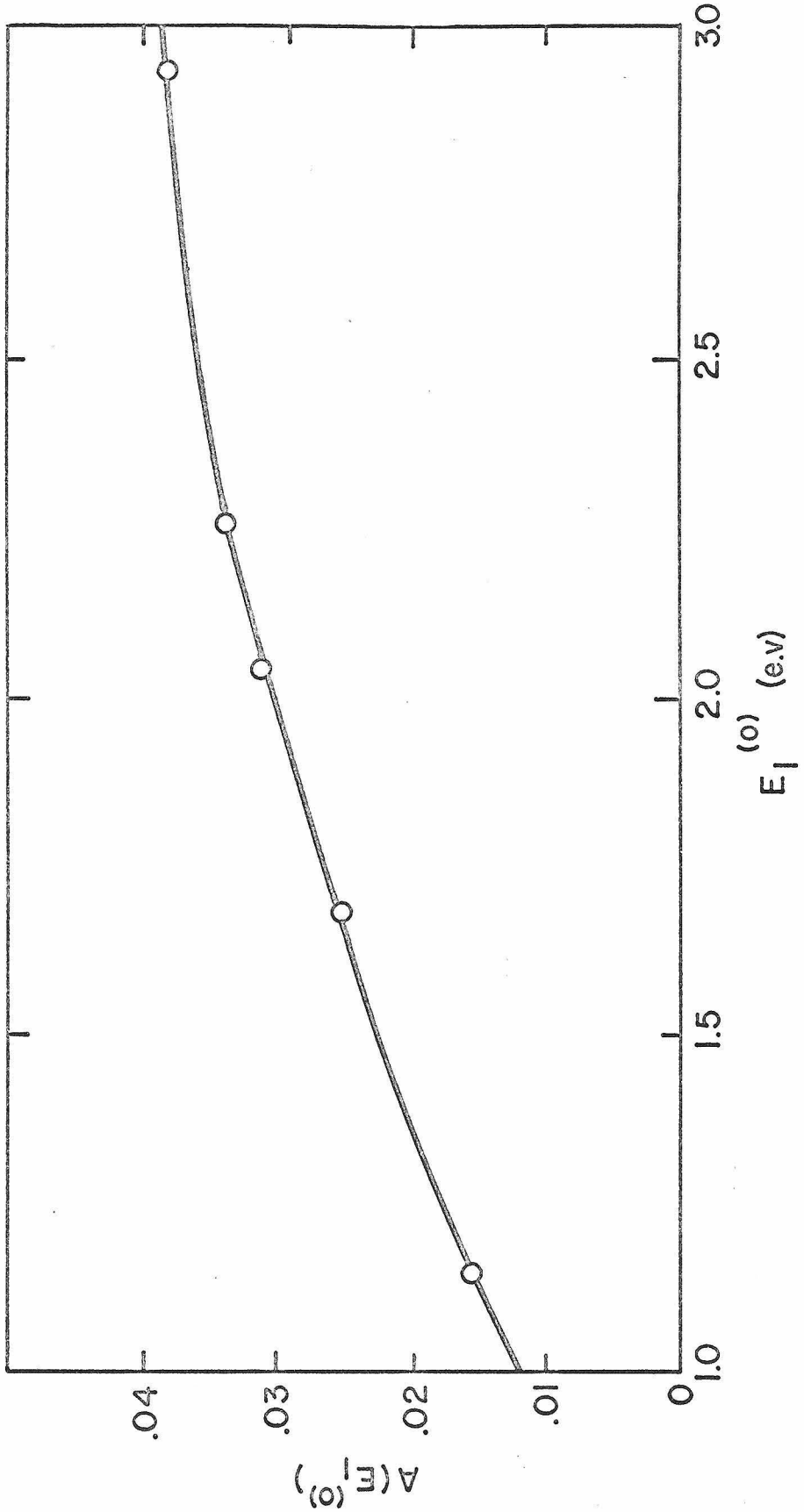
A(E_I^(o))
.4
.3
.2
.1
0
1.0
1.5
2.0
2.5
3.0
E_I^(o) (e.v)

6. DISCUSSION

6.1 Shape of $A(E_1^{(0)})$

The integral reaction yield A is a monotonically increasing function of the laboratory energy from 1.1 to 2.9 eV. Its slope is greater at low energies and appears to be leveling off at high energies.

The results for the H + CD_4 system can be compared qualitatively with those for the H + D_2 one.[16] The values of A for H + CD_4 are about an order of magnitude lower than those for H + D_2 at corresponding relative energies. This difference can be explained on the basis of the following arguments.

First, since the masses of H and D_2 are closer than those of H and CD_4 we expect a relatively more effective thermalization, due to elastic collisions, of H by D_2 than by CD_4. This would tend to make A smaller in the D_2 system than in the CD_4 system, the opposite of what is observed. However, as we will show in what follows, inelastic collisions are much more probable in the H + CD_4 system than in the H + D_2 one and this can account for the difference in the respective values of the integral reaction yields.

We will first consider inelastic collisions involving transfer of translational energy of the H atom to rotational energy of either the D_2 or CD_4. Since rotational relaxation times are in general much shorter than vibrational ones[17] rotational energy transfer is expected to be important compared to vibrational

transfer. There are no accurate theories to date covering the case where a large number of rotational levels are excited in a collision. However, approximate theories[18] indicate that if an interaction potential of the form $\exp(-\alpha R)$ is assumed, then the larger α's lead to larger transition probabilities between rotational states in collisions. In the above R is the internuclear distance and α is defined by:

$$\alpha = L^{-1}[m_C/(m_C + m_B)]\ (h/M^{1/2}k^{1/2}) \qquad (35)$$

where M is the reduced mass of the molecule, k is the oscillator force constant which is determined from spectroscopic data and m_B and m_C are the individual masses of the two atoms of the harmonic oscillator respectively. Hence, the larger the α the harder the collision between the atom and molecule. For the purpose of this discussion we will consider CD_4 to be a diatom D-CD_3 with the H atom colliding collinearly with the D. We may assume that the L's for D_2 and CD_4 are both 0.2Å.[19] This calculation leads to $\alpha_{D_2} = 0.26$ and $\alpha_{CD_4} = 0.44$. This indicates that CD_4 undergoes harder collisions with an H atom than does D_2 and therefore that its rotational transition probability should be greater. Also, the spacing of the rotational levels is related to translational rotational energy transfer; the closer the spacing, the more likely a transition.[18] Since CD_4 has more closely spaced rotational levels (B_e = 2.05 cm^{-1} [20]) available than D_2 (B_e = 30.43 cm^{-1} [21]) it should undergo more efficient rotational energy transfer. Finally, experimental relaxation times for D_2 and CD_4 determined by accoustical methods

verify the above assumptions. For D_2 the rotational relaxation time has been measured as 2.0×10^{-8} sec[22] at 273°K while for CD_4 this relaxation time is of the order of 1×10^{-9} sec[23] at 314°K. These relaxation times lead to energy transfer collision numbers Z_{rot} of 210 for D_2 and 14-17 for CD_4. Care is needed in applying the above argument since we are comparing $D_2 + D_2$ collisions with $CD_4 + CD_4$ ones and not $H + D_2$ collisions with $H + CD_4$ ones. However, it appears from the combined arguments above that the probability of inelastic collisions involving rotational energy transfer is greater for an H atom colliding with CD_4 than with D_2 by more than an order of magnitude.

To treat inelastic collisions involving transfer of translational energy of the H atom to vibrational energy of either the D_2 or CD_4 an approximate theory of Secrest and Johnson[24] can be used in which they consider only collinear collisions of the type A + BC where A, B and C are atoms. They assume an interaction potential between A and the harmonic oscillator BC of the form $V(x-y) = A_o \exp[-\alpha(x-y)]$. Here x and y are reduced coordinates where x is the distance between an atom of mass $m = m_A m_C / m_B(m_A+m_B+m_C)$ and the equilibrium position of the oscillator and y is the distance of a harmonic oscillator of unit mass from its equilibrium position. m_A, m_B and m_C are the masses of the colliding atom and the individual masses of the two atoms of the harmonic oscillator respectively, A_o is a constant having no effect on the results and α is as defined by Eq. (35) in the discussion of translational to rotational energy transfer above. Again, we will consider CD_4 to be a diatom

D-CD_3 with the H atom colliding collinearly with the D. The m's for D_2 and CD_4 are 0.20 and 0.43 respectively and the α's have been calculated above to be $\alpha_{D_2} = 0.26$ and $\alpha_{CD_4} = 0.44$.

Transition probabilities were calculated for each experimental energy using the method of Secrest and Johnson.[25] The probabilities that the molecule in question (either D_2 or CD_4) will be excited to a higher vibrational state are shown in Table IV. As can be seen, for an H atom colliding with CD_4 the probability of excitation is almost unity at all relative energies except 1.1 eV while for an H atom colliding with D_2 the probabilities range from 0.12 at 1.1 eV relative energy to 0.96 at 2.9 eV relative energy. Hence the probability of inelastic collisions involving vibrational energy transfer is greater for an H atom with a given initial energy colliding with CD_4 than with D_2.

The above arguments indicate that inelastic collisions are more important in CD_4 than in D_2 and that they may provide an explanation for the order of magnitude difference in the integral reaction yields for the two systems.

In support of the above assumptions, Rosenberg and Wolfgang[26] and Root and Rowland,[27] using experimental results interpreted by the Estrup-Wolfgang kinetic theory, have deduced that inelastic collisions are important in the overall mechanism for tritium recoil reactions with CD_4. Also, Biordi, Rouseau and Mains[28] have argued that in the flash photolysis of HI in the presence of deuterated hydrocarbons, collisions between hot hydrogen atoms and hydrocarbon molecules (C_2D_6, C_3D_8, n-C_4D_{10}) are quite inelastic

in the energy range from 0.8 to 2.2 eV.

An additional comparison of interest is that between the integral reaction yields of the present H + CD_4 system and those of the D + CH_4 system investigated by Martin and Willard[4] at 1849Å. These authors list their intercept value for a plot of $[D_2]/[HD]$ versus $[DBr]/[CD_4]$ as 5.0. From this we can calculate an integral reaction yield of 0.166. Our result at the same relative energy in the H + CD_4 system is 0.0381 which is 4.3 times smaller than their value. A small isotope effect in this direction is expected but not as great as that observed. For example, the integral reaction yield for D + H_2 at a relative energy of 1.4 eV is 1.4 times greater than the integral reaction yield for H + D_2 at the same relative energy.[1,16] Martin and Willard did their DBr-CH_4 photolyses at high DBr conversions (5-10%). In section 5.2 we showed that their HBr-CD_4 results done at high conversions were in error and hence it is possible that their DBr-CD_4 results have a similar error. If such an error exists it would lower the integral reaction yield making it more compatible with the H + CD_4 one. However, since their experiments were done at $[HBr]/[CD_4]$ ratios from 0.3 to 1.5 we do not expect the error for DBr-CH_4 to be as great as in the HBr-CD_4 experiments done at $[HBr]/[CD_4]$ ratios from 0.03 to 0.1. Nevertheless, it would be worthwhile to repeat their experiments taking into account the conversion effect and to determine how large an error is involved.

If their experimental error is assumed to be small, an explanation of the difference in the integral reaction yields of

$H + CD_4$ and $D + CH_4$ is needed. To provide this explanation we will first consider the effects of elastic collisions. The average energy lost by a moving sphere in an elastic collision with a sphere initially at rest is

$$f = \frac{2m_A m_B}{(m_A + m_B)^2} \tag{36}$$

Therefore, for the elastic collisions between $H + CD_4$ and $D + CH_4$, the f's are 0.0913 and 0.197 respectively. Hence we expect a more effective thermalization, due to elastic collisions, of D by CH_4 than of H by CD_4. This would tend to make A smaller in the $D + CH_4$ system, opposite to what is observed. Secondly, the effect of inelastic collisions in the $D + CH_4$ system can be examined as was done in the $H + CD_4$ and $H + D_2$ ones. For $D + CH_4$ the α, calculated from Eq. (35) assuming $L = 0.2\text{Å}$, is 0.52 compared to 0.44 for $H + CD_4$. This indicates that CH_4 should undergo harder collisions with a D atom than CD_4 undergoes with an H atom. However, this effect is compensated for by the closer spacing of vibrational levels in CD_4 than in CH_4 leading to greater probability of translational to vibrational energy transfer in $H + CD_4$ collisions than in $D + CH_4$ ones. However, Cottrell and Matheson[29] have measured vibrational relaxation times in CD_4 and CH_4 by the ultrasonic method and found that $\tau_{CD_4}/\tau_{CH_4} = 1.9$ at 298°K. This indicates that energy transfer is more efficient in $CH_4 + CH_4$ collisions than in $CD_4 + CD_4$ ones. They explained this on the basis of translational to rotational energy transfer. They argue that since CD_4 has a greater moment of inertia than CH_4

($I_{CD_4}/I_{CH_4} = 1.98$) it will undergo less efficient translational to rotational energy transfer than will CH_4. They conclude that the process they observe is the relaxation vibration → rotation → translation and that the second process is slower for CD_4 than for CH_4 making the overall relaxation time longer. If this trend holds for H + CD_4 and D + CH_4 collisions it could lead to more inelastic collisions in D + CH_4 making A smaller in this system. This is again opposite to what is observed. Hence, on the basis of these arguments and observations it does not seem likely that the observed differences in integral reaction yields between H + CD_4 and D + CH_4 are due to a more effective thermalization of the atoms in the former than in the latter.

Finally, we must consider whether these differences can be due to differences in the reactive cross sections of these systems. We can make a comparison with the H + D_2 and D + H_2 results to get an idea of the isotope effect to be expected. The cross section for the D + H_2 system is approximately 2.5 times greater at the same relative energy (0.7 to 1.1 eV) than for H + D_2[30] whereas the ratio of the corresponding integral reaction yields is about 1.4. Hence, this difference, although in the right direction, does not seem sufficient to explain the difference in integral reaction yields in the H + CD_4 and D + CH_4 systems. Hence, we are unable to adequately explain the differences in integral reaction yields of H + CD_4 and D + CH_4 on the basis of these arguments. However, further experiments on D + CH_4 are needed before any definite statement as to discrepancies between

the H + CD_4 and D + CH_4 systems can be made.

It was not experimentally possible because of low HD yields to determine the laboratory energy at which the integral reaction yield goes to zero. However, it is still interesting to compare the initial relative energy distribution function for H + CD_4 with D + H_2 to see what effect the different pairs of masses has on the width of this function. As in (I) the relative energy distribution function is given by

$$f(E) = \frac{1}{\mu v_1^*}\left(\frac{m_2}{\pi kT}\right)^{1/2}\left[\exp\left[-\frac{m_2}{kT}(v_1^* - v)^2\right] - \exp\left[-\frac{m_2}{kT}(v_1^* + v)^2\right]\right] \quad (37)$$

where μ is the reduced mass of the colliding system, m_2 is the mass of the target molecule, v_1^* is the initial laboratory velocity of the atoms, v is the relative velocity of the atom with respect to the molecule, k is the Boltzmann constant and T is the absolute temperature. The corresponding width as derived in (I) is:

$$\Delta E \sim 2\mu(6kTE_1^*/m_1m_2)^{1/2} \quad (38)$$

where E_1^* is the initial laboratory energy of the atoms. Note that the product of the masses of the atom and molecule appears in the denominator. Hence as the mass of the molecule becomes larger the width of the relative energy distribution becomes narrower for a given initial laboratory velocity. For example, for a laboratory energy E_1^* = 1.5 eV, E equals 0.39 eV for the H + D_2 system and 0.20 eV for the H + CD_4 system, and it is 0.48 eV for the D + H_2 system. This narrower distribution for H + CD_4 should make the determination of the threshold energy for this system easier than for D + H_2 and also helps in simplifying the extraction of reaction

cross sections from experimental integral reaction yield data as is discussed in the next section.

6.2 Reaction cross section from integral reaction yield

In this section we discuss how the cross section of reaction [1] is related to the measured integral reaction yields.

6.2.1. Boltzmann Equation

For the HBr-CD_4 system the behavior of the entire photolysis system can be described by a steady-state Boltzmann equation. In analogy to the DBr-H_2 system described in (I) we can write this equation as:

$$R_0 \phi_{v_H^*}(v_H) - K_t(v_H) G_{v_H^*}(v_H) + \int_{v_H'} H(v_H', v_H) G_{v_H^*}(v_H')\, dv_H = 0 \qquad (39)$$

In the above R_0 is the rate of initial H atom production due to photolysis. $\phi_{v_H^*}(v_H)$ is the normalized initial distribution function of H atom laboratory velocities. This is a narrow function peaked at v_H^* as indicated by our notation. $G_{v_H^*}(v_H)dv_H$ is the concentration of H atoms under steady-state photolysis conditions in the laboratory velocity range v_H to $v_H + dv_H$. $K_t(v_H)$ is defined as:

$$K_t = K^{CD_4} + K^{HBr} \qquad (40)$$

$$K^{CD_4} = K_R^{CD_4} + K_{NR}^{CD_4} \qquad (41)$$

$$K^{HBr} = K_R^{HBr} + K_{NR}^{HBr} \qquad (42)$$

$$K_R^{CD_4} = [CD_4]\int \phi_T^{CD_4}(v_H, v)\ v\ S_R^{CD_4}(v)\ dv \tag{43}$$

$$S_R^{CD_4} = \sum_i g_i^{CD_4}\ S_R^{CD_4,i} \tag{44}$$

$$K_{NR}^{CD_4} = [CD_4]\int \phi_T^{CD_4}(v_H, v)\ v\ S_{NR}^{CD_4}(v)\ dv \tag{45}$$

$$S_{NR}^{CD_4} = \sum_i g_i^{CD_4}\ S_{NR}^{CD_4,i} \tag{46}$$

$$K_R^{HBr} = [HBr]\int \phi_T^{HBr}(v_H, v')\ v'\ S_R^{HBr}(v')\ dv' \tag{47}$$

$$S_R^{HBr} = \sum_i g_i^{HBr}\ S_R^{HBr,i} \tag{48}$$

$$K_{NR}^{HBr} = [HBr]\int \phi_T^{HBr}(v_H, v')\ v'\ S_{NR}^{HBr}(v')\ dv' \tag{49}$$

$$S_{NR}^{HBr} = \sum_i g_i^{HBr,i} \tag{50}$$

In the above equations v is the relative velocity of H and CD_4 and v' the relative velocity of H and HBr. $\phi_T^{CD_4}$ is the distribution function of H-CD_4 relative velocities for H atoms with a laboratory velocity v_H and CD_4 molecules with a Boltzmann distribution of laboratory velocities and ϕ_T^{HBr} is a similar distribution function for H-HBr. $S_R^{CD_4}(v)$ is the reactive cross section for H-CD_4 averaged over internal states at temperature T and $S_{NR}^{CD_4}(v)$ is the non-reactive cross section averaged over internal states. S_R^{HBr} and S_{NR}^{HBr} are similarly the reactive and non-reactive cross sections for H-HBr averaged over the internal states of HBr. The $g_i^{CD_4}$ and g_i^{HBr} are the distribution functions for the internal states of CD_4 and HBr respectively. In applying Eq. (41) the assumption is made that thermalization of H by HBr is negligible with respect to the other processes and hence K_{NR}^{HBr} is set equal

to zero. This is valid because the masses of H and CD_4 are closer than those of H and HBr. Finally:

$$H(v'_H, v_H) = \frac{[CD_4]}{2} \int_{v_{CD_4}, \chi, \eta} \phi_T^{CD_4}(v'_{CD_4}) \sum_i g_i \sum_f v'_{if} \sigma_{i-f}^{CD_4}(v'_{if}, \chi, \eta) \left| \frac{\partial \cos \gamma_{if}}{\partial v_H} \right| \sin\chi \, dv'_{CD_4} \, d\chi \, d\eta \qquad (51)$$

where v'_{CD_4} is the laboratory velocity of CD_4 before collision, v'_{if} is the relative velocity vector of H and CD_4, χ and η are direction angles of this vector after collision and γ_{if} is the angle between v'_H and v'_{CD_4} before collision. The quantity $\sigma_{i\,f}^{CD_4}(v'_{if}, \chi, \eta)$ is the differential non-reactive cross section for the reaction

$$H + CD_4(i) \rightarrow H + CD_4(f)$$

in which the internal state of the two particle system changes from i to f, $\phi_T^{CD_4}(v'_{CD_4})$ is the Maxwell Boltzmann distribution function of CD_4 velocities in laboratory coordinates and g_i is the probability of an initial internal state i of CD_4. The independent variables in the above expression are v_{CD_4}, χ, η, v_H and ΔE_{if}, the change in internal energy of the CD_4. The relative velocity v' and the angle γ depend on these variables and hence on the initial and final states of the CD_4 molecule.

The physical interpretation of Eq. (39) can be explained very simply. The first term gives the rate of production of H atoms in the velocity range v_H to $v_H + dv_H$ directly from the photolysis source. The second represents their rate of removal from that

velocity range due to all collisions with CD_4 and reactive collisions with HBr. The third term represents the rate of production of H atoms in the velocity range v_H to $v_H + dv_H$ as a result of non-reactive collisions of H atoms at all other velocities v_H' with CD_4 molecules. Under steady-state conditions, the net rate of production of H atoms in any given velocity range must vanish.

6.2.2. Relation of $A(v_H^*)$ and the reaction cross section

In terms of the above quantities we can write $A(v_H^*)$ as:

$$A(v_H^*) = \frac{1}{R_o}\int K_R^{CD_4}(v_H)\, G_{v_H^*}(v_H)\, dv_H \qquad (52)$$

where $K_R^{CD_4}$ is defined by Eq. (43).

It can be shown that the Boltzmann equation given above can be reexpressed in terms of $A(v_H^*)$ as[31]

$$K_R^{CD_4}(v_H) - K_t(v_H)A(v_H) + \int H(v_H, v_H')\, A(v_H')\, dv_H' = 0 \qquad (53)$$

In the limit of dilute [HBr]

$$K_t(v_H) = K_R^{CD_4} + K_{NR}^{CD_4}$$

Hence from equation (53) we obtain $K_R^{CD_4}$ as :

$$K_R^{CD_4}(v_H) = \frac{K_{NR}^{CD_4}A(v_H) - \int H(v_H, v_H')\, A(v_H')\, dv_H}{1 - A(v_H)} \qquad (54)$$

$S_R^{CD_4}(v)$ can then be evaluated from a knowledge of the $\sigma_{NR}^{CD_4}$ (which suffices to determine both $K_{NR}^{CD_4}(v_H)$ and $H(v_H, v_H')$ in the above expression). Indeed it has been shown[31] that a correct procedure to use is as follows. The function

$$u^{CD_4}(v,T) = v^2 S_R^{CD_4}(v) \tag{55}$$

satisfies the diffusion equation:

$$\frac{\partial u^{CD_4}}{\partial T} = - \frac{k}{2m_{CD_4}} \frac{\partial^2 u^{CD_4}}{\partial v^2} \tag{56}$$

with the initial condition:

$$u^{CD_4}(v,0) = \frac{v}{[CD_4]} K_R^{CD_4}(v) \tag{57}$$

Therefore, integrating Eq. (56) numerically furnishes u(v,T) and therefore $S_R(v)$.

Thus $S_R^{CD_4}(v)$ is completely determined by a knowledge of $\sigma_{NR}^{CD_4}$ and the experimentally known $A(v_H)$. The σ_{NR} are not known but may be estimated from approximate model calculations or independent experiments.

6.3. Summary

In summary, a photochemical method was used to obtain the integral reaction yield $A(E_1^{(0)})$ for the H + CD_4 system. It was found that $A(E_1^{(0)})$ is a monotonically increasing function of laboratory energy in the range from 1.1 to 3 eV. The $A(E_1^{(0)})$'s for the H + CD_4 system are an order of magnitude lower than for the H + D_2 system for corresponding energies. This difference was attributed to the greater probability of inelastic collisions occuring in the H + CD_4 system than in the H + D_2 one. Finally, the relation of the integral reaction yield to the cross section was given and a method indicated of how in principle one can be

calculated from the other.

APPENDIX

The differential equations to be solved to obtain $[H_2]$ and $[HD]$ as a function of time are as follows:

$$\frac{d[H_2]}{dt} = \frac{\epsilon_{HBr} I_o}{NA} [HBr] \frac{\frac{k_3}{k_1}[HBr] + \frac{\frac{k_2}{k_1}[CD_4] + \frac{k_4}{k_1}[HBr] + [HBr]}{[HBr] + k_8/k_5[Br_2]}}{\frac{k_1 + k_2}{k_1}[CD_4] + \frac{k_3 + k_4}{k_1}[HBr]} \quad (58)$$

$$\frac{d[HD]}{dt} = \frac{\epsilon_{HBr} I_o}{NA} [HBr] \frac{[CD_4]}{\frac{k_1 + k_2}{k_1}[CD_4] + \frac{k_3 + k_4}{k_1}[HBr]} \quad (59)$$

where the symbols are as defined in the text. These equations were solved numerically in conjunction with Eqns. (19) and (20) in the text to obtain the theoretical $[H_2]/[HD]$ ratios listed in Table III.

TABLE II. Comparison of Theory and Experiment for a Fixed [HBr]/[CD_4] Ratio of 0.075.

Photolysis time (min.)	Experimental Conversion (%)	$\frac{[H_2]}{[HD]}$ exp.	$k_3/k_1 = 47.8$, $k_4/k_1 = 1.0$: theoretical conversion (%)	$\frac{[H_2]}{[HD]}$ calc.	$k_3/k_1 = 25.0$, $k_4/k_1 = 23.7$: theoretical conversion (%)	$\frac{[H_2]}{[HD]}$ calc.	$k_3/k_1 = 1.00$, $k_4/k_1 = 17.8$: theoretical conversion (%)	$\frac{[H_2]}{[HD]}$ calc.
5	0.62	39.8	0.62	40.3	0.62	40.2	0.62	40.2
10	1.2	38.8	1.2	39.2	1.2	39.1	[illegible]	39.0
15	1.7	37.6	1.7	38.2	1.7	38.1	[illegible]	37.9
20	2.3	37.2	2.3	37.3	2.3	37.1	2.3	36.9
25	2.8	36.1	2.8	36.4	2.8	36.2	2.8	36.0
30	3.3	35.5	3.3	35.6	3.3	35.4	3.3	35.2

TABLE III. Results of Calculations of Bromine Concentration as a Function of Conversion and $[HBr]/[CD_4]$

Photolysis Time (min.)	Extent HBr Conversion (%)	Eq. (17) $[Br_2]$ ($\times 10^{-4}$ M)	Eq. (18) $\frac{[Br_2]}{[HBr]}$	$[HBr]/[CD_4]$			
				0.03	0.1	0.3	1.0
				$[Br_2]$ ($\times 10^{-4}$ M)			
0	0.00	0.0000	0.00000	0.0000	0.0000	0.0000	0.0000
1	0.14	0.0387	0.00070	0.0380	0.0380	0.0382	0.0384
2	0.28	0.0775	0.00140	0.0756	0.0760	0.0760	0.0766
3	0.42	0.116	0.00211	0.112	0.113	0.113	0.114
4	0.56	0.155	0.00281	0.149	0.149	0.150	0.152
5	0.70	0.194	0.00351	0.184	0.184	0.186	0.188
6	0.84	0.232	0.00422	0.219	0.221	0.223	0.225
7	0.98	0.269	0.00493	0.255	0.256	0.258	0.261
8	1.1	0.308	0.00563	0.289	0.291	0.293	0.298
9	1.2	0.345	0.00634	0.322	0.325	0.328	0.336
10	1.4	0.384	0.00705	0.356	0.360	0.363	0.370

TABLE III (continued)

Photolysis Time (min.)	[HBr]/[CD_4]							
	0.03	0.1	0.3	1.0	0.03	0.1	0.3	1.0
	[Br_2]/[HBr]				[H_2]/[HD]			
0	0.00000	0.00000	0.00000	0.00000	39.4	42.8	52.6	86.7
1	0.00069	0.00069	0.00069	0.00069	39.1	42.6	52.3	86.3
2	0.00137	0.00137	0.00138	0.00139	38.9	42.3	52.0	86.3
3	0.00204	0.00204	0.00206	0.00207	38.6	42.0	51.7	85.7
4	0.00271	0.00271	0.00273	0.00276	38.3	41.7	51.4	85.4
5	0.00335	0.00335	0.00340	0.00342	38.1	41.4	51.1	85.1
6	0.00401	0.00402	0.00406	0.00412	37.8	41.2	50.9	84.7
7	0.00465	0.00467	0.00471	0.00479	37.5	40.9	50.6	84.5
8	0.00529	0.00531	0.00537	0.00546	37.3	40.7	50.3	84.2
9	0.00591	0.00594	0.00601	0.00607	37.1	40.4	50.1	83.9
10	0.00654	0.00657	0.00665	0.00680	36.8	40.2	49.8	83.6

REFERENCES

1. M. A. Eliason and J. O. Hirshfelder, J. Chem. Phys., 30, 1426 (1959).
2. J. M. White, D. R. Davis, J. A. Betts and A. Kuppermann, forthcoming (Paper I in this thesis).
3. R. J. Carter, W. H. Hamill and R. R. Williams, Jr., J. Am. Chem. Soc., 77, 6457 (1955).
4. R. M. Martin and J. E. Willard, J. Chem. Phys., 40, 3007 (1964).
5. This lamp was built by William B. DeMore at the Jet Propulsion Laboratory in Pasadena. We wish to thank him for permitting us to use it.
6. R. S. Mullikan, J. Chem. Phys., 8, 382 (1940).
7. (a) D. J. LeRoy, Disc. Faraday Soc., 14, 120 (1953); (b) M. R. Berlie and D. J. LeRoy, Can. J. Chem., 32, 650 (1954).
8. G. B. Skinner and G. H. Ringrose, J. Chem. Phys., 43, 4129 (1965).
9. J. B. Steiner, Proc. Roy. Soc., 173A, 531 (1939).
10. R. A. Fass, J. Phys. Chem., 74, 984 (1970).
11. R. M. Martin, Ph.D. Thesis, University of Wisconsin, 1964.
12. C. C. Chou and F. S. Rowland, J. Chem. Phys., 50, 2763 (1969).
13. P. J. Kuntz, E. M. Nemeth, J. C. Polanyi and W. H. Wong, J. Chem. Phys., 52, 4654 (1970).
14. (a) G. B. Kistiakowsky and E. R. Van Artsdalan, J. Chem. Phys., 12, 469 (1944); (b) G. C. Fettis, J. H. Knox and A. F. Trotman-Dickenson, J. Chem. Soc., 4177 (1960).

15. A. Persky and A. Kuppermann, forthcoming (Paper I).

16. A. Persky and A. Kuppermann, forthcoming (Paper II).

17. T. L. Cottrell and J. C. McCoubrey, Molecular Energy Transfer in Gases, (Butterworths, London, 1961) pp. 74-124.

18. K. Takanyanagi, Prog. Theoret. Phys. (Kyoto) Supple., 25, 1 (1963).

19. K. F. Herzfeld and T. A. Litovitz, Absorption and Dispersion of Ultrasonic Waves (Academic Press Inc., New York, 1959).

20. G. Herzberg, Infrared and Raman Spectra, (D. Van Nostrand Co., Inc., New York, 1945) p. 306.

21. G. Herzberg, Molecular Spectra and Molecular Structure, I Spectra of Diatomic Molecules (D. Van Nostrand Co., Inc., New York, 1950) p. 534.

22. E. S. Steward and J. L. Steward, J. Acoust. Soc. Amer. 24, 194 (1952).

23. B. T. Kelley, J. Acoust. Soc. Amer., 29, 1005 (1957).

24. D. Secrest and B. R. Johnson, J. Chem. Phys., 45, 4556 (1966).

25. We wish to thank Albert F. Wagner for performing this calculation.

26. A. H. Rosenberg and R. Wolfgang, J. Chem. Phys., 41, 2159 (1964).

27. J. W. Root and F. S. Rowland, J. Chem. Phys., 38, 2030 (1963).

28. J. C. Biodi, Y. Rouseau and G. J. Mains, J. Chem. Phys., 49 2642 (1968).

29. F. L. Cottrell and A. J. Matheson, Trans. Faraday Soc., 58, 2336 (1962).

30. A. Kuppermann, forthcoming.

31. A. Kuppermann and R. N. Porter, forthcoming.

6. CONCLUSION

Mixtures of $DBr-H_2$, $DI-H_2$ and $HBr-CD_4$ were photolyzed with monochromatic light. Thirteen different wavelengths were used in the $DBr-H_2$, $DI-H_2$ systems yielding deuterium atoms with initial laboratory energies ranging from 0.6 to 3.0 eV. By photolyzing analogous DX-He mixtures (where X = I or Br) we were able to obtain the integral reaction yield

$$A_{H + D_2}(\lambda) = \frac{k_1(\lambda)}{k_1(\lambda) + k_2(\lambda)}$$

where $k_1(\lambda)$ and $k_2(\lambda)$ are effective bimolecular rate coefficients for the processes:

$$D^* + H_2 \rightarrow DH + H \qquad [1]$$

$$D^* + H_2 \rightarrow D + H_2 \qquad [2]$$

These processes describe rates of reaction and thermalization which accompany the injection of monoenergetic atoms into thermal H_2 gas. We were able to show that results obtained using DBr as the source of monoenergetic atoms were consistent with those obtained using DI.

For the $HBr-CD_4$ system, photolyses were performed at 5 wavelengths giving H atoms with laboratory energies ranging from 1.15 to 3.0 eV. By analyzing the results of these photolyses we were able to calculate the integral reaction yield

$$A_{H + CD_4}(\lambda) = \frac{k_1'(\lambda)}{k_1'(\lambda) + k_2'(\lambda)}$$

where $k_1'(\lambda)$ and $k_2'(\lambda)$ correspond to the processes:

$$H^* + CD_4 \rightarrow HD + CD_3 \qquad [1']$$

$$H^* + CD_4 \rightarrow H + CD_4 \qquad [2']$$

For both the $D + H_2$ and $H + CD_4$ systems we were able to show that the integral reaction yield is a monotonically increasing function of energy over the energy ranges scanned. For $D + H_2$ A ranged from 0 at about 0.6 eV to 0.66 at 2.86 eV initial laboratory energy while for $H + CD_4$ A ranged from 0.015 at 1.15 eV to 0.040 at 3.0 eV initial laboratory energy. If we assume, in a first approximation, that the H_2 and CD_4 targets are stationary, the corresponding ranges of initial relative energies are 0.3 eV to 1.43 eV for $D + H_2$ and 1.15 eV to 3.0 eV for $H + CD_4$. These results show that there is almost an order of magnitude difference between the integral reaction yields for these two reactions at the same initial relative energies. We were also able to compare the $H + CD_4$ results with some for $H + D_2$ where there was likewise an order of magnitude difference favoring the latter. This difference was attributed to the greater probability of inelastic collisions occuring in the $H + CD_4$ system than in the $H + D_2$ one.

The relative initial velocity distribution functions between the atoms (D or H) and the molecules (H_2 or CD_4) were examined. The relative velocities were found to follow a distribution function of the form:

$$f_{v_1^*}(E)dE = \frac{1}{\mu v_1^*}\left(\frac{m_2}{2\pi kT}\right)^{1/2}\left[\exp - \frac{m_2}{2kT}(v_1^* - v)^2 - \exp - \frac{m_2}{2kT}(v_1^* + v)^2\right]dE$$

where m_2 is the mass of the molecule, v_1^* is the initial laboratory

velocity with which the atom is formed, v is the relative velocity, k is the Boltzmann constant and T is the absolute temperature. This distribution function has a width of the order of

$$E \sim 2\mu(6kTE_1/m_1m_2)^{1/2}$$

where μ is the reduced mass, E_1 is the laboratory energy of the atom and m_1 is the mass of the atom. This distribution function is narrower when the mass of the molecule is large compared to that of the atom which facilitates interpretation of the H + CD_4 results relative to the D + H_2 ones. We were able to show that the initial nominal phenomenological relative energy at which the experimental integral reaction yield for the D + H_2 system went to zero could differ by as much as 0.1 eV from the equivalent phenomenological threshold relative energy for the reactive cross section because of this spread.

Finally we were able to show how reaction cross sections can be extracted from the experimental integral reaction yield using a steady state Boltzmann equation. This determination depends on a knowledge of the differential non-reactive cross sections. Obtaining these non-reactive cross sections theoretically is easier for D + H_2 than for H + CD_4 and therefore a complete analysis of the D + H_2 system will be completed sooner than the one for H + CD_4.

In the course of the D + H_2 experiments additional information to that described above was obtained. From additional DX-HX-He experiments we were able to measure the abstraction fraction a defined as:

$$a = \frac{k_6}{k_6 + k_7}$$

where k_6 and k_7 correspond to the processes:

$$H + DX \rightarrow HD + X \qquad (6)$$

$$H + DX \rightarrow HX + D \qquad (7)$$

The results were a(DI) = 0.97 $\pm$ 0.05 and a(DBr) = 0.99 $\pm$ 0.03. In the course of doing these experiments, accurate extinction coefficients were measured for DI and HI in the wavelength range from 2900Å - 3400Å and for DBr and HBr in the wavelength region from 2100Å - 2600Å.

Finally, using the integral reaction yield versus energy plot for D + H_2 plus additional DI-H_2, DI-He experiments we were able to determine the fraction f of iodine atoms produced in the excited $^2P_{1/2}$ state in the photolysis of DI at 4 wavelengths. The results are: f(2800Å) = -0.08 $\pm$ 0.27, f(2537Å) = 0.46 $\pm$ 0.05 f(2400Å) = 0.60 $\pm$ 0.07 and f(2138Å) = 0.33 $\pm$ 0.1.

APPENDIX A

LIGHT SOURCES

1. Monochromators

1.1 Photolysis monochromator

A Bausch and Lomb high intensity monochromator with a model 33-86-01 ultraviolet grating and quartz optics was used to select a narrow band of radiation from continuous spectra lamps for a photolysis experiment. The grating is plane with 2700 groves/mm and is blazed for 2500A; the instrument blaze efficiency is approximately 30%. The dispersion of the monochromator is 32 Angstroms per millimeter at the exit slit. The monochromator had adjustable slits at both its entrance and exit allowing for band-passes from 1Å to 190Å. The instrument without final collimator had an f/3.5 divergent exit beam.

It was found that a factor of 2 more intensity could be obtained for a given monochromator setting if a 1-inch diameter, 2-inch focal length quartz lens was used to replace the Bausch and Lomb Model 33-80-51 achromatic condenser lens. The 1-inch lens was mounted so that it could be adjusted to give maximum intensity for a given monochromator setting.

After about 2 years continuous use the amount of scattered light in the monochromator had increased by approximately 10 times its original amount. At this point the monochromator was returned to Bausch and Lomb to be renewed, which involved replacing the grating and blackening the inside of the housing.

The wavelength dial of the monochromator was calibrated using a low pressure mercury lamp.

1.2 Monochromators for Testing and Calibrating

1.2.1 Jarrell Ash Scanning Monochromator

A Jarrell Ash 1/2 meter Ebert high resolution scanning monochromator with photomultiplier detector was used to scan the output of the light sources. It has a grating blazed for 5000Å and a resolution of 0.5Å. It used a RCA IP28 phototube which had a gain of 1.25×10^6 at 1.00 Kv. The photocathode of the tube is S5 (Cs-Sb) and its spectral response is shown in Figure 8. The monochromator wavelength scale was calibrated using a low pressure mercury lamp. The output of the Bausch and Lomb monochromator was scanned with the Jarrell Ash monochromator to calibrate the peak wavelength, to determine the width of the peak at half height and to check for scattered light coming through the monochromator. The Jarrell Ash instrument was used in preference to the McPherson described in the next section because it was more portable and also had a greater range of sensitivity. Its resolution is higher than that of the Bausch and Lomb one and could conveniently be used for the purposes above.

1.2.2 McPherson Scanning Monochromator

A McPherson Model 235 ultraviolet scanning monochromator was also used to scan some of our light sources. This instrument proved most useful in the wavelength region from 1800Å to 2200Å where the sensitivity of the phototube on the Jarrell Ash

monochromator began to drop.

2. Light Sources

Several light sources were used and are described below.

2.1 2500 watt Xenon Mercury Arc Lamp

This is a lamp manufactured by Hanovia (#929-B1). It is housed in a universal lamp housing model C-60-80 manufactured by Orion Optics Co. The housing contained a 3-inch diameter spherical mirror behind the lamp and a 2-inch diameter, 3-inch focal length collimating lens. These were adjusted to give maximum intensity. The power supply for the lamp was built by Hughes Electronics (Model #5000R41T). It was originally intended to power an Orion 6500 watt xenon lamp but was adaptable to the 2500 watt xenon-mercury lamp.

The lifetime of the lamp is rated at 1000 hours by the manufacturer. After 400 hours the intensity was down by 20% of its original value and the lamp had begun to darken on the top. It was replaced after 600 hours running time when the intensity was down by 40% and the lamp envelope was very dark.

The output of the collimating lens was passed through a nickel sulfate-cobalt sulfate filter (see section 5.2) to remove the intense undesired radiation in the visible and infrared. The radiation was then passed through the Bausch and Lomb monochromator. The output of the monochromator was monitored using an Eppley thermopile (see section 6.1). A spectrum of the lamp with

intensity plotted versus wavelength is shown in Figure 1. The lamp had been running for 1 hour at 2450 watts when this spectrum was taken. The monochromator was set for an 8Å bandpass and the Bausch and Lomb collimator was used at the exit of the monochromator. Comparison of this lamp with other high intensity continuum sources is given in section 3.

2.2 6500 watt Xenon Lamp

This lamp was built by Osram Optical Co. It was housed in the same housing as the 2500 watt xenon mercury lamp and powered by the same supply. The lifetime of the lamp is rated by the manufacturer at 1000 hours. However, it exploded during cool-down after 300 hours running time, extensively damaging the inside of the lamp housing. No specific reason could be found for the lamp failure.

The output of this lamp was passed through the $NiSO_4$-$CoSO_4$ filter and then through the Bausch and Lomb monochromator. The output of the monochromator was monitored by the Eppley thermopile. A spectrum of the lamp with intensity plotted versus wavelength is shown in Figure 2. When this spectrum was taken, the lamp was running at 5000 watts and the monochromator was set for a 16Å bandpass. For the measurement, the $NiSO_4$-$CoSO_4$ filter was removed to give the true intensity of the lamp.

2.3 Mercury BH6 Lamp

A 1000 watt General Electric BH6 lamp was tested and

Figure 1. Spectrum of 2500 watt Hanovia xenon mercury arc lamp. Bausch and Lomb monochromator set for a bandpass of 8 Å.

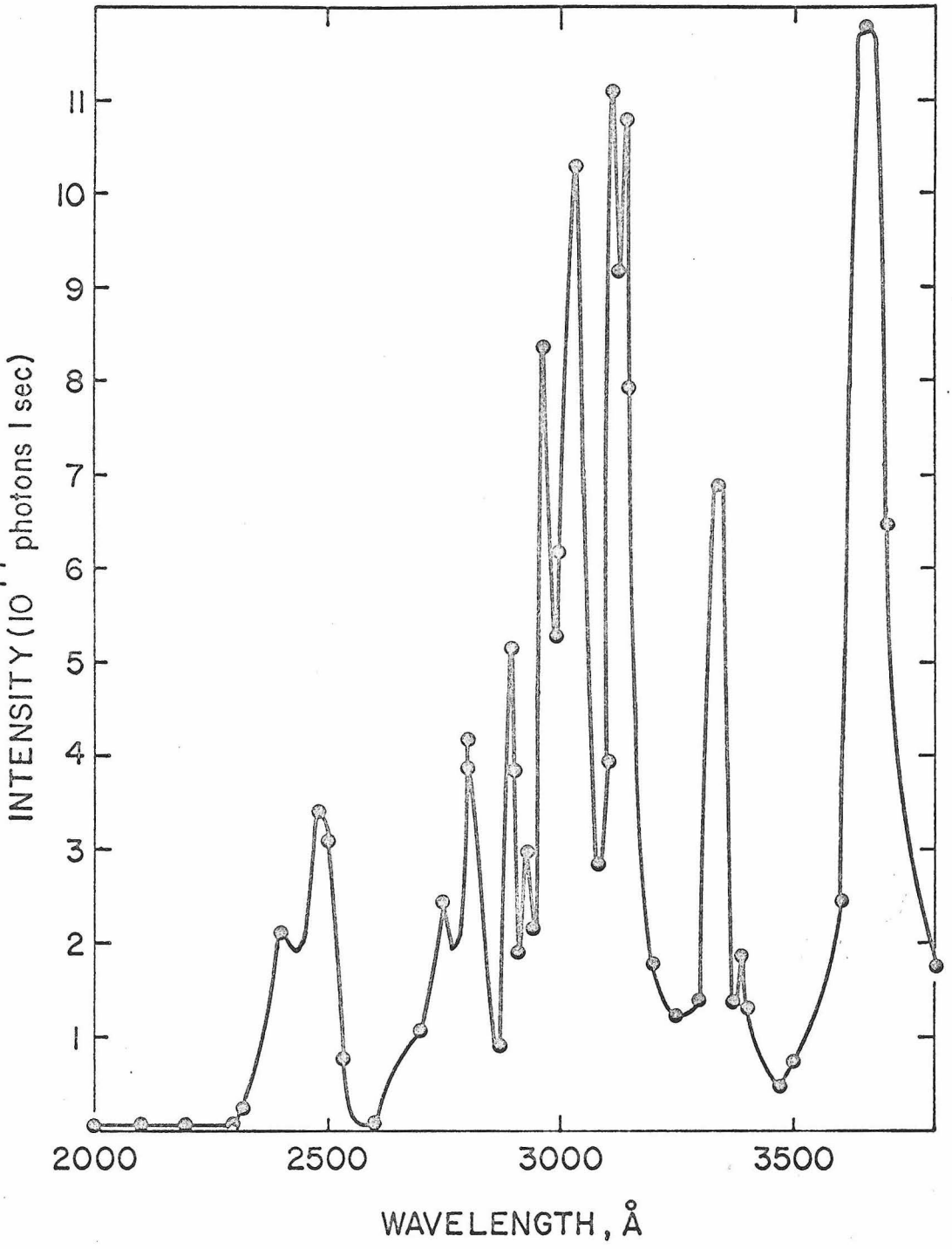
INTENSITY (10^{14} photons I sec)
1
2
3
4
5
6
7
8
9
10
11
2000
2500
3000
3500
WAVELENGTH, Å

Figure 2. Spectrum of 6500 watt xenon lamp. Bausch and Lomb monochromator set for a bandpass of 16Å.

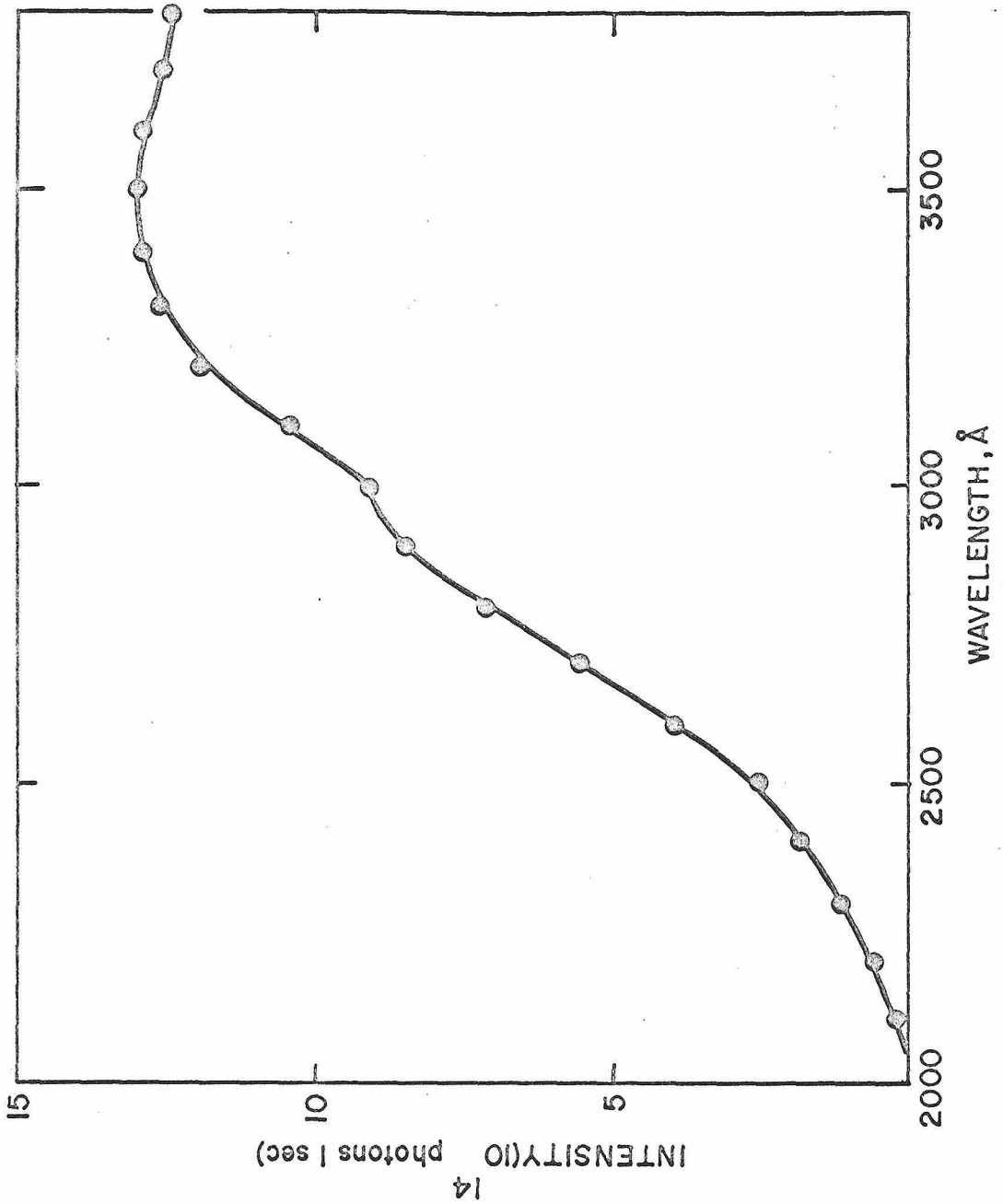
INTENSITY(10^14 photons / sec)
15
10
5
2000
2500
3000
3500
WAVELENGTH, Å

compared with several other high pressure mercury sources (see section 3). These are air-cooled capillary lamps with an effective illuminated area of 25mm by 1.5mm. The lamps were run in the vertical position in our tests although the manufacturer recommends that they be run horizontally. The mercury frequently had to be redistributed between electrodes when run in this position. The power supply for the lamp was General Electric Catalogue No. A14262. The average lifetime of a lamp was 30 hours. The intensity of the lamp decreased 20% during this period. The lamps are inexpensive so this is not a limiting factor.

A lens system consisting of a 2-inch diameter, 3-inch focal length quartz lens followed by a 2-inch diameter, 10-inch focal length lens was used to focus the light from the lamp into the monochromator. With this lens system, the maximum intensity was obtained with the lamp 23 cm from the monochromator. The output of the monochromator was monitored with the Eppley thermopile. A spectrum of the lamp is shown in Figure 3. For these measurements the bandpass of the monochromator was set at 20Å. The 1-inch diameter, 2-inch focal length lens was used at the exit of the monochromator to focus the light into the thermopile.

2.4 Hanovia Low Pressure Mercury Lamp

A SC 2537 low pressure mercury lamp built by Engelhard, Hanovia, Inc. was used for photolyses at 2537Å and 1849Å. The lamp draws 110 ma current at 280 volts. It consists of a tube 21.5 cm long and 2.5 cm in diameter with a suprasil quartz window

Figure 3. Spectrum of General Electric BH6 lamp. Bausch and Lomb monochromator set for a bandpass of 20Å.

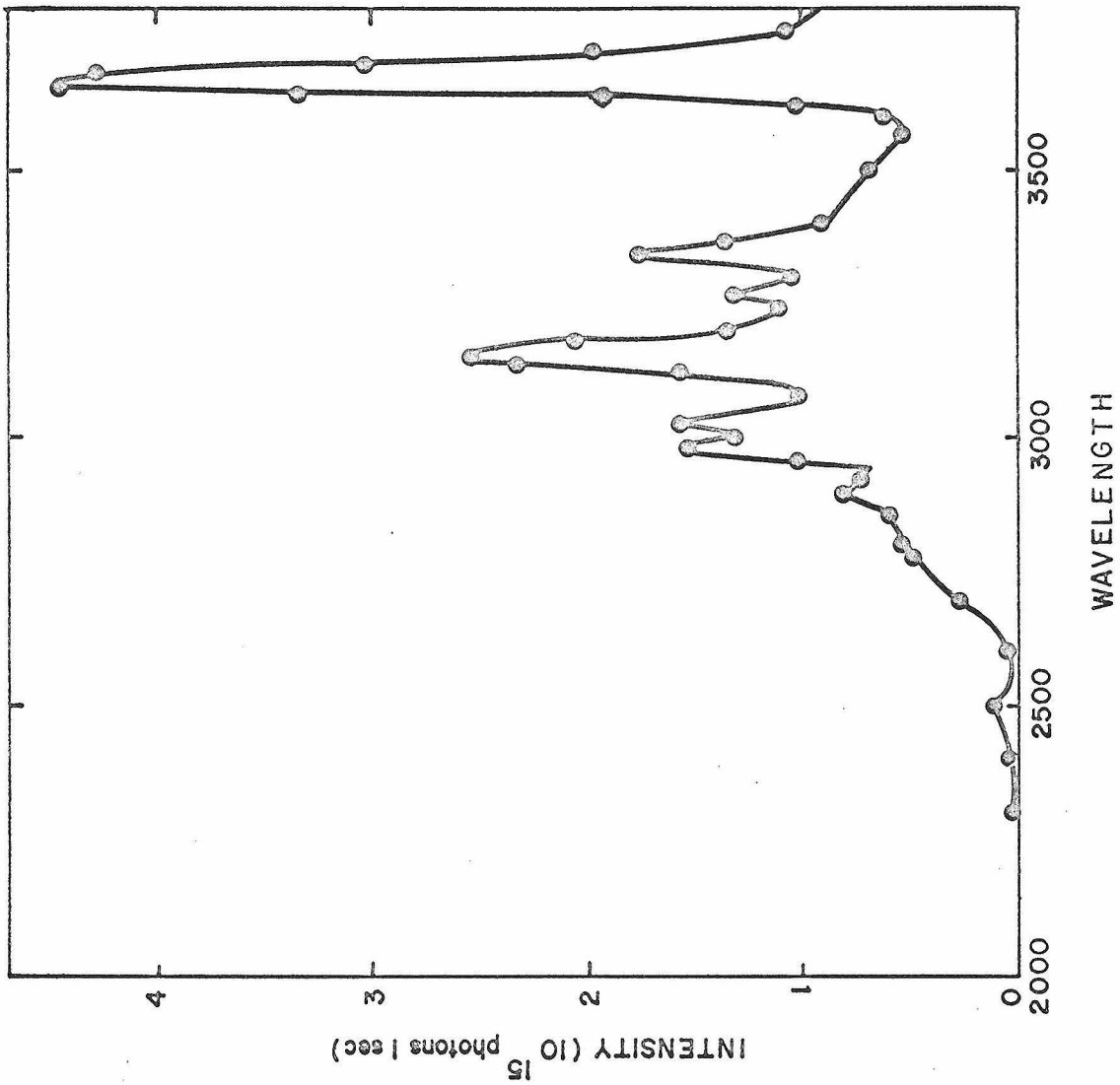
INTENSITY (10^{15} photons / sec)
0
1
2
3
4
2000
2500
3000
3500
WAVELENGTH

attached at one end. The electrodes are contained in legs attached to the main tube. A scan of the spectrum of this lamp with the McPherson monochromator showed that 92% of its light was 2537Å radiation, the remaining 8% being 1849Å radiation.

This lamp was also used as a microwave discharge lamp by using a microwave antenna to stimulate the lamp. A 2450 MHz. Raytheon microwave generator, model KV-104, was used to drive the discharge. The nominal relative output power applied to the antenna cable is read from a meter on the microwave generator. On this meter, 100% corresponds to 85 watts of radiative power. A study was made with the McPherson monochromator of the effect of the power applied on the relative amount of 1849Å radiation generated. It was found that 100% power gave 3.8% 1849Å radiation, 80% gave 7.9% 1849Å radiation and 50% gave 2.8% 1849Å radiation. Hence, the Raytheon unit was run at 80% power when 1849Å radiation was desired and at 100% when 2537Å radiation was needed. The intensity of the lamp increased approximately an order of magnitude when it was run in this manner as compared with the DC supply. The intensity of the lamp run both by electrode discharge and microwave discharge is compared with the intensities of other 2537Å lamps in section 4.

2.5 Germicidal Lamp

A General Electric germicidal lamp (#G4T4-1) was tested in an effort to obtain more intensity at 2537Å. The lamp is U-shaped and approximately 10 cm in length. The lamp was used lengthwise

so the radiation was incident on the cylindrical surface of the reaction vessel. Approximately 98% of the output of this lamp is 2537Å radiation, 2% being 1849Å radiation. A scan of the lamp with the McPherson monochromator showed the only other line appearing up to 3200 Å to be a doublet at 3130Å. This lamp is compared in intensity to other low pressure mercury lamps in section 4.

2.6 Phillips Spectral Lamps

Zinc, cadmium, low pressure mercury, indium and thallium Phillips spectral lamps were tested in the course of this research. The lamps are manufactured by Phillips in Holland and distributed by the Ealing Corporation in the United States. All of them draw 0.9 amperes current and dissipate from 15 to 25 watts power. They require an initial striking voltage of approximately 470 volts. The power supply for these lamps was also manufactured by Phillips (Cat. No. 26-295). They are all 17 cm high with an outside diameter of 3 cm. Their radiation is emitted from a cylinder approximately 10 mm in diameter and 25 mm long whose center is 11 cm from the tip of the basecap. A 2-inch diameter, 3-inch focal length quartz lens followed by a 2-inch diameter, 10-inch focal length lens was used to collect and collimate the output of the lamps. The lenses were adjusted for maximum intensity of radiation as measured by the RCA phototube.

2.6.1 Zinc Lamp

The spectrum of the zinc Phillips spectral lamp was scanned using the Jarrell Ash monochromator. The wavelengths at which the spectral lines occur as well as their relative intensities are given in Table I. The spectral lines at 2025Å and 2062Å can be removed by a cis-2-butene gas filter (100 torr, 5 cm pathlength, see section 5 for its spectrum) which renders the line at 2138Å photochemically useful. The intensity of this line for our lamp was 6.7×10^{15} photons/sec when the lamp was new. This dropped by 50% when the lamp had been run 250 hours at which time a new lamp was installed.

2.6.2 Cadmium Lamp

The spectrum of the Phillips cadmium lamp was scanned with the Jarrell Ash monochromator. The wavelengths at which spectral lines occur along with their relative intensities are given in Table II. The lines at 2288Å and 3260Å are useful for photochemistry. The 3260Å line can be isolated from the shorter wavelength lines by use of a 5 mm thick Corning0160 glass filter (see section 5 for spectrum). The intensity of this line was approximately 1×10^{16} photons/sec. The lines at 2288Å and 2265Å could not be separated from one another. When using the 2288Å one, a correction can be made to account for the 2265Å one. The line at 2145Å can be removed by a cis-2-butene gas filter (5 cm pathlength, 630 torr pressure). The combined intensity of the lines at 2288Å

Table I. Spectral Distribution of Zinc Phillips Spectral Lamp

wavelength (Å)	relative intensity
2025	0.200
2062	0.186
2138	1.00
3072	0.419
3282	0.110
3303	0.273
3345	0.294

Table II. Spectral Distribution of Cadmium Phillips Spectral Lamp

wavelength (Å)	relative intensity
2145	0.025
2265	0.118
2288	0.869
3261	1.00
3404	0.062
3467	0.091
3611	0.091

and 2265Å was 8×10^{15} photons/sec. The intensity gradually decreased as the lamp was used, dropping to about 50% of its original value after 300 hours use. The lamp was run for 8 hours at a time.

2.6.3 Low Pressure Mercury Lamp

The major line of the low pressure mercury Phillips spectral lamp is at 2537Å. The intensity of this line was 1.5×10^{16} photons/sec when the lamp was new. The intensity of the line at 1849Å was about 2% of the 2537Å one. This lamp is compared with other low pressure mercury lamps in section 4.

2.6.4 Thallium Lamp

The spectrum of the thallium Phillips spectral lamp was taken in the wavelength region from 2000Å to 5500Å with the Jarrel Ash monochromator. The major line of this lamp was 5350Å which is at too low an energy to be useful for our work. The other lines are not intense enough for photochemistry. The total intensity of the lamp was greater than 10^{16} photons/sec.

2.6.5 Indium Lamp

The spectrum of the indium Phillips spectral lamp was taken in the wavelength region from 2000Å to 4700Å with the Jarrel Ash monochromator. The lines at 4102Å and 4511Å are likely candidates for photochemical experiments although they are at too low an energy for our work. The wavelengths at which the spectral

Table III. Spectral Distribution of Thallium Phillips Spectral Lamp

wavelength (Å)	relative intensity
3229	0.17
3519	4.0
3529	1.3
3776	14.15
5350	27.7

Table IV. Spectral Distribution of Indium Phillips Spectral Lamp

wavelength (Å)	relative intensity
3039	0.7
3256	5.2
3259	2.3
4102	17.5
4511	19.1

lines occur along with the relative intensities of the lines are given in Table IV.

2.7 Iodine Lamp

An iodine lamp built by William B. DeMore at the Jet Propulsion Laboratories following the specifications given in a paper by Harteck, Reeves and Thompson[1] was tested and used in this research. It was designed to be run by an electrode discharge but was operated as a microwave discharge lamp in these tests because of the greater intensity emitted under this mode. The microwave source used to stimulate the lamp was described in section 2.4. Its output spectrum was scanned with the McPherson monochromator. The major line occurred at 2061Å. There were also lines at 1820Å, 1830Å and 1860Å which were less than 0.5% of the 2061Å one. These lines were removed by a 5 mm thickness of quartz placed in front of the reaction vessel. The intensity of the line at 2061Å was 1.8×10^{16} photons/sec measured using HBr as an actinometer.[2]

3. Comparison of High Intensity Continuum Lamps in the Wavelength Region from 2400Å to 3660Å

The intensities of several high intensity continuum lamps were compared over a range of wavelengths. The output of each lamp was passed through the Bausch and Lomb monochromator with a bandpass set for 16Å and the intensity was measured with the Eppley thermopile. The lamps considered are: (1) a 200 watt

Hanovia super pressure mercury lamp[3], (2) a 2500 watt Hanovia xenon mercury lamp, (3) a 6500 watt Osram xenon lamp and (4) a 1000 watt General Electric BH6 super pressure mercury lamp. These were run under the conditions described in section 2. Table V gives the absolute intensity of each lamp after passing the output through the Bausch and Lomb monochromator at 9 different wavelengths. Most of the wavelengths chosen for comparison correspond to the maxima of the high pressure mercury lamps. The 2500 watt xenon mercury lamp is the most intense of the lamps considered at these peak wavelengths. However, both the 200 watt super pressure mercury and the 1000 watt BH6 lamp have enough intensity for photochemical purposes and are less expensive than the 2500 watt xenon mercury one. The 6500 watt xenon lamp is useful at wavelengths where the high pressure mercury lamps have little intensity (such as 3250Å). Table V, along with the intensity versus wavelength plots in section 2, is useful in chosing which lamp to use for given photolysis conditions.

4. Comparison of Low Pressure Mercury Lamps

The lamps compared here are the Hanovia SC 2537 lamp (run by both electrode and mocrowave discharge), the Phillips low pressure mercury spectral lamp, and the General Electric germicidal lamp. The relative intensities were measured by photolyzing DBr with each lamp and measuring the rate of conversion of DBr per hour. Since DBr has a quantum yield of D_2 of 1, the absolute intensities could be calculated for all lamps except the germicidal lamp

Table V. Comparision of High Intensity Continuum Lamps

wavelength (Å)	200 watt mercury	2500 watt Xe-Hg	6500 watt xenon	1000 watt BH6
		(10^{14} photons/sec)		
2400	2.2	6.3	1.8	0.52
2483	4.2	10.8	2.5	1.4
2700	0.1	7.1	5.5	2.6
2800	2.3	16.8	7.1	4.2
2891	2.6	14.5	8.4	6.4
3030	3.3	37.8	9.1	13.4
3130	11.7	40.5	11.0	20.4
3340	3.5	20.6	13.2	14.4
3660	20.0	47.5	12.0	35.6

where the geometry used did not permit an accurate determination of the pathlength. The output of all lamps was passed through a 2-mm Corning 7910 glass filter to remove any 1849Å radiation. The Hanovia lamp was used with no lenses. The Phillips lamp had a 2-inch diameter, 3-inch focal length lens followed by a 2-inch diameter, 10-inch focal length lens to collect the light from the lamp. For both these lamps the light was directed through the quartz window of the reaction vessel containing the DBr. For the General Electric germicidal lamp the light was directed through the fused silica sides of the cylindrical reaction vessel to use the maximum amount of radiation. The results in terms of conversion of DBr and absolute intensity are shown in Table VI.

The SC 2537 lamp run as a microwave discharge lamp was the most intense source. The main disadvantage of running the lamp in this manner was the large quantity of heat generated by the discharge. A cooling coil had to be wrapped around the reaction vessel to keep it at room temperature.

Of the lamps operating on an electrode discharge, the germicidal lamp was best. This may have been because of the large area irradiated by the lamp. If the position of the lamp with respect to the reaction vessel is unimportant for the photolysis experiment being done, the germicidal lamps are the most economical high intensity low pressure mercury lamps available.

The SC 2537 lamp and the Phillips lamp are about equal in performance. The Phillips lamp has the advantage that its light can be focused into a smaller area.

Table VI. Comparison of Low Pressure Mercury Lamps at 2537Å

Lamp	Extent DBr Conversion (% per hour)	Absolute Intensity (10^{16} photons/sec)
SC 2537 electrode	0.057	1.12
SC 2537 microwave	0.51	10.0
Phillips Spectral Lamp	0.065	1.28
Germicidal Lamp	0.16	---

5. Filters

5.1 Glass Filters

High energy cut off filters were used with several of the light sources to remove unwanted lines and at the exit of the Bausch and Lomb monochromator to remove undesired high energy radiation. Corning 7910 (2 mm thick) and 0160 (2 mm and 5 mm thick) glass filters were used in the course of this work and their transmission characteristics are shown in Figure 4. The 7910 filter was used when wavelengths from 2400Å to 2537Å were desired. The 5 mm 0160 filter was used with the cadmium Phillips spectral lamp to isolate the 3261Å line and also at the output of the monochromator for wavelengths from 3250Å to 3400Å. Also shown are the transmission characteristics of a 2 mm thick piece of quartz similar to the quartz windows of the reaction vessel. All spectra were taken with a Cary 14 spectrophotometer.

5.2 $NiSO_4$-$CoSO_4$ Filter

A filter solution containing 10g of $CoSO_4 \cdot 7H_2O$, 20g of $NiSO_4 \cdot 6H_2O$ and 1 ml of 16M sulfuric acid per liter of water was used to remove much of the visible and infrared radiation from the 2500 watt xenon mercury lamp and the 6500 watt xenon lamp. The transmission characteristics of the filter for a 5 cm path-length are shown in Figure 6. A temperature dependence study was made on this filter at 25°C, 50°C and 65°C. Little if any temperature effect was observed.

A 5 cm long stainless steel cell with 4 cm diameter quartz

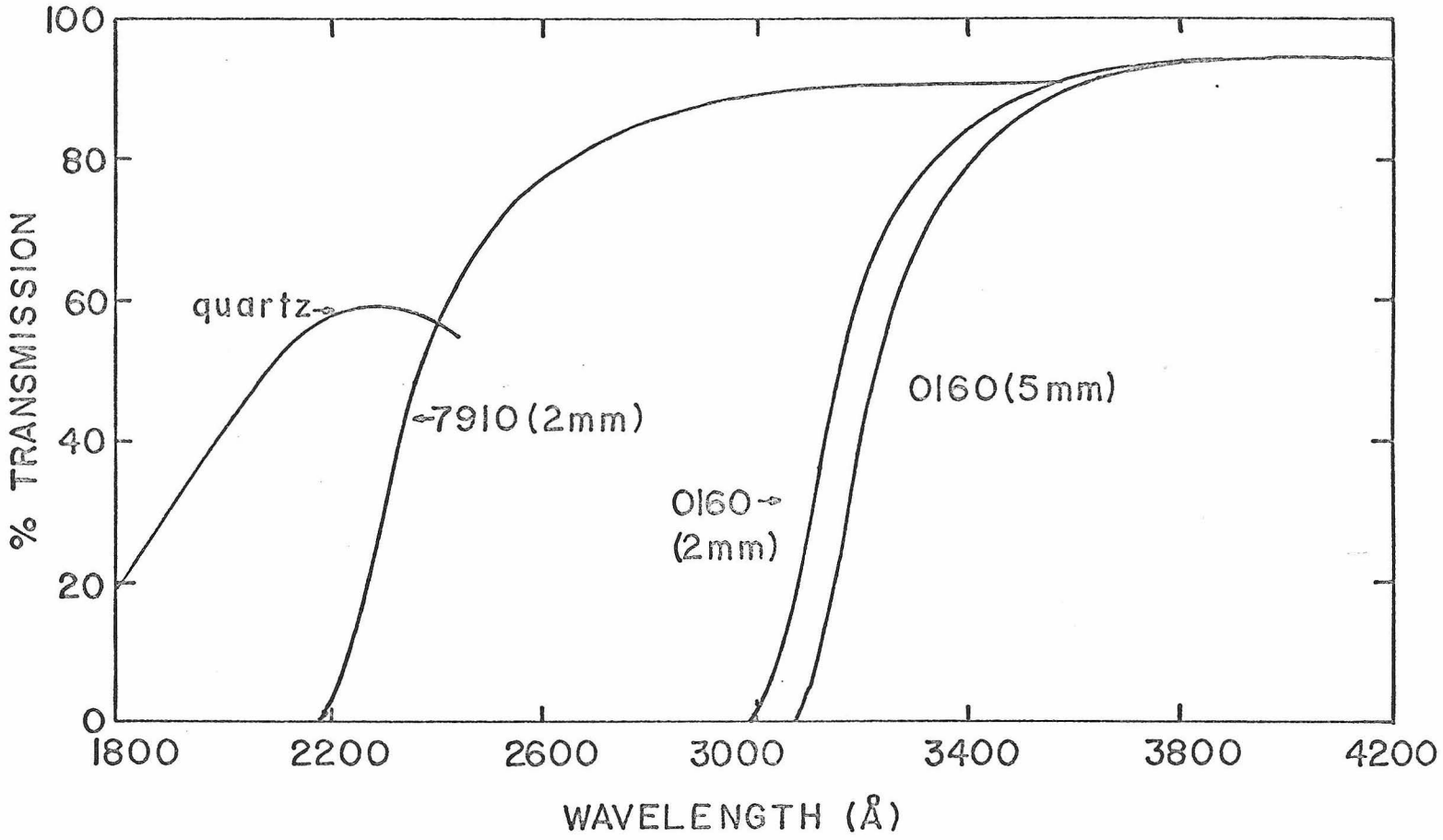

Figure 4. Transmission curves of glass filters.

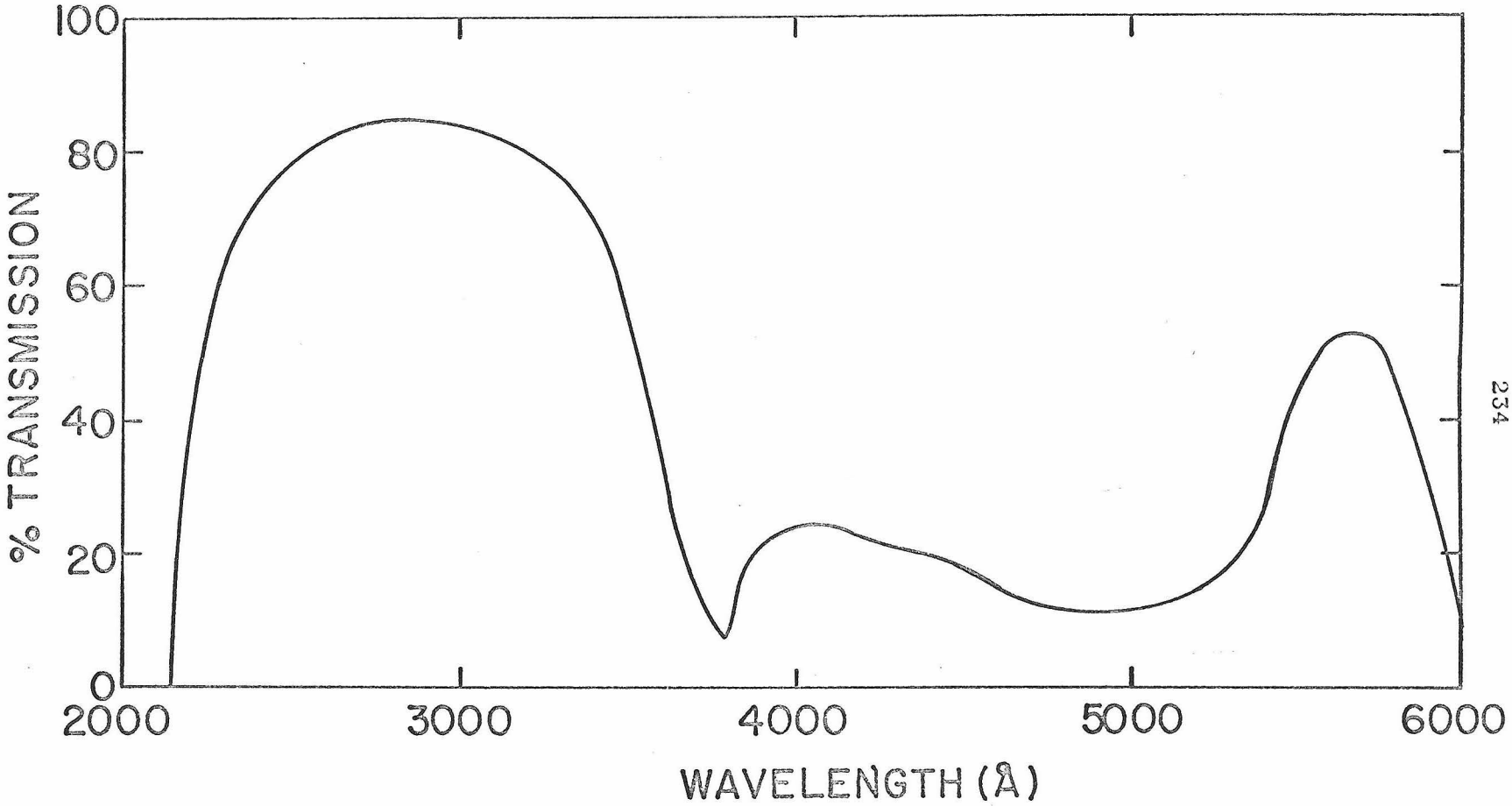

Figure 5. Transmission of $NiSO_4$ - $CoSO_4$ filter (5 cm pathlength).

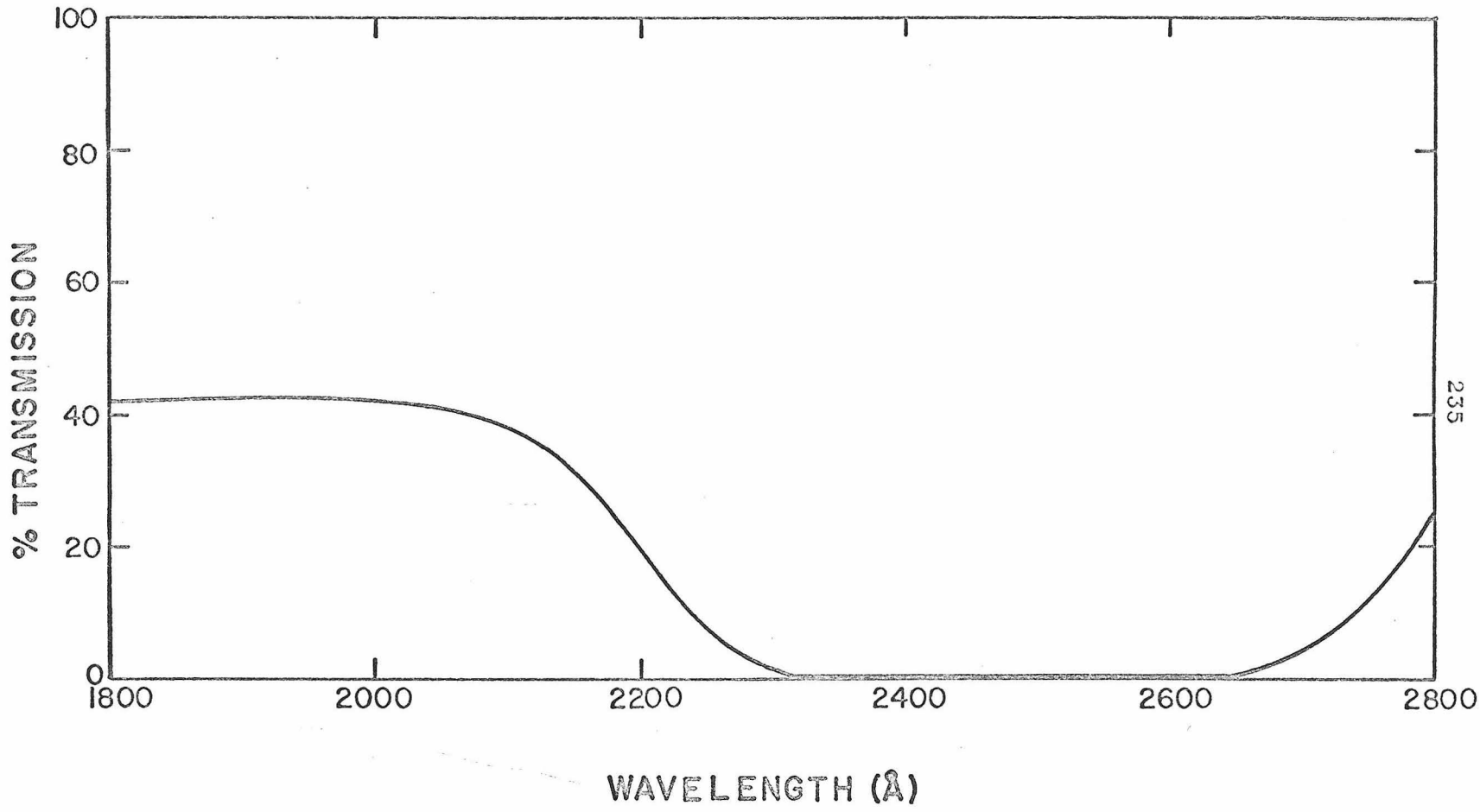

Figure 6. Transmission of Co^{60} gamma-irradiated lithium flouride filter.

windows sealed on with General Electric RTV-108 silicone rubber adhesive was used to contain the filter solution. This container was water cooled by a coil of copper tubing soldered around the circumference. Some difficulty was encountered in finding a suitable cell because of the high reactivity of the solution. A Pyrex cell was insufficiently heat conductive. Brass ruined the optical properties of the filter solution, and we could not get a nickle plate to adhere sufficiently well. Neither Varian's Torr Seal nor Fuller's Resiweld adhesives could long withstand the warm solution.

5.3 cis-2-butene Gas Filter

A cis-2-butene gas filter at 100 torr pressure, 5 cm path-length was used to isolate the 2138Å line of the zinc Phillips spectral lamp. The transmission of this filter is plotted as a function of wavelength in Figure 7. A 5 cm long, 5 cm diameter quartz cell was used to contain the gas. A similar filter at 630 torr pressure was used to remove the 2145Å line of the Cadmium Phillips spectral lamp. Its transmission curve is also shown in Figure 7. A Cary 14 spectrophotometer was used to measure these spectra.

6. Light Intensity Measuring Devices

6.1 Eppley Thermopile

An Eppley thermopile (serial number 5823) was used to measure the light intensity in some of our experiments. It is a surface

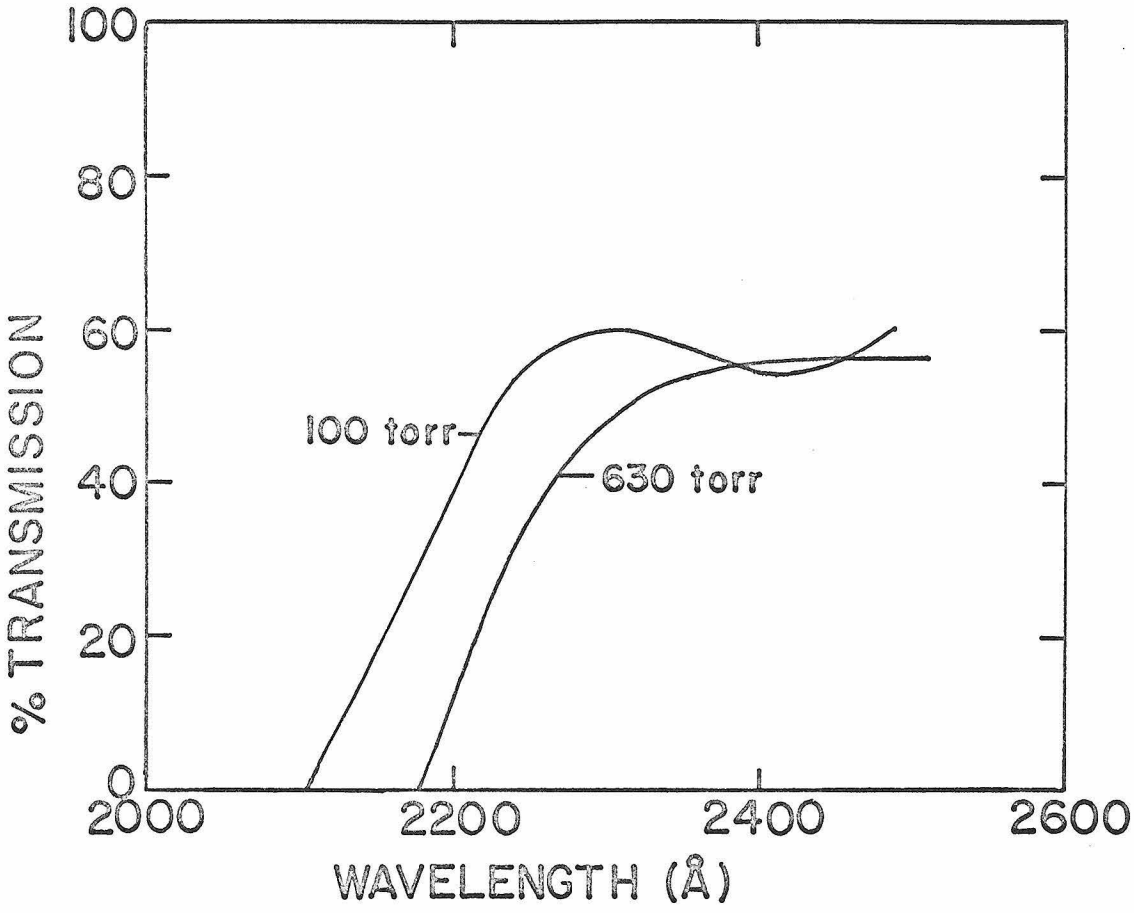

Figure 7. Transmission of cis-2-butene gas filters.

type thermopile with 12 bismuth silver junctions. It was contained in an aluminum housing with an aperature 3 mm wide and 10 mm high. It was calibrated by Eppley with an NBS standard lamp and was found to develop an emf of 0.056 microvolts when a radiant flux of 1.00 microwatts per square centimeter was incident upon it. A Keithley Model 150 microvolt-ammeter was used to measure the voltage developed by the thermopile.

6.2 RCA 935 Phototube

An RCA 935 phototube was frequently substituted for the Eppley thermopile. The phototube was housed in a housing made of anodized aluminum. The aperature to the phototube was 2.5 cm high and 1.25 cm across. A power supply-ammeter was built by our electronics shop to supply 250 VDC to the photocell and to measure currents from 0 to 50 microamps. A battery could probably be found that would take the place of the power supply.

The phototube has an S-5 response. RCA's data for the relative S-5 response (per energy interval) is shown in Figure 8. The photocell was also calibrated against the Eppley thermopile. The photocell sensitivity as a function of wavelength is given in Table VII. The photon flux is obtained from the output of the phototube in microamps by the formula

$$I = \frac{\text{output}}{\text{sens.}} \times 10^{14}$$

where I is the photon flux in units of photons/sec, the output is in microamps and the sensitivity is in units of microamps/

Table VII. RCA 935 Photocell Sensitivity

wavelength (Å)	sensitivity (amp/10^{14} photons/sec)
2000	0.05
2100	1.8
2200	2.0
2300	2.2
2400	2.4
2500	2.5
2600	2.6
2700	2.6
2800	2.5
2900	2.5
3000	2.5
3100	2.6
3200	2.6
3300	2.6
3400	2.6
3500	2.6
3600	2.5
3700	2.4
3800	2.3
3900	2.2
4000	2.1

Figure 8. Relative S-5 response (per energy).

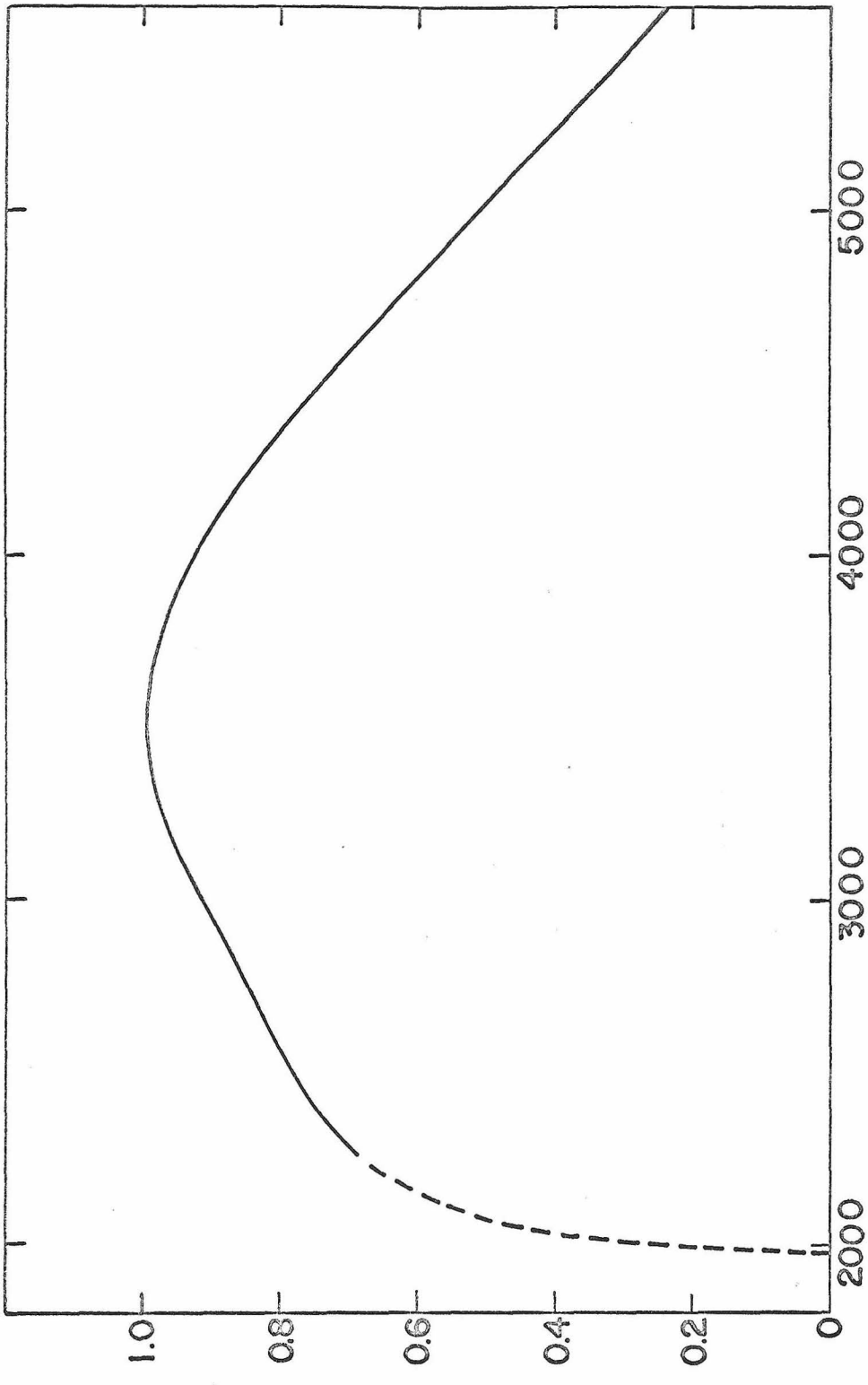
RELATIVE RESPONSE
0
0.2
0.4
0.6
0.8
1.0
2000
3000
4000
5000
WAVELENGTH (Å)

10^{14} photons/sec.

The phototube was found to be more useful than the thermopile because of its wider aperature.

7. Scattered Light in the Bausch and Lomb Monochromator

The amount of scattered light was checked by scanning the output of the Bausch and Lomb monochromator with the Jarrell Ash monochromator described in section 1. In a system such as ours in which the extinction coefficient of the substance being photolyzed increases rapidly with decreasing wavelength, a small amount of scattered light of short wavelength could lead to drastically wrong results for a given wavelength setting.

Figure 9 shows a plot of the output of the monochromator as a function of wavelength for the Xe-Hg lamp when the dial on the Bausch and Lomb instrument was set for 2480Å and the bandpass of the monochromator was set for 24Å. The width at half-height of the peak is 22Å in good agreement with the bandpass settings. Note that the peak at 2400Å has been completely removed by the monochromator and that the tail of the peak drops rapidly to zero at short wavelengths. A 2 mm Corning 7910 glass filter was placed at the exit of the monochromator at this wavelength to remove any short wavelength light present. From a scan of this type we could discover if scattered light was coming through the monochromator and could decide if a filter was needed to remove excessive short wavelength light. These considerations became increasingly important for long wavelengths since the extinction

coefficients became very small.

The peak absorbed wavelength could be found by making a plot of intensity times extinction coefficient versus wavelength. The peak of this plot sometimes differed from the peak intensity by 2 to 3 Angstroms.

REFERENCE

1. P. Harteck, R. R. Reeves, Jr., and B. A. Thompson, Z. Naturforschg., 19a, 2 (1964).

Figure 9. Output of Bausch and Lomb monochromator as a function of wavelength for the Xe-Hg lamp with the dial of the monochromator set at 2480Å and the bandpass set for 24Å.

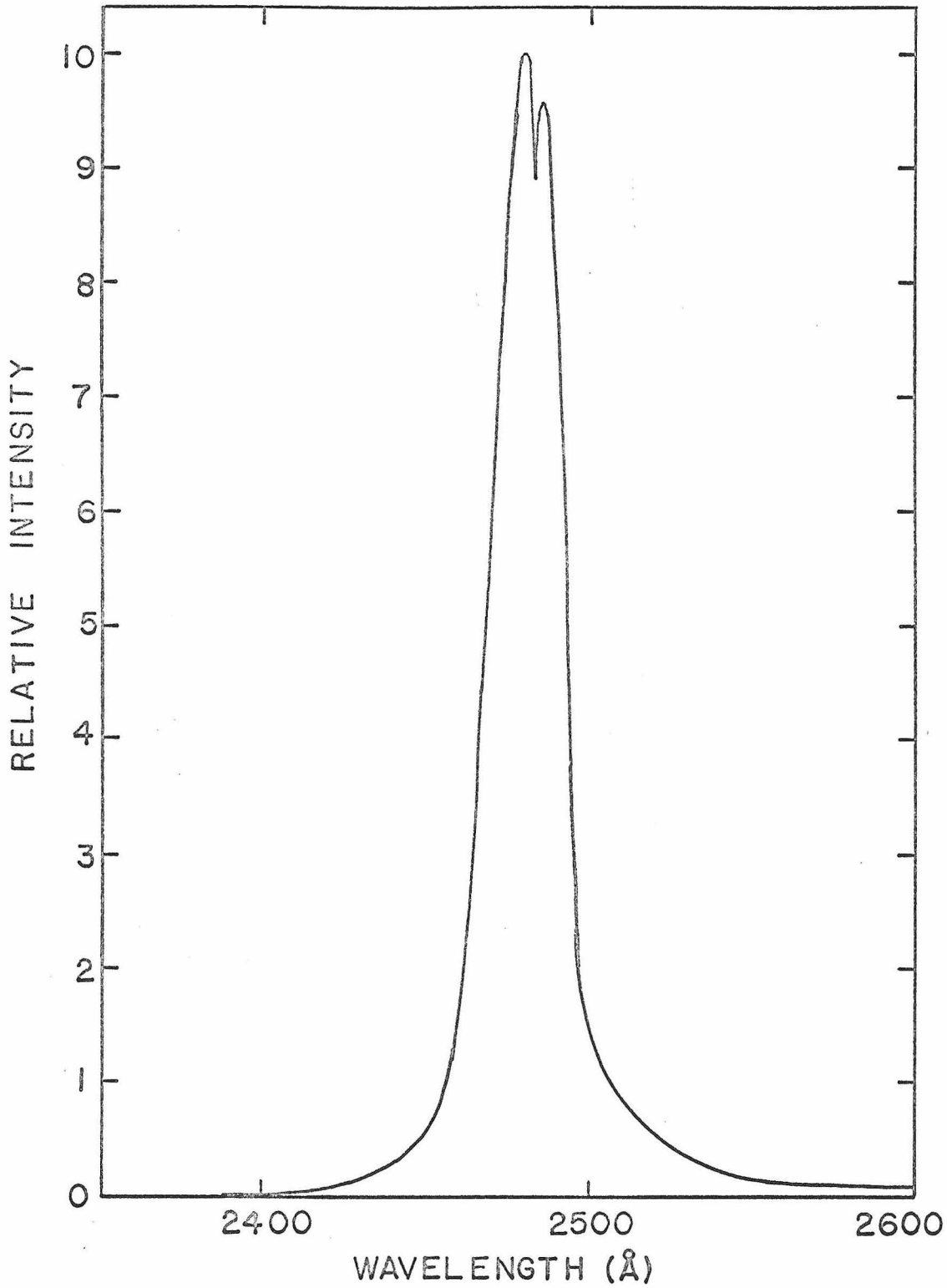
RELATIVE INTENSITY
0
1
2
3
4
5
6
7
8
9
10
2400
2500
2600
WAVELENGTH (Å)

APPENDIX B

ADDITIONAL EXPERIMENTAL TECHNIQUES FOR D + H_2

1. Reactant Mixing

A mercury free vacuum line utilizing an oil diffusion pump was used for mixing reactants. The vacuum line is essentially the same as described in J. M. White's thesis[1] with the addition of a separate section to handle DBr. This section was added in order to avoid contamination of the DBr by the DI or vice versa. A schematic sketch of the vacuum line is shown in Figure B1. Section I is the pumping section and utilizes the same mechanical and diffusion pumps as described in J. M. White's thesis. Section II is the section of the line for handling DI and section III is the section of the line for handling DBr. These two sections are separated by a cold trap C to prevent mixing of DI and DBr. Hydrogen and helium were added directly to the line from high pressure gas tanks through cold traps. The technique for filling the reaction vessels is as described in J. M. White's thesis.

2. Product Handling

The vacuum line for product handling was the same as described in J. M. White's thesis. One end of the reaction vessel was placed in liquid nitrogen for 15 minutes to remove the DBr or DI and the remaining gases were transferred via a toepler pump to a glass bulb for analysis.

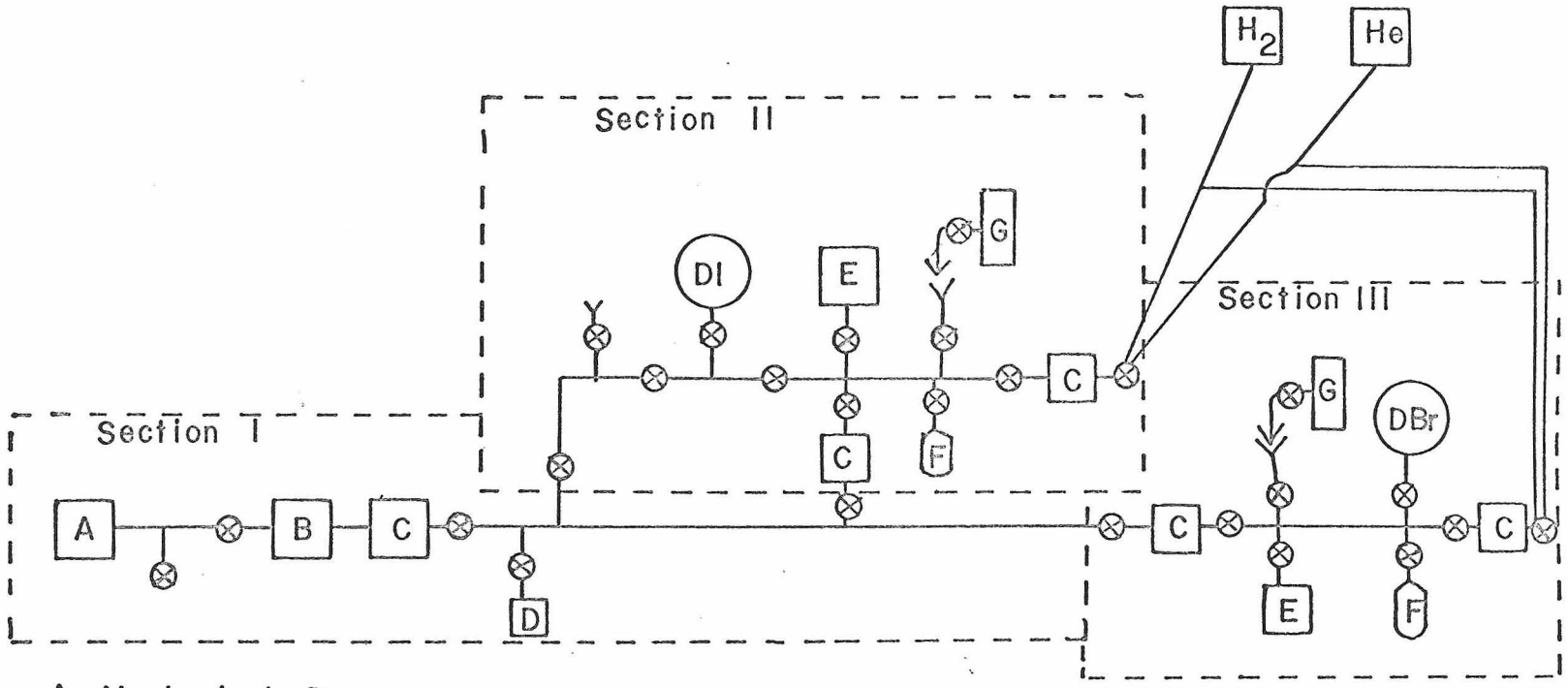

A. Mechanical Pump

B. Diffusion Pump

C. Cold Trap

D. Ion Gauge

E. Transducer

F. Cold Finger

G. Reaction Vessel

Figure B1. Schematic sketch of vacuum line.

3. Mass Spectral Analysis

A CEC-103C mass spectrometer was used for product analysis. The spectra were recorded photographically on an oscillograph recorder built into the mass spectrometer. The slowest automatic scan rate (1/6 octave/min) was used in analyzing the samples. A rigid time schedule was adhered to in these analyses so the same peaks were in register at a given time after the sample was introduced. For samples containing HD, D_2 and H_2, the m/e = 3 peak was scanned 3 times at 10 second intervals. Five seconds we allowed to adjust the ion accelerating voltage to the peak at m/3 = 4 and this peak was scanned 3 times at 10 second intervals. Five seconds were then allowed to adjust the ion accelerating voltage to the m/e = 2 peak and this peak was scanned 3 times at 10 second intervals. Hence there was 100 seconds elapsed time from the time the sample was introduced until the analysis was completed with m/e = 3 peaks at 5, 15 and 25 seconds elapsed time, m/e = 4 peaks at 40, 50 and 60 seconds elapsed time and m/e = 2 peaks at 75, 85 and 95 seconds elapsed time. For the samples containing H_2 a correction had to be made for the H_3^+ contributing to the peak at m/e = 3. This was done by running a given sample at 4 different inlet pressures and extrapolating the measured $[HD]/[H_2]$ and $[HD]/[D_2]$ ratios to zero pressure where the H_3^+ contribution to the m/e = 3 peak vanishes. The correction for the HD originally in the H_2 was made by the expression:

$$\left(\frac{[HD]}{[D_2]}\right)_{photolysis} = \left(\frac{[HD]}{[D_2]}\right)_{total} \left\{1 - \frac{\left(\frac{[HD]}{[D_2]}\right)_{tank}}{\left(\frac{[HD]}{[D_2]}\right)_{total}}\right\}$$

where the ratios $([HD]/[D_2])_{total}$ and $([HD]/[H_2])_{total}$ are from the observed peak ratios extrapolated to zero inlet pressure and $([HD]/[H_2])_{tank}$ is the ratio of the HD and H_2 peaks in the tank hydrogen used in the photolyses.

For samples containing HD, D_2 and He, the same time schedule was followed with the exception of not scanning the m/e = 2 peak. It was also not necessary to extrapolate the results to zero pressure. The m/e peaks for He and D_2 were separated enough so analysis of D_2 was possible. Even though the He peak was as much as 100 times larger than the D_2 peak, the contribution of the He peak to the D_2 peak was always less than 2% of the latter.

Carefully prepared calibration mixtures of HD, D_2 and H_2 and HD, D_2 and He with compositions analogous to photolysis mixtures were analyzed using the procedures described above to calibrate the mass spectrometer. The deviations of the peak height ratios of these mixtures from the known concentration ratios was always less than 3%.

Reproducibility for a given sample was always 2% or less.

REFERENCE

1. J. M. White, Ph.D. Thesis, University of Illinois, Urbana Illinois (1966).

APPENDIX C

ADDITIONAL EXPERIMENTAL TECHNIQUES FOR H + CD_4

1. Reactant Mixing

The vacuum line used was the same as that used for D + H_2 as described in Appendix B with bulbs of HBr and CD_4 attached in place of those of DBr and H_2 respectively. The procedure for preparing reactant mixtures was identical to the DBr-H_2 case described in detail in J. M. White's thesis, Paper I and Appendix B.

2. Product Handling

A new glass vacuum line using a mercury diffusion pump was constructed to process reaction products. The vacuum pumps are as described for D + H_2 in J. M. White's thesis and Appendix B.

In order to remove most of the unreacted CD_4 from the products H_2 and HD, (because of its contributions to m/e = 2 from the D^+ fragment and m/e = 3 from the HD^+ fragment of the CD_3H impurity) a dewar for pumping on liquid nitrogen was constructed. A schematic drawing of the dewar and toepler pump is shown in Figure C1. The reaction vessel A is placed on the standard taper joint at the top of the trap B and the trap is evacuated. One end of the reaction vessel is placed in liquid nitrogen to remove the HBr and some of the CD_4 before the remaining contents are passed through the trap. Liquid nitrogen is then added to the dewar through C. After nitrogen has been added, the opening C is closed with a ground glass joint. This joint has a small

diameter tube sealed into it in which a thermocouple is placed to measure the temperature in the dewar. The nitrogen is then pumped on through D with a Cenco Megavac Pump (pumping speed liters/min) until the temperature of the nitrogen reaches -212°C or lower as measured by the thermocouple. This usually takes from 15 to 20 minutes. The contents of the reaction vessel are then passed through the trap with the aid of a 1 1/2 liter toepler pump. One sweep of the toepler pump collects about 75% of the sample and reduces the $[CD_4]/([HD] + [H_2])$ ratio by at least 98.5%. Mixtures of HD, H_2 and CD_4 of known composition analogous to photolysis mixtures were prepared, passed through the dewar and analyzed to check for fractionation of H_2 and HD and to measure the efficiency of the dewar. The measured $[H_2]/[HD]$ ratios agreed with the known ones within 1%. After passing through the dewar, the sample was transferred to a sample bulb and then analyzed by the CEC mass spectrometer.

3. Mass Spectral Analysis

The products H_2 and HD were analyzed on the CEC-103C mass spectrometer. The spectrum of peaks was scanned automatically with the slowest automatic scan rate (1/6 octave/min) of the mass spectrometer. The output was measured with a strip-chart recorder connected to the amplifier jack of the mass spectrometer. This enabled us to obtain at least 3 times more sensitivity (when the instrument noise level was low) than with the oscillograph recorder used for the D + H_2 analysis as described in Appendix B.

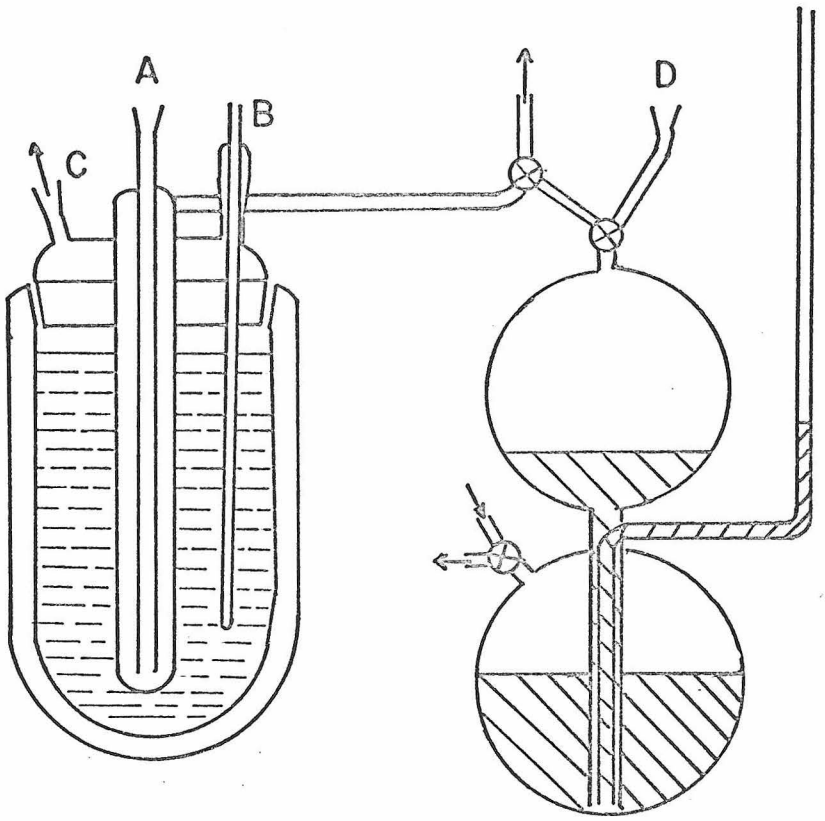

Figure C1. Schematic drawing of pumped liquid nitrogen dewar and toepler pump.

Each peak at m/e 3, 2 and 20 was scanned five times in succession and an average taken. To correct for peak heights decreasing with time, the peaks were scanned at reproducible times from when the sample was introduced. The peak at m/e 3 was scanned 5 times at 10 second intervals, 5 seconds were then allowed to adjust the accelerating voltage for the peak at m/e 2 and this peak was scanned 5 times at 10 second intervals. One minute was then allowed to adjust the accelerating voltage for the peak at m/e 20 since the magnet current range had to be changed to get this peak into register. This peak was then scanned 5 times at 10 second intervals. The same time schedule was used on all samples and calibration mixtures, alleviating the need to extrapolate the measured peak heights to zero time.

In order to correct for the contributions of the CD_4 to the m/e 2 peak and the CD_3H impurity to the m/e 3 peak, samples of "pure" CD_4 were analyzed and the ratios of the peaks at m/e 2 and m/e 3 to the peak at m/e 20 were determined. These were then used to correct for CD_4 in the sample by the formula:

$$\left(\frac{[H_2]}{[HD]}\right)_{photolysis} = \frac{[H_2]_{obs} - [CD_4]_{obs} \cdot C_{H2}}{[HD]_{obs} - [CD_4]_{obs} \cdot C_{HD}} .$$

In the above $[H_2]/[HD]$ is the true experimental value and $[H_2]_{obs}$, $[HD]_{obs}$ and $[CD_4]_{obs}$ are the observed peak heights at m/e 2, 3 and 20 respectively. C_{H2} and C_{HD} are ratios of peak heights of masses 2 and 3 to mass 20 in "pure" CD_4. The second term in the numerator was usually 20-30% of the measured peak $[H_2]_{obs}$ and the second term in the denominator was less than 10% of $[HD]_{obs}$.

Calibration mixtures whose composition was analogous to photolysis mixtures were analyzed by the same procedure and a correction was applied if necessary. Corrections varied slightly from day to day but never exceeded 3%. Reproducibility for a given sample was within 2%.

APPENDIX D

ADDITIONAL RESULTS FOR D + H_2

1. Photolyses at 1849Å

Photolyses of DBr-H_2 and DBr-He mixtures were carried out at this wavelength using the experimental techniques described in Paper 1 and Appendix B. A 6-inch long 1 1/2-inch diameter fused silica reaction vessel with optical quality quartz windows was used in this and all following experiments except where specifically stated otherwise. The Hanovia SC 2537 lamp described in Appendix A was used with the ^{60}Co gamma-irradiated filter. The intensity of this lamp at 1849Å was approximately 9×10^{13} photons/sec. Photolysis times for DBr-H_2 ranged from 1-2 hours with DBr conversions of from 0.2% to 0.5% while for DBr-He, photolysis times were 3 hours with conversions of approximately 0.8%.

The results of the DBr-H_2 experiments are given in Table DI while those of the DBr-He experiments are given in Table DII. The results of both sets are plotted in Figure D1. For the DBr-H_2 system, least squares analysis of the photolysis data gives a slope of 0.73 ± 0.02 and an intercept of 0.31 ± 0.01. For the DBr-He system the least squares slope and intercept are 0.1 ± 1.0 and 39.3 ± 0.7 respectively.

Table DI. Results of DBr-H_2 Photolyses at 1849Å

Expt.	P_{DBr} (torr)	P_{H_2} (torr)	Photolysis Time(hrs.)	$\frac{[DBr]}{[H_2]}$	$\frac{[D_2]}{[HD]}$	conv. (%)
1	42.0	47.7	1.0	0.880	0.965	0.30
2	51.7	173.7	1.0	0.298	0.523	0.25
3	60.2	64.1	1.0	0.938	0.990	0.21
4	55.3	166.8	1.5	0.331	0.549	0.39
5	50.0	49.5	1.6	1.01	1.079	0.43
6	53.2	105.2	1.8	0.506	0.663	0.42
7	40.7	90.2	1.5	0.451	0.653	0.48
8	61.1	93.6	2.3	0.652	0.452	0.57
9	54.9	121.3	1.5	0.452	0.657	0.35
10	57.5	47.8	1.0	1.202	1.167	0.23

Table DII. Results of DBr-He Photolyses at 1849Å

Expt.	P_{DBr} (torr)	P_{He} (torr)	Photolysis Time(hrs.)	$\frac{[DBr]}{[He]}$	$\frac{[D_2]}{[HD]}$	conv. (%)
1	29.1	92.6	5	0.314	39.2	1.25
2	35.3	45.9	3 1/2	0.771	40.4	0.85
3	32.0	68.8	4 1/3	0.465	40.0	1.16
4	32.0	61.3	4	0.522	39.3	1.06
5	41.0	36.2	3	1.132	38.3	0.80
6	37.2	84.8	4	0.439	38.8	1.00
7	32.6	99.8	4	0.326	40.4	0.98
8	41.0	41.6	3 1/2	0.985	40.7	0.86
9	29.7	55.4	4	0.536	38.1	1.01

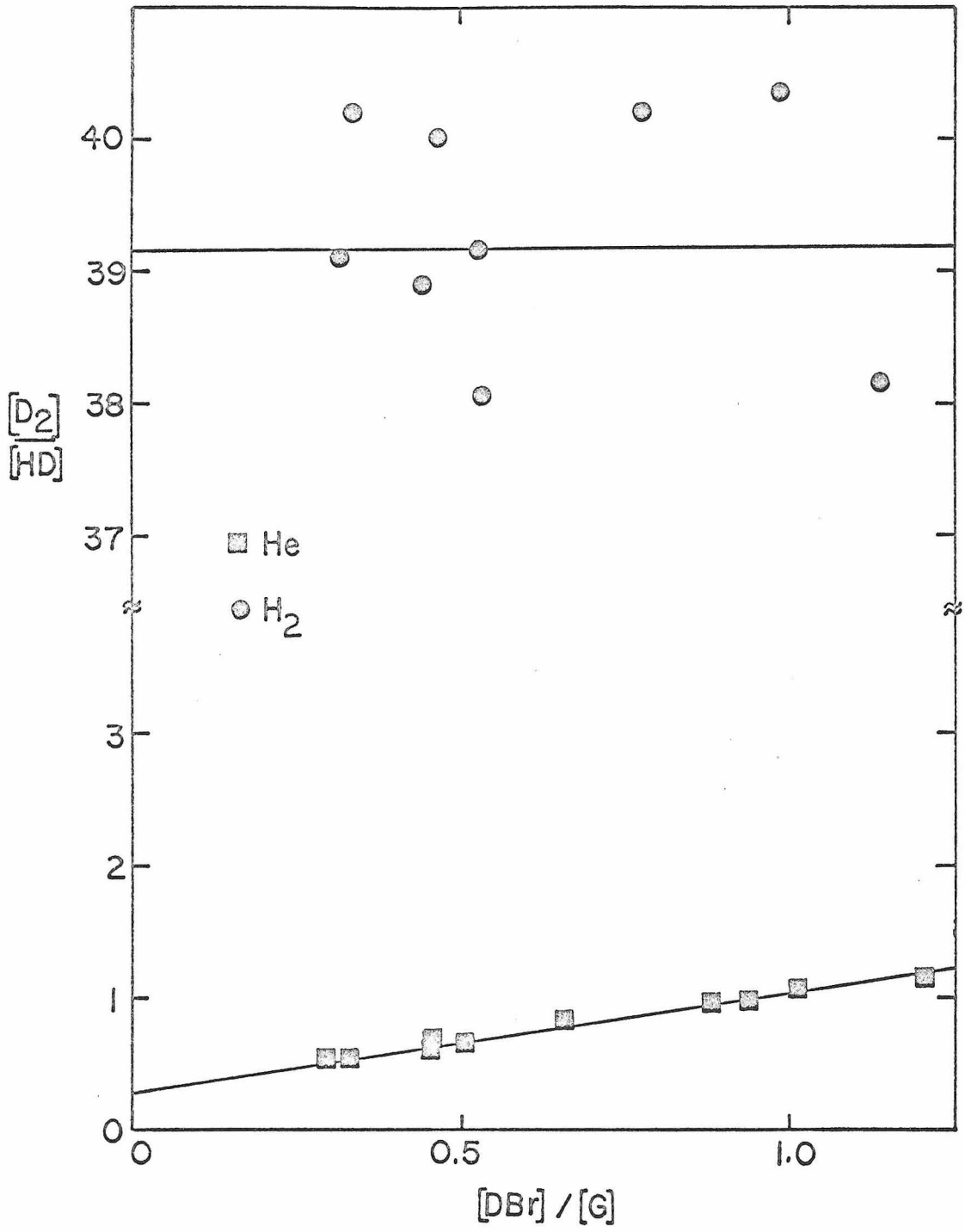

Figure D1. Results of DBr-H_2 and DBr-He photolyses at 1849Å.

2. Photolyses at 2138Å

Photolyses of DBr-H_2 and DBr-He mixtures were performed at this wavelength using the zinc Phillips spectral lamp with the cis-2-butene filter described in Appendix A. The intensity of the lamp was approximately 2 x 10^{15} photons/sec with the filter. The same experimental procedure as described previously was used. Photolyses lasted an average of 15 minutes resulting in conversions of approximately 0.45%.

The results of the DBr-H_2 photolyses are given in Table DIII and are plotted in figure D2. Least squares analysis of these data gives a slope of 0.91 ± 0.03 and an intercept of 0.735 ± 0.026. The results of the DBr-He photolyses are given in Table DIV and are plotted in figure D2. Least squares analysis gives a slope of 2.8 ± 0.2 and an intercept of 29.1 ± 0.2.

3. Photolyses at 2300Å

Photolyses of DBr-H_2 and DBr-He mixtures were done at 2300Å using a 6500 watt Orion xenon lamp with the Bausch and Lomb monochromator set for a 24Å bandpass. The width at half height of the peak was 22Å as measured by the Jarrell Ash monochromator. The 2:1 $NiSO_4$-$CoSO_4$ filter used to cut out visible and infrared radiation became clouded as photolyses proceded and was changed periodically. This caused the intensity exiting from the monochromator to vary by as much as 20% during a photolysis. The intensity at the beginning of a photolysis was usually about 1 x 10^{15} photons/sec. Photolyses lasted 2 1/2 hours and

Table DIII. Results of DBr-H_2 Photolyses at 2138Å

Expt.	P_{DBr} (torr)	P_{H2} (torr)	Photolysis Time(min.)	$\frac{[DBr]}{[H_2]}$	$\frac{[D_2]}{[HD]}$	conv. (%)
1	41.2	47.0	60	0.876	1.480	2.12
2	44.2	138.7	15	0.319	1.022	0.695
3	49.2	39.0	15	1.261	1.952	0.403
4	43.8	97.5	15	0.449	1.138	0.45
5	53.7	55.0	20	0.976	1.640	0.465
6	45.7	70.3	15	0.651	1.323	0.429
7	43.1	143.2	20	0.301	1.037	0.636
8	43.5	48.8	17	0.891	1.548	0.45
9	58.5	44.5	18	1.315	1.910	0.46
10	58.3	43.7	15	1.334	1.934	0.44

Table DIV. Results of DBr-He Photolyses at 2138Å

Expt.	P_{DBr} (torr)	P_{H_2} (torr)	Photolysis Time(min.)	$\frac{[DBr]}{[H_2]}$	$\frac{[D_2]}{[HD]}$	conv. (%)
1	58.5	58.2	15	1.005	32.1	0.42
2	53.4	171.4	15	0.311	30.2	0.40
3	35.4	91.4	15	0.388	29.8	0.43
4	54.2	40.1	15	1.350	32.9	0.43
5	38.1	145.8	20	0.261	30.0	0.48
6	60.5	44.5	15	1.360	32.8	0.41

Figure D2. Results of DBr-H_2 and DBr-He photolyses at 2138Å.

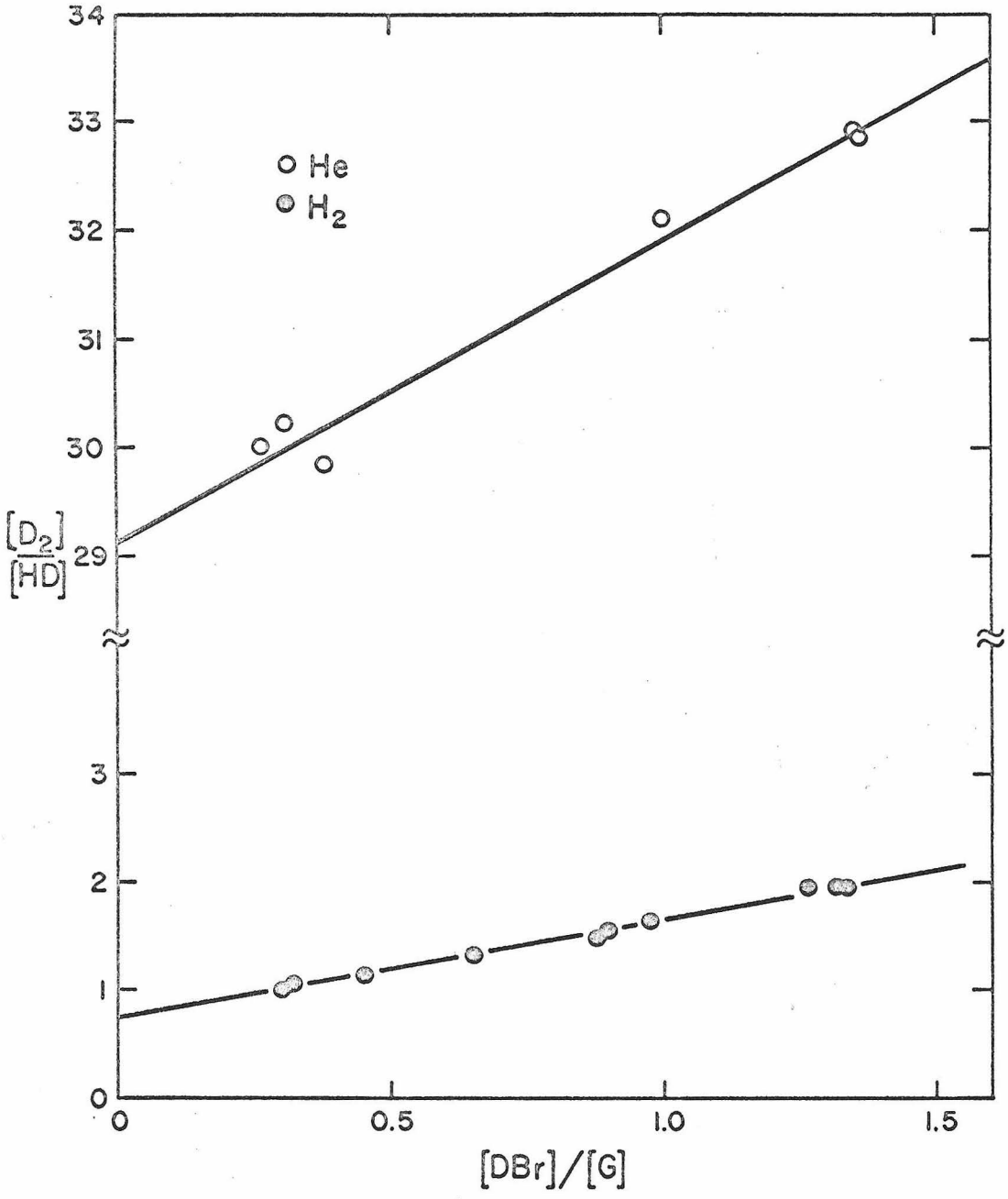
34
33
32
31
30
29
3
2
1
0
He
H_2
$\frac{[D_2]}{[HD]}$
0
0.5
1.0
1.5
[DBr]/[G]

Table DV. Results of DBr-H_2 Photolyses at 2300Å

Expt.	P_{DBr} (torr)	P_{H_2} (torr)	Photolysis Time(hrs.)	$\frac{[DBr]}{[H_2]}$	$\frac{[D_2]}{[HD]}$	conv. (%)
1	58.0	94.4	1.2	0.615	1.78	0.24
2	51.5	179.8	1.2	0.286	1.39	0.42
3	54.1	45.5	1.5	1.189	2.43	0.15
4	54.8	131.4	1	0.417	1.67	0.23
5	67.6	74.4	2	0.908	2.20	0.15
6	47.1	87.5	2	0.538	1.65	0.16
7	55.6	270.4	1.7	0.205	1.40	0.55
8	47.8	63.9	3	0.749	1.87	0.32

Table DVI. Results of DBr-He Photolyses at 2300Å

Expt.	P_{DBr} (torr)	P_{H_2} (torr)	Photolysis Time(hrs.)	$\frac{[DBr]}{[H_2]}$	$\frac{[D_2]}{[HD]}$	conv. (%)
1	41.4	73.7	2.5	0.561	25.9	0.34
2	75.0	74.2	2.5	1.011	26.9	0.41
3	48.6	153.0	3	0.317	25.5	0.45
4	48.9	71.4	3	0.685	26.5	0.50

Figure D3. Results of DBr-H_2 and DBr-He photolyses at 2300Å.

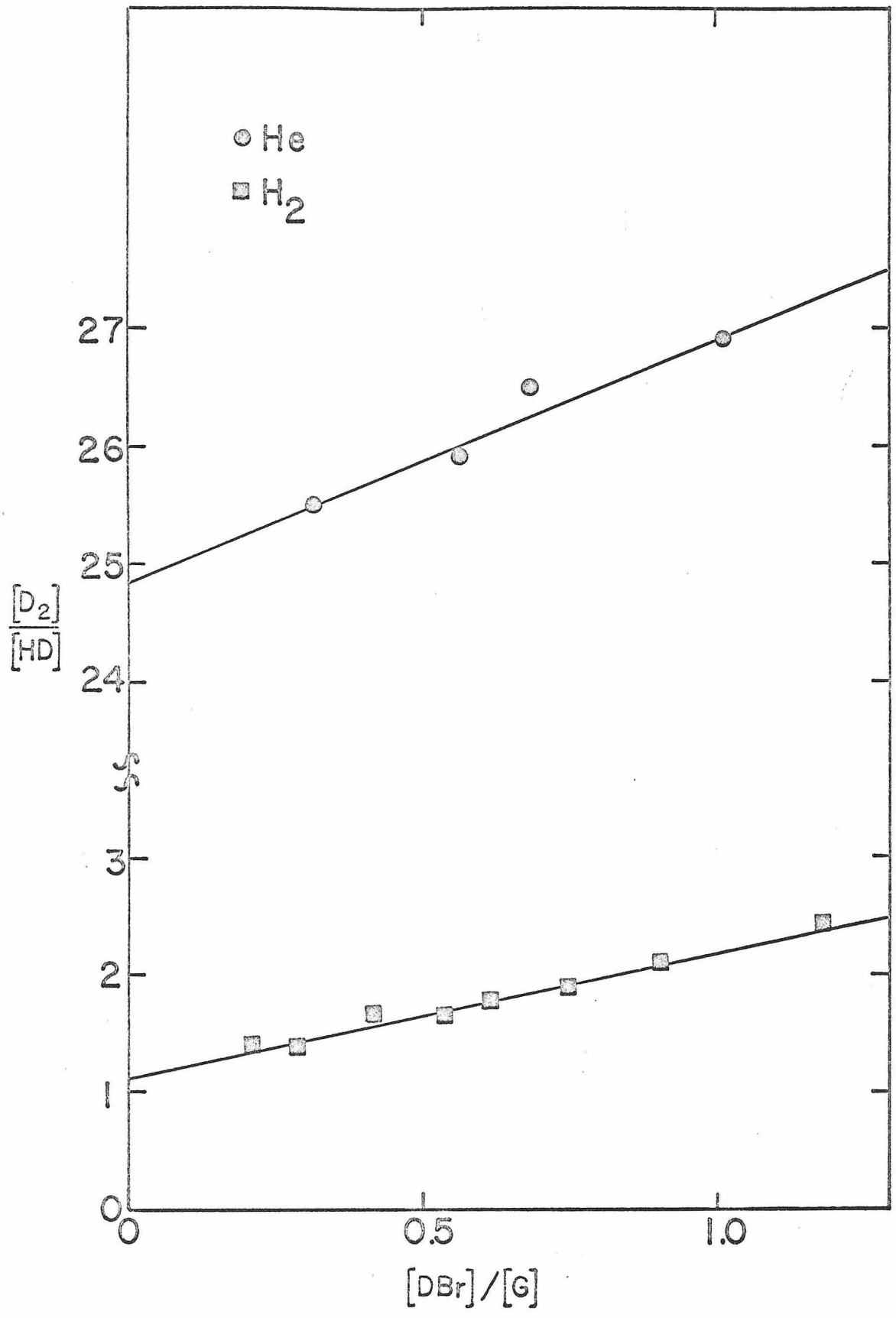
He
H2
27
26
25
24
3
2
1
0
0
0.5
1.0
[D2]/[HD]
[DBr]/[G]

resulted in conversions ranging from 0.15 to 0.30%.

The results of the DBr-H_2 photolyses are given in Table DV and are plotted in figure D3. Least squares analysis of these data gives a slope of 1.09 ± 0.08 and an intercept of 1.13 ± 0.05. The results of the DBr-He photolyses are given in Table DVI and are plotted in figure D3. Least squares analysis of these data gives a slope of 2.1 ± 0.4 and an intercept of 24.8 ± 0.2.

4. Photolyses at 2446Å

Photolyses of both DBr-H_2 and DBr-He mixtures were performed at this wavelength using the procedures described previously. The BH6 lamp was used in conjunction with the Bausch and Lomb monochromator set for a 32Å bandpass. The width of the peak at half height exiting from the monochromator was 34Å. The intensity was approximately 5 x 10^{14} photons/sec. Photolyses lasted an average of 3 hours with conversions of 0.35%.

Results of the DBr-H_2 experiments are listed in Table DVII and plotted in figure D4. Least squares analysis of these data gives a slope of 1.18 ± 0.04 and an intercept of 2.06 ± 0.02. Results of the DBr-He experiments are listed in Table DVIII and are plotted in figure D4. Least squares analysis of these data gives a slope of 2.9 ± 0.6 and an intercept of 16.4 ± 0.4.

Table DVII. Results of DBr-H_2 Photolyses at 2446Å

Expt.	P_{DBr} (torr)	P_{H_2} (torr)	Photolysis Time(hrs.)	$\frac{[DBr]}{[H_2]}$	$\frac{[D_2]}{[HD]}$	conv. (%)
1	49.1	59.7	2.8	0.822	3.01	0.345
2	50.9	176.5	3	0.288	2.38	0.351
3	50.6	57.5	3	0.877	3.14	0.352
4	49.0	133.0	3	0.368	2.49	0.349
5	46.3	43.6	2.5	1.061	3.28	0.344
6	31.5	68.7	3	0.459	2.64	0.353
7	47.8	164.1	3	0.291	2.38	0.351
8	46.1	77.5	3	0.595	2.75	0.348
9	38.7	60.9	3	0.635	2.83	0.349

Table DVIII. Results of DBr-He Photolyses at 2446Å

Expt.	P_{DBr} (torr)	P_{H_2} (torr)	Photolysis Time(hrs.)	$\frac{[DBr]}{[He]}$	$\frac{[D_2]}{[HD]}$	conv. (%)
1	42.9	140.9	4	0.304	17.1	0.45
2	50.2	52.3	2.9	0.960	19.1	0.37
3	41.5	79.5	4	0.512	18.2	0.46
4	37.6	61.5	4	0.611	18.3	0.47

Figure D4. Results of DBr-H_2 and DBr-He photolyses at 2446Å.

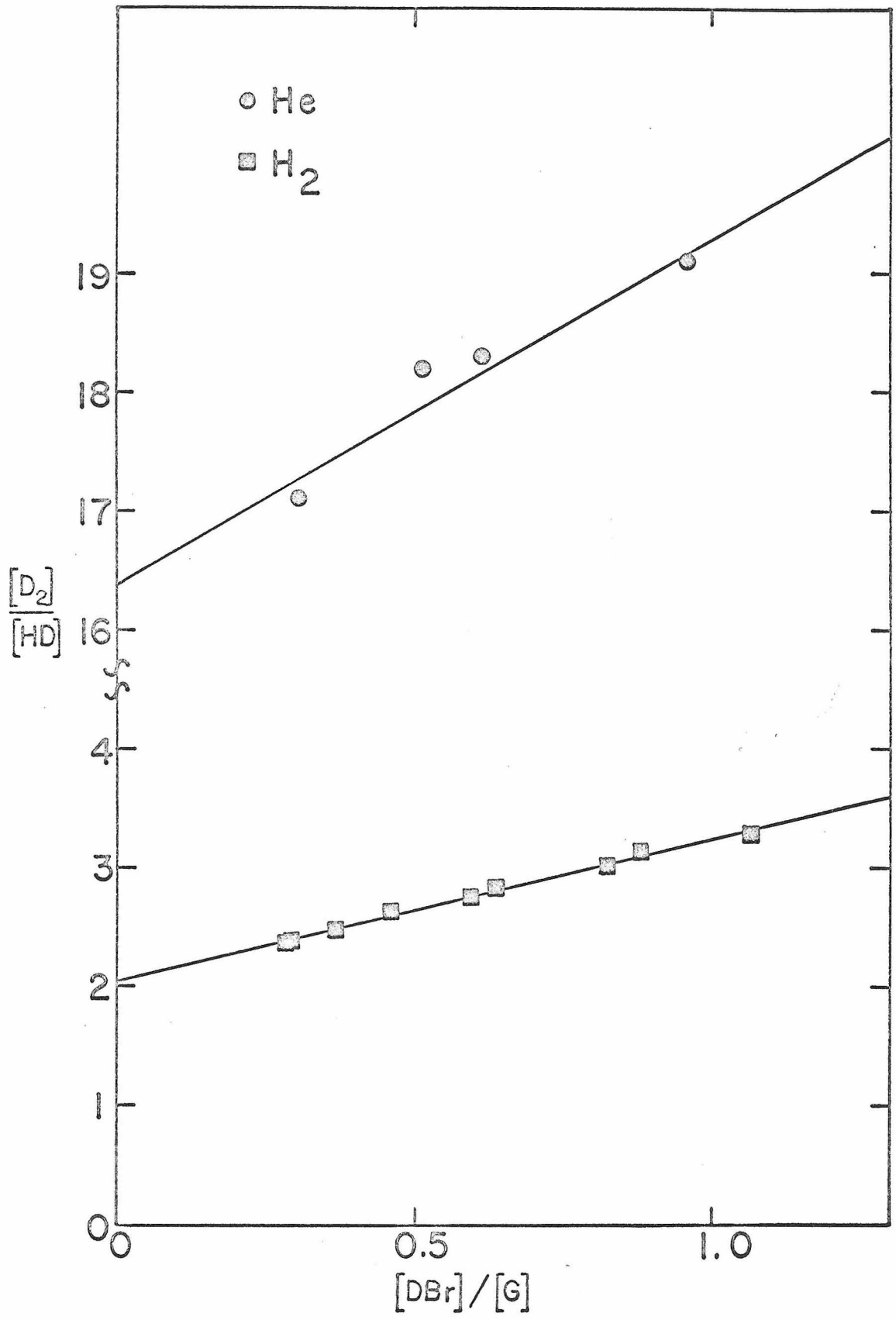
He
H2
19
18
17
[D2]/[HD]
16
4
3
2
1
0
0
0.5
1.0
[DBr]/[G]

5. Photolyses at 2483Å

Photolyses at this wavelength were carried out using the Hanovia 2500 watt mercury-xenon lamp. It was used in conjunction with the Bausch and Lomb monochromator with a bandpass of 24Å. A 7910 Corning glass filter was placed at the exit of the monochromator to remove any short wavelength radiation. The intensity of the lamp was approximately 3×10^{15} photons/sec. Photolyses lasted an average of 1 hour which resulted in conversions of 0.35%.

The results of the DBr-H_2 photolyses are given in Table DIX and Figure D5. Least squares analysis of these data gives a slope of 1.45 ± 0.07 and an intercept of 2.10 ± 0.06. The results of the DBr-He photolyses are given in Table DX and Figure D5. Least squares analysis of the data gives a slope of 2.2 ± 0.06 and an intercept of 13.3 ± 0.6.

6. Photolyses at 2500Å

Photolyses of both DBr-H_2 and DBr-He mixtures were carried out using the BH6 lamp with the Bausch and Lomb monochromator. The monochromator was set for a 32Å bandpass. The width of the peak at half-height was 30Å as measured with the Jarrell Ash monochromator. A 2mm thick Corning 7910 glass filter was placed at the exit of the monochromator to remove shorter wavelength radiation. The total intensity passing into the reaction vessel was 5.7×10^{14} photons/sec. Photolysis times ranged from 3.8 to 6 hours with conversions varying from 0.15% to 0.28%.

The results for DBr-H_2 photolyses are given in Table

Table DIX. Results of DBr-H_2 Photolyses at 2483Å

Expt.	P_{DBr} (torr)	P_{H_2} (torr)	Photolysis Time(hrs.)	$\frac{[DBr]}{[H_2]}$	$\frac{[D_2]}{[HD]}$	conv. (%)
1	77.3	55.1	1.2	1.402	4.16	0.40
2	31.7	110.3	1.1	0.288	2.56	0.43
3	41.9	71.8	1.0	0.582	2.84	0.33
4	49.0	66.0	1.0	0.742	3.24	0.35
5	54.8	47.9	1.0	1.142	3.73	0.36
6	56.7	179.7	1.0	0.316	2.45	0.33
7	48.5	37.3	1.0	1.301	3.97	0.34
8	32.7	83.2	1.0	0.393	2.79	0.37

Table DX. Results of DBr-He Photolyses at 2483Å

Expt.	P_{DBr} (torr)	P_{H_2} (torr)	Photolysis Time(hrs)	$\frac{[DBr]}{[He]}$	$\frac{[D_2]}{[HD]}$	conv. (%)
1	36.9	53.9	2.0	0.685	14.6	0.65
2	47.2	51.1	1.9	0.923	15.0	0.61
3	61.1	47.3	1.6	1.29	16.6	0.57
4	47.2	155.7	2.0	0.303	14.3	0.64

Figure D5. Results of DBr-H_2 and DBr-He photolyses at 2483Å.

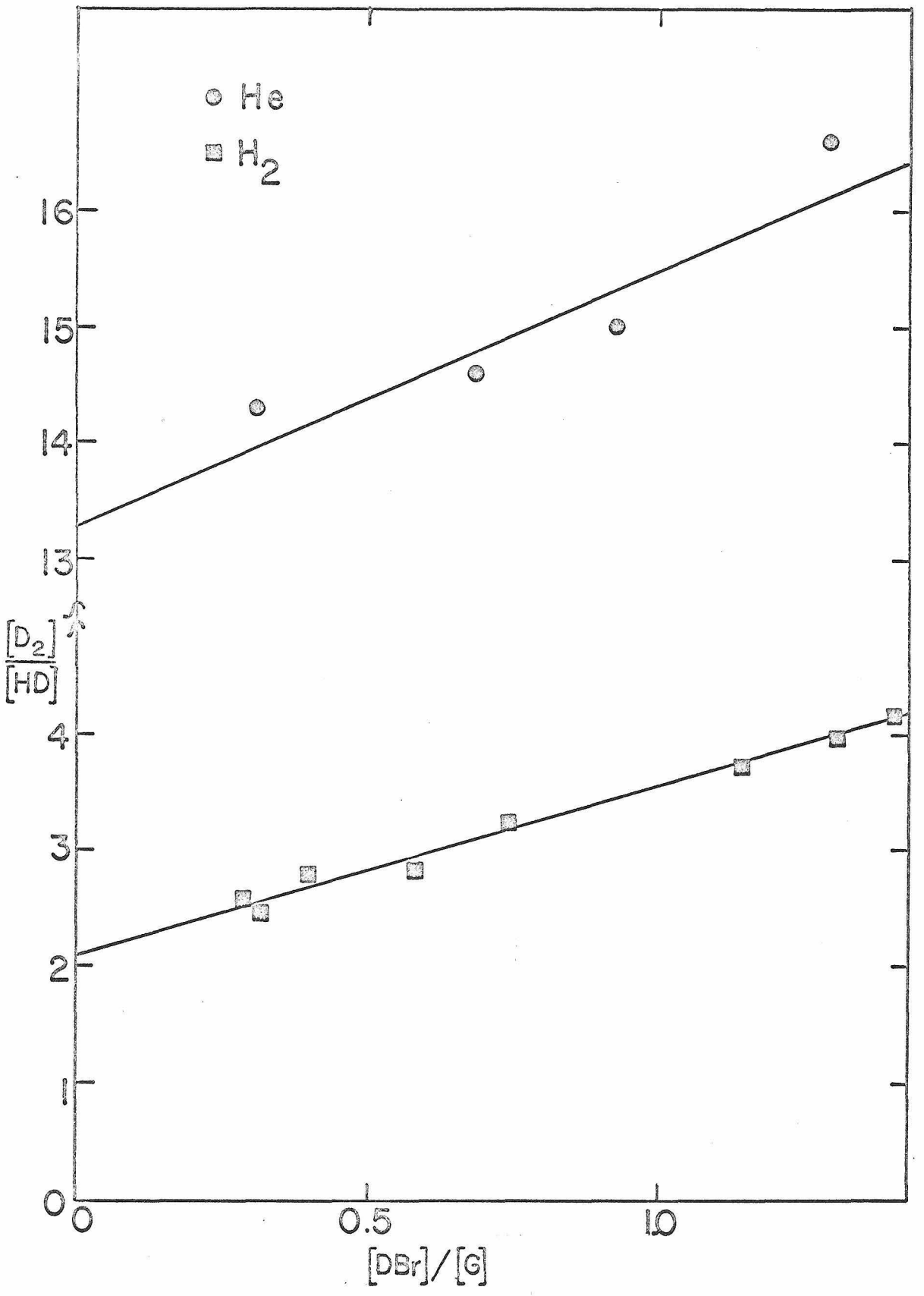
He
H2
16
15
14
13
[D2]/[HD]
4
3
2
1
0
0
0.5
1.0
[DBr]/[G]

Table DXI. Results of DBr-H_2 Photolyses at 2500Å

Expt.	P_{DBr} (torr)	P_{H_2} (torr)	Photolysis Time(hrs.)	$\frac{[DBr]}{[H_2]}$	$\frac{[D_2]}{[HD]}$	conv. (%)
1	34.1	83.3	4	0.410	2.97	0.26
2	40.9	31.2	4	1.310	3.61	0.19
3	33.4	34.5	3.8	0.969	3.44	0.15
4	22.2	77.6	4.5	0.286	2.70	0.18
5	30.3	46.3	5.0	0.655	3.11	0.23
6	32.1	91.2	6.0	0.352	2.80	0.28
7	44.5	77.5	5.5	0.575	2.93	0.23

Table DXII. Results of DBr-He Photolyses at 2500Å

Expt.	P_{DBr} (torr)	P_{H_2} (torr)	Photolysis Time(hrs.)	$\frac{[DBr]}{[He]}$	$\frac{[D_2]}{[HD]}$	conv. (%)
1	27.3	91.4	4	0.299	16.55	0.21
2	43.0	44.6	3	0.964	18.12	0.16
3	28.8	97.1	3	0.296	16.65	0.13
4	35.9	69.1	3	0.519	17.13	0.17
5	40.7	40.8	3	1.00	17.36	0.19
6	34.4	44.9	3	0.765	17.12	0.18

Figure D6. Results of DBr-H_2 and DBr-He photolyses at 2500Å.

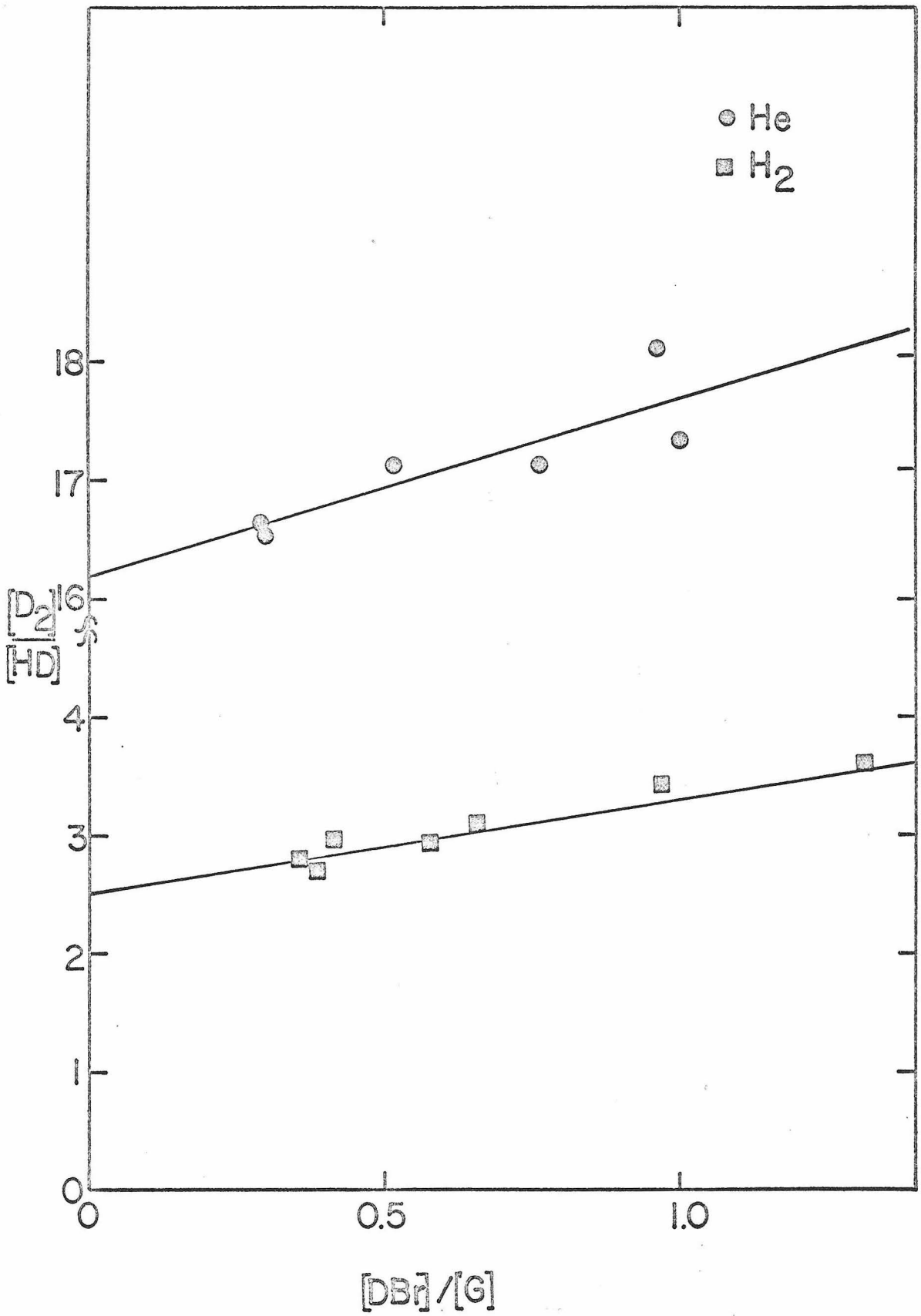
He
H2
18
17
16
4
3
2
1
0
0
0.5
1.0
[D2]/[HD]
[DBr]/[G]

DXI and Figure D6. Least squares analysis of the data gives a slope of 0.88 ± 0.08 and an intercept of 2.51 ± 0.06. The results for the DBr-He photolyses are given in Table XII and Figure 6. Least squares analysis of the data gives a slope of 1.5 ± 0.5 and an intercept of 16.2 ± 0.4.

7. Photolyses at 2537Å

Two different series of photolyses were done at 2537Å. One used the Hanovia SC 2537 low pressure mercury lamp with the 2mm Corning 7910 glass filter while the other used the same SC 2537 lamp at one end of the reaction vessel and the low pressure mercury Phillips spectral lamp at the other end. Intensities of both lamps were approximately 1×10^{16} photons/sec. The two series were done at intervals 3 months apart. The second series was also a study of the effect of DBr conversion on the experiments. For the first set of experiments photolysis times ranged from 8 to 11 hours resulting in DBr conversions of from 0.57% to 0.86%. In the second set of experiments, one group of experiments had photolysis times of 4 hours resulting in 0.53% conversion and another group had photolysis times of 10 hours resulting in 1.02% conversion.

The results for the first series of DBr-H_2 and DBr-He experiments are given in Tables DXIII and DXIV respectively, and both are plotted in Figure D7. Least squares analysis of the data gives a slope of 1.32 ± 0.05 and an intercept of 2.36 ± 0.04 for the DBr-H_2 experiments and a slope of 2.0 ± 0.1 and an

Table DXIII. Results of DBr-H_2 Photolyses at 2537Å, Set I

Expt.	P_{DBr} (torr)	P_{H_2} (torr)	Photolysis Time(hrs.)	$\frac{[DBr]}{[H_2]}$	$\frac{[D_2]}{[HD]}$	conv. (%)
1	50.3	176.3	8.0	0.285	2.70	0.70
2	44.3	140.6	10.5	0.315	2.73	0.76
3	50.4	64.8	7.5	0.778	3.40	0.57
4	42.5	37.7	7.1	1.128	3.95	0.56
5	37.3	122.6	9.75	0.304	2.84	0.75
6	36.0	67.7	8.0	0.531	3.01	0.62
7	32.1	83.5	11.0	0.384	2.91	0.86
8	50.8	32.6	9.7	1.57	4.39	0.699

Table DXIV. Results of DBr-He Photolyses at 2537Å, Set I

Expt.	P_{DBr} (torr)	P_{H_2} (torr)	Photolysis Time(hrs.)	$\frac{[DBr]}{[He]}$	$\frac{[D_2]}{[HD]}$	conv. (%)
1	40.4	101.0	9.9	0.399	10.91	0.70
2	58.9	48.4	8.0	1.219	12.68	0.61
3	27.7	95.0	10.5	0.292	10.87	0.77
4	34.6	75.6	11.0	0.458	11.10	0.85

Figure D7. Results of photolyses at 2537Å, Set I.

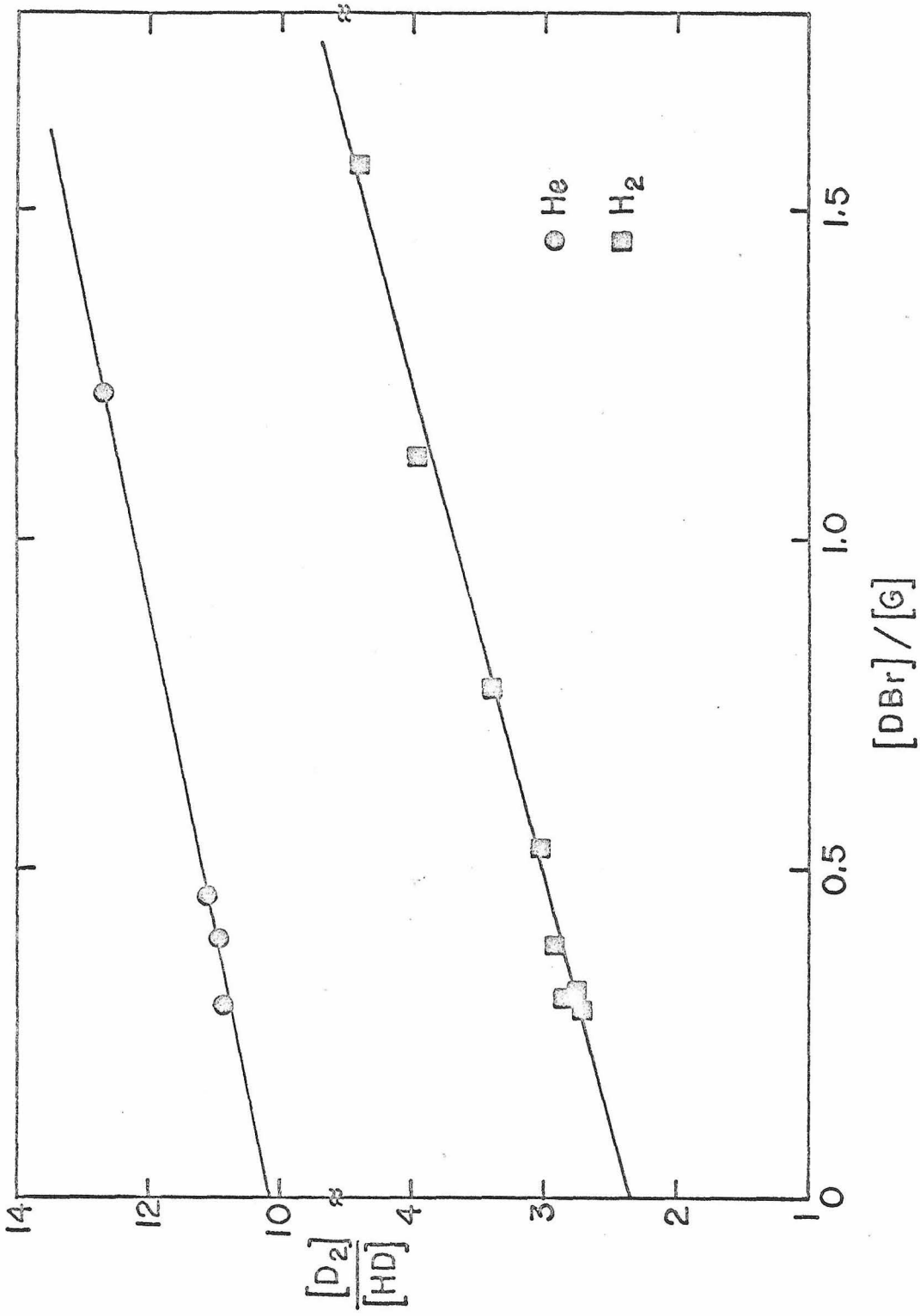
He
H2
[D2]/[HD]
[DBr]/[G]
0
0.5
1.0
1.5
2
3
4
10
12
14

Table DXV. Results of Variable Conversion DBr-H_2 Photolyses at 2537Å

Expt.	P_{DBr} (torr)	P_{H_2} (torr)	Photolysis Time(hrs.)	$\frac{[DBr]}{[H_2]}$	$\frac{[D_2]}{[HD]}$	conv. (%)
1	78.1	78.8	4.0	0.991	3.96	0.53
2	55.7	176.3	4.0	0.316	3.08	0.54
3	52.9	112.8	10.0	0.469	3.24	1.02
4	60.7	40.6	10.0	1.492	4.55	1.02
5	73.5	49.6	4.0	1.482	4.56	0.54
6	51.9	176.5	10.0	0.294	3.04	1.02
7	66.4	212.5	4.0	0.312	2.98	0.52
8	77.0	72.5	10.0	1.062	3.98	1.03
9	52.3	76.4	4.0	0.685	3.51	0.55
10	56.9	73.0	10.0	0.779	3.70	1.01
11	53.0	88.0	4.0	0.602	3.62	0.51
12	55.6	182.8	10.0	0.304	3.12	1.05
13	45.0	107.2	4.0	0.419	3.31	0.51

Table DXVI. Results of DBr-He Photolyses at 2537Å, set II

Expt.	P_{DBr} (torr)	P_{H_2} (torr)	Photolysis Time(hrs.)	$\frac{[DBr]}{[He]}$	$\frac{[D_2]}{[HD]}$	conv. (%)
1	62.0	39.9	4.5	1.554	15.4	0.57
2	45.7	161.0	4.0	0.284	14.4	0.54
3	56.3	55.9	4.0	1.026	14.3	0.53
4	43.5	151.6	10.2	0.287	14.1	1.04
5	47.1	194.7	5.0	0.241	13.0	0.61
6	50.5	71.6	4.1	0.705	13.7	0.56

Figure D8. Results of variable conversion photolyses at 2537Å, Set II.

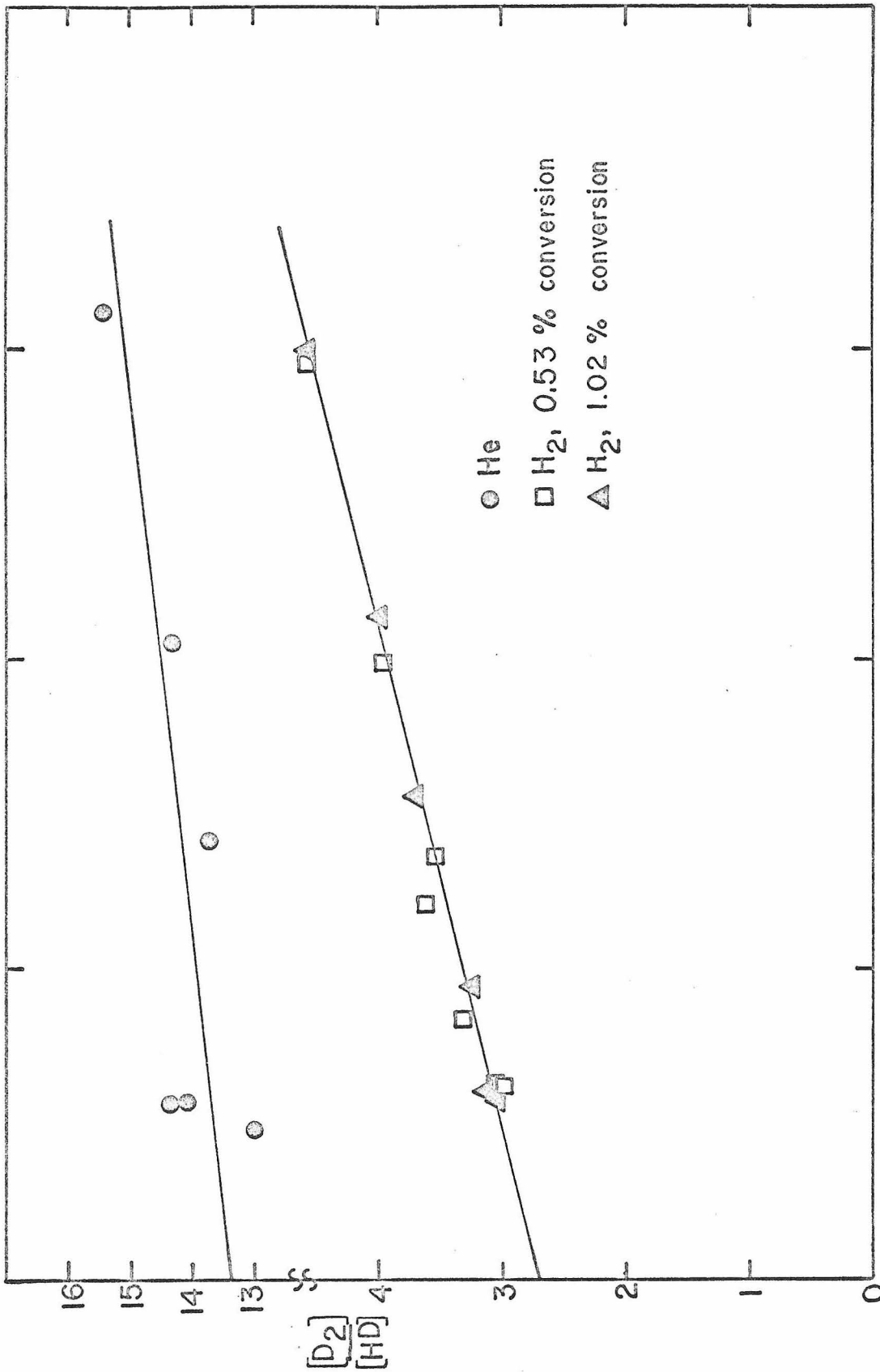
He
H2, 0.53 % conversion
H2, 1.02 % conversion
[D2]/[HD]
[DBr]/[G]
0
0.5
1.0
1.5
1
2
3
4
13
14
15
16

intercept of 10.18 ± 0.09 for the DBr-He experiments. The results for the second series of DBr-H_2 and DBr-He experiments are tabulated in Tables DXV and DVI respectively and plotted in Figure D8. Least squares analysis of all DBr-H_2 data gives a slope of 1.25 ± 0.05 and an intercept of 2.70 ± 0.04. The slope and intercept from the data of experiments at 0.53% conversion are 1.27 ± 0.09 and 2.70 ± 0.04 while those from the experiments at 1.02% conversion are 1.23 ± 0.04 and 2.70 ± 0.03. Hence we are able to conclude that the extent of conversion of DBr has no effect on the results for conversions less than 1%. Least squares analysis of the DBr-He experiments gives a slope of 1.1 ± 0.5 and an intercept of 13.4 ± 0.4. The descrepancies between data sets I and II can be most plausibly explained by a change in the condition of the internal surfaces of the reaction vessel over the period of 3 months. An average of the two sets of data were used in the results given in Paper 1.

8. Photolysis of DI at 2891Å

Photolyses at this wavelength were done using the Hanovia 2500 watt mercury-xenon lamp in conjunction with the Bausch and Lomb monochromator. The monochromator was set for a 16Å bandpass. The width at half height of the peak at 2891Å was 11Å as measured with the Jarrell Ash monochromator. A 2 mm thick pyrex filter (transmission 20% at 2890, 1% at 2700Å) was placed at the exit of the monochromator to cut out any short wavelength radiation. The intensity of light exiting through the monochromator with the

Table DXVII. Results of DI-H_2 Photolyses at 2891Å

Expt.	P_{DI} (torr)	P_{H_2} (torr)	Photolysis Time(hrs.)	$\frac{[DI]}{[H_2]}$	$\frac{[D_2]}{[HD]}$	conv. (%)
1	27.8	37.0	2.0	0.752	3.76	0.51
2	31.2	30.2	2.0	1.035	4.32	0.52
3	47.0	48.6	1.5	0.966	4.22	0.46
4	50.6	32.0	2.0	1.584	5.35	0.50
5	64.0	37.9	2.0	1.689	5.57	0.51
6	46.2	156.3	2.0	0.295	2.90	0.51
7	28.9	101.5	2.1	0.284	3.00	0.53

Table DXVIII. Results of DI-He Photolyses at 2891Å

Expt.	P_{DI} (torr)	P_{He} (torr)	Photolysis Time(hrs.)	$\frac{[DI]}{[He]}$	$\frac{[D_2]}{[HD]}$	conv. (%)
1	47.1	145.6	2.5	0.323	14.0	0.56
2	41.0	123.6	2.5	0.332	15.0	0.56
3	52.6	44.7	3.0	1.176	16.1	0.62
4	34.6	46.2	3.0	0.750	15.6	0.62
5	44.3	48.1	3.0	0.920	15.7	0.62

Figure D9. Results of DI-H_2 and DI-He photolyses at 2891Å.

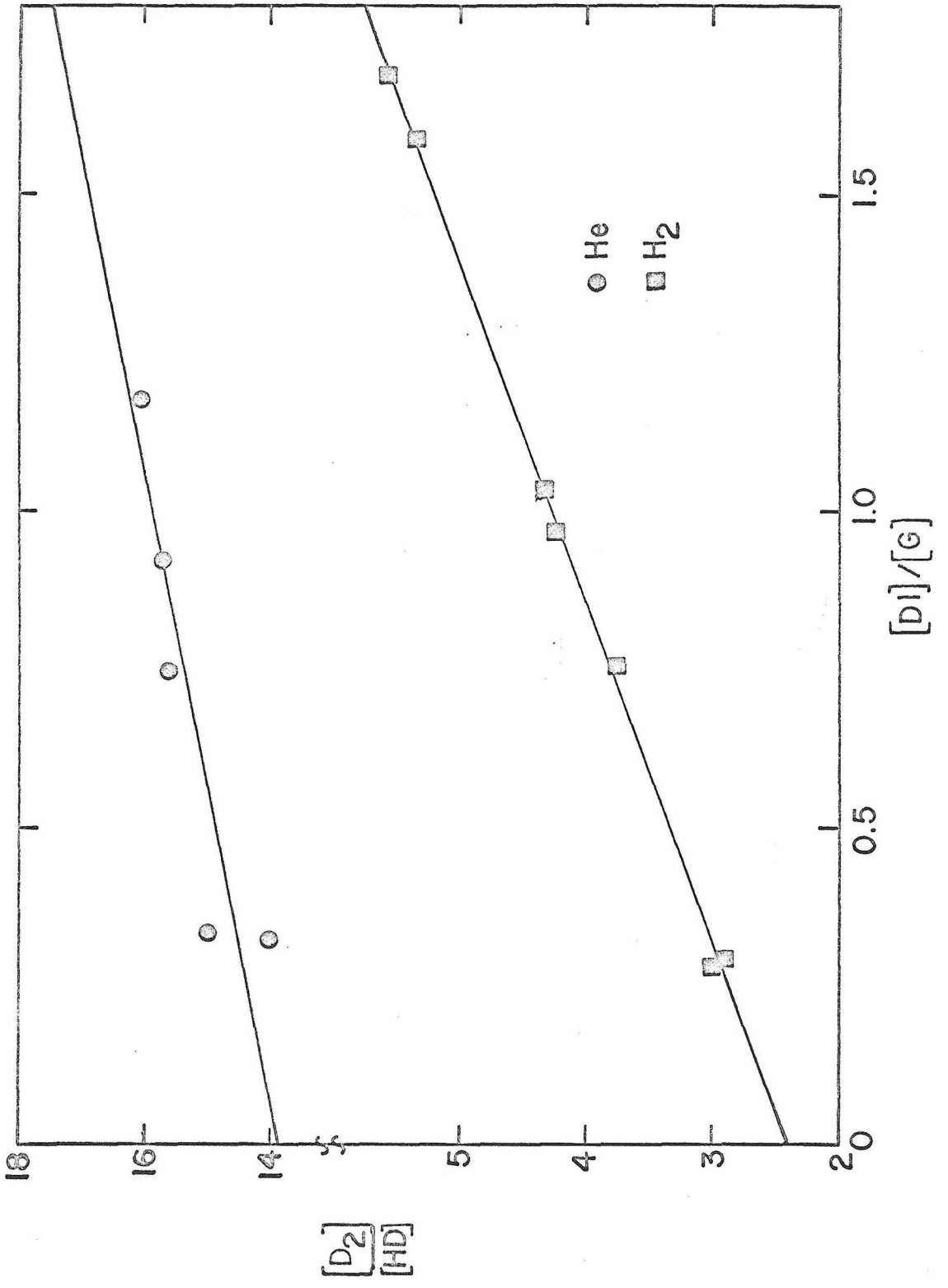
He
H2
[D2]/[HD]
[D]/[G]
18
16
14
5
4
3
2
0.5
1.0
1.5

filter was 2.8×10^{15} photons/sec. A 3-inch long, 2-inch diameter fused silica reaction vessel with optical quality quartz windows was used for the photolyses. Photolysis times were two hours which resulted in a conversion of 0.61%.

The results for the DI-H_2 and DI-He experiments are tabulated in Tables DXVII and DXVIII respectively and plotted in Figure D9. Least squares analysis of the DI-H_2 photolysis data gives a slope of 1.87 ± 0.03 and an intercept of 2.40 ± 0.03. Least squares analysis of the DI-He photolysis data gives a slope of 2.0 ± 0.8 and an intercept of 13.9 ± 0.6.

9. Photolysis of DI at 3030Å - Study of DI Conversion

Photolyses were performed at 3030Å to determine the effect of extent DI conversion on the experiments. The Hanovia 2500 watt xenon-mercury lamp was used for photolysis in conjunction with the Bausch and Lomb monochromator set for a bandpass of 24Å. The width of the peak at half-height as measured with the Jarrell Ash monochromator was 20Å. The intensity coming through the reaction vessel was approximately 6×10^{15} photons/sec. Photolyses lasted 30 minutes, 1 hour and 2 hours resulting in conversions of 0.55%, 1.2% and 2.1% respectively.

Results of the DI-H_2 experiments are tabulated in Table DXIX and plotted in Figure D10. Least squares analysis of all data gives a slope of 1.44 ± 0.11 and an intercept of 3.06 ± 0.10. For the 0.55% conversion experiments the slope is 1.46 ± 0.21 and the intercept is 3.00 ± 0.18, for the 1.2% conversion runs

Table DXIX. Results of DI-H_2 Photolyses at 3030Å

Expt.	P_{DI} (torr)	P_{H_2} (torr)	Photolysis Time(hrs)	$\frac{[DI]}{[H_2]}$	$\frac{[D_2]}{[HD]}$	conv. (%)
1	39.9	40.8	2.0	0.976	4.23	2.1
2	36.4	113.8	2.0	0.320	3.33	2.1
3	32.3	19.4	2.0	1.074	4.71	2.1
4	32.0	29.8	2.0	1.074	4.71	2.1
5	29.9	51.8	2.0	0.576	4.00	2.1
6	36.8	26.9	1.0	1.368	4.95	1.2
7	38.4	76.7	1.0	0.501	3.79	1.2
8	33.8	96.4	1.0	0.351	3.62	1.2
9	51.4	171.6	1.0	0.299	3.68	1.2
10	29.4	26.6	0.5	1.106	4.54	0.55
11	35.0	60.1	0.5	0.582	3.95	0.55
12	36.3	22.8	0.5	1.590	5.46	0.55
13	30.8	93.1	0.5	0.331	3.44	0.55
14	37.6	134.8	0.45	0.279	3.57	0.55
15	36.1	30.9	0.5	1.169	4.65	0.55
16	35.7	116.0	0.5	0.308	3.27	0.55
17	40.8	54.4	0.55	0.750	4.00	0.56

Table DXX. Results of DI-He Photolyses at 3030Å

Expt.	P_{DI} (torr)	P_{He} (torr)	Photolysis Time(hrs)	$\frac{[DI]}{[He]}$	$\frac{[D_2]}{[HD]}$	conv. (%)
1	35.0	115.0	1.5	0.304	8.95	1.7
2	34.5	25.7	1.5	1.342	9.74	1.7
3	38.0	43.4	1.5	0.875	9.94	1.7
4	37.6	128.3	1.5	0.293	9.81	1.7

Figure D10. Results of DI-H_2 and DI-He photolyses at 3030Å.

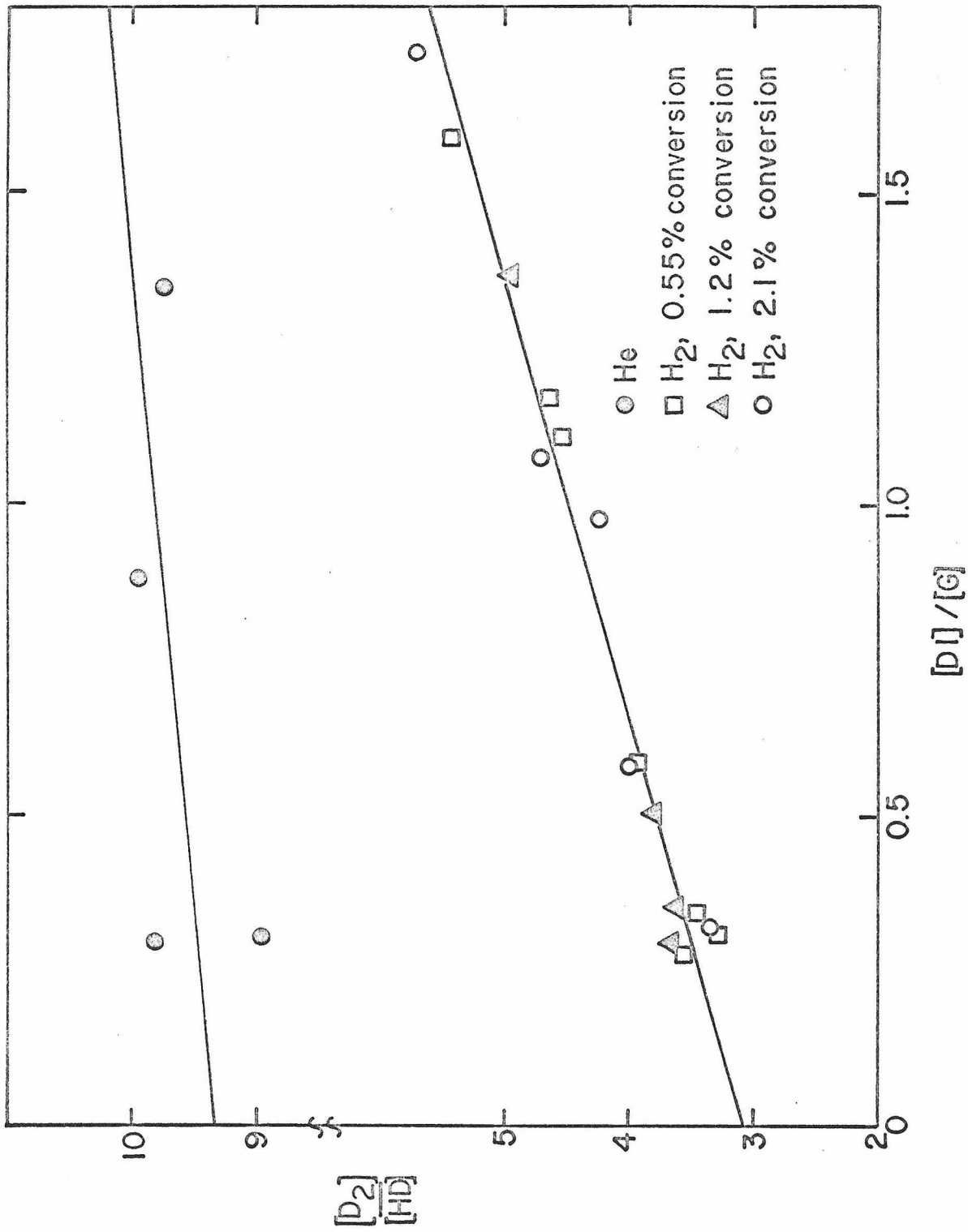
10
9
5
4
3
2
0
0.5
1.0
1.5
[D2]/[HD]
[D]/[G]
He
H2, 0.55% conversion
H2, 1.2% conversion
H2, 2.1% conversion

the slope is 1.29 ± 0.23 and the intercept is 3.2 ± 0.1, and for the 2.1% conversion experiments the slope is 1.6 ± 0.1 and the intercept is 2.9 ± 0.2. These results show no trend with DI conversion and lead to the conclusion that the amount of DI decomposition is not important if conversions are kept below 2%.

The results for the DI-He experiments are tabulated in Table DXX. The conversion was not varied in these experiments since even a large error in the intercept would lead to a small error in the integral reaction yield in which we are interested. Least squares analysis of the data gives a slope of 0.42 ± 0.55 and an intercept of 9.3 ± 0.4.

10. Photolysis of DI-H_2 and DI-He Mixtures at 3261Å

Experiments at this wavelength were performed using the cadmium Phillips spectral lamp with a 5 mm Corning 0160 glass filter to eliminate the short wavelength lines. A 16 cm long, 2.5 cm diameter pyrex reaction vessel with a 3.2 cm inside diameter teflon sleeve was used. The intensity of the lamp with the filter was approximately 5×10^{15} photons/sec. Photolyses lasted from 7 to 22 hours resulting in conversions ranging from 0.27% to 0.78%.

Results for the DI-H_2 photolyses are tabulated in Table DXXI and plotted in Figure D11. Least squares analysis of the data gives a slope of 1.5 ± 0.3 and an intercept of 3.4 ± 0.3. Results of the DI-He photolyses are tabulated in Table DXXII and plotted in Figure D11. Least squares analysis of this data gives a

Table XXI. Results of DI-H_2 Photolyses at 3261Å

Expt.	P_{DI} (torr)	P_{H_2} (torr)	Photolysis Time(hrs.)	$\frac{[DI]}{[H_2]}$	$\frac{[D_2]}{[HD]}$	conv. (%)
1	28.1	32.5	9.0	0.863	4.25	0.36
2	38.8	26.7	8.8	1.454	5.94	0.36
3	25.3	89.0	22.0	0.284	3.78	0.78
4	31.8	52.9	10.6	0.601	4.67	0.40
5	27.9	26.0	14.5	1.073	4.73	0.32
6	25.2	24.5	8.0	1.029	4.95	0.27
7	22.8	51.0	13.5	0.447	4.29	0.49

Table DXXII. Results of DI-He Photolyses at 3261Å

Expt.	P_{DI} (torr)	P_{H_2} (torr)	Photolysis Time(hrs.)	$\frac{[DI]}{[He]}$	$\frac{[D_2]}{[HD]}$	conv. (%)
1	29.6	109.1	7.9	0.272	5.10	0.27
2	25.4	22.6	9.0	1.122	5.80	0.38
3	38.2	24.3	7.1	1.572	6.15	0.23
4	30.3	45.7	6.9	0.663	6.00	0.22
5	27.0	70.7	12.9	0.382	5.75	0.48
6	28.8	29.8	8.2	0.968	6.30	0.28

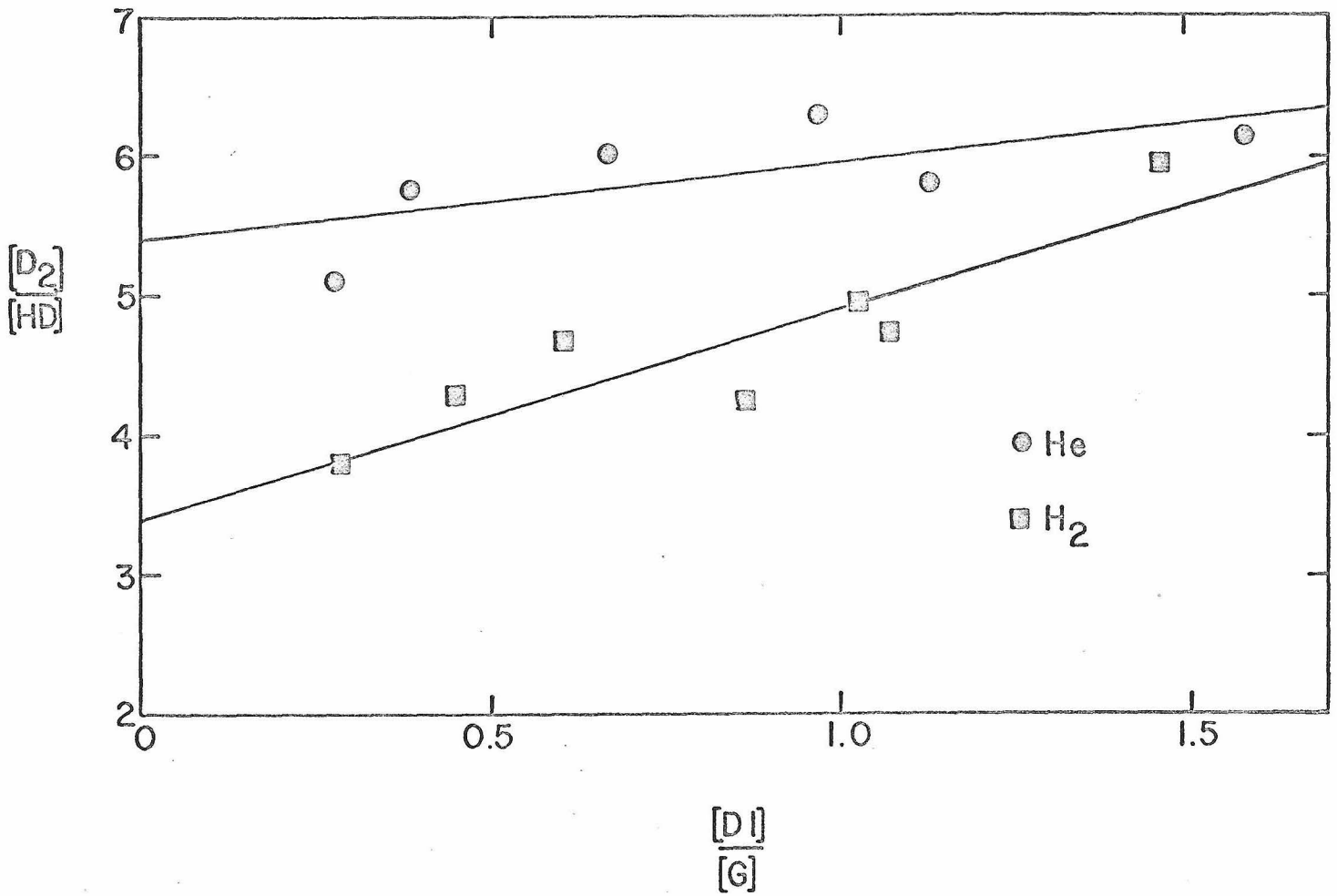

Figure D11. Results of DI-H_2 and DI-He photolyses at 3261Å.

slope of 0.59 ± 0.31 and an intercept of 5.4 ± 0.3.

11. Experiments to Determine the Fraction of Excited Iodine Atoms Produced in the Photolysis of DI.

11.1 DI Photolysis at 2138Å

Several experiments were performed at 2138Å to determine the fraction of iodine atoms produced in the excited $^2P_{1/2}$ state in the photolysis of DI. The analysis of this and the following experiments is found in Paper 3. The zinc Phillips spectral lamp with the cis-2-butene filter was used for photolysis. The intensity of the lamp with the filter was approximately 2×10^{15} photons/sec. The 3-inch long, 2-inch diameter fused silica reaction vessel was used. Photolysis times ranged from 10-15 minutes with conversions of 0.5%.

The results of these experiments are given in Table DXXIII and plotted in Figure D12. Least squares analysis of the DI-H_2 data gives a slope of 1.35 ± 0.02 and an intercept of 0.45 ± 0.02. The intercept of the helium experiments is taken as 9.4 ± 0.5.

11.2 DI Photolysis at 2400Å

The experiments at this wavelength were done using the General Electric BH6 lamp in conjunction with the Bausch and Lomb monochromator with a bandpass set for 32Å. The 3-inch long, 2-inch diameter fused silica reaction vessel was used. The intensity of the lamp was 3.7×10^{14} photons/sec. Photolyses lasted

Table DXXIII. Results of DI experiments at 2138Å

Expt.	Gas	P_{DI} (torr)	P_{H_2} (torr)	Photolysis Time(min.)	$\frac{[DI]}{[gas]}$	$\frac{[D_2]}{[HD]}$	conv. (%)
1	H_2	41.4	135.9	10	0.304	0.847	0.76
2	H_2	40.7	40.1	15	1.010	1.820	0.82
3	H_2	38.3	130.4	15	0.294	0.872	0.83
4	H_2	36.3	27.7	15	1.301	2.20	0.82
5	He	40.4	140.8	20	0.287	9.63	0.89
6	He	34.7	26.6	15	1.304	10.47	0.81

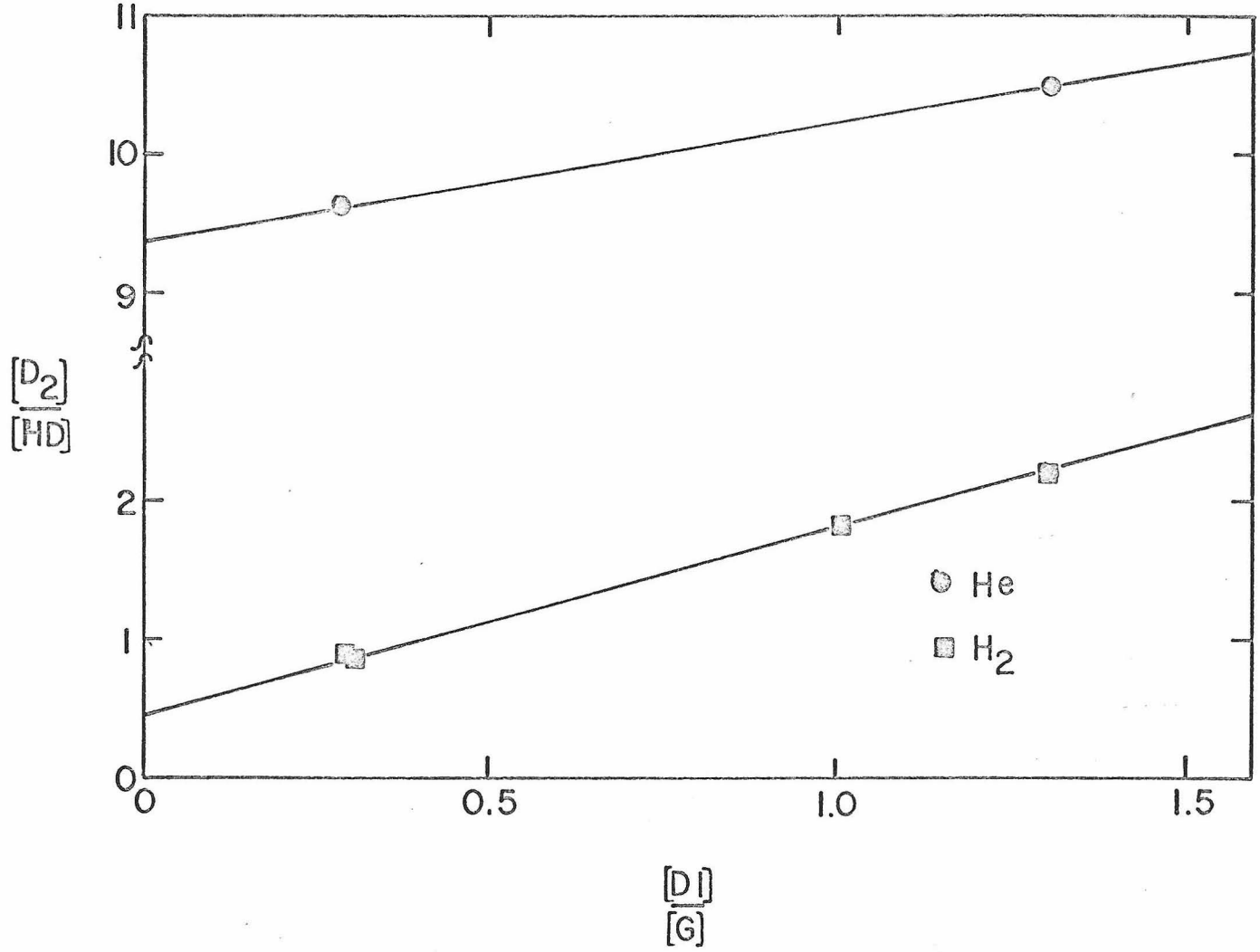

Figure D12. Results of DI-H_2 and DI-He photolyses at 2138Å.

Table DXXIV. Results of DI Experiments at 2400Å

Expt.	Gas	P_{DI} (torr)	P_{H_2} (torr)	Photolysis Time(min.)	$\frac{[DI]}{[gas]}$	$\frac{[D_2]}{[HD]}$	conv. (%)
1	H_2	28.4	95.2	60	0.299	1.68	1.03
2	H_2	35.6	32.6	30	1.092	2.98	0.51
3	H_2	53.5	36.5	30	1.465	3.69	0.50
4	H_2	50.2	153.0	30	0.328	1.87	0.51
5	H_2	32.9	29.0	30	1.135	3.16	0.52
6	He	36.5	114.1	30	0.320	13.2	0.51
7	He	45.5	33.4	30	1.362	16.7	0.50
8	He	37.2	43.4	30	0.858	14.8	0.51

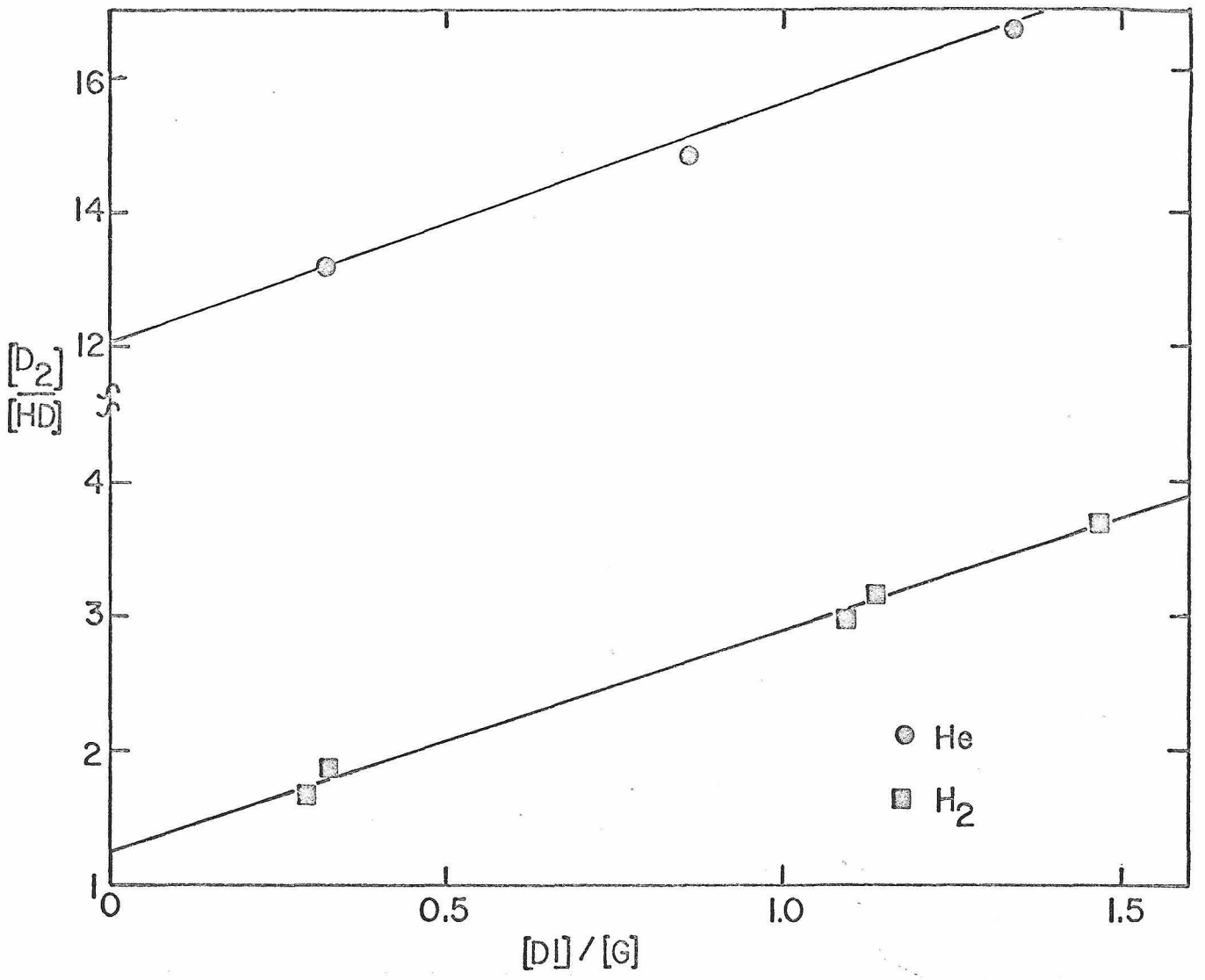

Figure D13. Results of DI-H_2 and DI-He photolyses at 2400Å.

30 minutes with a conversion of 0.6%.

The results of these experiments are tabulated in Table DXXIV and plotted in Figure D13. Least squares analysis for the DI-H_2 data gives a slope of 1.65 ± 0.07 and an intercept of 1.25 ± 0.07. Least squares analysis for the DI-He data gives a slope of 3.5 ± 0.2 and an intercept of 12.1 ± 0.2.

11.3 DI Photolysis at 2805Å

The Hanovia 2500 watt xenon-mercury lamp in conjunction with the Bausch and Lomb monochromator with a bandpass of 20Å was used for photolysis at this wavelength. A 2 mm thick Corning 7910 glass filter was placed at the exit of the monochromator to remove any shorter wavelength radiation. The 3-inch long, 2-inch diameter fused silica reaction vessel was used. The intensity exiting from the monochromator was 1.8×10^{15} photons/sec. Photolyses lasted from 15 to 45 minutes with conversions ranging from 0.4 to 0.9%.

Results of both the DI-H_2 and DI-He experiments are tabulated in Table DXXV and plotted in Figure D14. Linear least squares analysis of the DI-H_2 data gives a slope of 2.0 ± 0.4 and an intercept of 1.4 ± 0.4. The intercept of the DI-He experiments was taken as 11.2 ± 0.5 on the basis of the three experiments which were done.

Table DXXV. Results of DI Experiments at 2805Å

Expt.	Gas	P_{DI} (torr)	P_{H_2} (torr)	Photolysis Time(min)	$\frac{[DI]}{[gas]}$	$\frac{[D_2]}{[HD]}$	conv. (%)
1	H_2	23.2	77.9	15	0.298	1.79	0.56
2	H_2	45.6	37.4	15	1.221	4.00	0.57
3	H_2	30.0	29.3	15	1.023	3.28	0.58
4	H_2	39.8	81.5	15	0.488	2.76	0.56
5	He	33.2	137.2	15	0.319	11.25	0.58
6	He	29.2	34.6	20	0.844	11.30	0.58
7	He	32.8	46.9	15	0.700	11.40	0.57

Figure D14. Results of DI-H_2 and DI-He photolyses at 2805Å.

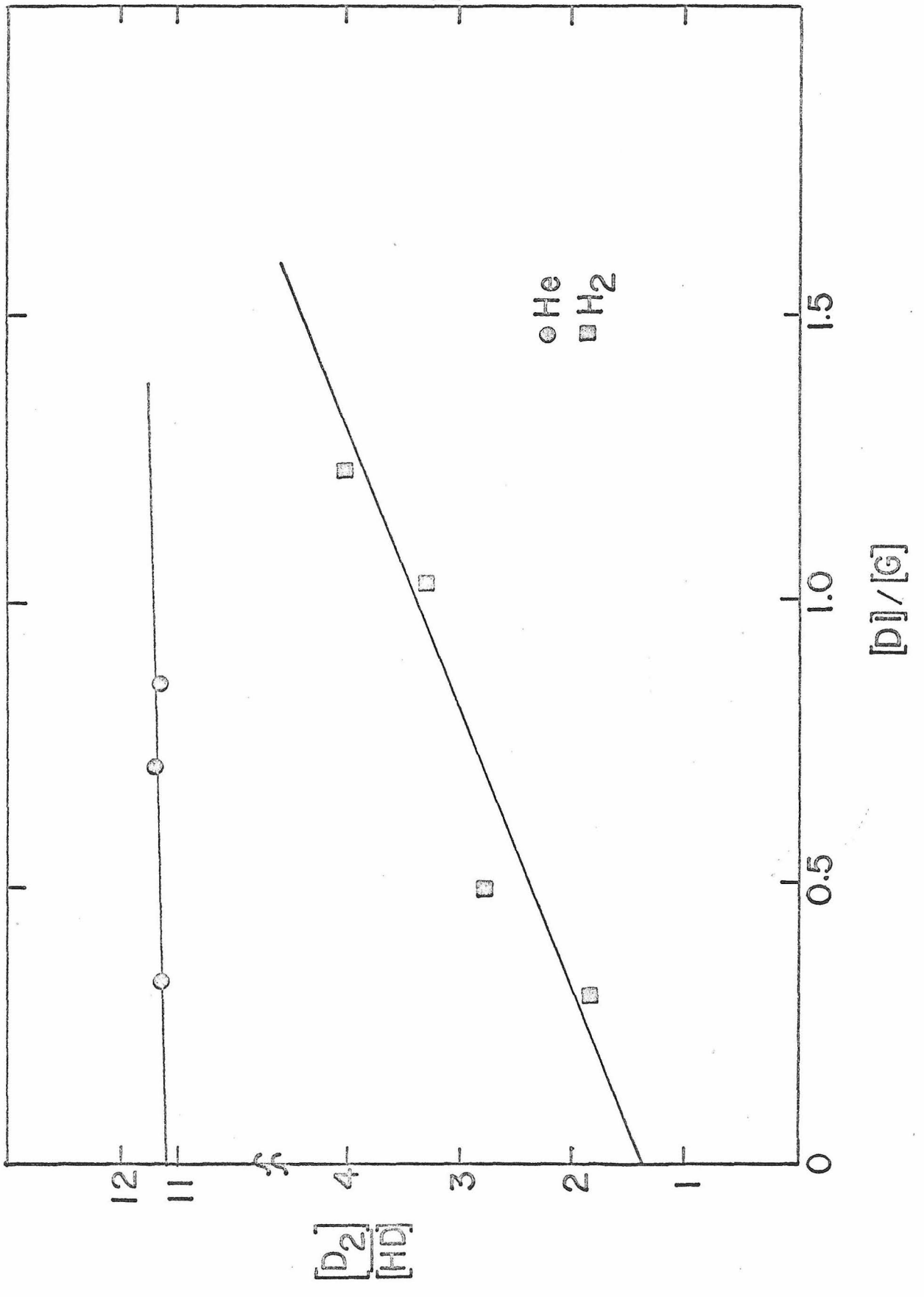
[D2]/[HD]
[D]/[G]
He
H2
0
0.5
1.0
1.5
1
2
3
4
11
12

APPENDIX E

ADDITIONAL EXPERIMENTAL RESULTS FOR H + CD_4

1. Preliminary Experiments

Preliminary experiments were run at wavelengths of 2138Å, 2061Å and 2288Å. The 1 1/2-inch diameter, 6-inch long fused silica reaction vessel described in Paper 4 was used for all experiments. The experimental procedure was the same as that described in Paper 4 and Appendix C. The first experiments were done with HBr/CD_4 ratios ranging from 0.03 to 0.15 in accordance with the ratios used by Martin and Willard[1] and by Carter, Hamill and Williams[2] for the same system.

1.1 Preliminary experiments at 2138Å

The photolyses at this wavelength were done using the zinc Phillips spectral lamp with the cis-2-butene filter. The photolyses lasted 3 hours resulting in approximately 1.5% conversion.

The results of the first series of experiments performed at 2138Å are shown in Table EI and in the lower curve of Figure E1. They had a slope of 10.6 ± 6.0 and an intercept of 17.4 ± 0.6. About 2 months later, a second series of experiments was performed at this wavelength to check for internal consistency of the results. These were done under the same experimental conditions with the exception that the conversion was 0.5%. The results of these experiments are shown in Table EII and the upper line in Figure E1. They had a slope of 105 ± 6 and an intercept of

Table E1. Results of HBr-CD_4 Photolyses at 2138Å With [HBr]/[CD_4] Ratios from 0.03 to 0.1. Conversion 1.5%

Expt.	P_{HBr} (torr)	P_{CD_4} (torr)	Photolysis Time(hrs.)	$\frac{[HBr]}{[CD_4]}$	$\frac{[H_2]}{[HD]}$
1	10.54	230.7	3.0	0.0456	23.4
2	10.52	261.2	3.0	0.0403	22.0
3	11.71	107.2	3.0	0.109	28.9
4	11.76	152.4	3.0	0.0771	26.0
5	11.37	333.6	3.0	0.0342	20.2
6	8.63	345.6	3.0	0.0250	19.0
7	9.80	123.9	3.0	0.0792	26.1
8	9.79	80.6	3.0	0.121	29.0
9	11.49	150.7	3.0	0.0762	26.2
10	10.22	174.9	3.0	0.0585	23.2
11	10.11	100.1	3.0	0.101	29.1

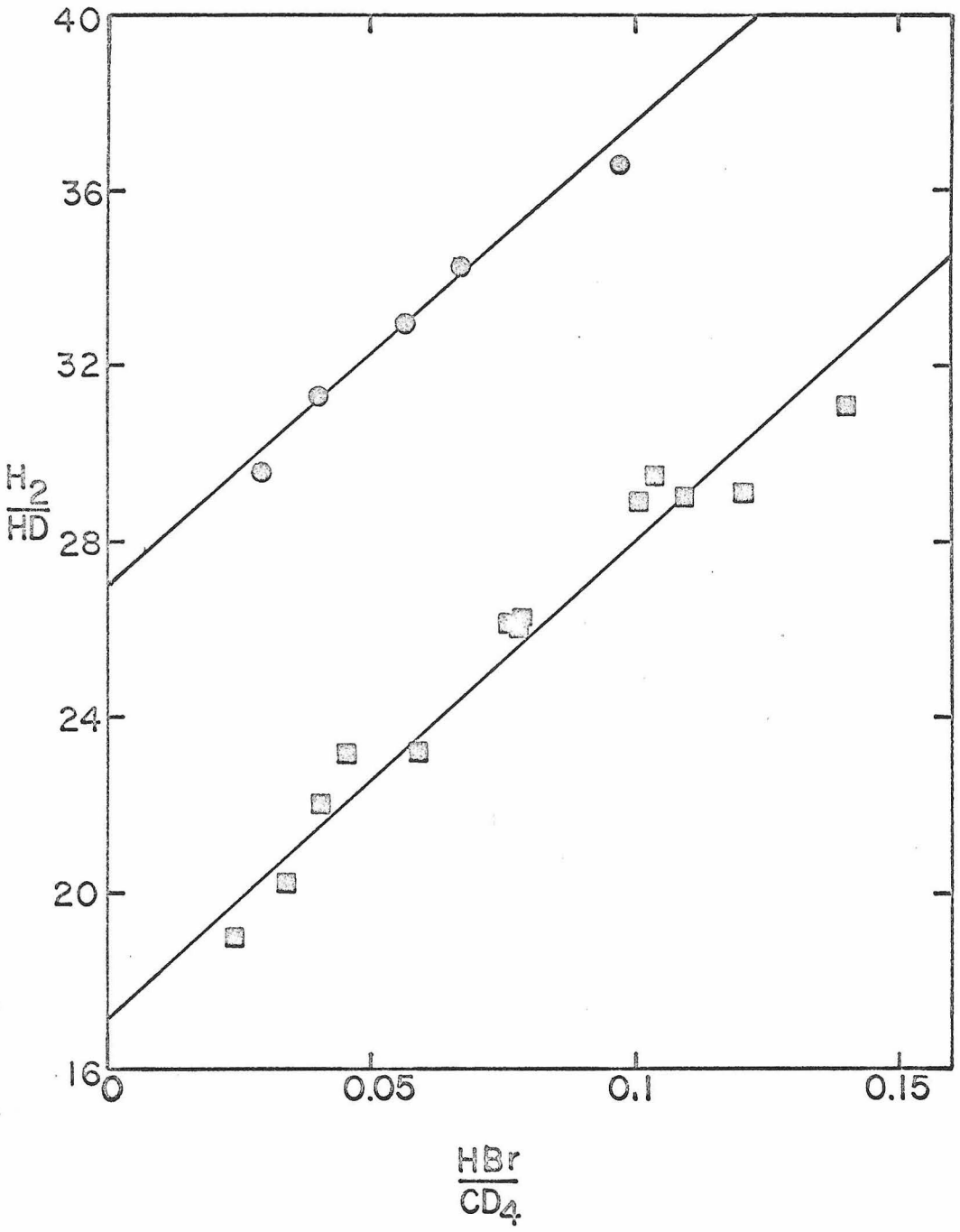

Figure E1. Results of preliminary photolyses at 2138Å.

27.2 ± 0.8. The intercept was 40% higher than the intercept of the first series of experiments. These two series of experiments suggested a conversion effect in experiments with $[HBr]/[CD_4]$ ratios ranging from 0.03 to 0.15 and motivated the conversion experiments described in Section 1.3.

1.2 Preliminary Experiments at 2061Å

Preliminary experiments at 2061Å were done using an iodine lamp powered by a microwave source. The intensity of the lamp was not constant for these experiments, varying by as much as a factor of 2 during a photolyses. The experimental results showed as much as 15% scatter. A plot of $[H_2]/[HD]$ versus $[HBr]/[CD_4]$ yielded an average intercept of 21 ± 2. This intercept is higher than the intercept of the first series of experiments run at 2138Å. This behavior was not expected since the $D + H_2$ and $H + D_2$ systems always showed a decrease in intercept with decreasing wavelength. This led us to perform further experiments to check the consistency of the method.

1.3 Preliminary experiments at 2288Å

A cadmium Phillips spectral lamp with the cis-2-butene filter described in Paper 4 and Appendix A was used for these experiments.

The two sets of experiments at 2138Å indicated that a conversion effect might be causing the irreproducibilities observed in the early experiments. Hence a set of experiments was performed at 2288Å in which the $[HBr]/[CD_4]$ ratio and the intensity

Table E2. Results of HBr-CD_4 Photolyses at 2138Å with [HBr]/[CD_4] Ratios From 0.03 to 0.15. Conversion 0.5%

Expt.	P_{HBr} (torr)	P_{CD_4} (torr)	Photolysis Time(hrs.)	$\frac{[HBr]}{[CD_4]}$	$\frac{[H_2]}{[HD]}$
1	10.71	160.2	1	0.0669	34.2
2	10.91	272.1	1	0.0401	31.5
3	12.87	228.9	1	0.0563	32.8
4	10.80	103.9	1	0.0969	36.3
5	11.11	323.9	1	0.0291	29.6

were kept constant and the time (and hence the conversion) varied. This wavelength was chosen for these experiments because of the shorter photolysis times required. The results of the above experiments is given in Table EIII and in Figure E2. There is a considerable variation of $[H_2]/[HD]$ with time indicating a conversion effect at this $[HBr]/[CD_4]$ ratio. These data are further analyzed in Paper 4.

Also two sets of experiments with photolysis times of 10 minutes and 5 minutes respectively were performed with $[HBr]/[CD_4]$ ratios varying from 0.03 to 0.12. The results of these experiments are given in Table EIV and are plotted in Figure E3. For the experiments with 10 minute photolysis times the slope was 67.2 ± 2.9 and the intercept was 31.9 ± 0.2. For the experiments with 5 minutes photolysis time the slope was 67.8 ± 2.2 and the intercept was 34.5 ± 0.3.

Photolysis experiments of Compton and Martin[3] on the HBr-C_4D_{10} system indicated that a conversion effect observed at $[HBr]/[C_4D_{10}]$ ratios of 0.03 to 0.15 disappeared when $[HBr]/[C_4D_{10}]$ ratios were greater than 0.3. Hence we did two series of experiments at $[HBr]/[CD_4]$ ratios ranging from 0.3 to 1.2 with conversions of 0.45% and 0.9% to see if Compton and Martin's observations were true for our system. The results of these experiments are tabulated in Table EV and plotted in Figure E4. For the experiments at 0.45% conversion, least squares analysis of the photolysis data gives a slope of 49.1 ± 1.8 and an intercept of 37.7 ± 0.9. For the experiments at 0.9% conversion the least

squares slope and intercept were 49.3 ± 1.2 and 37.1 ± 0.8 respectively. Least squares analysis of the combined data gives a slope of 48.7 ± 0.9 and an intercept of 37.8 ± 0.5. Hence the slopes and intercepts of two series of experiments done at two different conversions agree within experimental error and indicate that no conversion effect is present at $[HBr]/[CD_4]$ ratios ranging from 0.3 to 1.2.

The results in Table EIII where $[HBr]/[CD_4]$ equals 0.77 and the time is varied extrapolate to zero time to give an $[H_2]/[HD]$ ratio of 41.5. The least squares fit of the experiments with $[HBr]/[CD_4]$ ranging from 0.3 to 1.2 gives $[H_2]/[HD]$ equal to 41.4 at $[HBr]/[CD_4]$ equal to 0.0775. Hence the two are in good agreement. Also the intercepts in Figure E3 extrapolate to zero conversion to give a zero conversion intercept of 37.5 which is in experimental agreement with the 37.8 above.

Hence, the above experiments lead to the conclusion that the extent of HBr conversion is unimportant if $[HBr]/[CD_4]$ ratios are greater than 0.2.

Table EIII. Results of Variable Conversion Experiments at 2288Å With $[HBr]/[CD_4]$ Ratios Approximately Constant

Expt.	P_{HBr} (torr)	P_{CD_4} (torr)	Photolysis Time(min.)	$\frac{[HBr]}{[CD_4]}$	$\frac{[H_2]}{[HD]}$	conv. (%)
1	10.29	131.5	10	0.0783	38.9	1.23
2	33.8	426.5	10	0.0792	38.6	1.24
3	10.48	139.3	15	0.0751	37.6	1.77
4	10.37	137.7	30	0.0752	35.6	3.34
5	10.57	145.4	30	0.0727	35.4	3.35
6	9.70	126.3	5	0.0768	39.8	0.62
7	10.36	136.6	5	0.0758	39.7	0.65
8	10.05	131.3	20	0.0765	37.2	2.28
9	10.40	138.8	25	0.0769	36.1	2.81

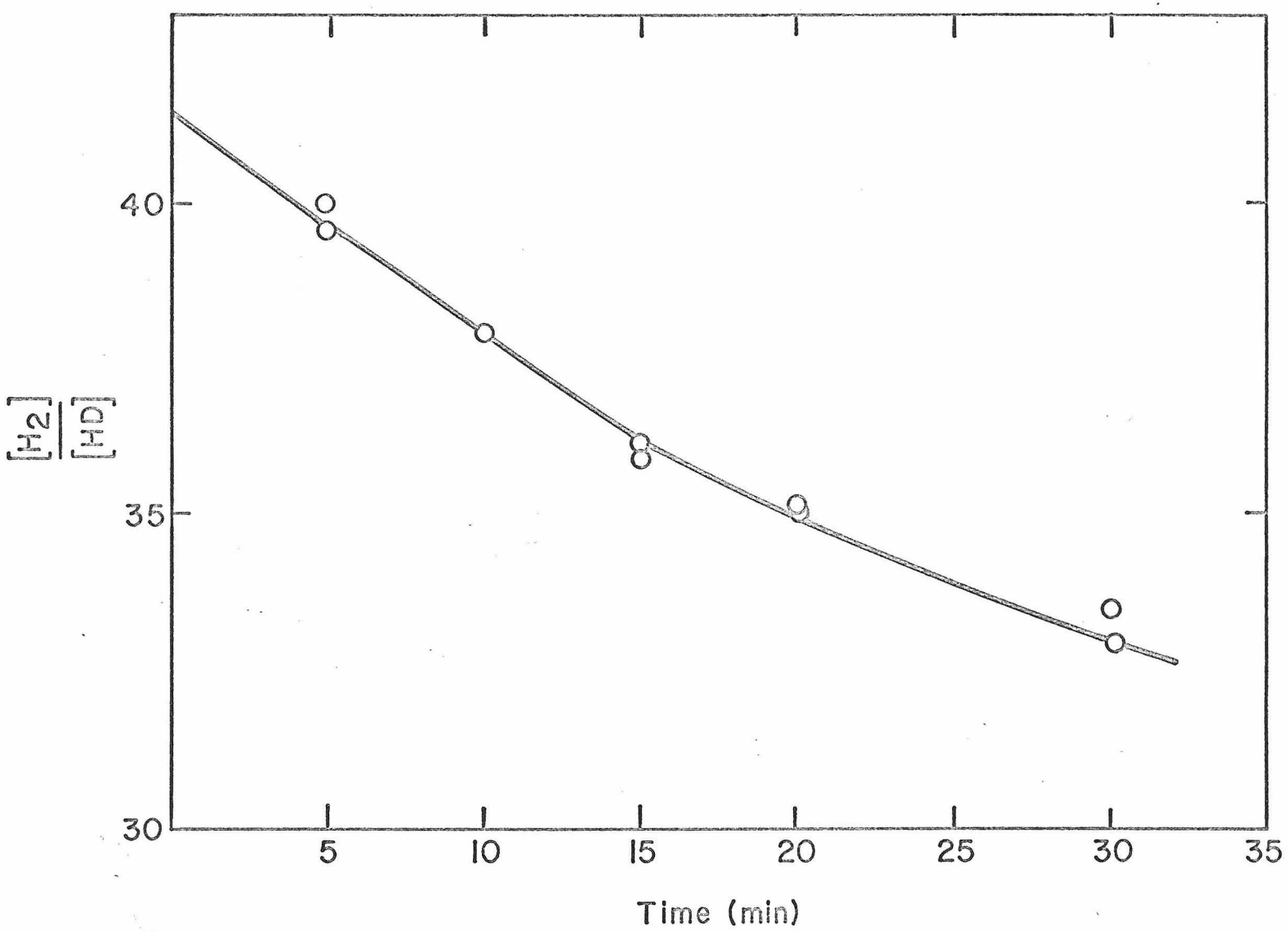

Figure E2. Results of photolyses at 2288Å with variable photolysis times.

Table E4. Results of Variable Conversion Experiments at 2288Å With $[HBr]/[CD_4]$ Ratios From 0.03 to 0.12

Expt.	P_{HBr} (torr)	P_{CD_4} (torr)	Photolysis Time(min.)	$\frac{[HBr]}{[CD_4]}$	$\frac{[H_2]}{[HD]}$
1	10.11	81.9	10	0.1236	40.3
2	10.51	113.3	10	0.0928	38.0
3	10.46	144.6	10	0.0723	37.0
4	10.12	185.3	10	0.0546	35.4
5	10.00	307.1	10	0.0326	34.2
6	10.13	350.4	5	0.0289	36.6
7	10.10	307.8	5	0.0328	36.6
8	10.16	134.9	5	0.0753	39.5
9	10.13	131.8	5	0.0769	39.9

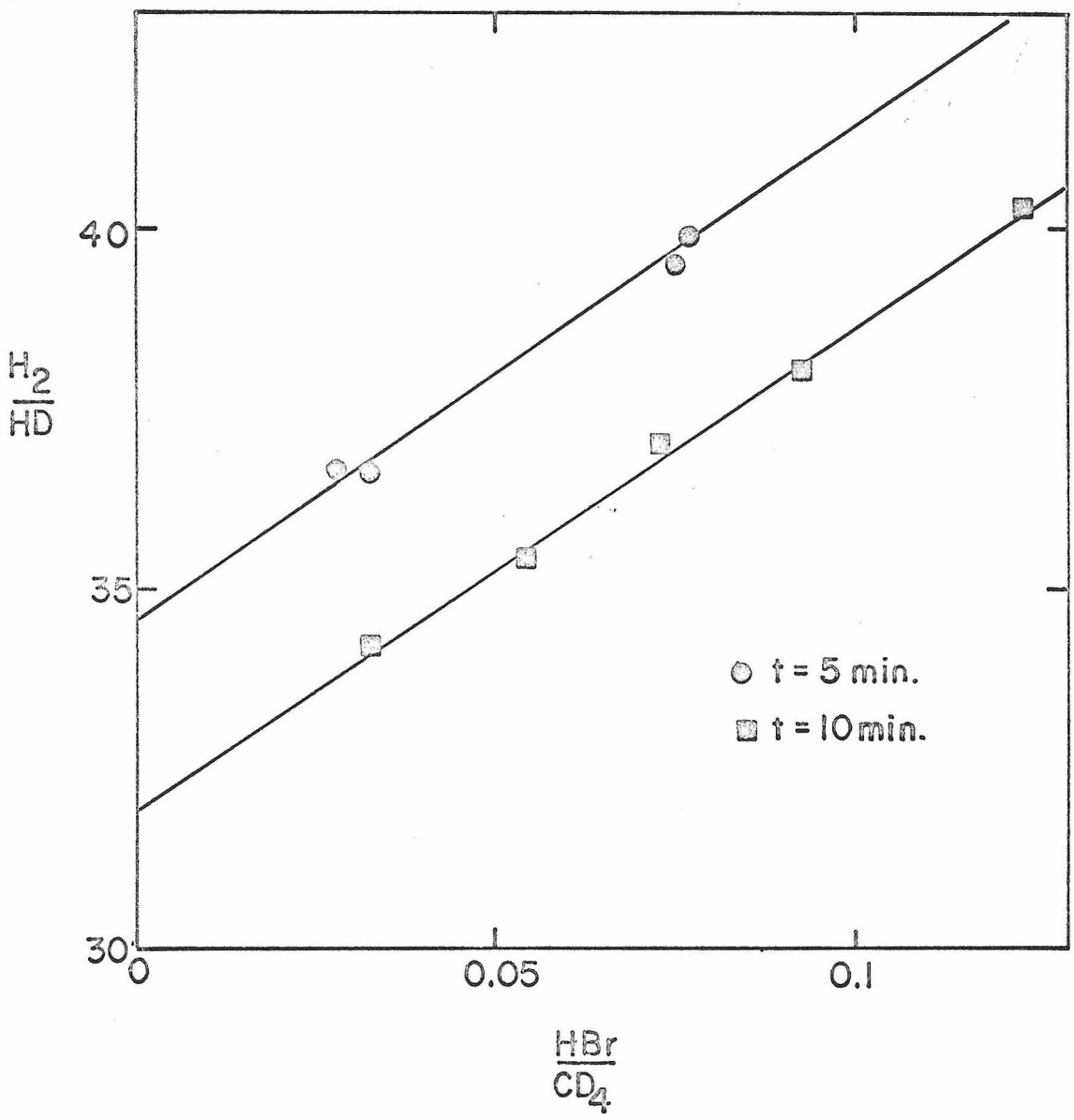

Figure E3. Results of preliminary experiments at 2288Å.

Table EV. Results of Variable Conversion Experiments at 2288Å With $[HBr]/[CD_4]$ Ratios From 0.25 to 1.0

Expt.	P_{HBr} (torr)	P_{CD_4} (torr)	Photolysis Time(min.)	$\frac{[HBr]}{[CD_4]}$	$\frac{[H_2]}{[HD]}$	conv. (%)
1	27.8	72.2	10	0.385	55.5	1.21
2	24.4	45.6	10	0.534	63.9	1.20
3	28.3	35.9	5	0.788	76.2	0.61
4	28.7	109.5	5	0.262	50.6	0.62
5	26.5	63.5	5	0.417	57.5	0.61
6	61.2	58.2	10	1.052	89.4	1.21
7	43.8	56.3	10	0.778	74.5	1.20
8	46.6	69.8	5	0.668	71.7	0.62
9	43.1	87.1	5	0.495	61.5	0.61
10	37.8	150.9	10	0.251	49.8	1.22
11	36.5	142.0	5	0.257	51.1	0.61

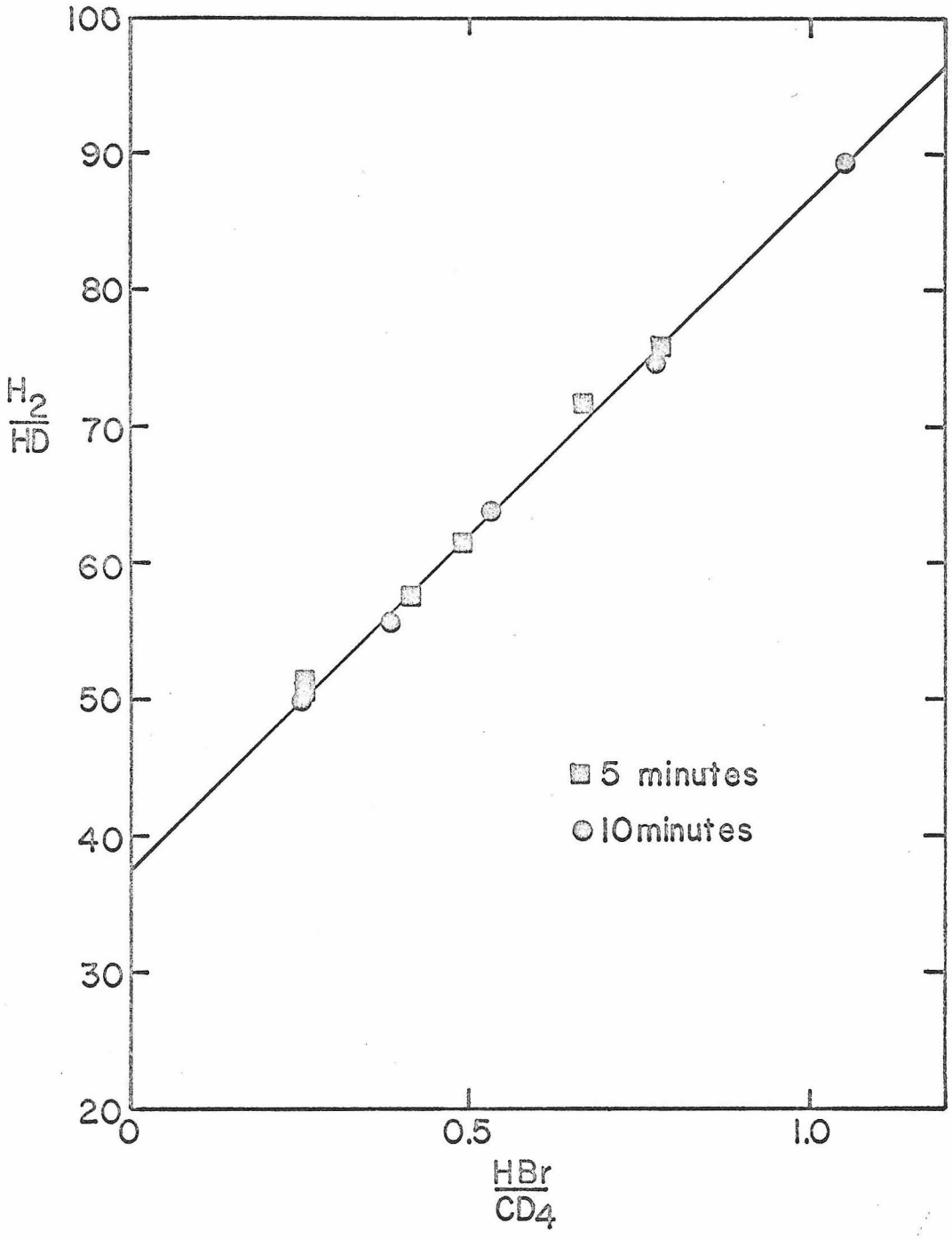

Figure E4. Results of HBr-CD_4 photolyses at 2288Å.

2. Photolysis at 2537Å

A General Electric germicidal lamp was used in conjunction with a 2 mm thick Corning 7910 glass filter for photolyses at this wavelength. One side of the reaction vessel was irradiated instead of the window as in other experiments. To verify that this geometry gave consistant results, a photolysis was done with the Hanovia SC 2537 low pressure mercury lamp where only the window of the reaction vessel was irradiated. At an $[HBr]/[CD_4]$ ratio of 0.388, the $[H_2]/[HD]$ ratio was 87.5 with the Hanovia lamp while at an $[HBr]/[CD_4]$ ratio of 0.378, the $[H_2]/[HD]$ ratio was 86.9 with the germicidal lamp. This is within experimental error and shows that the geometry of the photolysis system is unimportant. Photolyses in all experiments lasted 20 minutes. The conversion was measured in only the first experiment of each series at a given wavelength by adding a known amount of He to the reaction vessel after the photolysis, measuring [HD]/[He] on the mass spectrometer and then obtaining the conversion from the formula:

$$c = \frac{[HD]}{[He]}\left(1 + \frac{2[H_2]}{[HD]}\right) \Big/ \frac{[HBr]}{[He]}$$

The measured conversion in the first experiment was 1.0%.

The results of these experiments are listed in Table EIV and a plot of $[H_2]/[HD]$ versus $[HBr]/[CD_4]$ is shown in Figure E5. Least squares analysis of the data gives a slope of 63.8 ± 1.1 and an intercept of 61.8 ± 0.7.

Table EVI. Results of Experiments at 2537Å - Conversion 1.0%

Expt.	P_{HBr} (torr)	P_{CD_4} (torr)	Photolysis Time(min.)	$\frac{[HBr]}{[CD_4]}$	$\frac{[H_2]}{[HD]}$
1	49.2	129.9	20	0.378	86.9
2	53.7	78.0	20	0.688	106.0
3	36.3	166.2	23	0.218	74.6
4	64.3	64.6	20	0.995	124.8
5	49.8	70.2	20	0.710	108.0
6	51.8	102.1	20	0.507	94.6
7	50.4	173.3	20	0.291	79.8
8	41.0	42.0	22	0.978	123.5

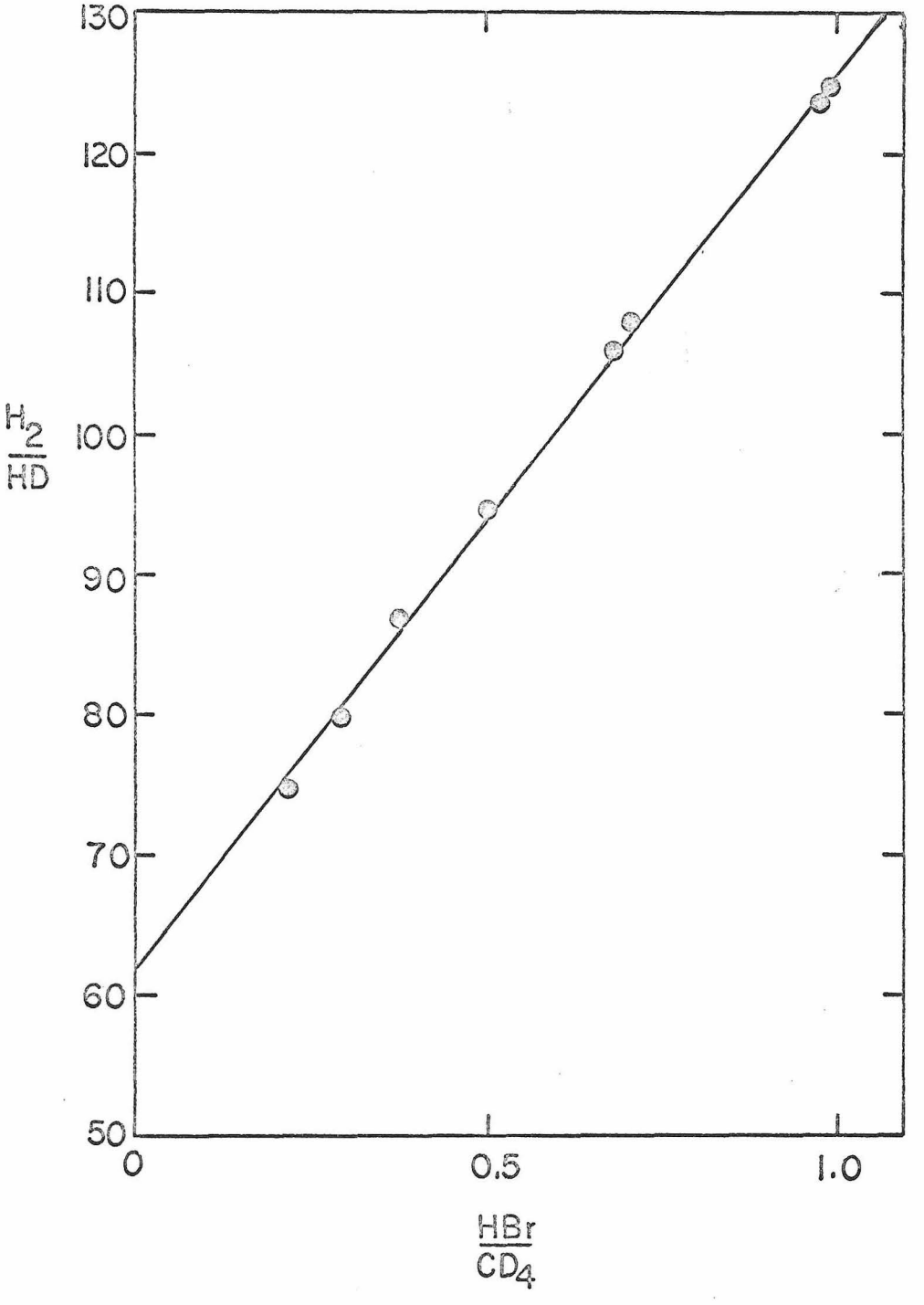

Figure E5. Results of HBr-CD_4 photolyses at 2537Å.

3. Photolyses at 2138Å

Experiments at this wavelength were performed using the zinc Phillips spectral lamp with the cis-2-butene filter described in Appendix A. Photolyses lasted 1 1/2 hours which resulted in an HBr conversion for the first experiment performed of 0.8%.

The results of these experiments are given in Table EVII and a plot of $[H_2]/[HD]$ versus $[HBr]/[CD_4]$ is shown in Figure E6. Least squares analysis of the data gives a slope of 50.5 ± 1.1 and an intercept of 30.3 ± 0.8.

4. Photolyses at 2061Å

Experiments at this wavelength were carried out using an iodine lamp powered by a microwave source. Since a large amount of heat was generated by the lamp, a cooling coil was wrapped around the reaction vessel to keep it at room temperature. The remainder of the experimental procedure was as described previously. Photolyses lasted 30 minutes for all experiments. The measured conversion for the first experiment was 0.56%.

The results of these experiments are given in Table EVIII and a plot of $[H_2]/[HD]$ versus $[HBr]/[CD_4]$ is shown in Figure E7. Least squares analysis of the data gives a slope of 53.0 ± 0.6 and an intercept of 27.8 ± 0.4.

Table EVII. Results of Experiments at 2138Å - Conversion 0.8%

Expt.	P_{HBr} (torr)	P_{CD_4} (torr)	Photolysis Time(hrs.)	$\frac{[HBr]}{[CD_4]}$	$\frac{[H_2]}{[HD]}$
1	49.8	67.4	1.5	0.740	68.5
2	66.1	55.7	1.5	1.188	89.5
3	47.6	151.6	1.5	0.314	46.5
4	48.0	92.1	1.5	0.521	55.5
5	38.2	155.2	1.5	0.246	42.2
6	66.2	69.8	1.5	0.948	79.5
7	52.2	103.6	1.5	0.503	56.5
8	68.0	77.2	1.5	0.881	74.0

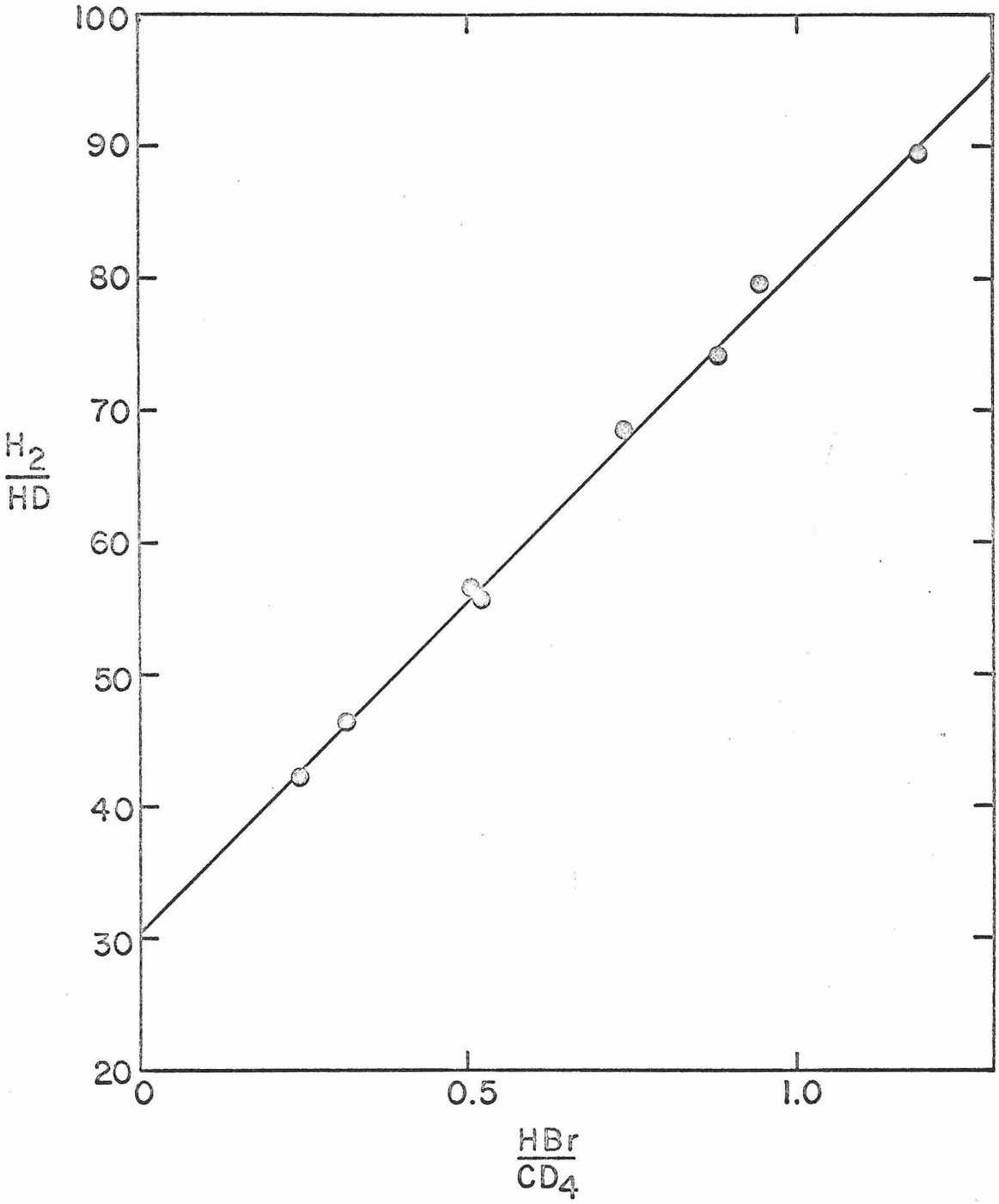

Figure E6. Results of HBr-CD_4 experiments at 2138Å.

Table EVIII. Results of Experiments at 2061Å - Conversion 0.56%

Expt.	P_{HBr} (torr)	P_{CD_4} (torr)	Photolysis Time(min.)	$\frac{[HBr]}{[CD_4]}$	$\frac{[H_2]}{[HD]}$
1	40.0	86.4	30	0.463	52.7
2	49.6	135.7	30	0.356	46.5
3	52.4	55.3	30	0.947	78.5
4	44.2	71.3	30	0.620	60.3
5	47.5	160.8	30	0.295	43.1
6	40.0	63.9	30	0.627	60.9
7	49.9	60.0	30	0.832	71.5
8	37.5	105.8	30	0.355	47.4
9	49.5	54.5	30	0.909	76.0

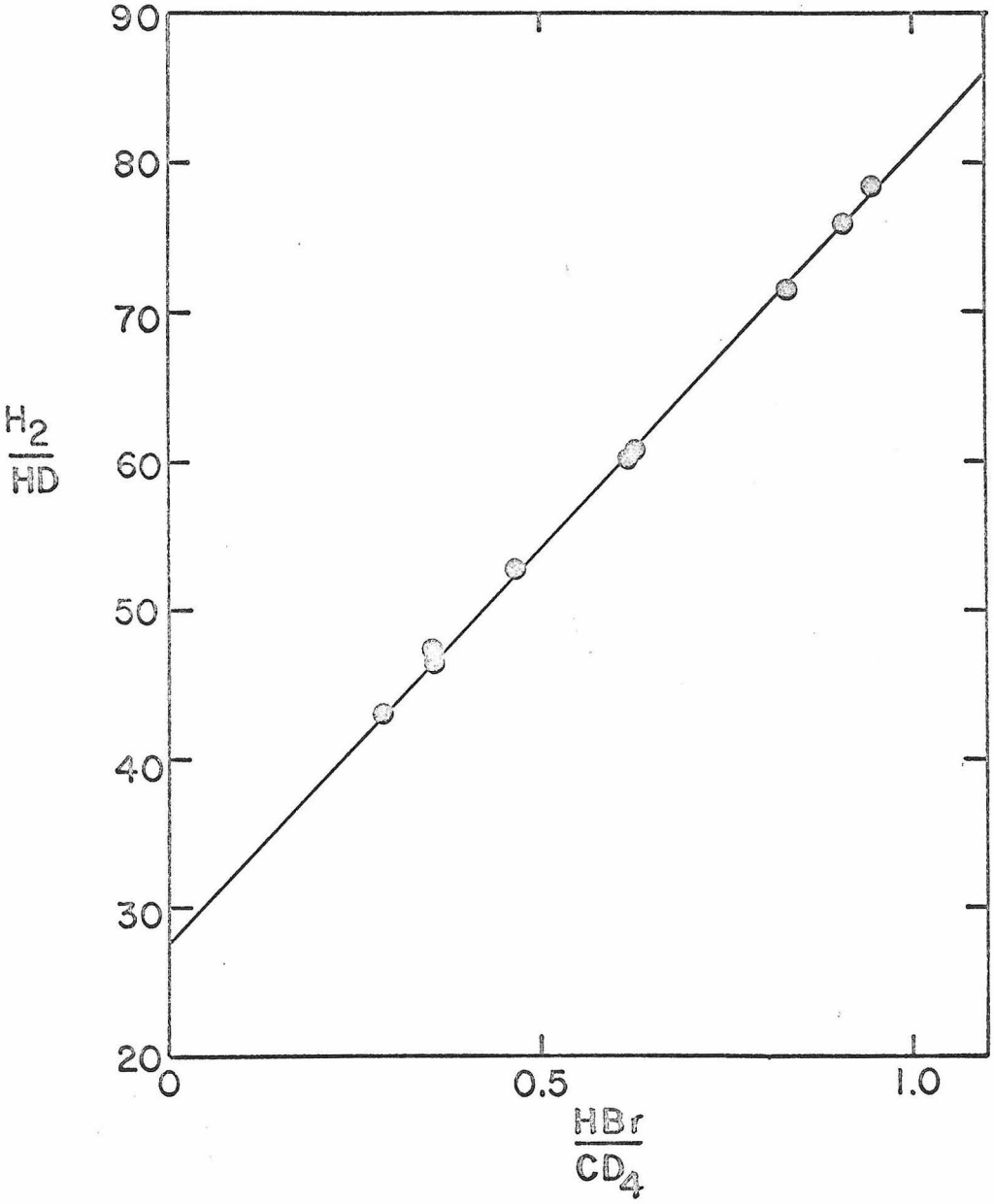

Figure E7. Results of HBr-CD_4 experiments at 2061Å.

5. Photolyses at 1849Å

The photolyses at this wavelength were done with the Hanovia SC 2537 lamp with the ^{60}Co gamma-irradiated filter. This lamp was powered by the microwave source as described in Appendix A to give greater intensities. A cooling coil was wrapped around the cell to keep it at room temperature. The remainder of the procedure was as described previously. Photolyses lasted 30 minutes for each experiment. The measured HBr conversion for the first experiment was 0.6%.

The results of these experiments are given in Table EIX and a plot of $[H_2]/[HD]$ versus $[HBr]/[CD_4]$ is shown in Figure E8. Least squares analysis of the data gives a slope of 56.5 ± 1.5 and an intercept of 24.6 ± 1.1.

REFERENCES

1. R. M. Martin and J. E. Willard, J. Chem. Phys., 40, 3007 (1964).

2. R. J. Carter, W. H. Hamill and R. R. Williams, Jr., J. Am. Chem. Soc., 77, 6457 (1955).

Table EIX. Results of Experiments at 1849Å - Conversion - 0.60%

Expt.	P_{HBr} (torr)	P_{CD_4} (torr)	Photolysis Time(min.)	$\frac{[HBr]}{[CD_4]}$	$\frac{[H_2]}{[HD]}$
1	40.0	65.6	30	0.610	57.7
2	42.0	112.6	30	0.376	46.0
3	54.0	56.7	30	0.953	79.2
4	53.6	95.2	30	0.563	55.9
5	34.6	127.1	30	0.272	40.6
6	39.5	48.1	30	0.821	69.1
7	65.9	54.8	20	1.202	93.5
8	43.5	102.0	20	0.450	51.4

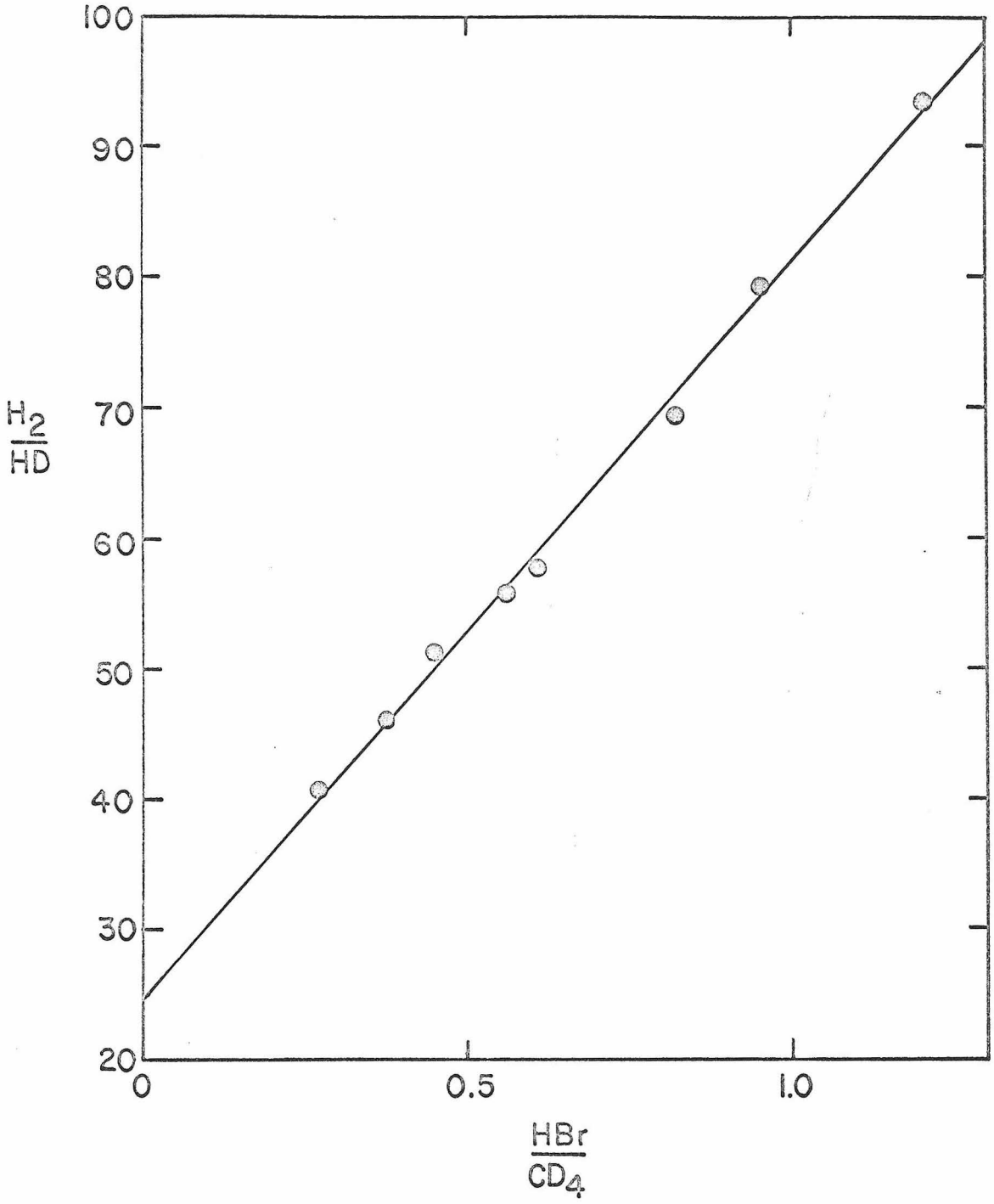

Figure E8. Results of HBr-CD_4 photolyses at 1849Å.

APPENDIX F

CALCULATION OF ROTATIONAL AND TRANSLATIONAL ENERGY SPREADS IN DBr AND DI

1. Rotational Energy Spread

The relative rotational populations for DBr and DI at 298°K are listed in Table F1 and plotted as a function of J(J+1) in figures F1 and F2. The average rotational energy of DBr is 0.025 eV while for DI it is 0.020 eV. These energies correspond to average values of J(J+1) of 23.8 and 48.8 respectively. As a measure of the energy spread we use an interval, symmetric about the average J(J+1), which contains approximately 70% of the molecules. This was done by a method of trial and error. Table FII shows the fraction of the total population present in various J(J+1) intervals for DBr. For DBr the chosen interval contains J(J+1) values from 0 to 47 which corresponds to an energy spread of 0.025 eV on either side of the average and includes 71% of the molecules. For DI the chosen interval includes J(J+1) values from 7 to 90 which corresponds to an energy spread of 0.018 eV on either side of the average and includes 73% of the molecules.

2. Translational Energy Spread

The translational energies of DBr and DI follow a Boltzmann distribution function of the form:

$$g(E_{DX}^{lab})\, dE_{DX}^{lab} = 4\pi\left(\frac{m_{DX}}{2\pi kT}\right)^{3/2}\left(\frac{2}{m_{DX}}\right)^{1/2}\left(E_{DX}^{lab}\right)^{1/2}\exp(-E/kT)\, dE_{DX}^{lab}$$

A plot of $E_{DX}^{lab\ 1/2}\exp(-E_{DX}^{lab}/kT)$ as a function of E_{DX}^{lab}/kT is shown in figure F3. Table FIII shows the approximate percentage of DX molecules contained in each energy interval. Again, an interval is selected which is symmetric about the average energy of 3/2 kT (1.5 in figure F3) and contains 70% of the molecules. The chosen interval was for values of E_{DX}^{lab}/kT from 0.4 to 2.6 which contains 71% of the population. This interval corresponds to a translational energy spread in DX of 0.57 eV.

Table FI. Relative Rotational Populations for DBr and DI

J	J(J+1)	DBr $N_J/N \times 10^2$	DI $N_J/N \times 10^2$
0	0	4.00	1.60
1	2	11.09	4.64
2	6	15.69	7.25
3	12	17.23	9.22
4	20	16.02	10.40
5	30	13.12	10.87
6	42	9.47	10.61
7	56	6.18	9.79
8	72	3.67	8.59
9	90	1.98	7.08
10	110	0.98	5.76
11	132	0.43	4.45
12	166	0.11	3.31
13	182	0.07	2.35
14	210		1.62
15	240		1.09
16	272		0.69

Table FII. Fraction of Population in Various Rotational Energy Intervals in DBr

J(J+1) Interval	Fraction (in percent)
0 to 5	4.49
5 to 10	9.63
10 to 15	10.23
15 to 20	9.94
20 to 23	5.63
23 to 25	3.56
25 to 30	8.30
30 to 40	13.82
40 to 50	10.07
50 to 70	13.18
70 to 90	6.70
90 to 110	3.11
110 to 130	1.43

Table FIII. Fraction of Population in Various Translational Energy Intervals

E/0.026	Fraction (in percent)
0.0 - 0.2	4.27
0.2 - 0.4	9.25
0.4 - 0.6	9.82
0.6 - 0.8	9.52
0.8 - 1.0	8.90
1.0 - 1.4	15.35
1.4 - 1.5	0.46
1.5 - 2.0	16.39
2.0 - 3.0	15.30
3.0 - 4.0	6.76
4.0 - 5.0	2.49
5.0 - 6.0	1.42

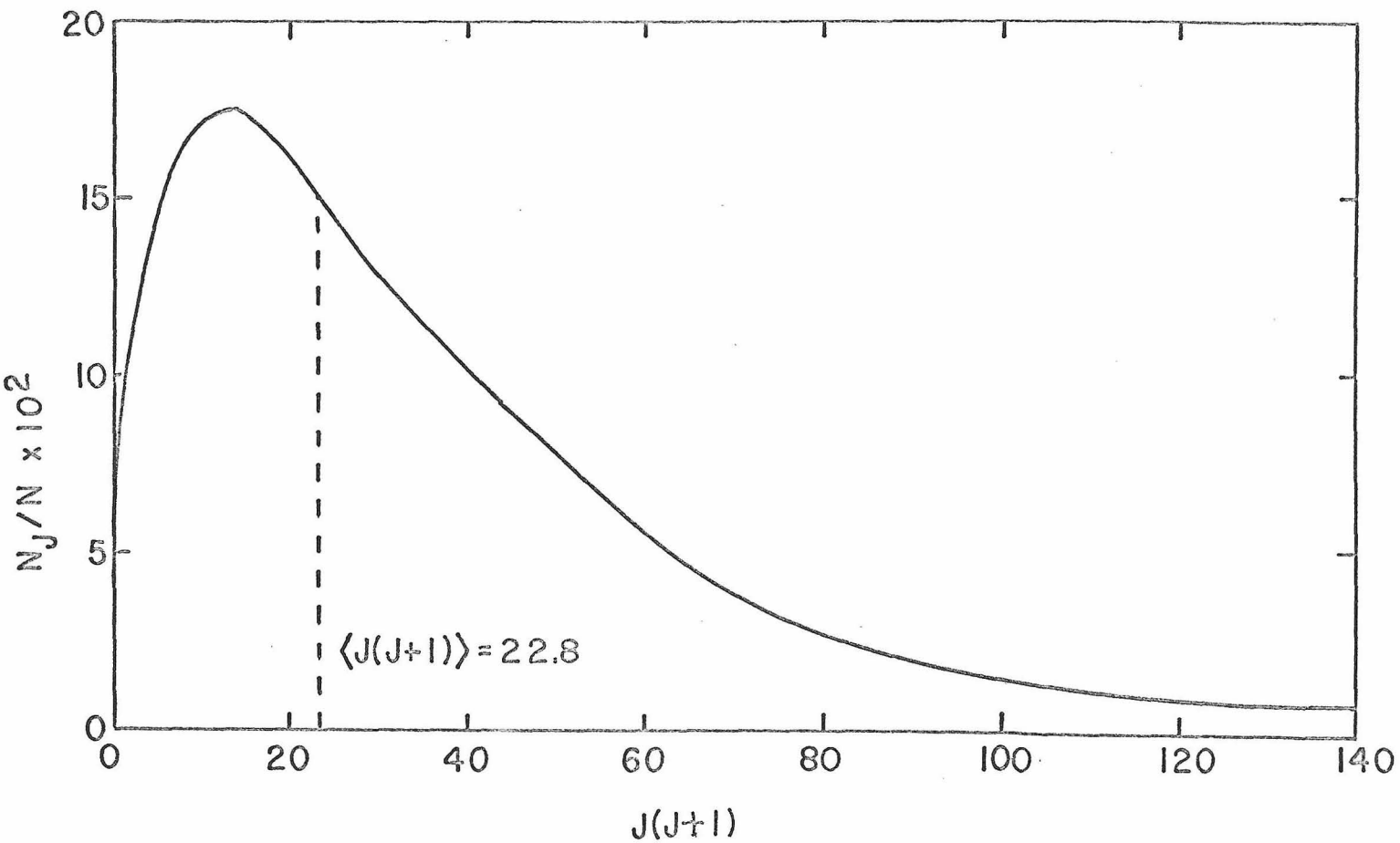

Figure F1. Population of rotational energy levels of DBr at room temperature.

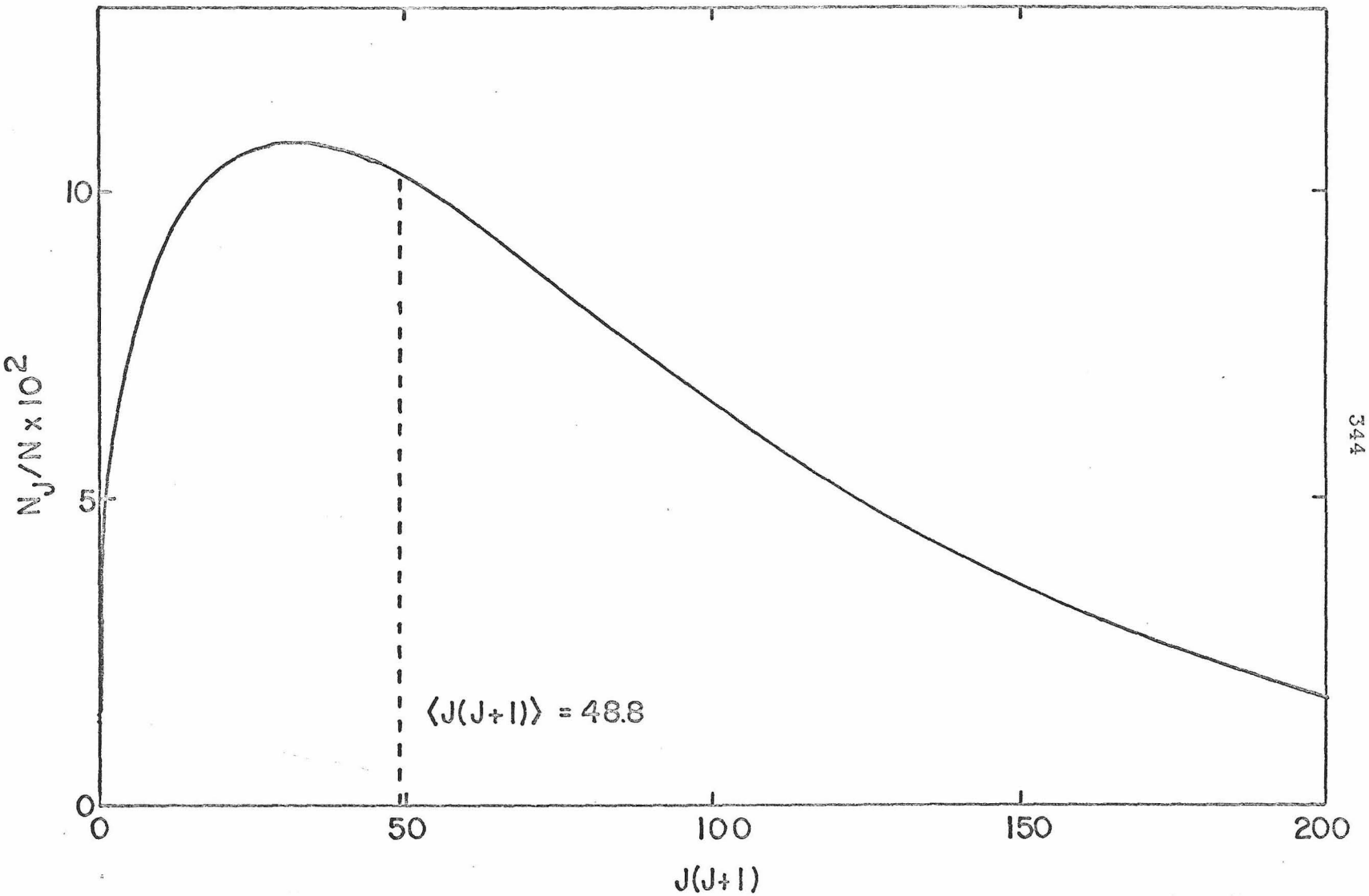

Figure F2. Population of rotational energy levels of DI at room temperature.

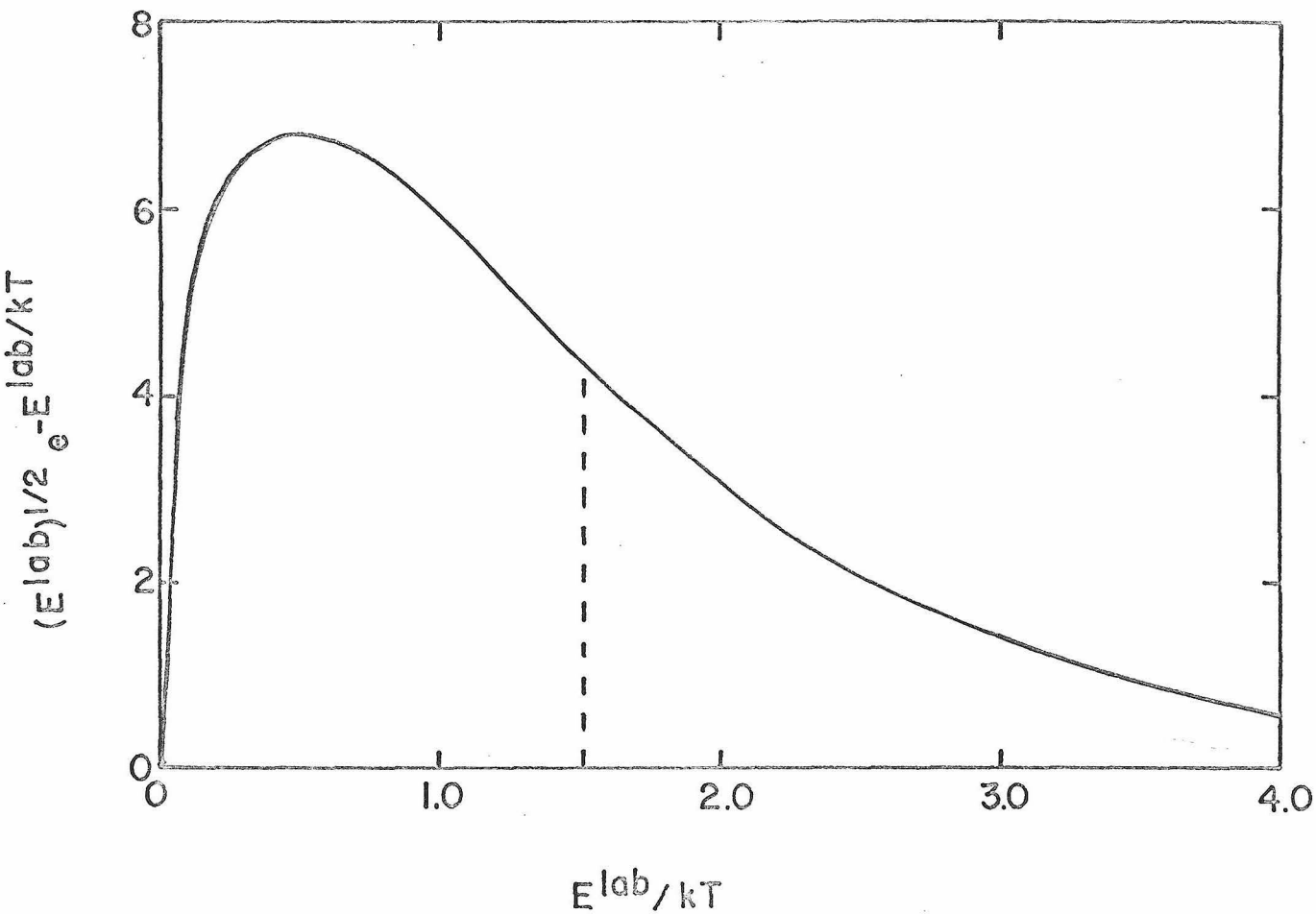

Figure F3. Boltzmann distribution of translational energies at 300°K.